BINDING SERVICES
Tel +44 (0)29 2087 4949
Fax +44 (0)29 20371921
e-mail bindery@cardiff.ac.uk

The role of keratan sulphate proteoglycans in the maintenance of mouse corneal stromal ultrastructure

Thesis submitted to Cardiff University, University of Wales
for the degree of

Doctor of Philosophy

in the Discipline of Structural Biophysics

Nicola Beecher (BSc Hons)

The Strucural Biophysics Group
School of Optometry and Vision Sciences
Cardiff, Wales, United Kingdom
Year 2006

ProQuest LLC
789 East Eisenhower Parkway
P.O. Box 1346
Ann Arbor, MI 48106-1346

DECLARATION

This work has not previously been accepted in substance for any degree and is not concurrently submitted in candidature for any degree.

Signed.....N. Beecle.....(Candidate) Date.7.11.2006.

STATEMENT 1

This thesis is being submitted in partial fulfilment of the requirements for the degree of PhD.

Signed...N. Beecle.....(Candidate) Date.7.11.2006

STATEMENT 2

This thesis is the result of my own independent work/investigation, except where otherwise stated.

Signed.....N. Beecle.....(Candidate) Date.7.11.2006

STATEMENT 3

I hereby give consent for my thesis, if accepted, to be available for photocopying and for inter-library loan, and for the title and summary to be made available to outside organisations.

Signed.....N. Beecle.....(Candidate) Date.7.11.2006

Acknowledgements

I would sincerely like to thank my supervisors, Professor Keith Meek and Dr Andrew Quantock, for their guidance, support, and enthusiasm throughout my PhD studies. I have been most fortunate in having two very friendly and approachable mentors. It has really been a privilege to know them and work with them, and I hope that our paths cross again in the future.

I would also like to pay thanks to Dr Craig Boote and Dr Sally Hayes, not least for their friendship, but also for the good advice they imparted me with in the collection and analysis of X-ray diffraction data. My thanks also extend to Dr Gunter Grossmann at the SRS for his help with data collection.

My thanks go to Dr Robert Young and Dr Phillip Lewis who, as very good friends and colleagues, have provided me with excellent guidance and advice with regards to transmission electron microscopic procedures. My thanks also go to Dr Hann for his help with the electron microscope.

Thanks to all the people who have kept my spirits lifted throughout my time at Cardiff University. To Melody, Rosie, Sally, Craig, Phil, Rob, and Che for being steadfast in their positive outlook on life; I am so glad to have formed such good friendships with you. Also great thanks to James Douche for sparking some very interesting discussions to start the day! Happily, I have found the journey through my PhD studies to be one of the most challenging, yet rewarding, times of my life.

Thanks to all my family for their support; especially to my Dad, my Grancha, my brother, Richard, and to Gaynor and Steven, the best in-laws I could ever wish for.

To my Mum, who I know is with me every day in spirit, thank you for being the best Mum you could be, and for your earlier encouragement of my academic pursuits. I don't believe I would have come so far if it hadn't been for you.

To my lovely husband, Rob, thank you so much for all of your love, support and encouragement, and for taking a genuine interest in my work. You've been unwavering in your attempts to make me smile. I've never known anyone to place so much faith in me as you do.

To my son, Morgan, the most beautiful person that walks the planet; I'm so very proud to have completed this thesis, but you are, by far, my greatest achievement in life. I dedicate this thesis to you.

For Morgan

Abstract

The cornea is a remarkable connective tissue that is transparent to visible light as a consequence of the regularly arranged, uniformly-sized collagen fibrils that constitute it. Evidence suggests that this intricate collagen fibril architecture is maintained by the presence of keratan sulphate-carrying proteoglycans (KSPGs) within the corneal stroma. The KSPGs, lumican, keratocan, and mimecan are believed to be involved in the regulation of collagen fibril diameter and fibril spacing. KSPGs have recently been investigated using transgenic technology, which allows the manipulation of gene expression in order to determine the significance of a gene product in a biological system. Thus, to ascertain the role of KSPGs in this thesis transgenic mice were used.

Two methodologies were employed to investigate the structural organisation of collagen within normal and mutant mouse corneas; small angle X-ray diffraction (XRD) provided quantitative information on collagen fibril spacing, collagen fibril diameter and degree of local order in the fibrillar array averaged throughout the tissue, and transmission electron microscopy (TEM) afforded a view of collagen fibril morphology within the tissue.

Previous research has shown that a homozygous-null mutation for lumican affects corneal collagen fibril architecture. But no information exists about whether these structural changes develop in adulthood or start early in life. Thus, the role of lumican during neonatal corneal stromal development between days 8 and 14 was explored. Collagen fibril spacing is considerably higher in lumican-null corneas until day 14, and fibril diameter is, on average, smaller-than-normal. TEM provided evidence of stromal disorder in mutants and fibril fusion at day 14, indicating that lumican plays a key role in development of the neonate cornea.

Next, the effect of a cysteine-serine substitution in the N-terminal region of lumican was investigated to determine the importance of this region in lumican-collagen interaction. Mutant collagen fibrils are appreciably larger in diameter, signifying failure of lumican to bind collagen and regulate fibril growth. This chapter also investigated the consequences of lumican over-expression, to reveal that excess lumican has no significant effect on mutant corneal stromal ultrastructure.

The role of mimecan in the corneal ECM via ablation of gene expression was explored. The extent of ultrastructural alteration was minimal with mutants having collagen fibril spacing and fibril diameter that were essentially unchanged. This work indicated that mimecan plays a minor role in the maintenance of matrix structure in the cornea.

Finally, to better understand what structural motifs contribute to KSPG effectivity, the significance of a carbohydrate sulphotransferase gene, *Chst5*, in the mouse corneal stroma was investigated. The ablation of *Chst5*, responsible for the production of a carbohydrate sulphotransferase enzyme, revealed that smaller fibril spacing and fibril diameters, and stromal disorganisation are the result.

KSPGs are structurally and functionally distinctive. Mimecan appears to have little influence over matrix morphogenesis, and it is possible that absence of mimecan is

compensated for by the upregulation of other PGs. In contrast, lumican is an important component of the ECM; the structure of lumican bestows this molecule the ability to regulate matrix morphogenesis, as exemplified by absence of lumican and also N-terminal mutation of the core protein. Indeed, the sulphated form of KS is required within cornea, as the absence of a carbohydrate sulphotransferase gene renders the corneal stroma structurally altered.

"Nature is nowhere accustomed more openly to display her secret mysteries than in cases where she shows traces of her workings apart from the beaten path; nor is there any better way to advance the proper practice of medicine than to give our minds to the discovery of the usual law of Nature by careful investigation of cases of rarer forms of disease. For it has been found, in almost all things, that what they contain of useful or applicable [nature] is hardly perceived unless we are deprived of them, or they become deranged in some way."

From a letter written by William Harvey, shortly before his death in 1657. Quoted by Archibald Garrod in his article "The Lessons of Rare Maladies", *The Lancet*, Volume 211, Issue 5465, pp.1055-1060 (26th May 1928).

Table of Contents

List of Publications

Beecher, N., Chakravarti, S., Joyce, S., Meek, K.M., Quantock, A.Q. 2006. Neonatal development of the corneal stroma in wild-type and lumican-null mice. *Investigative Ophthalmology and Visual Science* 47 (1), 146-150.

Beecher, N., Carlson, C., Allen, B.R., Kipchumba, R., Conrad, G.W., Meek, K.M., Quantock, A.J. 2005. An X-ray diffraction study of corneal structure in mimecan-deficient mice. *Investigative Ophthalmology and Visual Science* 46 (11), 4046-4049.

Hayashida, Y., Akama, T.O., Beecher, N., Lewis, P.N., Young, R.D., Meek, K.M., Kerr, B., Hughes, C.E., Caterson, B., Tanigami, A., Nakayama, J., Fukada, M.N., Tano, Y., Nishida, K., Quantock, A.J. Matrix morphogenesis in cornea is mediated by the modification of keratan sulphate by GlcNAc 6-*O* sulphotransferase. *Proceedings of the National Academy of Sciences of the United States of America* 103 (36), 13333-13338.

Bibliography

List of Figures

List of Tables

Abbreviations

Alanine	Ala
Aldehyde dehydrogenase class 1	ALDH1
Alpha	α
Anterior banded region	ABR
Any amino acid	X
Aspartic acid	Asp
Asparagine	Asn
Basement membrane complex	BMC
Beta	β
Carbon	C
Chlorine	Cl
Chondroitin sulphate/dermatan sulphate	CS/DS
Coherence distance	t
Complimentary DNA	cDNA
Cupromeronic Blue	CuBlue
Cysteine	Cys
Deoxyribonucleic acid	DNA
Embryonic day	E
Embryonic stem	ES
Endoplasmic reticulum	ER
Ethanol	EtOH
Extracellular matrix	ECM
Fibril-associated collagens with interrupted triple helices	FACITs
Fucose	Fuc
Galactose	Gal
Glucuronate	GlcA
Glutamic acid	Glu
Glycine	Gly
Glycosaminoglycans	GAGs
Height-to-width (ratio)	H/W
Hydrogen	H
Hydroxylysine	Hyl
Hyproxyproline	Hyp
Iduronate	IdoA
Interfibrillar	IF
Interfibrillar spacing	IFS
Iron	Fe
Keratan sulphate	KS
Knockout	KO
Lead	Pb
Leucine rich repeats	LRRs
Macular Corneal Dystrophy	MCD
Magnesium chloride	Mg^{2+}
Mannose	Man
Mucopolysaccharidoses	MPS
N-acetylgalactosamine	GalNAc
N-acetylglucosamine	GlcNAc
Peak width at half-height	P/W

Post-coitus	p.c.
Posterior non-banded region	PNBR
Potassium chloride	KCl
Potassium	K^+
Proline	Pro
Proteoglycans	PGs
Refractive index	RI
Serine	Ser
Sialic acid	NeuAc
Small leucine rich proteoglycan	SLRP
Smooth muscle actin	SMA
Sodium	Na^+
Sodium chloride	NaCl
Sodium hydroxide	NaOH
Synchrotron Radiation Source	SRS
Threonine	Thr
Thrombospondin	TSP
Transketolase	TKT
Tyrosine	Tyr
Transmission electron microscope	TEM
Uranyl acetate	UA
Wild-type	WT
X-ray diffraction	XRD
Xylose	Xyl

Chapter 1. Introduction

1.1 Structure and function of the cornea

The cornea is a collagenous connective tissue that comprises one-sixth of the outer tunic of the eye, the sclera making up the remaining five-sixths (Klyce and Beuerman, 1988). The unique properties of this remarkable optical structure set it apart from other connective tissues as it is tough yet transparent, a characteristic that enables the efficient transmission of light. When light strikes the cornea it is refracted onto the retina via the lens, and as the degree of light bending depends upon corneal curvature and on the difference between the refractive indices (RI) of two media, it is clear from Figure 1.1 that the air-cornea interface significantly contributes to the human eye's optical power.

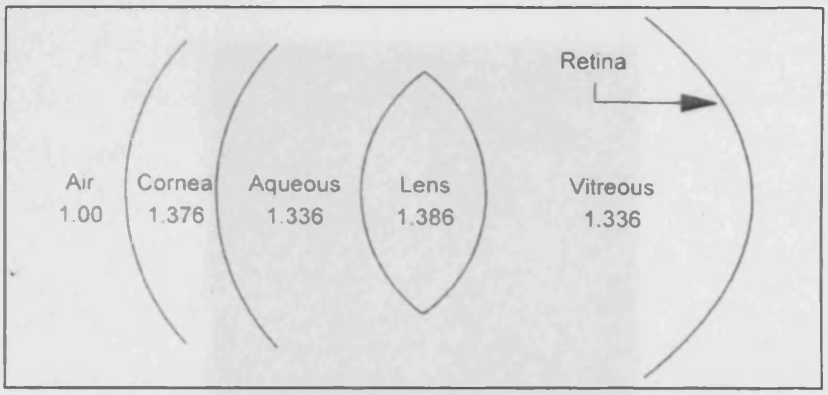

Figure 1.1. Indices of refraction of the optical media of the human eye (from McIlwain, 1998).

Indeed, this interface is so crucial optically that even minor corneal surface and curvature imperfections can affect image formation (McIlwain, 1998; Meek, 2002). It is imperative that the cornea remains transparent, so its avascular structure ensures that light travels through the tissue unabated. In the absence of blood vessels, the anterior tear film provides oxygen requirements, and most nutrient requirements are obtained from the aqueous humor via the posterior corneal surface (Klyce and Beuerman, 1988).

The opaque nature of the sclera acts, in part, as a barrier to stop light entering the eye from directions other than the optical axis, thus preventing interference with the image.

The adult human cornea is approximately 11.7 mm diameter horizontally and 10.6 mm diameter vertically (Forrester *et al*, 1999), with an average central thickness of 0.52 mm that flattens and thickens at the periphery to about 0.67 mm, lending it a hyperboloid shape (Bron *et al*, 1997). Although a relatively thin structure, the cornea's mechanical strength is provided by the stromal collagen matrix. The collagen fibrils resist tensile forces, while the soluble polymers inflate the matrix to resist compressive forces (Scott, 1992). These aspects will be discussed in more detail later.

The cornea is a highly differentiated tissue consisting of 5 distinct layers (Figure 1.2). In order from anterior to posterior they are epithelium, Bowman's layer, stroma, Descemet's membrane and endothelium.

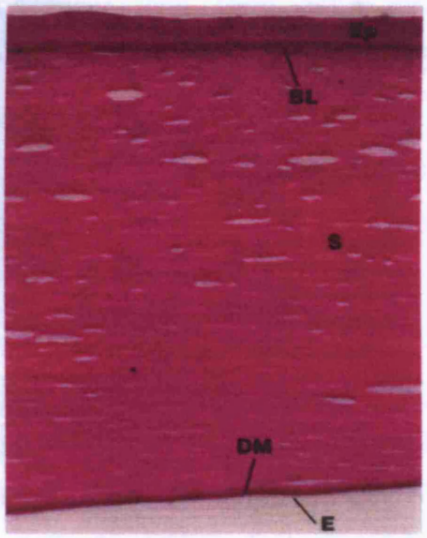

Figure 1.2. Low-power light micrograph showing the five layers of the human cornea. Ep, epithelium; BL, Bowman's layer; S, stroma; DM, Descemet's membrane; E, endothelium. (from Forrester *et al*, 2002).

1.1.1 Epithelium

The corneal epithelium is a non-keratinised, stratified squamous epithelium that represents 10% of the corneal thickness in man (50-60 μm). This layer principally supplies the eye with a smooth refracting surface together with the lubricating tear film at the front of the eye (Smolin and Thoft, 1994). The epithelium is the site of an active chloride (Cl) secretory process which acts as a structural barrier to reduce excess tear fluid absorption by coupling the transport of fluid to its Cl secretion

(Klyce, 1977). This layer also acts as a mechanical barrier protecting the underlying corneal layers. When damaged, the rapid migration of cells from the basal layer restores the epithelium (Gipson and Anderson, 1977).

1.1.2 Bowman's layer

Bowman's layer is an 8-12 μm thick layer (Komai and Ushiki, 1991) consisting of randomly arranged collagen fibrils, mainly types I, III, V (Jacobsen *et al*, 1984) and VII (Polack, 1961). The presence of Bowman's layer in the adult rabbit is controversial, but an acellular zone reminiscent of Bowman's layer is present in developing rabbit cornea (Cintron *et al*, 1983) averaging 3 μm in thickness (Hayashi *et al*, 2002). A rudimentary Bowman's layer has been observed in the mouse cornea (Haustein, 1983), although just 0.7-0.8 μm thick (Hayashi *et al*, 2002). It is postulated that Bowman's layer may form as a result of cytokine-mediated interactions occurring between corneal epithelial cells and keratocytes (Section 1.1.3) that include chemotactic and apoptotic effects on the keratocytes (Wilson and Hong, 2000), and although the function of this layer is not clear, insertion of stromal lamellae into the Bowman's layer may serve to maintain the precise shape of the corneal surface (Bron, 2001).

1.1.3 Stroma

The stroma constitutes approximately 90% of the corneal thickness in man (Jester *et al*, 1999) and is continuous with the sclera at the limbus. Although the majority of the stroma is water, the most abundant dry constituent is collagen at 71% (Maurice, 1957). Figure 1.3 shows a transverse section of 3 lamellae in the human stroma. At its centre, the human cornea consists of 200-250 collagenous lamellae, 2 μm thick each extending from limbus-to-limbus. The lamellae are oriented at various angles to one another, typically to less than 90^{o} in the anterior stroma, but almost orthogonal in the posterior region (Maurice, 1984). This arrangement enables the collagen fibrils to withstand the tension in the globe caused by the intraocular pressure (Benedek, 1971; Maurice, 1957) and ensures the efficient transmission of light.

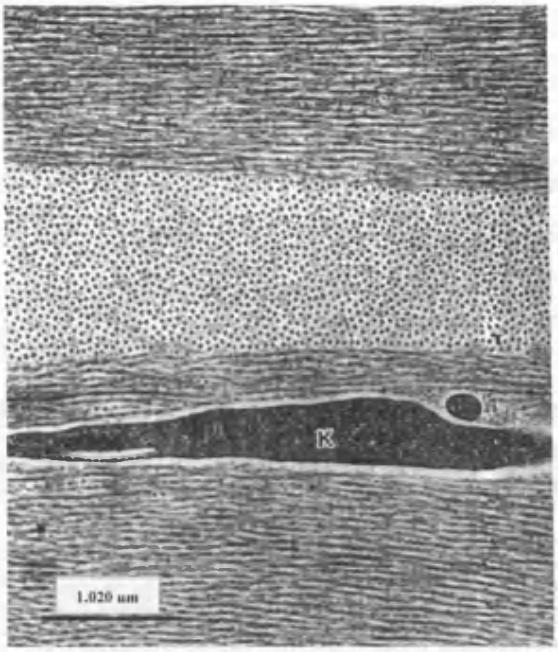

Figure 1.3. Collagen fibrils in the cornea have a uniform diameter and are arranged in the same direction within each lamella. K = keratocyte (x16, 666) (modified from Komai and Ushiki, 1991).

Keratocytes, the flat cellular components of the corneal stroma, interdigitate between collagen lamellae and constitute approximately 10% of the corneal stroma (Kaye, 1969; Maurice, 1969; Maurice and Riley, 1970) (Figure 1.3).

Keratocytes are responsible for the synthesis of corneal collagen types I (Ruggiero *et al*, 1996), III (Nakayasu *et al*, 1986), V (Ruggiero *et al*, 1996), VI (Linsenmayer *et al*, 1986), glycosaminoglycans (GAGs) (Section 1.3.1) and other matrix constituents, such as thrombospondins (TSP) 2 and 3 during corneal wound healing (Armstrong *et al*, 2002). Keratocytes are interconnected with adjacent keratocytes via cellular processes, signifying the presence of a functional communicating network (Kang and Ko, 2005). Keratocyte nuclei are a major source of backscattering of light in normal human corneas, but the cytoplasm is transparent due to the 'crystallins' in the cell. These water-soluble proteins transketolase (TKT) and aldehyde dehydrogenase class 1 (ALDH1) contribute to the transparent and refractive properties of the cornea by accumulating to high concentrations and minimising the RI fluctuations by short-range interactions within the cytoplasm of the keratocytes (Jester *et al*, 1999). Evidence from wounded rabbit corneas reveals that a decrease in the level of these proteins leads to increased light scatter by keratocytes (Jester *et al*, 1999).

1.1.4 Descemet's membrane

This 8-10 μm thick homogenous layer consists of collagen types IV (Nakayasu *et al*, 1986), VI (von der Mark *et al*, 1984), and VIII (Sawada *et al*, 1990) and glycoproteins, and serves as a basement membrane to support the endothelium from which it is secreted (Gurwood, 2000). Between the stroma and Descemet's membrane there is a very thin layer (approximately 0.5 μm in man) consisting of irregularly deposited collagen fibrils (Komai and Ushiki, 1991). Collagen fibrils in the innermost part appear to be embedded in Descemet's membrane (Figure 1.4).

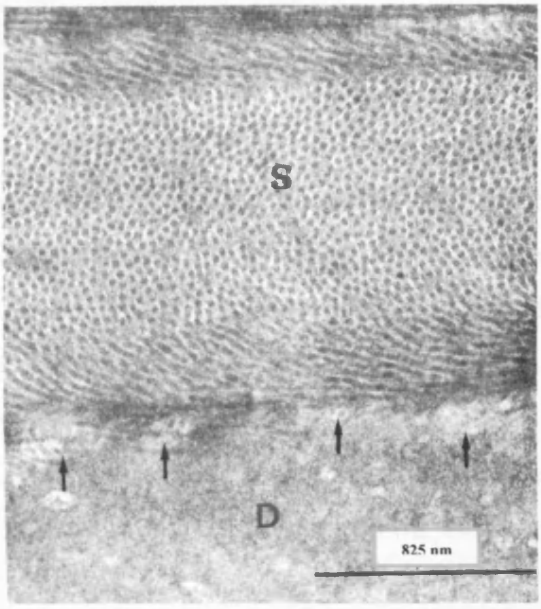

Figure 1.4. The innermost layer of the corneal stroma observed by TEM. Collagen fibrils adjacent to Descemet's membrane (D) are arranged randomly in a very thin sheet (arrows), which appear to be embedded in the amorphous substance of Descemet's membrane. S = stroma (x26, 666) (modified from Komai and Ushiki, 1991).

1.1.5 Endothelium

The endothelium is a 4-6 μm thick single layer of tightly packed, hexagonal-shaped cells that cover the posterior surface of the cornea. An energy-dependent system located in the endothelium maintains normal corneal hydration (Hodson, 1971). Endothelial cells are amitotic, and significant damage sustained by this layer leads to oedema and stromal swelling as exemplified by the surgical removal of rabbit corneal endothelium and development of considerable oedema which persists until the 1-2 months following surgery (Anseth, 1969). However, a little mechanical damage is rectified by the spreading of healthy neighbouring cells (Forrester *et al*, 1999).

1.1.6 Structure of the mouse cornea

A light microscopy examination of the adult mouse cornea by Haustein (1983) revealed a total corneal thickness of approximately 90 μm. Of this, 25 μm are epithelium, 60 μm stroma, and 2.5 μm each of Descemet's membrane and endothelium. Although Bowman's layer was not visible under the light microscope, EM revealed that a sub-epithelial fibrous region might be considered as a rudimentary Bowman's layer (Haustein, 1983). Nevertheless, rat cornea does not exhibit the clear transition zone between the superficial stromal lamellae and this sub-epithelial fibrous layer that human cornea does (Quantock *et al*, 2005), and so is not truly comparable to Bowman's layer in man.

1.2 Collagen

Collagen is the major macromolecular constituent of cornea. The collagens are a family of structural glycoproteins that constitute a quarter of the total protein in mammals (Marshall *et al*, 1993). To date, 27 genetically distinct types of collagen have been identified (Boot-Handford *et al*, 2003; Pace *et al*, 2003; Jenkins *et al*, 2005), and are grouped according to their characteristics, as shown in Table 1.1. Collagen types I-IX, XII and XIV are located in ocular tissue, but only collagen types I, III, V, VI, and XII are found in the corneal stroma, as illustrated in Figure 1.5.

GROUP	COLLAGEN TYPE
Fibril-forming collagens	I, II, III, V, XI
Fibril associated collagens (FACITs)	IX, XII, XIV, XVI, XIX
Non fibrillar collagens	
Short chain collagens	VIII, X
Basement membrane collagen	IV
Anchoring fibril	VII
Microfibrillar	VI
BP-antigen	XVII
Multiplexins	XV, XVIII
Membrane intercalated	XIII, XVII

Table 1.1. The different collagen types of vertebrates (adapted from Robert *et al*, 2001).

1.2.1 Collagen types

1.2.1.1 Fibril-forming collagens

Collagen types I, II, III, V and XI participate in the formation of fibrils with molecules packed in quarter-staggered arrays (Section 1.2.2). Collagen types I, III, and V have similar structures (Lander, 1999). Analysis of dissected regions of the calf cornea showed a uniform distribution of the collagen populations from centre to limbus (89% type I, 10% type V, less than 1% type III). There was a general uniformity throughout the depth of the stroma, with the exception that type III collagen was concentrated around Bowman's layer (Lee and Davison, 1984).

Type I is the prominent collagen in the mammalian cornea (Newsome *et al*, 1982). Located in the ECM of the corneal stroma, this collagen offers tensile strength to the tissue (Yue *et al*, 1979). The mechanism by which this and other fibril-forming collagens are able to resist tensile forces will be outlined in Section 1.2.2.

Type III collagen is associated with the stromal lamellae and with the substratum of the epithelium, where it may be necessary for function, adhesion and other important aspects of this layer (Newsome *et al*, 1982). Amounts of type III collagen have been found to decline with increasing age, but this is not detrimental to transparency (Schmut, 1977). However, increased amounts of type III collagen are deposited at the wound site one week post-wounding in human cornea (Ljubimov *et al*, 1998).

Type V is located throughout the corneal stroma (Nakayasu *et al*, 1986) and at the stromal-epithelial and -endothelial interfaces. Type V collagen has been shown to be co-distributed with type I collagen within the same fibril in avian stroma, forming heterotypic collagen fibrils (Birk *et al*, 1988). Type V collagen is speculated to influence and regulate collagen fibril diameter as an increased concentration of this collagen leads to the development of smaller diameter heterotypic fibrils (Birk *et al*, 1990).

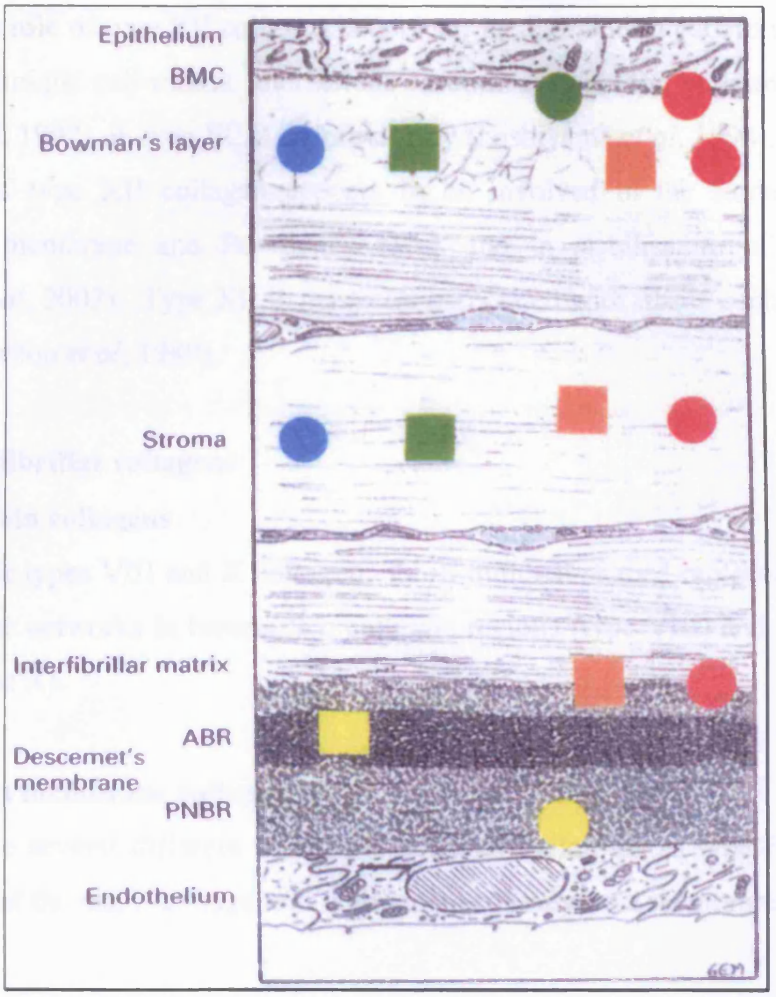

Figure 1.5. The distribution of collagens I-VIII in aged human cornea. Collagen types I (blue circle), III (green square), V (brown square), and VI (red circle) are evenly distributed throughout Bowman's layer and the corneal stroma. Types V (brown square) and VI (red circle) are also present in the interfacial matrix. Type IV collagen (yellow circle) is present in Descemet's membrane. Both types VI (red circle) and VII collagen (green circle) are present in the basement membrane complex (BMC) immediately underneath the epithelium. Type VIII collagen (yellow square) is present in the anterior banded region (ABR) of Descemet's membrane. PNBR = posterior non-banded region (from Marshall *et al*, 1993).

1.2.1.2 Fibril associated collagens with interrupted triple helices (FACITs)

This class includes types IX, XII, XIV, XVI, and XIX collagens (Hay, 1991). These collagens do not themselves form fibrils, but may serve as molecular bridges between fibrillar collagens and other ECM components by co-aggregating with fibril forming collagens and modulating outside interactions of fibrils by domains projecting from their surfaces (Svensson *et al*, 2001). Type XII collagen is located in the corneal stroma as well as the corneal epithelial basement membrane and Bowman's layer.

Although the role of type XII collagen is unclear, its distribution pattern suggests it is involved in unique cell-matrix interactions in corneal epithelial and stromal tissues (Wessel *et al*, 1997) or even ECM deformability (Nishiyama *et al*, 1994). Indeed, the long form of type XII collagen appears to be involved in the formation of the Descemet's membrane and Bowman's layer and in stabilisation of the limbus (Akimoto *et al*, 2002). Type XII is generally associated with fibrils containing type I collagen (Gordon *et al*, 1989).

1.2.1.3 Non-fibrillar collagens

- **Short chain collagens**

These include types VIII and X collagen; short, dumbell-shaped molecules that form part of unique networks in basement membrane regions (type VIII) and hypertrophic cartilage (type X).

- **Basement membrane collagens**

These include several different molecules collectively known as type IV collagens. They represent the major collagenous components of basement membranes.

- **Microfibrillar collagens**

This group includes molecules that form specialised structures in a variety of tissues. For instance type VII collagen acts as an anchoring fibril. Type VI is a non-fibril forming collagen and a component of the secondary (mature) corneal stroma (Linsenmayer *et al*, 1986). Type VI collagen constitutes 100 nm periodic filaments throughout the ECM, and its presence during all stages of corneal development and association with type I collagen fibrils suggests that it acts as a bridging molecule by binding to type I collagen (Bonaldo *et al*, 1990), possibly contributing to the mechanical properties of connective tissues as a whole.

- **Multiplexins**

Types XV and XVIII collagen currently belong to this group, molecules with multiple short triple-helical domains that are found mostly in basement membrane regions.

- **Membrane intercalated collagens**

Types XIII and XVII collagen are cell-surface molecules with multiple extracellular triple-helical domains, connected to a cytoplasmic region by a transmembrane segment.

1.2.2 Structure and assembly of collagen fibrils

Collagen fibrillogenesis is an extensive multistep process involving both intracellular and extracellular assembly reactions. In fibrillar collagens and some short chain collagens, each collagen molecule contains only one triple-helical molecular domain that accounts for almost the entire length of the 300 nm long molecule (Wess *et al*, 1998). Collagens such as FACITs, basement membranes, and multiplexins contain several short triple-helical domains that are separated by non-triple-helical sequences.

Collagen type I is the classic fibril forming collagen. The foundation unit of the collagen fibril is tropocollagen, a processed molecule found in the ECM. The precursor of tropocollagen is procollagen, a higher molecular weight form with additional extension peptides, called propeptides, at both NH_2 and COOH termini. Procollagen is synthesized by keratocytes and released into the ECM in secretory vesicles. The formation of procollagen into tropocollagen requires the action of procollagen peptidases which remove the amino (NH_2) and then carboxy (COOH) terminal propeptides leaving a short, non-triple helical telopeptide at each end of the tropocollagen molecule (Fessler *et al*, 1975).

Tropocollagen is a triple helix (Ramachandran and Kartha, 1954) of three polypeptide chains, two identical $\alpha 1(I)$ chains and one $\alpha 2(I)$ chain. Each chain is a left-handed helix with around 3.3 residues per turn (Ramachandran and Kartha, 1955). The tropocollagen molecule is formed within the cell by the combination of three pro-α-chains in a right-handed manner before excretion to the ECM (Figure 1.6).

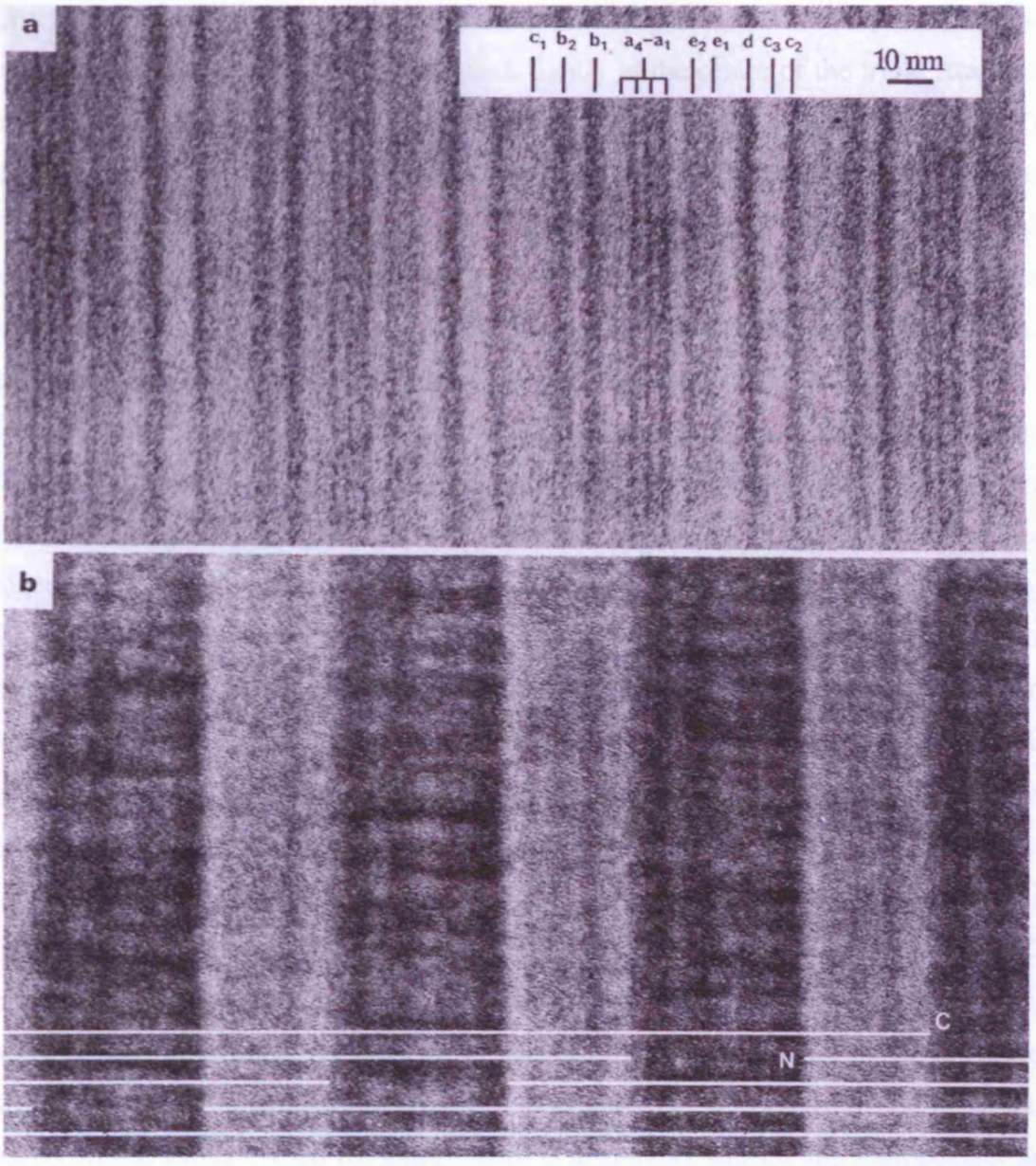

Figure 1.6. Matching of (b) the negative staining pattern with (a) the positive staining pattern. The fibril is from a reconstituted gel of calf skin collagen. The broad stain-penetrable/stain excluding zoning in (b), arising from the 'gap/overlap' staggering of molecules in a fibril, is characteristic of the negative staining pattern. Positive straining in (a) reveals that each D-period consists of 12 staining bands, a1 through e2, that denote the axial position along the collagen fibril; a1 and a2 are in the gap zone, a3 is at the gap/overlap zone, a4, b1, b2, and c1 are in the overlap zone, c2 is at the other gap/overlap junction, and c3, d, e1, and e2 are in the gap zone. Note that in (a) bands c1 and c3 stain very weakly, and are generally very difficult to stain (Professor Karl Kadler, personal communication) (from Chapman *et al*, 1990).

The high content of Glycine (Gly) in fibrillar collagens is a necessity as it is the smallest possible amino acid that can pack tightly at the centre of the triple stranded collagen fibril monomer (Ramachandran and Kartha, 1954). Bella *et al* (1994) demonstrated that the presence of Gly is crucial for fibril formation by substituting Gly with Alanine (Ala) in a collagen-like synthetic peptide, which resulted in crystal rather than fibril formation. Thus, the occurrence of Gly as every third residue gives rise to a polymer of tripeptide units with the formula $(Gly\text{-}X\text{-}Y)_n$, where X is often, but not exclusively, proline, and Y is often hydroxyproline (van der Rest *et al*, 1990). Ramachandran and Kartha (1955) suggested that the –OH groups of hydroxyproline help to stabilise the triple-helix. The formation of an extra hydrogen bond between the –OH group and a water molecule links the backbones of neighbouring chains together. This hypothesis was later confirmed (Ramachandran *et al*, 1973). Hydroxylysine is required for the transformation of reducible collagen cross-links into more stable, non-reducible cross-links of mature collagen fibres, as the modification of the ε-amino group of both lysine and hydroxylysine completely halts cross-link transformation *in vitro* (Davis *et al*, 1975). Hydroxylysine also serves to form attachment sites for polysaccharides (Mathews and van Holde, 1995).

Individual tropocollagen molecules are approximately 4.4 times the length of the 67 nm repeat period (called the *D*-periodicity) when arranged parallel to the fibril axis, and are 'staggered' about one-quarter their length. This arrangement, shown in Figure 1.6, is termed the 'quarter-staggered array' (Schmitt *et al*, 1955; Hodge and Petruska, 1963; Smith, 1968). When a collagen fibril is negatively stained, the stain collects in the short space present between the NH_2-terminal of one molecule and the COOH-terminal end of the next. These spaces are known as 'hole' or 'gap' zones (Gross, 1974). These zones are present due to the incomplete overlapping of adjacent collagen molecules within the repeating structure. The spaces allow penetration of certain enzymes required for formation of the aldehyde-derived crosslinks that stabilise fibrils and others that degrade the fibrils. They also allow the functional domains of collagen molecules to project outwards to the surface of the fibril. The light bands are the regions in which no stain has accumulated and there is complete molecular overlapping. These are termed 'overlap zones'. The basic repeating unit of

the structure, the *D*-periodicity, consists of one hole zone (0.4-D units long) and one overlap zone (0.6-D units long).

The collagen molecules themselves are organised into 4 nm diameter circular microfibrils of a centre-to-centre spacing of approximately 4 nm, that are tilted by approximately 15° to the fibril axis in a right-handed helix (Holmes *et al*, 2001). This tilting lends corneal collagen fibrils an axial period of 65 nm as opposed to the 67 nm axial period found in collagen of tendon or bone (Marchini *et al*, 1986). Orgel *et al* (2001) described the lattice-like arrangement of microfibrils within a fibril as 'quasihexagonal' because although they are packed on a hexagonal lattice, not all molecular segments are identical. The intermolecular and intermicrofibrillar crosslinks within the collagen fibril add a high degree of tensile strength to fibrillar connective tissues (Orgel *et al*, 2001).

1.2.3 Collagens in corneal development

The development of the corneal stroma in mammals such as chick (Linsenmayer *et al*, 1984) principally involves the synthesis of a primary stroma by the corneal epithelium that consists of striated fibrils of collagen types I and III (Hendrix *et al*, 1982). The primary stroma acts as the foundation for the subsequent development of the secondary (mature) stroma. The primary corneal stroma is the only matrix present until embryonic day 6 (E6) of development (Linsenmayer *et al*, 1986). However, a primary stroma is not observed in the mouse (Haustein, 1983; Cintron *et al*, 1983), rabbits, or primates (Cintron *et al*, 1983).

In the mouse, mesenchymal cells first appear in the corneal stroma at E14 and differentiate into corneal keratocytes (Haustein, 1983) and produce the first large heterotypic fibrils of collagen types I and V (Birk *et al*, 1988). Type VI collagen appears very rapidly at this stage of embryogenesis (Bruns *et al*, 1986), and possibly directs the migration of the invading keratocytes. In a transient stage in embryogenesis, filaments of types IV, VI, and IX collagen extend from the epithelial side to the endothelial side of the developing cornea (Fitch *et al*, 1988). Type IV collagen is present during this phase as a non-basement membrane form consisting of long strings penetrating the corneal stroma from the epithelial basement membrane

(Linsenmayer *et al*, 1990), and in doing so is believed to stabilise the whole structure throughout development (Bonaldo *et al*, 1990).

Prior to E14 of chick development, the cornea is easily separated at the limbus, but with progressive development the cornea becomes stronger and is not so easily manipulated (Coulombre and Coulombre, 1958). To investigate collagen fibril arrangement within the depths of the mature human corneal stroma, Radner and Mallinger (2002) removed the extrafibrillar material of 12 corneas by sodium hydroxide (NaOH) treatment, dehydrated them in a series of graded tertiary butanols, froze them at -24°C and dried them in an exsiccator. Each cornea was then cut vertically with a razor blade, and the stroma was stretched along its anterior-posterior axis by pulling apart the epithelial and endothelial edges, thus exposing the interlamellar spaces. Figure 1.7 illustrates their findings of numerous lamellae interlaced in various patterns. The strength of mature cornea reported by Coulombre and Coulombre (1958) therefore appears to be due, in part, to the interlacing of the lamellae in the mid- and posterior stroma (Maurice and Monroe, 1990; Radner and Mallinger, 2002).

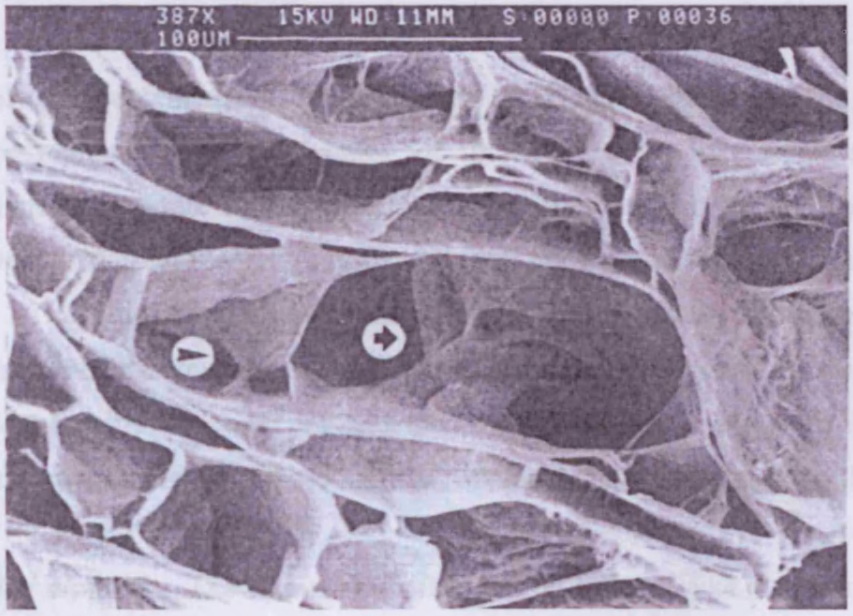

Figure 1.7. The interlamellar spaces of the corneal stroma give the appearance of a polymorphic honeycomb. Lamellae appear as cross-sectioned sheets. Within the central interlamellar opening a large interweaving zone (arrow) can be seen, in which several types of interlacing are found close together. To the left of this zone a lamella crosses upwards through a larger one (arrow head) (from Radner and Mallinger, 2002).

1.2.4 Corneal stromal morphology

Biophysical studies have shown that approximately 66% of the stromal lamellae in human cornea are preferentially aligned orthogonally along the superior-inferior and nasal-temporal directions, while around 34% lie within a 45° sector (Daxer and Fratzl, 1997; Newton and Meek, 1998b). This preferential alignment is exemplified by the appearance of two sets of lobes on an XRD pattern and has so far been found in humans (Meek *et al*, 1987; Daxer and Fratzl, 1997) and the chick primary corneal stroma (Quantock *et al*, 1998). Boote *et al* (2005) used wide-angle XRD to quantify the relative number of stromal collagen fibrils directed along the superior-inferior and nasal-temporal corneal lamellar directions and demonstrated that, on average, the two directions are populated in equal proportions at the corneal centre. The fibril tension in the isotropically arranged collagen helps to balance the intraocular pressure, while the extra preferentially aligned fibrils bear the additional tensile stress along the superior-inferior and nasal-temporal meridians exerted by the rectus muscles and the orbicularis (Boote *et al*, 2005). XRD studies have demonstrated the presence of a circumferential annulus of collagen fibrils in the limbus of human (Newton and Meek, 1998a) and mouse (Quantock *et al*, 2003) cornea, which may help maintain the correct curvature of the cornea.

Generally, the corneal stroma is regarded as consisting of two zones, the anterior and posterior regions. This segregation of the stroma into two separate regions is appropriate as they are morphologically quite different. Komai and Ushiki (1991) conducted a comprehensive study of collagen fibril organisation within the corneal stroma. They reported that the collagen fibrils are regularly spaced and of fairly uniform diameter throughout the stroma, ranging between 25 and 35 nm. However, fibrils of the posterior stroma appear to be more well-ordered, as a study into the total scattering cross-section of these regions revealed that the values for the posterior stroma ($(2.35 \pm 0.27) \times 10^{-2}$Å) were lower than anterior ($(3.15 \pm 1.14) \times 10^{-2}$Å) (Freund *et al*, 1995). The anterior lamellae are flat and tape-like in appearance (up to 30 μm wide and 1.2 μm thick), while those of the posterior region look like broad sheets, being typically wider (up to 200 μm) and thicker (up to 2.5 μm) (Komai and Ushiki, 1991). The posterior lamellae extend, uninterrupted, from limbus-to-limbus, an arrangement which may confer additional strength. On the other hand, the

anterior stroma displays a prominent anteroposterior lamellar interweave (Davson, 1984; Klyce and Beuerman, 1988; Komai and Ushiki, 1991) which, together with insertion of lamellae into Bowman's layer (Bron, 2001), may help to maintain corneal curvature (Muller *et al*, 2001) and give structural stability to this layer under conditions of extreme hydration. Indeed, the posterior region is more hydrated (Turss *et al*, 1971; Lee and Wilson, 1981) and more easily swollen with a lower RI (1.373) than the anterior stroma (1.380) (Patel *et al*, 1995). The significance of these hydration properties is apparent when considering the GAG content of each in bovine corneal stroma. While keratan sulphate (KS) has less capacity to retain water than chondroitin sulphate (CS), it has a greater affinity for water (Castoro *et al*, 1988); as the KS:CS ratio is higher in the posterior region this may explain, in part, why deeper stromal regions are more prone to swelling (Bettelheim and Goetz, 1976; Castoro *et al*, 1988).

1.3 Proteoglycans

1.3.1 Proteoglycans and glycosaminoglycans

The proteoglycan (PG) family consists of molecules that fulfil a variety of biological functions, ranging from regulating cell migration and adhesion, to modulating growth factor activities. PGs are grouped into distinct gene families and subfamilies based mainly on genetic homology of the protein core (Section 1.3.3); the basement membrane PGs, nervous tissue PGs, large extracellular PGs, and small leucine-rich PGs (SLRPs) (Hay, 1991).

SLRPs are the second most abundant biological material of the corneal stroma and are fundamental for transparency (Funderburgh, 2000). Each SLRP consists of a core protein covalently bonded to one or more GAG chains (Iozzo, 1999). There are different types of GAG, distinguished by the sugar residues and linkage to the protein core. The most common GAG types of corneal stroma are keratan sulphate (KS) (a glucosaminoglycan), chondroitin sulphate (CS), and dermatan sulphate (DS) (galactosaminoglycans). These GAGs are long chains consisting of repeating disaccharide units (Hardingham and Fosang, 1992) that are held together by molecular bonds (Scott, 1992). The specific units constituting KS, CS, and DS are outlined in Table 1.2.

GAG	Repeating disaccharide unit
KS	N-acetylglucosamine (GlcNAc) and galactose (Gal)
CS	N-acetylgalactosamine (GalNAc) and glucuronate (GlcA)
DS	N-acetylgalactosamine (GalNAc) and iduronate (IdoA)

Table 1.2. The repeating disaccharide units of KS, CS, and DS GAGs (information obtained from Fosang and Hardingham, 1996).

In cornea, CS/DS GAG is found; a hybrid GAG composed of both iduronate and glucuronate disaccharide units (Soriano *et al*, 2000). DS is a structural isomer of CS, in which some glucuronate is epimerised to iduronate (Fosang and Hardingham, 1996). Human corneal GAGs compose 1.5mg/g of tissue wet weight; KS and CS/DS each constitute approximately 50% of total GAG (Soriano *et al*, 2000).

The GAGs of each SLRP are covalently bonded to the protein core. The CS/DS linkage region consists of a typical trisaccharide unit of (Gal-Gal-GlcA/IdoA) and a xylose (Xyl) *O*-linked to a serine (Ser) residue of the protein core by xylosyltransferase (Stuhsatz *et al*, 1971; in Axelsson and Heinegard, 1978; Hardingham and Fosang, 1992).

1.3.2 Structure and biosynthesis of KS

KS was first identified in extracts of cornea (Suzuki, 1939), and was isolated from bovine cornea by Mayer *et al* (1953). KS is also present in skeletal and cartilage tissue, but as the linkage structures differ, corneal and skeletal/cartilage KS are designated KSI and KSII respectively (Funderburgh, 2000).

Corneal KS is *N*-linked to asparagine (Asn) residues in the protein core, whereas cartilage KS is *O*-linked to serine (Ser) or threonine (Thr) residues (Funderburgh, 2000).

KSI structure

Figure 1.8 illustrates the typical structural features of KSI GAG.

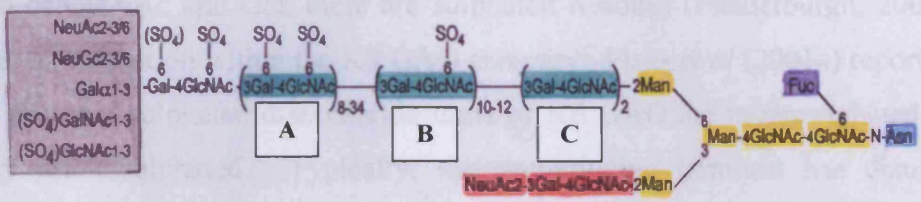

Figure 1.8. A summary of the structural features of corneal KSI GAG. Numbers to the lower right of the large parenthesis show the approximate number of *N*-acetyllactosamine monomers in each chain. Numbers separated by a forward slash present optional attachment locations. Sulphates in parentheses indicate partial or incomplete sulphation of monomers at this site. Sources of these structural assignments, each signified by a specific coloured block or letter, are given in the text (adapted from Funderburgh, 2000).

KSI consists of a common linkage oligosaccharide core of three mannose (Man) and two *N*-acetylglucosamine (GlcNAc) residues (yellow blocks), that are *N*-linked to an Asn residue in the protein core (blue block). The KS chain GAG is modified with fucose (Fuc) (purple block) at GlcNAc (Plaas *et al*, 2001a). The KSI illustrated is a monoantennary extension model, in which the KS chain extends only at the carbon (C)-6 branch of the linkage oligosaccharide. However, evidence suggests that both mono- and biantennary extension of the linkage oligosaccharide occur (Nilsson *et al*, 1983; Oeben *et al*, 1987; Plaas and Wong-Palms, 1993; Tai *et al*, 1996), and that linkage location on the protein core may influence the type of extension. Figure 1.8 shows that the C-3 KS chain terminates with a single lactosamine residue capped by sialic acid (NeuAc) (red blocks) (Toda and Seno, 1970; Oeben *et al*, 1987; Dickenson *et al*, 1991; Tai *et al*, 1997; Plaas *et al*, 2001a). As the C-6 branch demonstrates, each KS chain can, in fact, be capped by a variety of structures (Tai *et al*, 1996) (grey box – top to bottom):

- α(2-3)- and α(2-6)-linked *N*-acetylneuraminic acids,
- α(2-3)- and α(2-6)-linked *N*-glycolylneuraminic acids,
- α(1-3)-linked galactose,
- β(1-3)-linked sulphated *N*-acetylgalactosamine and;
- β(1-3)-linked sulphated *N*-acetylglucosamine.

The KS chain itself consists of repeating disaccharide units of (-3Galβ1-4GlcNAcβ1-) termed poly-*N*-acetyllactosamine (green blocks) (Funderburgh, 2000). At the 6-*O*-position of GlcNAc and Gal, there are sulphated residues (Funderburgh, 2000), but the level of sulphation within the KS GAG can vary. Plaas *et al* (2001a) reported that half of the total sulphated disaccharide units of KS GAG are monosulphated, and a majority are disulphated. Typically, the nonreducing terminus has disulphated disaccharides (A), the central portion consists of monosulphated disaccharides (B), and chains near the linkage oligosaccharide region are composed of nonsulphated disaccharides (C) (Oeben *et al*, 1987).

KS biosynthesis

With the exception of hyaluronan, GAG biosynthesis on the core protein is performed by glycosyltransferases and sulphotransferases located in the Golgi apparatus (Ruter and Kresse, 1984). Four enzymes are responsible for corneal KSI biosynthesis:

- β1,3-*N*-acetylglucosaminyltransferase
- β1,4-galactosyltransferase
- GlcNAc 6-*O* sulphotransferase (hCGn6ST)
- Gal 6-*O* sulphotransferase (KSG6ST)

The former two enzymes elongate the poly-*N*-acetyllactosamine backbone of KS by transferring GlcNAc or Gal to the nonreducing terminus of the oligosaccharide linkage core on the core protein. The latter two enzymes transfer sulphate to the 6-*O*-position of GlcNAc or Gal, thereby modifying the poly-*N*-acetyllactosamine to form KS composed of mono- and disulphated disaccharides.

The process by which corneal KS biosynthesis takes place has been speculated. A popular hypothesis was that sulphate is added simultaneously with carbohydrate chain polymerisation (DeLuca *et al*, 1973; Degroote *et al*, 1997). Similarly, Akama *et al* (2002) postulated that sulphation of the GlcNAc residue of KS by GlcNAc 6-*O* sulphotransferase is coupled to elongation of the poly-*N*-acetyllactosamine chain by β1,3-*N*-acetylglucosaminyltransferase and β1,4-galactosyltransferase. To test this theory, the authors conducted an *in vitro* investigation of the substrate specificity of

the aformentioned enzymes using synthetic oligosaccharide substrates. They determined that 1) the sulphated poly-*N*-acetyllactosamine chain is produced by both glycosyltransferases and GlcNAc 6-*O* sulphotransferase in a cooperative manner, and 2) sulphation of Gal residues by Gal 6-*O* sulphotransferase is not coupled with the elongation step, but occurs during/after production of GlcNAc sulphated poly-*N*-acetyllactosamine carbohydrate (Akama *et al*, 2002). Figure 1.9 illustrates this corneal KS biosynthetic pathway for mono- and disulphated disaccharide sequences.

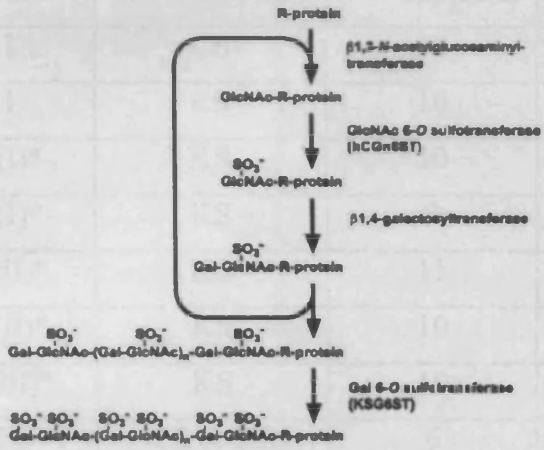

Figure 1.9. Proposed biosynthetic pathway of corneal KS. Since GlcNAc 6-*O* sulphotransferase only transfers sulphate onto the nonreducing terminal GlcNAc of a substrate carbohydrate, sulphation of GlcNAc may be coupled to elongation of the poly-*N*-acetyllactosamine backbone. GlcNAc-sulphated poly-*N*-acetyllactosamine is a completed product that represents about 50% of the corneal KS content. The remaining structure is further sulphated on the Gal residues by Gal 6-*O* sulphotransferase to produce highly sulphated KS disaccharides (from Akama *et al*, 2002).

1.3.3 Corneal KSPGs

The precise roles of corneal KSPGs have yet to be determined, but they appear to be heavily involved in the proper development and regulation of collagen fibril spacing and collagen fibril diameter (Chakravarti *et al*, 1998; 2000). The core proteins of corneal KSPGs were first isolated from bovine tissue, designated 37A, 37B, and 25 (Funderburgh and Conrad, 1990). These corneal KSPGs were later identified as lumican (37B) (Blochberger *et al*, 1992), keratocan (37A) (Corpuz *et al*, 1996), and mimecan (25) (Funderburgh *et al*, 1997). Lumican, the dominant KSPG was first to be identified in the cornea (Blochberger *et al*, 1992). The second most prevalent PG,

although a CS/DS PG, is decorin (Danielson *et al*, 1997), named so because it associates with, and 'decorates', the collagen fibrils. Table 1.3 shows that the SLRP family consists of three major classes. Classification is based on genetic homology of the protein core, the conserved pattern of amino acid spacing among the N-terminal cysteine (Cys) residues, and also the number of leucine-rich repeats (LRRs) each SLRP contains.

Proteoglycan	Class	GAG chain(s)	No. of LRRs	N-terminal sequence
Decorin	I	CS	10	(CX_3CXCX_6C)
Biglycan	I	CS	10	(CX_3CXCX_6C)
Fibromodulin	II(I)*	KS	10	(CX_3CXCX_9C)
Lumican	II(I)*	KS	9	(CX_3CXCX_9C)
Keratocan	II(II)*	KS	11	(CX_3CXCX_9C)
PRELP	II(II)*	KS	10	(CX_3CXCX_9C)
Osteoadherin	II(III)*	KS	10	(CX_3CXCX_9C)
Epiphycan	III	CS or DS	6	(CX_2CXCX_6C)
Mimecan	III	KS	6	(CX_2CXCX_6C)

Table 1.3. Structural classification of SLRPs. *number in brackets represents subfamily designation of Class II. C = Cys, X = any amino acid in N-terminal sequence (Information obtained from Iozzo, 1999).

SLRPs share a common structure that can be divided into four domains (Iozzo, 1999): (I) signal peptide of 16-20 residues; (II) negatively charged N-terminal domain containing four conserved Cys residues; (III) tandem LRR region; and (IV) C-terminal domain of approximately 50 amino acids containing two conserved Cys residues.

Domain I

The signal peptide targets the nascent polypeptides to the endoplasmic reticulum (ER) for secretion into the ECM. Only class I members, decorin and biglycan, contain a propeptide that may function as a recognition signal for xylosyltransferase, the first enzyme involved in the synthesis of CS/DS GAG chains (Iozzo, 1999).

Domain II

The negatively charged N-terminal peptide of lumican, keratocan, and fibromodulin have sulphotyrosine residues at the N-terminal end of the mature core proteins (Funderburgh *et al*, 1995; Oldberg *et al*, 1989; Corpuz *et al*, 1996; Otvos *et al*, 1996), that may affect interactions with cationic domains of ECM or cell surface proteins. Generally, the N-terminal end contains a cluster of highly conserved Cys residues with the general consensus $CX_{2-3}CXCX_{6-9}C$, where X is any amino acid, and the subscripts denote the number of intervening residues.

Domain III

The central domain of the core protein comprises up to 80% of the primary structure, and is usually composed of 8 to 10 tandem repeats of LRRs in conserved positions. The presence of this LRR domain has led to speculation that the three-dimensional structure of SLRPs is similar to an intracellular protein, ribonuclease inhibitor (Weber *et al*, 1996). The LRRs of this protein create a horseshoe-shaped coil of parallel, alternating α-helices and β-sheets, stabilised by interchain H-bonds. This domain also contains the consensus sequences for *N*-linked glycosylations.

Domain IV

The C-terminal domain is the least characterised part of the primary structure, but like the N-terminal region, it contains two conserved Cys residues. The function of this domain remains elusive (Danielson *et al*, 1997), although evidence suggests that the Cys residues within both the N- and C-termini of the core protein are essential for intrachain disulphide bond formation and binding to collagen fibrils (Hocking *et al*, 1998).

1.3.3.1 Lumican

Lumican was initially isolated and sequenced from chick cornea (Blochberger *et al*, 1992), and was renamed due to the important role it plays in the acquisition and maintenance of corneal transparency. Lumican is designated to SLRP class II(I) due to its genetic homology to fibromodulin (50%), biglycan (32%), and decorin (32%) (Iozzo *et al*, 1999). The full length *Lum* gene spans 6.9kb of the mouse genome, and resides on the distal portion of mouse chromosome 10, a region of homology to

human chromosome 12q (Chakravarti and Magnuson, 1995; Taylor *et al*, 1997). Lumican core protein has a complete molecular mass of 38 kDa. Lumican consists of a 20 hydrophobic amino acid signal peptide, 4 Cys residues at the N-terminus and 2 Cys residues at the C-terminus flanking a central LRR region $(LXXLXLXXNXL/I)_{10-11}$ (Funderburgh *et al*, 1995; Ying *et al*, 1997), where X denotes any amino acid, and L is leucine or another hydrophobic amino acid. There are 3 potential *N*-linked glycosylation sites located within the LRR domain (Funderburgh *et al*, 1995) that may serve as a site for the post-translational addition of KS chains (Hocking *et al*, 1998). Murine stromal cells begin to express lumican at E12 (Ying *et al*, 1997). In descending order, lumican is expressed most highly in cornea, keratocytes, breast muscle, intestine, heart, liver and sclera. Evidence has suggested that lumican interacts with collagen fibrils via its N-terminal region (Carlson *et al*, 2003). However, Rada *et al* (1993) showed that lumican inhibits fibrillogenesis *in vitro*, as do decorin (Vogel *et al*, 1984) and fibromodulin (Hedbom and Heinegard, 1993). Therefore, as the LRR region is the most conserved part, it is possible that the repeats may be interacting with collagen.

1.3.3.2 Keratocan

Corpuz *et al* (1996) first cloned and sequenced keratocan from bovine cornea. Keratocan is designated to SLRP class II(II) (Iozzo *et al*, 1999). The keratocan gene (*Kera*) spans 6.5kb of the mouse genome and, like *Lum*, has been mapped to the distal region of chromosome 10 (Funderburgh *et al*, 1998). The core protein of keratocan has a molecular mass of approximately 38kDa, consisting of a 20 amino acid signal peptide, 4 Cys residues at the N-terminus, and 2 Cys residues at the C-terminus that flank an LRR region with the consensus sequence $(LXXLXLXXNXL)_{10}$ (Liu *et al*, 1998). There are 3 potential *N*-linked glycosylation sites for addition of KS chains located within the LRR domain (Dunlevy *et al*, 1998). A Tyr-sulphation motif has been located for protein sulphation (Liu *et al*, 1998). Keratocan expression is first detected in developing cornea and other tissues on E13.5, but is found to be exclusively expressed in mouse cornea by E18.5 (Liu *et al*, 2003).

1.3.3.3 Mimecan

Mimecan was first cloned and sequenced from bovine cornea (Funderburgh *et al*, 1997) and belongs to SLRP class III (Iozzo, 1999). Mimecan is encoded by a single

copy gene located on chromosome 9q22 in humans, and is most abundant in cornea, sclera, cartilage, aorta, and skin. Like keratocan and lumican, this proteoglycan is found in KSPG form only in cornea. Although there are 3 potential N-linked glycosylation sites for KS attachment, it has been proposed that mimecan carries no more than one sulphated KS chain (Funderburgh *et al*, 1997). Mimecan is initially secreted as a full-length protein with a molecular mass of 34kDa. The most commonly found mimecan transcript in adult bovine cornea is 2.5kb when cleaved *in situ*. However, two additional mimecan transcripts of 2.4kb and 2.6kb have been shown by Northern blot analysis (Tasheva *et al*, 1997) and evidence suggests that there are as many as 8 differentially spliced transcripts (Tasheva *et al*, 1999). There are also two mimecan transcripts in human cornea, but the biological significance of multiple mimecan transcripts remains unknown (Tasheva *et al*, 1997), particularly as the proteins of each are exactly the same. Mimecan consists of an 18 amino acid signal peptide, with 4 Cys residues at the N-terminus and 2 Cys residues at the C-terminus (Ujita *et al*, 1995), flanking the LRR region $(LXXLXLXXNXL)_6$ (Funderburgh *et al*, 1997). Dunlevy *et al* (2000) reported that during chick embryonic development, mimecan mRNA concentrations are 38-fold lower than those of lumican, suggesting that mimecan may be a minor KSPG in the adult cornea.

The highly conserved LRR domain flanked by hypervariable Cys-rich disulphide-bonded N- and C-terminal regions of lumican, keratocan, and mimecan are believed to impart unique characteristics upon these SLRPs with which to fulfil distinct functions as structural proteins within the corneal stromal ECM.

1.3.4 Proteoglycan-corneal collagen fibril binding sites

Corneal PGs interact with the specific bands of collagen through their protein core (Rada *et al*, 1993). A TEM investigation of rabbit corneal stroma revealed that keratanase digestion leaves only the 'd' and 'e' bands occupied with PGs, while chondroitinase ABC digestion renders only 'a' and 'c' binding sites occupied (Scott and Haigh 1985). Meek *et al* (1986) utilised XRD and TEM to determine that PGs are bound at the 'a', 'c', 'd', and 'e' binding sites on bovine corneal stromal collagen fibrils. The 'a' and 'c' bands are binding sites for KSPGs, and the 'd' and 'e' bands are binding sites for CS/DS PGs (Scott, 1990). The fibril-associated PGs are the KSPG, lumican, and the CS/DS PG, decorin (Mao and Bristow, 2001). Together,

these discoveries strongly support the hypothesis of "one PG: one binding site" (Scott, 1988). Figure 1.10 illustrates the PG-collagen fibril binding site model proposed by Scott (1988).

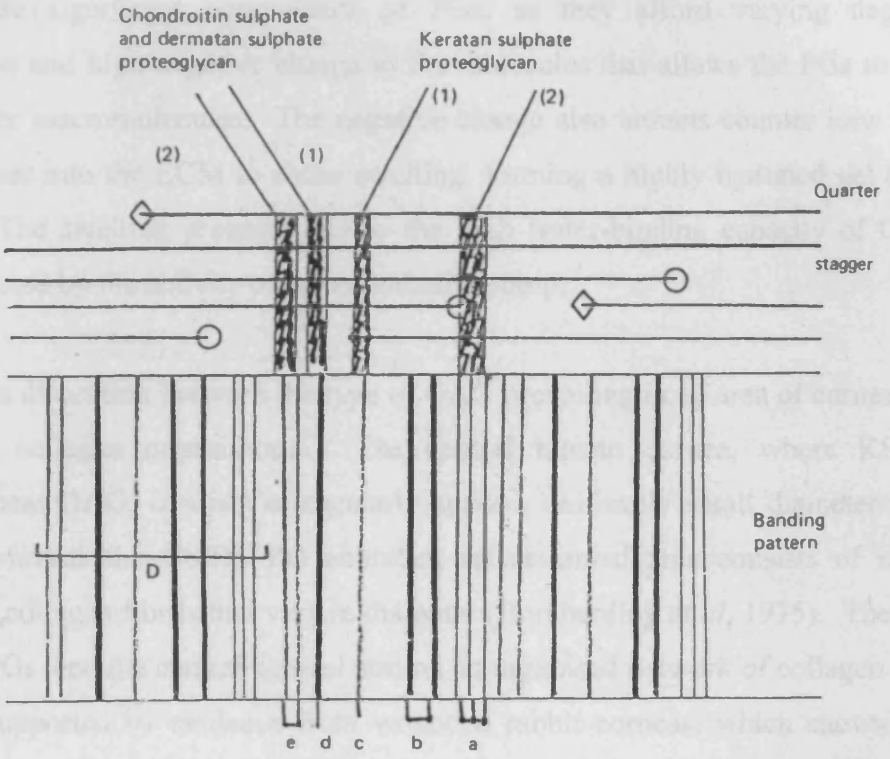

Figure 1.10. Map of binding sites of PGs along the collagen fibril. The a-e banding pattern within the *D*-period of the collagen type I fibril (lower portion) is shown against the arrangement of collagen molecules in quarter-stagger (upper portion). ◇, N-terminal; ○, C-terminal. D, *D*-period. The locations of PGs are displayed across the quarter-stagger diagram, to correlate with the 'a', 'c', 'd', and 'e' banding pattern. The CS/DSPG and KSPG groupings are based on the staining of keratanase-, chondroitinase- (ABC and AC), or hyaluronidase-digested tissue plus biochemical morphometric analysis of tendon. Dermatan sulphate PG1, dermatan sulphate PG2, keratan sulphate PG1, and keratan sulphate PG2 are the corneal PGs so designated (from Scott, 1988).

Interestingly, rabbit corneal PGs locate at the four specific binding sites along the collagen type I fibril, while PGs in sclera, skin and tendon locate at only two binding sites, 'd' and 'e' (Scott and Haigh, 1985). This is a significant finding that indicates the requirement for KSPGs within this specialised tissue. The genetic and structural differences between lumican, keratocan, and mimecan, coupled with the fact that they

are only sulphated in the cornea, have led to speculation that they play distinct roles in the regulation of collagen fibril organisation.

1.3.5 The significance of KS in the cornea

GAGs are significant components of PGs, as they afford varying degrees of sulphation and high negative charge to the molecules that allows the PGs to interact with other macromolecules. The negative charge also attracts counter ions that can draw water into the ECM to cause swelling, forming a highly hydrated gel (Lander, 1999). The swelling pressure due to the high water-binding capacity of GAGs is counteracted by the activity of the endothelial pump.

There is a direct link between the type of GAG prevailing in an area of cornea and the level of collagen organisation. The central human cornea, where KS is the predominant GAG, consists of regularly spaced, uniformly small diameter collagen fibrils, whereas the CS/DS PG abundant sclera-limbal area consists of randomly arranged collagen fibrils that vary in diameter (Borcherding *et al*, 1975). The concept that KSPGs lend the central corneal stroma an organised network of collagen fibrils is further supported by evidence from wounded rabbit corneas, which shows that the wound area and surrounding tissue contains high levels of CS and DS and low levels of KS (Anseth, 1961a). These opaque corneal scars display large interfibrillar spaces that return to normal with an increase in KS levels (Hassell *et al*, 1983). Certainly, the appearance of the sulphated proteoglycan form of lumican after E12 in the chick cornea (Anseth, 1961b) is believed to facilitate the arrangement of collagen fibrils (Cornuet *et al*, 1994).

1.4 Transparency

1.4.1 Theory of corneal transparency

Several theories have been presented in an attempt to explain why the cornea is transparent. Smith (1969) proposed the uniform RI theory, in which the close similarity between the RI of the fibrils and ECM components results in a minimal light scattering and thus transparency. However, this theory was later ruled out as a species study conducted by Leonard and Meek (1997) revealed that, in fact, collagen fibrils have a higher RI value at 1.411 when compared with the 1.365 RI value measured for the ECM. The corneal transparency theory proposed by Maurice (1957)

was based on a calculation suggesting that although corneal collagen fibril diameters (~30 nm) and centre-to-centre spacing (~60 nm) are much less than the wavelength of light (400-700 nm), there are so many collagen fibrils that the light has to travel through that their summed scattering would render the corneal stroma an opaque tissue like skin. Thus, Maurice's lattice theory (1957) states that even though each collagen fibril can scatter light, they do not act as independent scattering centres. The uniformity of their diameter and spacing will cause destructive interference of light in all directions except the forward one so the tissue will appear transparent. However, Maurice's (1957) statement that fibrils must be arranged in a 'perfect' lattice is not entirely true. A degree of short-range order is all that is necessary for the destructive interference of scattered light (Goldman and Benedek, 1967; Hart and Farrell, 1969).

1.4.2 Essential requirements of corneal transparency

The several modern theories of corneal transparency generally agree that transparency is principally dependent on three factors (Farrell and McCally, 2000):

1) Each fibril is an ineffective scatterer. Although collagen fibrils are the main scattering elements in the cornea, they are nonetheless relatively weak scatterers of light because their diameter, approximately 32 nm in the mouse (Meek *et al*, 2003b), is much smaller than the wavelength of light (400-700 nm) and their RI is fairly close to that of the surrounding ground substance.

2) Nevertheless, the large number of fibrils requires that destructive interference of scattered light takes place. The collective light scattering of collagen fibrils significantly increases the destructive interference effects of non-forward scattered light waves. If fibrils scattered light independently of one another, constructive interference effects would be greater (Freund *et al*, 1995).

3) The cornea is thin. Corneal thickness dictates the amount of light scattering, which is proportional to the number of scattering centres encountered by the incident wave passing through the cornea. Thus, as the mouse cornea is thin at approximately 80 to 90 μm (Haustein, 1983; Scott and Bosworth, 1990) light scattering is minimal.

As light scattering from the corneal stroma is based on the combined scattering from all fibrils in the path of the radiation, the fraction of incident light transmitted through a cornea without scattering ($F\lambda$) may be expressed by the formula:

$$F(\lambda) = e^{-\rho\sigma t} \quad \text{.....Equation 1}$$

$F(\lambda)$ falls off exponentially with the product of the total scattering cross-section (σ), the collagen fibril number density (ρ), and the thickness of the tissue (t) (Farrell, 1994). Detailed calculations of corneal transparency are not trivial, particularly because σ is itself a complex function of the wavelength of light, the diameters of the collagen fibrils, their mode of packing, and the ratio of the RI of the hydrated fibrils to the RI of the ECM (Farrell, 1994).

The degree to which the cornea is hydrated has a bearing on corneal transparency. Corneal collagen fibril spacing increases on swelling in a unidirectional manner (Goodfellow *et al*, 1978), and if severe enough, this will often result in the formation of water pockets termed 'lakes' (Benedek, 1971). However, increases in hydration do not appear to affect collagen fibril diameter to any great extent (Muller *et al*, 2001; Meek *et al*, 2003a). KSPGs have been implicated in the regulation of collagen fibril spacing and collagen fibril diameter in corneal stroma, and therefore its transparency. The exact nature of KSPGs has not been entirely ascertained, but with the application of transgenic technology these aspects are being explored.

1.5 Transgenic technology

Transgenic technology (or genetic engineering) is a powerful tool in biological research, as the development of transgenic animals gives new insights into physiological functioning and provides models of human disease. Transgenic animals are defined as having a stable, experimentally induced modification to the genome, involving either the addition of exogenous sequences (a transgene) or the alteration of sequences of an endogenous gene. The main aim of transgenesis is to introduce the transgene into the germline so that it is inherited by offspring.

In recent years, the development of genetically engineered mice has aided in the investigation of protein structure/function. In particular, to ascertain the roles of KSPGs in cornea, two types of genetically engineered mice have been investigated; transgenic mice (Carlson *et al*, 2005), and gene-targeted (knockout) mice (Chakravarti *et al*, 1998; Tasheva *et al*, 2002; Liu *et al*, 2003). Transgenesis is a broad field of biology, and so a detailed discussion is beyond the scope of this thesis. However, the key principles of the techniques used to generate these mice are briefly summarised as follows.

1.5.1 Transgenic mice

Transgenic mice were first produced by a technique called pronuclear microinjection (Gordon *et al*, 1980; Gordon and Ruddle, 1981). As the name suggests, this technique involves the physical microinjection of the transgene (DNA construct) directly into the male pronucleus of a fertilised egg, which generally results in stable germline transmission of the microinjected DNA (Gordon and Ruddle, 1981). Essentially, the transgene does not replace an endogenous gene, but is simply an addition to the genome (consequently, the transgene is accompanied by a promoter sequence to ensure its transcription in the genome). Transgene integration occurs randomly, not necessarily as single copies, and with unpredictable levels of expression (Gordon and Ruddle, 1981). A major use for transgenic mice created in this way is to examine the effects of gene over-expression.

1.5.2 Gene-targeted (knockout) mice

One of the best ways to ascertain the role of a protein in a biological system is to ablate its expression by interfering with the gene that encodes it. Gene targeting in mouse embryonic stem (ES) cells allows for particular genes of interest to be disrupted by effectively replacing the endogenous gene of interest with a DNA construct that contains a selectable marker gene (ideally one conferring antibiotic resistance) in place of target sequences (Doetschman *et al*, 1987; Thomas and Capecchi, 1987). In this way, the integrated gene cannot be transcribed, and the marker gene allows for the positive selection of transfected ES cells.

Gene targeting differs from pronuclear microinjection on two counts. Firstly, whereas DNA is physically introduced in pronuclear microinjection, gene targeting typically

involves the introduction of DNA into ES cells by subjecting them briefly to an electrical potential that partially disrupts the cell membrane, allowing some exchange between the contents of the cell and the surrounding culture. Secondly, in gene targeting the replacement of a gene requires homologous recombination, so the DNA construct is flanked by sequences that are identical to target sequences of the endogenous gene.

Despite the different approach of these techniques, both procedures involve the introduction of the transfected cells into the uterus of a pseudopregnant foster mother to be carried to term. Heterozygous offspring (i.e. mice containing one copy of the transgene) are identified using the DNA from a tail snip. Any heterozygous mice found will be mated together and, according to the Mendalian ratio, 25% of the resulting offspring will be homozygous for the transgene.

1.5.3 Collagen fibrillogenesis and corneal transparency of SLRP gene-targeted mice

Since its discovery in chick cornea (Blochberger *et al*, 1992), the role of lumican in collagen fibrillogenesis and transparency has received much attention. In particular, it has been determined that transparency of embryonic chick corneas starts to increase only when the PG form of lumican begins to accumulate (Cornuet *et al*, 1994) and that lumican operates during the early stages of fibrillogenesis (Ezura *et al*, 2000), thereby pointing to an important role for lumican during the development of the cornea.

The generation of SLRP gene-targeted mice has enabled researchers to develop a better understanding of their *in vivo* structure/function, not just in cornea but a range of connective tissues. To date, six SLRP genes have been disrupted; the corneal SLRPs decorin (Danielson *et al*, 1997), lumican (Chakravarti *et al*, 1998), mimecan (Tasheva *et al*, 2002), and keratocan (Liu *et al*, 2003), as well as the non-corneal SLRPs biglycan (Xu *et al*, 1998) and fibromodulin (Svensson *et al*, 1999). The evidence collected from these investigations is persuasive in pointing to key regulatory roles for SLRPs in the development of mature collagen fibrils. Using animal models, our understanding of the influence of SLRPs within the corneal stroma will give insight into the development and, ultimately, treatment of corneal

diseases in man. The examination of decorin-null mice provided the first *in vivo* demonstration that these macromolecules are important for collagen fibrillogenesis (Danielson *et al*, 1997). This CS/DS carrying SLRP is fairly ubiquitously expressed, and decorin-null mice exhibit abnormal fibril morphology in skin that compromises the tensile strength of this tissue, yet there is no apparent corneal phenotype (Danielson *et al*, 1997). However, evidence gathered from mice lacking expression of the KSPGs lumican, keratocan, and mimecan is fairly compelling in highlighting the important role they play in the governance of corneal collagen fibril architecture.

The mimecan-null mouse presents a moderate reduction in skin tensile strength resulting from abnormal collagen fibril morphology whereby the fibrils are thick and irregularly contoured (Tasheva *et al*, 2002). However, examination of the cornea reveals normal tissue thickness, with only very subtle changes at the ultrastructural level; specifically, slightly more loosely packed, thicker fibrils in the posterior stroma (Tasheva *et al*, 2002). The ablation of keratocan expression via gene targeting is not expected to affect connective tissues other than cornea, as this KSPG is expressed exclusively in cornea of mature mice. Unlike the mimecan-null cornea, the keratocan-null cornea suffers a decrease in thickness (Liu *et al*, 2003) with slight increases in fibril spacing and diameter in the posterior stroma (Meek *et al*, 2003b). Interestingly, however, the disruption to fibril architecture in mimecan-null (Tasheva *et al*, 2002) and keratocan-null (Liu *et al*, 2003; Meek *et al*, 2003b) corneas is not extensive enough to compromise corneal transparency. Conversely, a null homozygous mutation for lumican is severe, with extensive disruption to fibril morphology in skin and cornea (Chakravarti *et al*, 1998). The cornea is significantly thin with abnormal stromal matrix architecture (Chakravarti *et al*, 1998; 2000; Saika *et al*, 2000; Quantock *et al*, 2001). Lumican-null mice develop bilateral corneal opacification by the fifth week of age, and light scattering in mutant corneas hails predominantly from the posterior stroma (Chakravarti *et al*, 1998) likely the result of the abnormally thick, irregularly contoured fibrils in deeper tissue regions. This phenomenon has since been confirmed (Chakravarti *et al*, 2000; Saika *et al*, 2000; Jester *et al*, 2001).

These research efforts have disclosed that lumican, keratocan, and mimecan ensure the correct development of corneal stromal collagen fibrils, and also the maintenance

of interfibrillar spacing and proper tissue hydration. Although it has been purported that corneal KSPGs of mouse are less extensively sulphated than those of higher vertebrates such as rabbit, cow, and man (Young *et al*, 2005), the manifestation of abnormal fibril architecture in their absence supports the necessity for their expression in the mouse to control collagen fibrillogenesis.

Information about the structure and arrangement of collagen fibrils in KSPG-null corneas has been successfully collected using X-ray diffraction (Meek *et al*, 2003b; Quantock *et al*, 2001), a non-invasive technique which allows the study of hydrated, and usually unprocessed tissues (Huang and Meek, 1999).

1.6 Synchrotron X-ray diffraction

Synchrotron X-ray diffraction (XRD) enables the investigation of the arrangement of a variety of fibrous biological tissues at the ultrastructural level. The first published report detailing the use of synchrotron XRD to study the cornea was by Meek *et al* (1981). XRD works on the principle that the scattering elements of a tissue (i.e. collagen fibrils) are of reasonably regular spatial distribution in order for the X-rays to interfere.

At the Synchrotron Radiation Source (SRS) Daresbury Laboratory in the North West of England, there are more than 30 different stations each set up for particular experimentation. Each station relies upon the production of synchrotron radiation. A synchrotron is a machine that accelerates electrons (or other charged particles) with a velocity close to that of the speed of light, causing them to emit an intense beam of light known as synchrotron radiation. This light radiation covers the infrared to gamma-ray spectrum, with the X-rays produced being far more powerful than conventional X-rays produced by lab-based generators. Meek and Quantock (2001) have outlined the principles of synchrotron radiation production as applied to fibre diffraction studies of cornea. The synchrotron comprises 3 main components; 1) a linear accelerator (or electron gun), 2) a booster synchrotron, and 3) a storage ring.

The linear accelerator is responsible for firing high-energy electrons into the booster synchrotron, where the energy and velocity of these particles is greatly increased. The electrons are then transferred to a 2GeV storage ring of 96 m circumference. The

stainless steel high-vacuum tubes within the storage ring store the injected electrons. A form of polygun, comprising a series of dipole electromagnets, produces a dipole magnetic field that deflects and steers the path of the particles into an almost circular shape. This motion causes the particles to emit electromagnetic waves (for up to 20 hours at a time) tangential to the source, and this is the synchrotron radiation. Synchrotron light in the SRS is emitted from 16 dipole bending magnets and 4 special types of magnets for narrower and brighter light, called insertion devices. While emitting light, the electron beam loses a lot of energy, replenished by radio frequency waves that push along the electron beam in 4 different places around the storage ring circumference. The synchrotron radiation is supplied to each station, some of which utilise the X-ray part of the spectrum.

1.6.1 SRS Station 2.1

Two SRS stations that use the X-ray spectrum for the study of tissue ultrastructure are Station 2.1 (low-angle XRD) and Station 14.1 (high-angle XRD). Information obtained for the interpretation of average collagen fibril spacing and collagen fibril diameter of each experimental corneal sample was obtained on Station 2.1 (Figure 1.11).

At Station 2.1, the experimental hutch contains a gas proportional area X-ray detector and the specimen stage, the position of which can be adjusted with respect to the incoming synchrotron light. In the data collection room the experimental parameters are adjusted in order to optimise the results of the data collected. Each sample is, in turn, placed in a specimen holder between two sheets of Mylar to limit evaporation. The specimen holder is then inserted into the path of the X-ray beam by placing it in the specimen stage in the sample area (Figure 1.12a). The focused beam of monochromatic X-rays is passed through the whole thickness of the corneal sample for a usual exposure time of 2 minutes. X-rays are scattered by corneal collagen fibrils in much the same way as light, and when the X-ray detector captures these reflections they can be analysed to gain information about scattering elements in the tissue. Between the X-ray detector and specimen holder is an evacuated tube typically of 8.25 m length, which is responsible for reducing air scatter (Figure 1.12b). All data is stored on a local computer within the data collection room to later be downloaded onto the departmental system for further analysis.

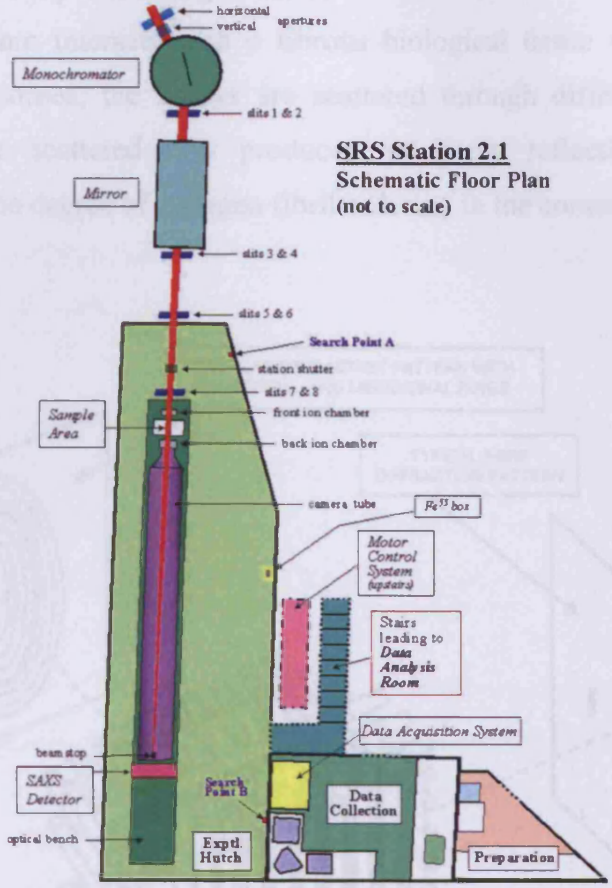

Figure 1.11. Schematic floor plan of Station 2.1 at the SRS in Daresbury, UK. X-rays are focused by a mirror-monochromator and are collimated by means of apertures. They then enter the experimental area where they pass through the specimen. The diffracted X-rays travel within an evacuated tube and are recorded on an electronic detector. The station is operated remotely from an adjacent data collection room (image from source: http://www.srs.ac.uk/srs/).

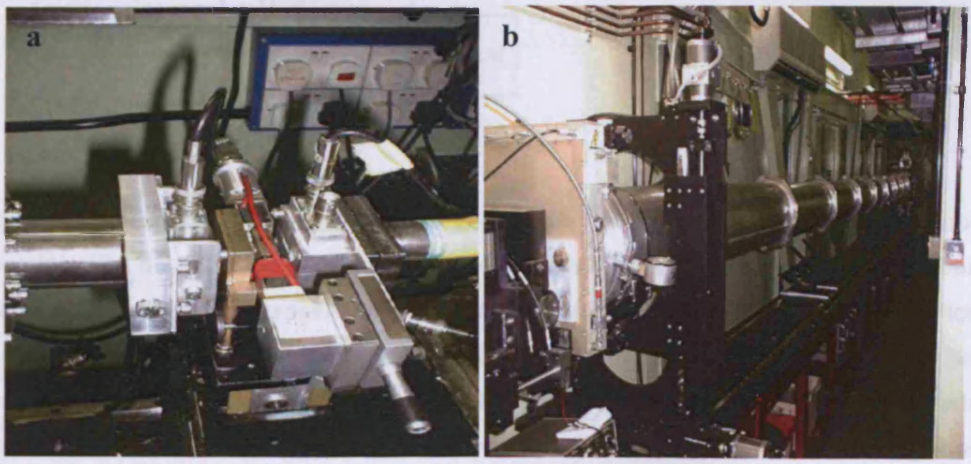

Figure 1.12. (a) Specimen holder in the sample area of Station 2.1. (b) Between the X-ray detector (far left) and specimen holder (far right) is the 8.25 m long evacuated tube.

1.6.2 Low-angle X-ray scattering of cornea

When an X-ray beam interacts with a fibrous biological tissue with a lattice-like structure, such as cornea, the X-rays are scattered through different angles. The interference of the scattered rays produces an X-ray reflection, which gives information about the degree of collagen fibril ordering in the cornea (Figure 1.13).

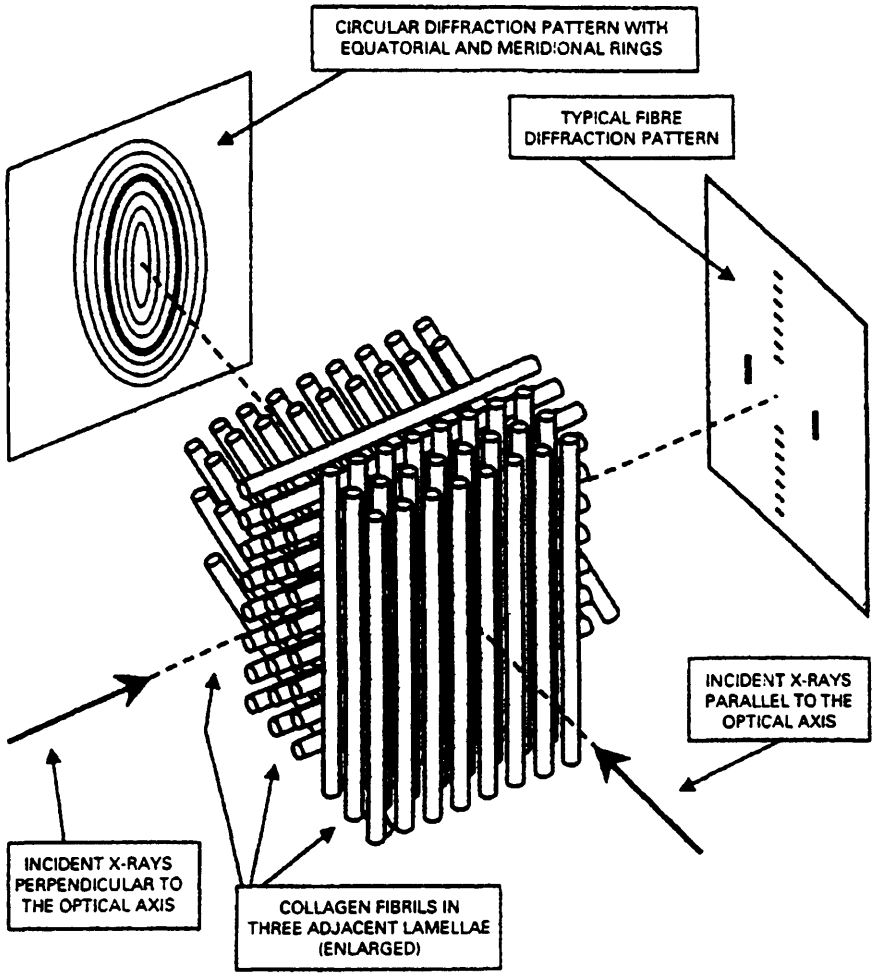

Figure 1.13. A schematic diagram showing how X-rays may be passed either through the front of the cornea (parallel direction i.e. parallel to the optical axis if the cornea were *in situ*), or through the edge of a corneal strip (perpendicular direction). In both cases, the resulting diffraction pattern is an average from all the fibrils in the different lamellae encountered by the X-ray beam in its passage through the specimen. If X-rays in the parallel direction encounter equal numbers of fibrils in all directions within the plane of the cornea, the resultant meridional and equatorial reflections appear as rings (from Meek and Quantock, 2001).

As Figure 1.13 shows, low-angle meridional reflections arise from the axial ordering of the collagen molecules within fibrils, known as the *D*-periodicity. A unique feature of cornea is its additional production of low-angle equatorial reflections that arise due to the uniformity of collagen fibril diameters and degree of lateral order in the packing of the fibrils within the lamellae. Through analysis, these low-angle equatorial reflections provide average values for the fibril Bragg spacing within the corneal stroma (Meek and Quantock, 2001).

Collagen fibrils run parallel to each other within a single lamella, and if there is no preferential orientation of lamellae the net effect throughout the specimen is to have no preferred fibrillar orientation. Where this occurs the intensity is spread over 360° and the pattern is circular (Figure 1.13). Although the low-angle diffraction pattern of a number of species is thus a series of concentric rings (i.e. the meridional reflections), Meek *et al* (1987) found that the human cornea displays an equatorial diffraction pattern consisting of 2 sets of lobes, indicating an overall orthogonal arrangement of lamellae in the inferior-superior and nasal-temporal directions.

1.6.3 The use of X-ray diffraction and transmission electron microscopy

Low-angle XRD and transmission electron microscopy (TEM) are techniques that can be used to observe tissue structure on a small scale and are complimentary in the degree of detail they can reveal. XRD covers the range 0.1 nm to approximately 100 nm, and electron microscopy from about 3 nm to 1 μm in tissues. Both methods rely on the scattering power of the electrons within the atoms of the specimen (Woodhead-Galloway, 1982). XRD is a useful technique as tissue processing is not required prior to analysis, unlike TEM, which involves staining, fixation, and embedding of tissue (Fullwood and Meek, 1993). Additionally, XRD can be used to study tissue that is close to physiological hydration. Nevertheless, the nature of XRD means that an X-ray beam passes through the whole tissue thickness and, although it samples many thousands of fibrils at a time, it will give only average data measurements. This means that small variations in collagen fibril spacing and diameter cannot be detected. TEM is by necessity a highly selective procedure which, when used in combination with XRD, can yield information on localised tissue differences. It is for this reason that XRD and TEM are complimentary techniques.

1.7 Thesis aims

The primary aims of this thesis are to better understand the role of the corneal KSPGs, lumican and mimecan, within corneal stroma, using XRD to gain quantitative information about stromal collagen architecture, and TEM to obtain information about collagen morphology. The role of lumican will be studied during neonatal development in the wild-type and lumican-null mouse cornea (Chapter 3), and a wider appreciation for this macromolecule will be developed through mutation of its N-terminal region and also via its over-expression in the mouse cornea (Chapter 4). The implications of a mimecan deficiency will be explored in order to learn more about the nature of this KSPG in the mouse cornea (Chapter 5). Additionally, the impact of KPSG undersulphation will be investigated within the corneal stroma of the mouse to appreciate which functional motifs of KSPGs are important for the control of matrix morphogenesis in the mouse cornea (Chapter 6).

Chapter 2. General Materials and Methods

2.1 Introduction

The procedures described within this section were used throughout, unless stated otherwise in the following chapters. Sample analysis was undertaken using low-angle XRD on Station 2.1 at the Synchrotron Radiation Source (SRS), Daresbury Laboratory, Cheshire, UK.

2.1.1 Tissue samples

Mouse corneas were excised from the eye, with or without sclera attached. Fresh corneal tissue can be analysed by XRD. However, the overseas shipment of corneas and scheduled beam times required corneas to be treated in one of the following ways.

- Fixed with 4% paraformaldehyde (in 0.1M phosphate buffer) and stored at 4°C for one week (Chapter 3)
- Wrapped in clingfilm, frozen in isopentane cooled in liquid nitrogen, and stored at -80°C (Chapter 4)
- Wrapped in clingfilm, frozen in liquid nitrogen, and stored at -80°C (Chapters 5 and 6).

Freezing is an accepted way of storing corneas for investigation of extracellular matrix structure by synchrotron XRD, and although it is known that fixation for electron microscopy causes shrinkage within tissue, the degree of shrinkage via the use of paraformaldehyde is though to be minimal (Fullwood and Meek, 1994). Unfortunately, it was not possible to measure tissue hydration as these small corneas would rapidly lose water on exposure to the air which would thereby render the calculated values inaccurate.

2.2 Low-angle XRD

2.2.1 Determining the position of the X-ray beam

Sample preparation involved placing each cornea in an airtight sample cell (specimen holder) constructed from 2 sheets of Mylar that limit tissue dehydration. Prior to data collection the position of the X-ray beam was determined by mounting a piece of green X-ray sensitive paper onto graph paper which was the same size and shape as

the airtight cell. The graph paper was then placed into the cell and exposed to the X-ray beam for approximately 10 seconds. A small red mark was burnt onto the paper at the point where the X-ray beam made contact. Thus, each tissue sample was positioned according to the red mark to ensure that the X-ray beam passed through the centre of the cornea.

2.2.2 Collection of low-angle XRD data

Low-angle XRD patterns were obtained using an evacuated camera of 8.25 m length and a focused monochromatic X-ray beam of 0.154 nm fixed wavelength of dimensions 1 mm (horizontal) x 0.5 mm (vertical), with the beam direction parallel to the corneas' optical axis.

Corneas stored in paraformaldehyde solution were gently dabbed on tissue paper to remove excess fixative. Those samples that were frozen remained wrapped in clingfilm to prevent dehydration and were kept frozen on dry ice before data were recorded. Accurate positioning of the cornea in the airtight cell was determined by placing the transparent cell on top of the exposed graph paper, and using a pair of tweezers to place the centre of the cornea within the cell directly over the red mark. The cell was sealed, put into the specimen stage, and the shutters were opened to allow a 2 minute X-ray exposure of the cornea. Patterns were recorded on a 512 x 512 pixel multiwire gas-proportional area detector. A lead beamstop was positioned between the cornea and detector to absorb any undeviated X-rays.

Prior to data collection of corneas stored in clingfilm, it was necessary to ensure that this material did not contribute to the XRD pattern. A folded piece of clingfilm was placed in the sample holder and exposed to the beam for 2 minutes. The clingfilm was found to produce a weak isotropic background scatter (this scattering would later be removed when the overall background scatter is subtracted). In order to calibrate patterns collected, each experiment involved the collection of an XRD pattern from a vertically positioned piece of hydrated rat tail tendon.

Following data collection on Station 2.1, the low-angle XRD patterns were downloaded to a SUN Microsystems computer at Cardiff. The XRD patterns were analysed using Unix based image analysis software (BSL, produced by Dr. G. Mant,

Daresbury Laboratory) and Windows based statistics (Statsoft Statistica Basic programme) and spreadsheet (Microsoft Excel) packages to obtain average values for collagen fibril (interfibrillar) Bragg spacing, collagen fibril diameter, height/width (H/W) ratio, and coherence distance (t).

As beam intensity falls off gradually as a function of time, typically over a period of several hours, each XRD pattern was normalised to correct for beam decay and changes in X-ray absorption (due to tissue hydration and thickness variations) using a reading from the appropriate ion chamber (Figure 1.11). Additionally, when using the multiwire detector it was necessary to record its spatial sensitivity by exposing it to Fe^{55} for a specified time. This ensured that any non-linearities in its response could subsequently be compensated for by dividing the detector response pattern, point-by-point, from each normalised image (Meek and Quantock, 2001).

2.3 Data analysis

2.3.1 Conventional analysis of XRD data

A vertical transect was taken through the centre of the normalised pattern (inset) and integrated horizontally to produce an X-ray intensity profile of the 1st order equatorial X-ray pattern (I) as a function of radial position (R) (which is directly related to the scattering vector, K) (Figure 2.1A).

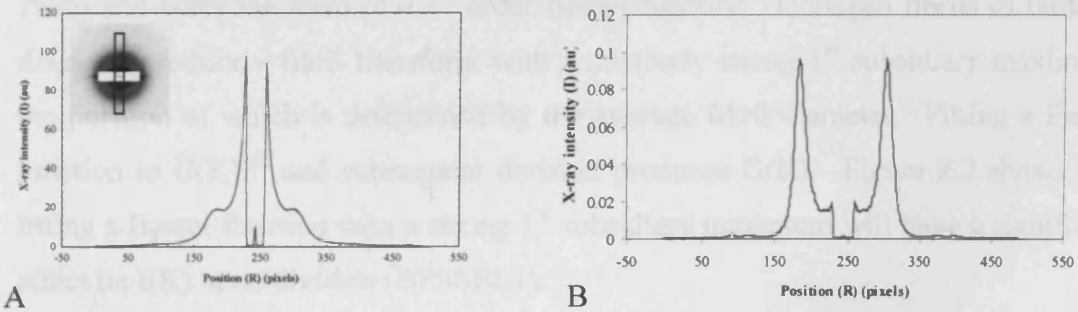

A B

Figure 2.1. (A) Inset image is an XRD pattern from wild-type cornea. A vertical transect is taken through the centre of this pattern and the intensity of X-rays (I) are plotted as a function of position (R), where R is directly related to the scattering vector, K. (B) XRD pattern from bovine cornea (kindly provided by Dr Justyn Regini) demonstrating that the murine 1st order equatorial reflection and 1st subsidiary maximum are comparatively much weaker.

This symmetrical pattern was then folded about its centre to produce an average intensity distribution profile, thereby improving the signal-to-noise ratio.

The intensity distribution I(K), consists of three elements; the interference function, G(K) (which describes the short-range order of fibrils), the scattering amplitude for a single cylinder, F^2 (i.e. collagen fibril), and also the background scatter from non-fibrillar stromal components such as cells and sometimes clingfilm, B(K), where K is the scattering vector. The relationship between these components is described in Equation 2:

$$I(K) = G(K)F^2 + B(K) \quad \text{.....Equation 2}$$

The aim of XRD pattern analysis is to obtain the interference function value, G(K), which contains information about the Bragg spacing of the collagen fibrils. Therefore, Equation 2 can be rearranged and the sequence outlined below followed:

$$G(K) = \frac{I(K) - B(K)}{F^2} \quad \text{.....Equation 3}$$

The first step is to subtract B(K) to isolate the scattering produced by the collagen fibrils, $G(K)F^2$. G(K) (created by regularly arranged collagen) consists of a fairly sharp first-order peak and a weak second-order peak, and levels off to a constant value at higher reciprocal distances (Worthington and Inouye, 1985); whereas F^2 represents scattering from the collagen fibrils themselves (Worthington and Inouye, 1985) and takes the form of a 1st order Bessel function. Collagen fibrils of uniform diameter produce a fibril transform with a relatively strong 1st subsidiary maximum, the position of which is determined by the average fibril diameter. Fitting a Bessel function to $G(K)F^2$ and subsequent division produces G(K). Figure 2.2 shows that fitting a Bessel function with a strong 1st subsidiary maximum will have a significant effect on I(K) upon division (BESSEL1).

However, weaker 1st subsidiary maxima formed by the scattering of collagen fibrils of less uniform diameter associate with Bessel functions that are broader and flatter (BESSEL2 to BESSEL4). This thesis involved the study of mouse collagen fibrils that generally produce a very weak 1st subsidiary maximum. Figure 2.2 shows that a Bessel function fitted to a wide distribution is rendered very broad and flat (BESSEL5), therefore revealing that F^2 contributes very little at low K.

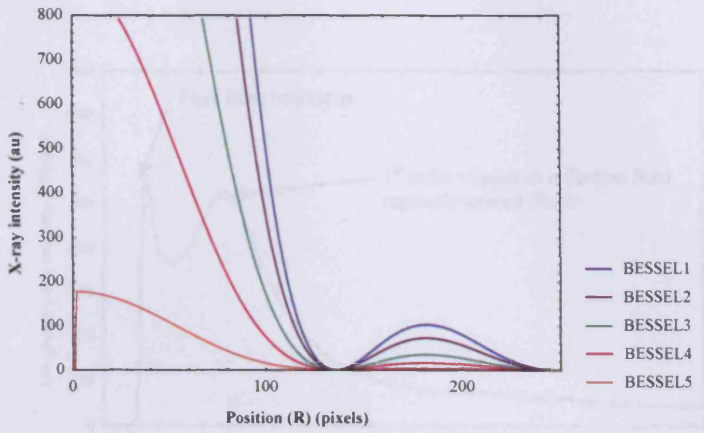

Figure 2.2. A series of Bessel functions illustrating that the strength of the 1st subsidiary maximum to be fitted will affect the contribution of F^2 on division.

Also, obtaining an accurate Bessel fit proved very difficult, and in most instances it was not possible to fit the Bessel function to the entire 1st subsidiary maximum. Therefore, the decision was made to superimpose the Bessel function over the data, without division, in order to simply estimate the 1st subsidiary maximum position and therefore the average collagen fibril diameter in each individual case. Therefore, Equation 4 outlines the procedure followed:

$G(K)F^2 = I(K) - B(K)$.....Equation 4

Step 1:Obtaining the intensity distribution I(K)

The scatter intensity distribution (I) is a function of radial distance (R) from the centre of the pattern. However, the scattered intensity measured is fundamentally a linear sample of I(K). Therefore, in order to correct for the fact that a linear scan was taken across a circular or arced X-ray pattern, the intensity at each position (I) was multiplied by its radial position (R) to form IR (Figure 2.3).

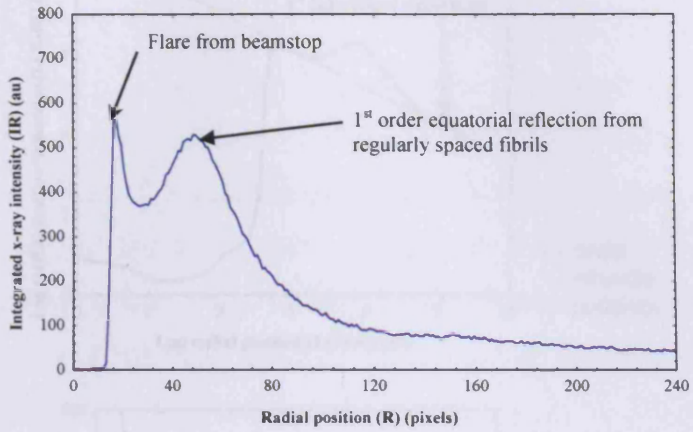

Figure 2.3. Scattering intensity (I) multiplied by radial position (R) corrects for the use of a linear scan across a circular X-ray pattern, thereby taking into account the fact that only a small sample of the pattern was used to form the integrated intensity distribution profile.

Step 2(A) Conventional removal of background scatter B(K)

To obtain $G(K)F^2$ from Equation 4 it was first necessary to subtract B(K). A linear background (LOGBACK) was generated for the natural log graph of IR against R, by selecting the coordinates of three points (FITLOGIR) from either side of the 1st subsidiary maximum (Figure 2.4A) these being the only points where we know $G(K)F^2$ must be zero (Daxer and Fratzl, 1997). These coordinates were used to generate a power function of the form:

$$B(K) = CK^m \quad \text{.....Equation 5}$$

where m and c are constants. The linear background was then anti-logged (ANTILOGB) and subtracted from the original plot of R against IR to form a new background-subtracted intensity profile (IR-ALB) (Figure 2.4B).

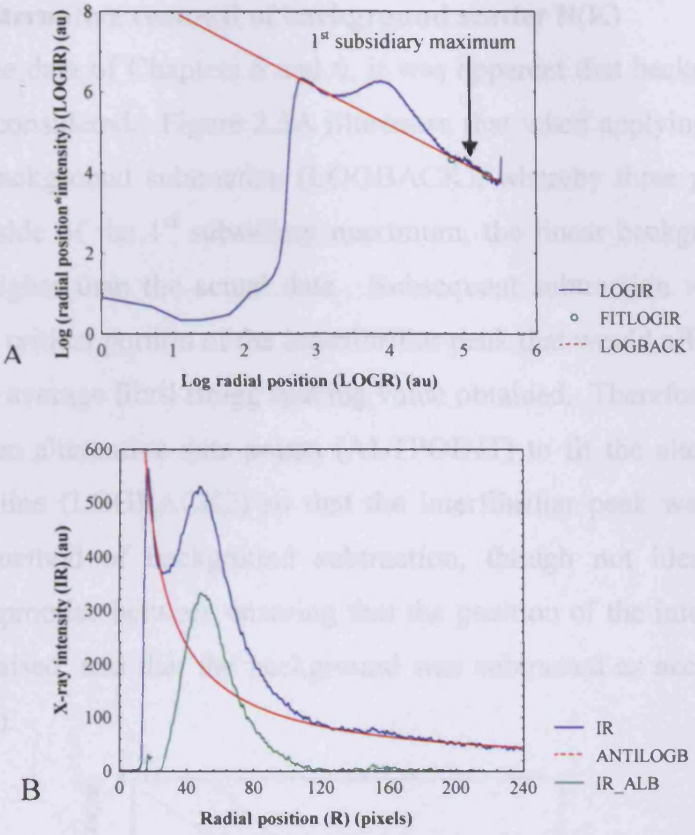

Figure 2.4. A linear background was generated (LOGBACK) for the log graph of scattering intensity against radial position (A), followed by removal of background scatter (ANTILOGB) resulting in IR-ALB (B).

Removal of diffuse X-ray scatter produced by other tissue components produced just the peaks associated with the low angle X-ray reflections of the cornea. From the 1st order equatorial peak, the average collagen interfibrillar Bragg spacing was determined (Step 4).

In mouse, the Bessel function from the distribution of fibril diameters should not contribute significantly to scatter at low K values (i.e. towards the beamstop) for reasons outlined earlier. Therefore, the intensity is expected to fall to zero on each side of the interfibrillar peak. However, sometimes the analysis of XRD patterns collected in Chapters 3 and 4 involved the subtraction of a second background to remove residual scattering at low K. The amount of unsubtracted background scatter varied from pattern-to-pattern and may have affected the position of each equatorial peak to different extents, so this extra step (which proved successful) was necessary to ensure that Bragg spacing values obtained were accurate.

Step 2(B) Alternative removal of background scatter B(K)

Regarding the data of Chapters 5 and 6, it was apparent that background subtraction had to be reconsidered. Figure 2.5A illustrates that when applying the conventional method of background subtraction (LOGBACK), whereby three points are selected from either side of the 1st subsidiary maximum, the linear background generated is positioned higher than the actual data. Subsequent subtraction would result in the removal of a critical portion of the interfibrillar peak that would affect its position and therefore the average fibril Bragg spacing value obtained. Therefore, it was necessary to select three alternative data points (ALTPOINT) to fit the alternative power-law background line (LOGBACK2) so that the interfibrillar peak was preserved. This alternative method of background subtraction, though not ideal, was deemed a suitable compromise between ensuring that the position of the interfibrillar peak was not compromised, and that the background was subtracted as accurately as possible (Figure 2.5B).

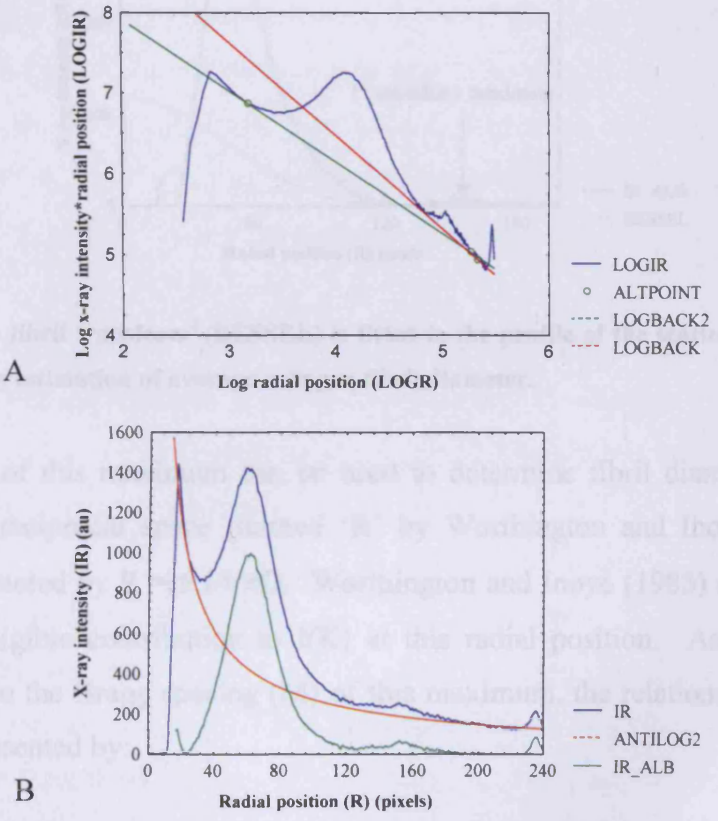

Figure 2.5. Subtracting the conventionally fitted background (LOGBACK) would compromise the final interfibrillar peak position, so alternative points were selected (ALTPOINT) with which to plot the background (LOGBACK2) (A). Subtraction of the anti-logged background (ANTILOG2) from IR sufficiently removed background scatter to produce IR-ALB (B).

Step 3: Determination of collagen fibril diameter

Collagen fibrils may be well approximated as infinitely long cylinders. At this stage of analysis, $G(K)F^2$ has been obtained, with F^2 representing the scattering amplitude for a single cylinder. Figure 2.6 shows that the 1st subsidiary maximum of the fibril transform is a low, broad peak produced by the scattering of collagen fibrils of varying diameters. Normally, G(K) can be obtained by fitting the 1st subsidiary maximum of a 1st order Bessel function to the background-subtracted image profile (IR-ALB) followed by division. In this thesis, however, the Bessel function was simply fitted at the 1st subsidiary maximum position without division in order to measure the average collagen fibril diameter within each particular cornea (Figure 2.6).

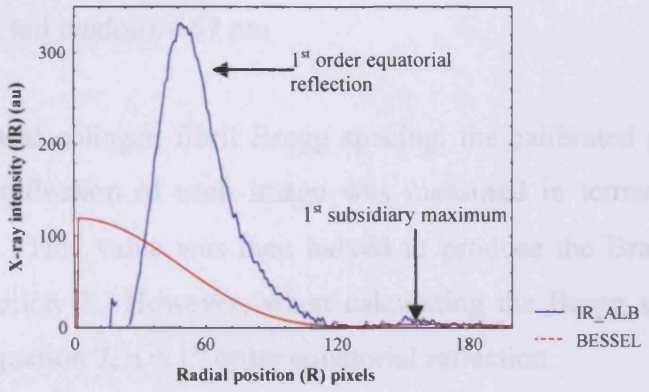

Figure 2.6. The fibril transform[2] (BESSEL) is fitted to the profile of the scattering intensity (IR-ALB) to gain an estimation of average collagen fibril diameter.

The position of this maximum can be used to determine fibril diameter, D. When measured in reciprocal space (termed 'R' by Worthington and Inouye, 1985), the position is denoted by $R = 5.14/\pi D$. Worthington and Inoye (1985) stated that G(K) makes a negligible contribution to I(K) at this radial position. As D is inversely proportional to the Bragg spacing (M) of this maximum, the relationship between M and D is represented by:

$$D = \frac{2x\ 5.14M}{2\pi} \quad \text{.....Equation 6}$$

Step 4: Calculating average fibril Bragg spacing using rat tail tendon calibration

The low-angle X-ray patterns were calibrated using the position of the sharp meridional 3rd order X-ray reflection and known 67 nm *D*-period of hydrated rat tail tendon. The scattering angle (2θ) of the rat tail tendon was calculated by entering the relevant values into the Bragg equation (Equation 7) and used to calibrate the radial position, R.

$n\lambda = 2.d.\sin\theta$.....Equation 7

where,

n (order of meridional peak) = 3

λ (fixed low-angle wavelength) = 0.154 nm

d (*D*-period of rat tail tendon) = 67 nm

To calculate corneal collagen fibril Bragg spacing, the calibrated position of the 1st order equatorial reflection of each image was measured in terms of the scattering angle value (2θ). This value was then halved to produce the Bragg angle (θ), and entered into Equation 7. However, when calculating the Bragg spacing of corneal collagen using Equation 7, n = 1st order equatorial reflection.

To convert Bragg spacing to actual interfibrillar spacing a multiplication factor of 1.12 is used, which assumes a liquid-like packing of collagen (Worthington and Inoye, 1985). However, the Bragg values are quoted within this thesis for consistency with other biophysical investigations.

Step 5: Determining the H/W ratio

The shape of the interfibrillar peak derived from the X-ray data gives an indication of the degree of nearest neighbour fibril packing. This shape, when measured in real space, may be quantified in terms of peak height (H) divided by peak width at half-height (W), and gives a measure of the degree of fibrillar order. The higher the H/W ratio value, the more local order in the array of collagen fibrils (Meek *et al*, 2003b).

Step 6: Determining the coherence distance (t) of collagen

As well as providing a measure of collagen fibril Bragg spacing, the 1st order equatorial peak allows an estimate of the degree of local order in the arrangement of the collagen fibrils in the cornea. The angular width of an interfibrillar reflection (β) is related to a parameter (t) that gives a measure of the degree of order in the lattice by the approximation:

$$\beta \approx \frac{2\lambda}{(t \cos \theta)} \quad \text{.....Equation 8}$$

where θ is the Bragg angle. Termed the coherence distance (t) by Regini *et al* (2004), Stokes (1955) described this parameter as "the order of the average distance over which the exact periodicity [of collagen arrangement] begins to fail". In order to obtain (t) the Bragg equation (Equation 7) may be combined with Equation 8. Beforehand, the numerical constant 2 in Equation 8 is replaced by 1 as Stokes (1955) stated that "more exact treatments give a value closer to unity".

$$\beta t \cos\theta = 2d \sin\theta \quad \text{.....Equation 9}$$

$$\beta t = 2d \frac{\sin\theta}{\cos\theta} \quad \text{.....Equation 10}$$

$$\beta t = 2d \tan\theta \quad \text{.....Equation 11}$$

At small angles, $\tan\theta \approx \theta$, therefore,

$$\beta t = 2d\theta \quad \text{.....Equation 12}$$

$$t = \frac{2d\theta}{\beta} \quad \text{.....Equation 13}$$

2.3.2 Statistical analysis

The collagen fibril Bragg spacing, collagen fibril diameter, and H/W ratio data collected in each chapter underwent statistical analysis using SPSS 11 for Windows. The General Statistics section (Appendix 1) outlines the statistical parameters

considered before comparing data sets, and also the most appropriate way that data sets should be displayed. Data sets that followed a normal Gaussian distribution were presented in terms of mean value ± standard error (SE). Alternatively, when at least one data set was not normally distributed, the most appropriate presentation took the form of a Box-and-Whiskers plot. Also, creating a Box-and-Whiskers plot in SPSS 11 allowed for the detection of values that deviate from the mean of a data set, called outliers and extremes. Appendix 1 describes in more detail the criteria that SPSS 11 uses to detect and classify these values, but essentially any point that lies more than 1.5 interquartile ranges beyond the quartiles is a "mild" outlier, while a point that lies beyond three interquartile ranges is an "extreme" outlier. These values can arise from measurement errors or natural variability in a population etc, and it was therefore important to determine whether such values should be included in statistical analysis, largely because the presence of a rogue value could have a strong effect on the average standard deviation of the data set and therefore the statistical outcome. All values that were found to be unusual were included in statistical analysis as I was satisfied that natural variability was the only cause.

As the coherence distance values are purely approximations, only descriptive statistics (i.e. mean, standard deviation etc) were calculated.

2.4 Transmission electron microscopy (TEM)

The complete process of tissue preparation for TEM leads to the transformation of a biological hydrated tissue into a dehydrated tissue preserved in a static state within a plastic resin matrix.

2.4.1 PG localisation with Cupromeronic Blue (CuBlue)

Corneal samples were fixed overnight on a rotator at room temperature in 0.05% (w/v) CuBlue in 2.5% (v/v) glutaraldehyde in 25mM sodium acetate buffer, containing 0.1M magnesium chloride (pH 5.7) to achieve a critical electrolyte concentration for staining of proteoglycans (Scott and Haigh, 1985). Remaining on the rotator throughout, they were then washed with 2.5% (v/v) glutaraldehyde in sodium acetate and magnesium chloride (3 x 15 min), and stained with aqueous 0.5% sodium tungstate solution (3 x 15 min) followed by washing with a 0.5% sodium tungstate: 50% ethanol (EtOH) solution (3 x 15 min). The samples were then

gradually dehydrated using a series of alcohol solutions: 15 min 50% (v/v) EtOH, 15 min 70% (v/v) EtOH, 15 min 90% (v/v) EtOH, then 2 x 15 min 100% EtOH. Prior to the infiltration of the tissue with Agar 100 resin, the samples were immersed in propylene oxide for 2 x 15 minutes. The rationale is that EtOH and resin are immiscible, so the propylene oxide acts as an intermediate to ensure that the resin can properly penetrate the tissue for more effective sectioning.

The following resin solution series was used: 1:1 (v/v) Agar 100 resin:propylene oxide for 1 hour, 100% Agar 100 resin for 1 hour, and then 100% Agar 100 resin overnight, during which time the tops of the vials were left off to allow any remaining propylene oxide to evaporate. This was then followed by 100% Agar 100 resin for 3 hours, after which the samples were placed in moulds and 100% Agar 100 resin was added to them. The samples were put in the oven (60°C) to polymerise for at least 48 hours according to the manufacturers recommendation (Agar Scientific) that this period is sufficient to achieve optimal polymerisation.

2.4.2 Block trimming and sectioning

Once the samples were embedded in resin, the polymerised blocks were placed into an Ultracut E Ultramicrotome (Reichert-Jung, Germany) (Figure 2.7C) and trimmed into a trapezoid cutting face (Figure 2.7A) using a stainless steel razor blade. Glass knives were made using a Leica EMKMR2 knifemaker (Wein-Austria) and plastic troughs (TRUFs) or silver tape were attached to some of the knives using dental wax (Figure 2.7B). This was necessary to hold water onto which the sections, cut with the glass knife, could float. All sections were cut to a 90 nm thickness and exhibited gold interference colour. These gold sections are recommended for a clear visualisation of collagen fibrils without compromising contrast (Melcher and Chan, 1978). To remove compression wrinkles, sections were flattened by exposure to chloroform vapour. A thin piece of filter paper was dipped into chloroform and immediately held above the sections for a few seconds. The sections were then collected on uncoated 300-size hexagonal mesh copper or nickel grids (Figure 2.7D). Upon removal from the water the sections adhered to the grids and were dried on a sheet of velin, a special lint-free tissue. Once completely dried, the grids were stained.

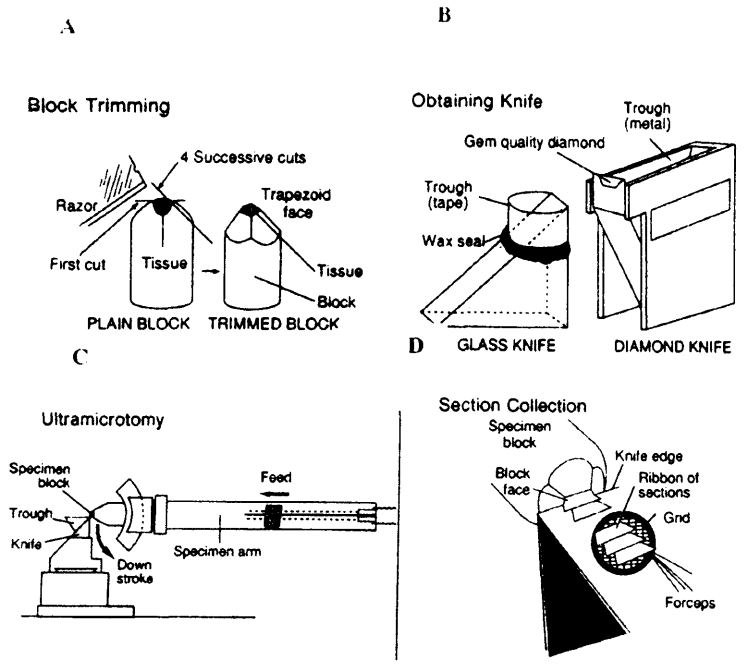

Figure 2.7. The four steps involved in ultramicrotomy process are (A) cutting the resin block using a razor blade to expose the underlying tissue and to form a trapezoid cutting face, (B) making glass knives with which to cut ultrathin sections, (C) placing the trimmed block in the ultramicrotome, and (D) cutting the ultrathin sections using a knife edge followed by picking up the floating sections with a copper grid (from Bozzola and Russell, 1992).

2.4.3 Staining grids

(A) Staining with saturated aqueous uranyl acetate (UA) and Pb citrate

Staining of sections was achieved by placing each grid, section-side-down, onto a 30 µl drop of saturated aqueous uranyl acetate, covered to avoid evaporation, and placed in an oven at 40°C for 40 minutes. Following this, each grid was washed by dipping (20 times) into three successive containers of filtered, distilled water, after which grids were placed onto velin paper to dry. Each grid was then lowered section-side-down onto a 30 µl drop of aqueous Reynolds lead citrate for 7 minutes to stain, followed by dipping (20 times) in three successive containers of fresh filtered distilled water. Again, each grid was then carefully picked up using forceps and transferred, section-side-up, onto velin paper to dry. To ensure that drying was complete, the grids were placed, section-side-up, onto a circular rubber grid holder and into a desiccator for at least 24 hours.

(B) Staining with saturated ethanolic uranyl acetate (UA) and Pb citrate

Each grid was placed, section-side-down, onto a 30 µl drop of saturated ethanolic UA, covered to avoid evaporation, and left for 50 minutes at room temperature to stain. Next, each grid was washed, by dipping (20 times) into four successive dilutions of EtOH:

- 100% EtOH
- 90% (v/v) EtOH
- 50% (v/v) EtOH
- 25% (v/v) EtOH

The remaining two washes consisted of dipping in filtered distilled water, after which each grid was placed onto velin paper to dry. Each grid was then lowered section-side-down onto a 30 µl drop of aqueous Reynolds lead citrate for 7 minutes to stain, followed by dipping (20 times) in three successive containers of fresh filtered distilled water. Again, each grid was then carefully picked up using forceps and transferred section-side-up onto velin paper to dry. To ensure that drying was complete, the grids were transferred section-side-up onto a circular rubber grid holder and placed in a desiccator for at least 24 hours.

2.4.4 Observing the tissue in the microscope

Observation of sections was undertaken using a Philips EM208 transmission electron microscope. Image magnification was calibrated with reference to the 8.75 nm lattice spacing of beef liver catalase crystals (Agar Scientific).

Chapter 3. Neonatal development of wild-type and lumican-null corneal stroma

3.1 Introduction

One of the most distinguishing properties of the cornea is its ability to transmit most of the incident light in the visible spectrum. This is accomplished because the collagen lamellae, which lie at different degrees to each other in the plane of the corneal surface, consist of collagen fibrils of approximately uniform diameter and regular arrangement (Maurice, 1957). Research suggests that this intricate stromal structure is largely governed by the KSPGs, particularly the major corneal KSPG, lumican (Blochberger *et al*, 1992). Several lines of evidence to support this concept come from the generation of KSPG-deficient mice.

3.1.1 Lumican knockout mouse corneas

The corneas of keratocan-deficient (Liu *et al*, 2003; Meek *et al*, 2003b) and mimecan-deficient (Tasheva *et al*, 2002) mice do not display obvious signs of corneal opacity. On the other hand, mice homozygous for a null mutation in lumican (Chakravarti *et al*, 1998; 2000) present a severe phenotype, having thin, cloudy corneas. Figure 3.1 illustrates that a lumican deficiency in mice affects corneal transparency during postnatal development. It is also age-dependent, as more and more corneas develop opacity over time (Chakravarti *et al*, 1998).

At the ultrastructural level in the mature lumican-null mouse, disruption of corneal stromal architecture is evident (Chakravarti *et al*, 1998). Electron microscopy has shown that in the anterior stroma, both wild-type (Figure 3.2A) and lumican-null (Figure 3.2B) corneas are similarly well-ordered. However, the posterior regions of wild-type and lumican-null corneas are markedly different, in that collagen fibrils of the wild-type posterior stroma are well-ordered and consistently thin throughout (Figure 3.2C), whereas the lumican-null posterior stroma (Figure 3.2D) consists of irregularly packed fibrils, a minor population of which are large and irregularly shaped, thought to be the result of fibril fusion (Chakravarti *et al*, 1998). This stromal region also suffers a 40% reduction in thickness. Increased backscattering of light originates from deeper tissue regions of mutant corneas, indicating that this disorganised area is the likely cause of corneal opacity (Chakravarti *et al*, 2000).

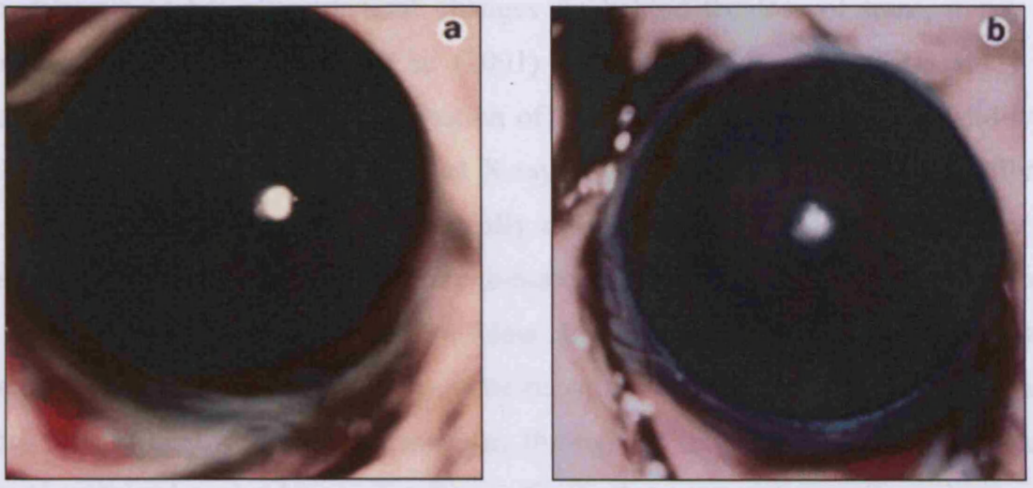

Figure 3.1. Full view photobiomicroscopy of wild-type (a) and lumican-deficient (b) eyes. Wild-type mice have clear corneas. Lumican-null mutants show a continuous cloudiness with a clear ring-like peripheral zone (from Chakravarti *et al*, 1998).

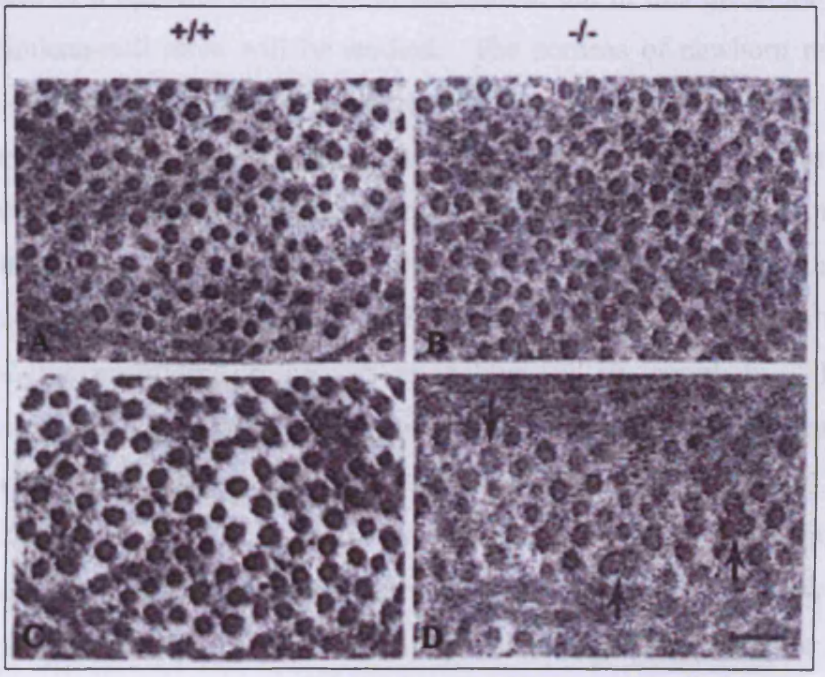

Figure 3.2. Transmission electron micrograph of collagen fibril structure in the anterior and posterior stroma of lumican-null and wild-type corneas. Fibril structure and packing are comparable in the anterior stroma of wild-type (A) and lumican-null mice (B). In contrast to fibrils in posterior stroma of wild-type (C), some fibrils in the posterior stroma of lumican-null mice (D) are abnormally large in diameter, with irregular contours (arrows). These structures are indicative of abnormal lateral growth. Bar = 100 nm (from Chakravarti *et al*, 2000).

To determine what ultrastructural changes lie behind the loss of transparency in lumican-null mice, Quantock *et al* (2001) undertook a low-angle XRD study of mature mouse corneas. The examination of 2-month-old and 6-month-old wild-type and lumican-null corneas revealed that X-ray reflections arising from collagen fibrils in lumican-null corneas were substantially diffuse and that collagen fibrils were in disarray compared to the situation in age-matched, wild-type counterparts (Quantock *et al*, 2001). More significantly, no clear and consistently measurable subsidiary maxima were detected in the X-ray patterns of the 6-month-old lumican-null mice. This finding confirmed that on average, throughout the whole cornea, the mutant tissue contained a population of collagen fibrils that were not as uniform in size as those of normal mouse corneas.

The majority of investigations into corneal structure and function have focused on the consequences of a lumican-deficiency in adulthood, but in this thesis the corneas of neonatal lumican-null mice will be studied. The corneas of newborn mice are not fully developed (Smith *et al*, 2002), and at birth the eyes are completely covered by the fused eyelids. Eye-opening appears to stimulate structural changes in the cornea (Zieske, 2004). The period from murine eyelid formation and fusion, through to their eventual re-opening less than 2 weeks after birth was investigated by Findlater *et al* (1993). At 15.5 days post-coitus (p.c.) the cornea is visible with the primitive eyelids represented by protruding ridges of epithelium at its periphery. It is these proliferating epithelial cells that form the eyelids with such rapidity that within 24 hours the eyes are completely covered by the fused eyelids. At 20 days p.c. mice are born with their eyes closed and remain so up to neonatal day 10. By neonatal day 12 eyelid separation is all but complete (Findlater *et al*, 1993). Alterations in stromal thickness and cellularity occur in the days preceding eyelid opening in the mouse (Song *et al*, 2003).

3.1.2 Corneal stromal thickness changes in neonatal wild-type and lumican-null mice

Research using confocal microscopy through focussing to monitor changes in the thickness of neonatal wild-type and lumican-deficient mouse corneas has provided evidence that lumican is an essential component of corneal development. The first part of this two-part study by Song *et al* (2003) investigated stromal thickness changes in the wild-type cornea during the first 30 days after birth. At birth, the wild-type corneal stroma was thin (62.9 ± 4.9 μm) and translucent. Development of the corneal stroma was characterised by a transient increase in thickness that started at neonatal day 8 (55.2 ± 6.3 μm) and peaked at day 12 (89.8 ± 11.6 μm); a 60% increase during the four days preceding eyelid opening. Following eyelid opening on day 12, stromal thickness steadily decreased to 66.9 ± 7.5 μm at day 20, to increase to adult thickness by day 30 (81.5 ± 10.7 μm). Stromal light scattering decreased by 50% between neonatal days 1 and 12.

Having determined stromal thickness changes during normal corneal development, the second part of the study by Song and associates (2003) focused on stromal development of the lumican-deficient cornea for the first 12 weeks after birth in comparison with age-matched wild-type counterparts. Figure 3.3 shows that normal stromal development again involved transient stromal thickening at week 2 and a rapid decrease in stromal light scattering. In contrast, the stroma of lumican-deficient mice, pre eye-opening, was thinner (60.0 ± 4.9 μm) and failed to undergo transient stromal thickening (in fact, the stroma became thinner from week 2 to 3 (50.7 ± 8.4 μm)) (Song *et al*, 2003). The mutant cornea also displayed significantly increased light scattering that remained elevated above that of the wild-type corneas, indicating that transparency was not developing normally.

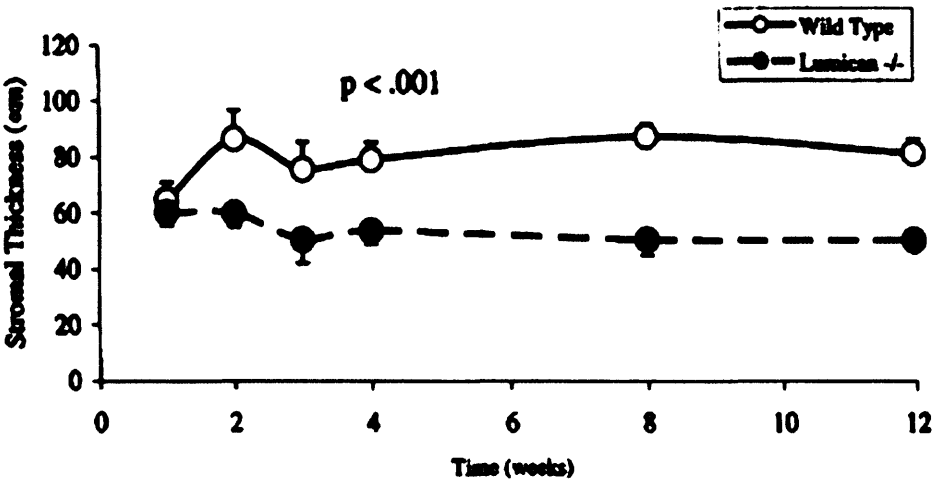

Figure 3.3. Differences in stromal thickness between neonatal wild-type and lumican-deficient mice. Stromal thickening up to day 12 is ablated in the lumican-deficient mouse cornea (from Song *et al*, 2003).

This evidence indicates that absence of lumican and its sulphated KS chains renders the mutant corneal stroma unable to undergo this transient thickening evident in the wild-type stroma.

3.1.3 Experimental aims

During neonatal development between days 8 and 14 the corneal stroma of the mouse undergoes critical changes in tissue thickness, cell density, and light scattering. Using XRD and TEM, the ultrastructural changes that take place within the corneas of wild-type and lumican-deficient newborn mice around the time of eye opening (days 8 to 14) were investigated. The following aims of this study were addressed:

- XRD measurements of average collagen fibril spacing and collagen fibril diameter were taken through neonatal days 8 to 14 to give insight into what developmental changes take place in the wild-type and mutant stroma at the ultrastructural level. Specifically, attempts were made to establish whether the transient stromal thickening at neonatal day 12 reported in wild-type mice (Song *et al*, 2003) could be attributed to a homogenous increase in stromal collagen fibril spacing, and also whether an absence of lumican during this early stage of development has a bearing on collagen fibril architecture, because changes in light scattering and failure to undergo the transient stromal thickening in the mutant cornea have been reported (Song *et al*, 2003). Calculation of the H/W ratio and coherence distance

from the interfibrillar peak provided representative values for the degree of fibril ordering within each cornea.

- Although lumican deficiency results in bilateral corneal opacification that generally develops with increasing age of the mouse (Chakravarti *et al*, 2000), it was important to address the possibility that ultrastructural abnormalities might be evident in the neonatal stage, despite the fact that lumican-null corneas are not noticeably cloudy at birth.

- A TEM study was undertaken to investigate whether fibril fusion occurs during the neonatal stage of corneal development, or if it is a later event only, as the posterior stroma of mature lumican-null mice contains a population of large, irregularly shaped collagen fibrils (Chakravarti *et al*, 1998).

3.2 Materials and methods

3.2.1 Tissue samples

Normal mouse (CD-1) corneas at neonatal development day 8 (n = 10), day 10 (n = 10), day 12 (n = 12), and day 14 (n = 12), along with lumican-null corneas at day 8 (n = 12), day 10 (n = 12), day 12 (n = 12), and day 14 (n = 12) from a colony with a null-homozygous mutation for lumican, were kindly supplied by Dr. Shukti Chakravarti of the Departments of Medicine, Cell Biology and Ophthalmology, Johns Hopkins University, Baltimore, Maryland. The lumican-null mice were generated as published (Chakravarti *et al*, 1998). Dr. Chakravarti carefully dissected each cornea at the limbus, and immediately immersed them in 4% paraformaldehyde in 0.1M phosphate buffer prior to transportation to Cardiff University. Chemical fixation via paraformaldehyde was deemed the most suitable storage method as this mild fixative rapidly penetrates thin tissue to preserve its fine structure (Glauert and Lewis, 1998). On arrival, the corneas remained in the fixative solution at 4°C for a further week until low-angle XRD analysis was undertaken.

3.2.2 Low-angle XRD

3.2.2.1 Collection of XRD data

The corneas were analysed on Station 2.1 at the SRS, Daresbury Laboratory. XRD patterns were collected as outlined in Section 2.2.2, with the exception that a detector response from a 9 hour exposure to a radioactive source (Fe^{55}) was then subtracted from each X-ray pattern to correct for any non-linearities in the detector.

Data analysis was undertaken as outlined in Section 2.3 to obtain average values for collagen fibril Bragg spacing (Step 4), collagen fibril diameter (Step 3), H/W ratio (Step 5), and coherence distance (Step 6). Step 2(A), the conventional removal of background scatter, was followed during the analysis of data.

3.2.3 Transmission electron microscopy

The details of tissue staining and embedding, block trimming and sectioning, and section observation are outlined in Section 2.4. As previous staining of sections with saturated aqueous UA (Section 2.4.3A) gave very little contrast of collagen fibrils in transverse section, fresh sections were stained using ethanolic UA (Section 4.2.3B).

3.3 Results

Details of statistical analysis within this study can be found in Appendix 2.

Neonatal Day	n	IFS (nm)	CFD (nm)	H/W ratio	t (nm)
	1	56.0	29.7	5.3	190
	2	64.4	31.8	5.3	252
	3	63.0	31.1	5.1	266
	4	66.0	32.0	7.9	265
$8^{+/+}$	5	61.0	31.3	3.6	273
	6	62.6	32.8	3.1	272
	7	64.0	28.1	1.6	234
	8	66.0	30.9	5.0	261
	9	63.0	30.9	3.2	219
	10	63.3	31.1	5.8	244
	1	59.7	29.7	6.1	254
	2	65.6	30.9	5.0	255
	3	68.3	31.3	8.1	249
	4	64.0	31.5	5.2	261
$10^{+/+}$	5	61.0	31.1	4.7	241
	6	62.6	32.2	6.0	259
	7	67.6	32.0	6.6	259
	8	59.3	30.7	6.9	247
	9	58.6	32.4	6.9	241
	10	64.4	31.5	6.8	260
	1	58.6	31.5	5.1	243
	2	62.0	35.2	10.0	277
	3	57.7	31.1	7.6	229
	4	59.0	32.2	6.8	264
	5	60.0	32.6	5.1	238
$12^{+/+}$	6	61.3	31.7	5.9	221
	7	59.7	32.4	6.0	254
	8	60.0	31.8	7.9	234
	9	61.3	32.2	6.9	253
	10	66.2	34.3	10.6	287
	11	64.0	32.6	5.9	255
	12	58.4	32.8	5.6	241
	1	62.6	32.8	5.9	246
	2	63.0	34.5	6.8	253
	3	55.7	33.7	5.3	244
	4	59.7	32.2	10.2	229
	5	66.0	33.5	9.7	254
$14^{+/+}$	6	55.0	30.2	5.6	211
	7	59.0	32.0	7.9	231
	8	61.3	32.6	7.6	253
	9	59.0	30.2	7.2	227
	10	62.4	32.4	8.1	238
	11	61.5	32.4	8.4	231
	12	57.5	31.3	5.4	220

Table 3.1. Collagen fibril Bragg spacing (IFS), collagen fibril diameter (CFD), H/W ratio, and coherence distance (t) values for wild-type specimens (n) at neonatal days 8, 10, 12, and 14.

Neonatal Day	n	IFS (nm)	CFD (nm)	H/W ratio	t (nm)
$8^{-/-}$	1	68.3	28.9	3.2	244
	2	70.7	28.8	2.6	259
	3	70.0	31.1	2.3	266
	4	73.0	28.9	3.9	240
	5	68.0	28.4	2.6	243
	6	66.0	30.9	3.1	236
	7	62.4	28.1	4.3	219
	8	69.0	28.8	2.4	226
	9	62.6	28.1	3.8	227
	10	66.2	28.6	2.6	219
	11	69.0	28.8	1.5	208
	12	69.4	30.2	4.4	223
$10^{-/-}$	1	67.4	30.2	3.6	228
	2	65.0	29.4	3.9	209
	3	67.0	30.7	8.1	219
	4	61.3	29.7	4.5	207
	5	66.5	27.4	3.6	254
	6	64.4	31.1	3.0	243
	7	63.5	30.4	4.0	230
	8	66.0	31.7	4.7	218
	9	66.5	30.6	6.5	213
	10	66.2	31.3	3.5	208
	11	67.6	32.4	4.6	238
	12	66.5	29.7	2.7	219
$12^{-/-}$	1	66.5	29.2	3.7	200
	2	65.0	31.5	3.0	222
	3	62.0	30.6	2.8	203
	4	66.7	29.1	3.5	222
	5	70.0	30.6	2.6	232
	6	66.2	30.4	2.3	236
	7	61.0	30.4	2.5	198
	8	60.4	30.7	4.2	213
	9	63.0	28.7	3.4	197
	10	62.4	30.2	2.9	198
	11	63.0	30.1	2.6	197
	12	62.6	30.7	6.5	224
$14^{-/-}$	1	60.0	29.7	5.0	223
	2	55.4	30.6	2.1	197
	3	59.5	27.6	5.0	221
	4	63.0	31.3	2.9	236
	5	64.7	32.4	4.0	215
	6	59.7	32.2	2.9	215
	7	61.1	30.6	4.1	212
	8	66.0	31.5	4.5	224
	9	60.0	29.2	4.1	190
	10	62.0	31.1	4.3	208
	11	58.0	32.4	3.7	214
	12	62.0	31.5	4.5	207

Table 3.2. Collagen fibril Bragg spacing (IFS), collagen fibril diameter (CFD), H/W ratio, and coherence distance (t) values for lumican-null specimens (n) at neonatal days 8, 10, 12, and 14.

3.3.1 Collagen fibril Bragg spacing

Changes in collagen fibril spacing occur during normal neonatal developmental days 8 and 14 (Kruskal-Wallis H test; $P = 0.057$) (Table 3.1). As Figure 3.4 illustrates, fibril spacing does not change appreciably between day 8 and day 10 remaining at around 63 nm (Mann-Whitney; $P = 0.940$). Fibril spacing falls, but not significantly, to 60.7 nm by day 12 (Independent samples t-test; $P = 0.069$) and remains essentially unchanged at day 14 (Independent samples t-test; $P = 0.698$). Through each successive time point, the change in spatial distribution is not pronounced, but when the values for days 12 and 14 are compared with fibril spacing at day 8 it is apparent that the stromal collagen fibrils are becoming progressively more closely packed with time (Mann-Whitney; day 8 – day 12, $P = 0.044$; day 8 - day 14, $P = 0.023$).

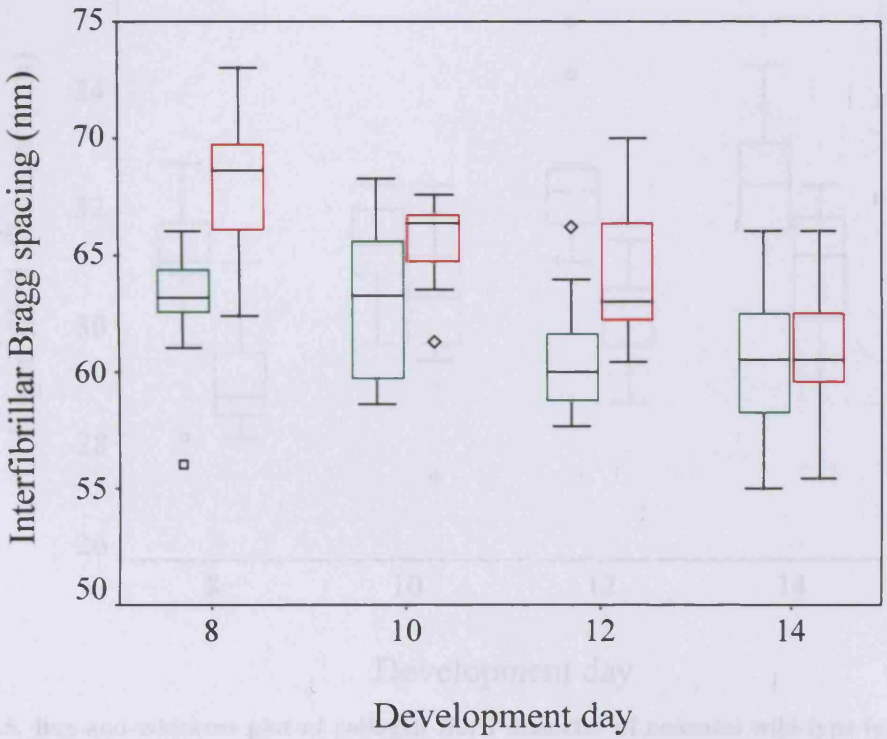

Figure 3.4. Box-and-whiskers plot of collagen fibril Bragg spacing (nm) of neonatal wild-type (green) and lumican-null (red) corneas. □ = extreme value, ◇ = outlier value.

To establish whether an absence of lumican affects collagen fibril spacing around eye opening, the corneas of mutant mice at days 8, 10, 12, and 14 were examined (Table 3.2). At days 8, 10, and 12 the lumican-null corneas have wider fibril spacing than their wild-type counterparts. Later, however, at day 14 when the average collagen fibril spacing falls, no difference is detected between mutant and wild-type (Independent samples t-test; $P = 0.565$) (Figure 3.4).

3.3.2 Collagen fibril diameter

Collagen fibril diameter in the normal mouse cornea during development lies in the 31 nm - 32.5 nm range, and changes over time (oneway ANOVA; $P = 0.002$). Figure 3.5 shows that there is initially very little change between day 8 and day 10 ($P = 0.900$). Again, through successive time points, the average collagen fibril diameter does not appear to change appreciably (day 10 – day 12, $P = 0.091$; day 12 – day 14; $P = 0.968$). Nevertheless, when compared to day 8 the average collagen fibril diameter is larger at day 12 (day 8 - day 12, $P = 0.016$) and remains so at day 14 (day 8 - day 14, $P = 0.048$).

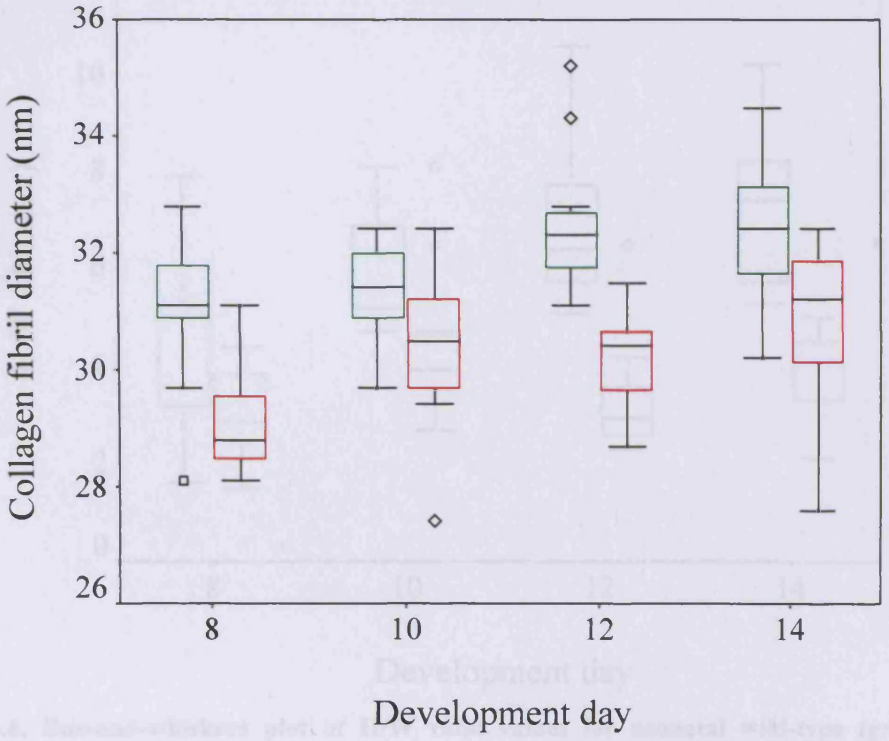

Figure 3.5. Box-and-whiskers plot of collagen fibril diameter of neonatal wild-type (green) and lumican-null (red) corneas. □ = extreme value, ◇ = outlier value.

Comparison of wild-type and mutant corneas disclosed that the average collagen fibril diameter of mutants is lower in the range 29.1 nm – 30.8 nm, with the difference significant or close to significance at each time point.

3.3.3 H/W ratio of corneal collagen interfibrillar peaks

The ordering of collagen fibrils increases during normal corneal stromal development (oneway ANOVA; $P<0.001$). Examination of successive time points shows that fibril ordering gradually increases, although not significantly so (day 8 – day 10, $P = 0.118$; day 10 – day 12, $P = 0.722$; day 12 – day 14, $P = 0.932$). However, fibril ordering is higher at days 12 and 14 when compared with that of day 8 (day 8 - day 12, $P = 0.007$; day 8 – day 14, $P = 0.001$), which suggests that the organisation of collagen fibrils increases subtly every 2 days, but that it nonetheless improves throughout the study period.

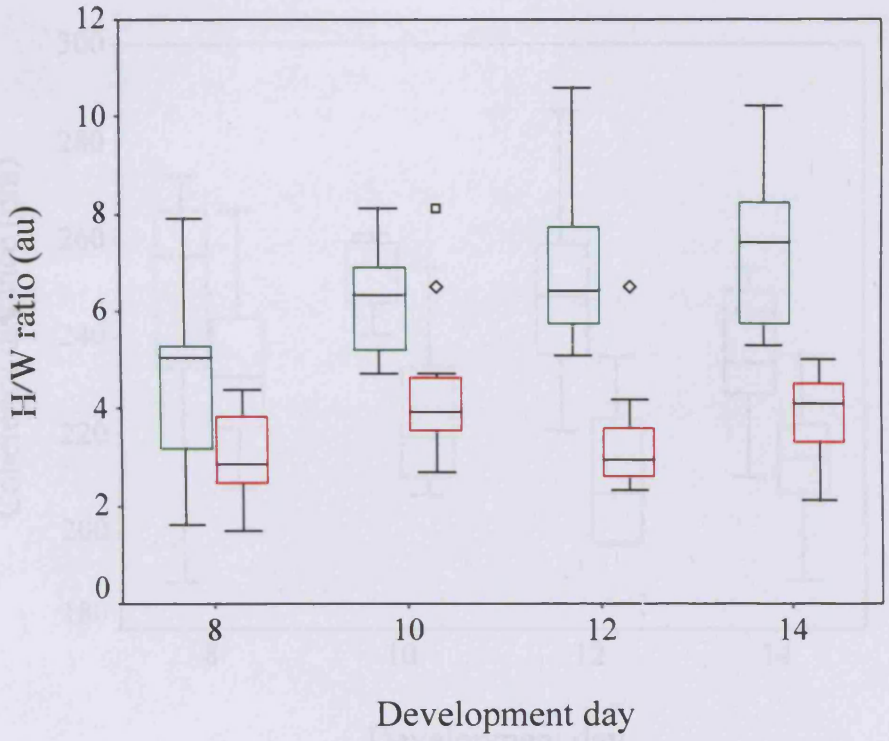

Figure 3.6. Box-and-whiskers plot of H/W ratio values for neonatal wild-type (green) and lumican-null (red) collagen interfibrillar peaks. At all time points, the collagen fibril ordering within the lumican-null cornea is lower than wild-type. □ = extreme value, ◇ = outlier value.

The lumican-deficient corneal collagen fibrils are at all times more disordered as the average H/W ratio of the lumican-deficient corneal interfibrillar peaks is substantially lower (Figure 3.6).

3.3.4 Coherence distance of corneal collagen interfibrillar peaks

The coherence distance data reveal that the short-range ordering of collagen fibrils remains reasonably steady during normal development, ranging between 236 nm and 253 nm. However, the coherence distance of the array of mutant corneal collagen fibrils was at all times lower with respect to wild-type counterparts, extending around 14 - 38nm less (Figure 3.7). Bearing in mind the extent of variation within each group, and that the fall in short-range ordering equates to no more than one fibril thickness, on-the-whole the mutant stromal matrix around eye opening appears to be less well ordered.

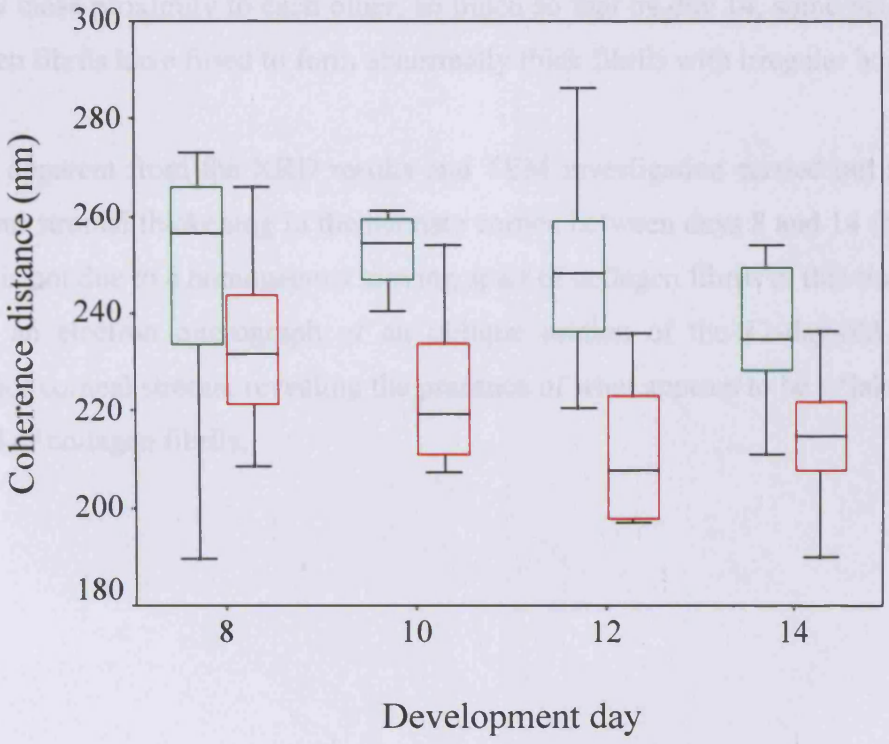

Figure 3.7. Box-and-whiskers plot of coherence distance values for neonatal wild-type (green) and lumican-null (red) murine corneal stroma depicting a difference in lattice structure at all development days.

3.3.5 Transmission electron microscopy

A TEM investigation was performed in order to determine whether there is any evidence of lateral fibril fusion during the period of neonatal development studied here. Unfortunately, wild-type corneal samples were mixed up following data collection so corneas could not be selected on the basis of average XRD values,

although the development day that the corneas were harvested from was logged. Therefore, the selection of wild-type and lumican-null tissue samples had to be made on a random basis. As Figure 3.8 shows, collagen fibrils of the posterior wild-type corneal stroma (left) are circular in cross-section and fairly well ordered. Indeed, through successive time points the collagen fibrils seem to become more compacted, signifying the development of a well-ordered corneal stromal matrix. However, on examination of transverse sections of the lumican-null posterior corneal stroma (right), collagen fibrils are widely spaced and disorganised. Significantly, the micrograph taken from the corneal stroma of the 12-day-old lumican knockout mouse presents evidence of the first signs of lateral fusion; in some areas collagen fibrils are in very close proximity to each other, so much so that by day 14, some neighbouring collagen fibrils have fused to form abnormally thick fibrils with irregular borders.

It was apparent from the XRD results and TEM investigation carried out so far that transient stromal thickening in the neonate cornea between days 8 and 14 (Song *et al*, 2003) is not due to a homogenous moving apart of collagen fibrils at this time. Figure 3.9 is an electron micrograph of an oblique section of the 12-day-old wild-type posterior corneal stroma, revealing the presence of what appears to be a 'lake', an area devoid of collagen fibrils.

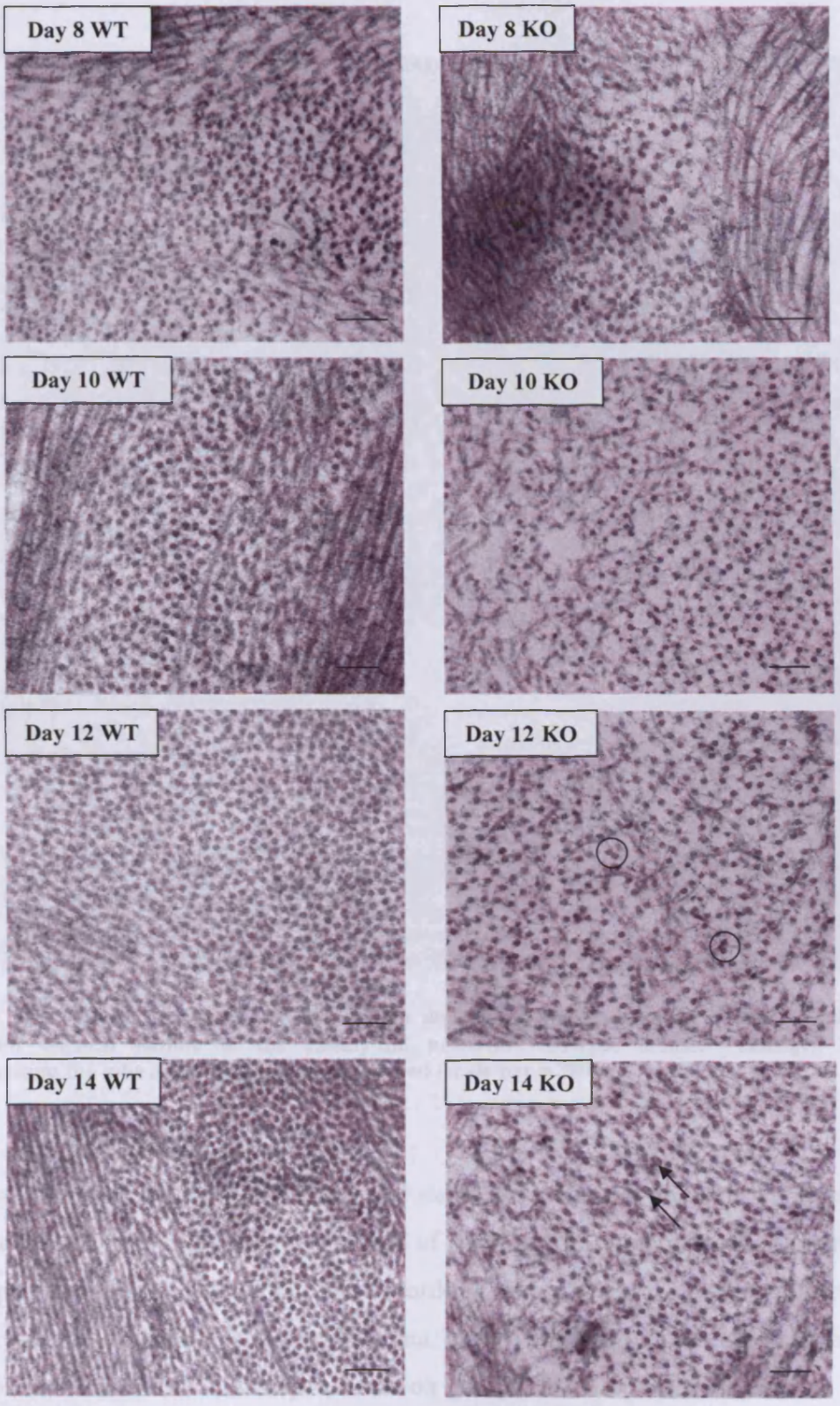

Figure 3.8. TEM revealing that collagen fibrils in the wild-type (WT) posterior stroma become increasingly more well-ordered with time. In contrast, lumican knockout (KO) collagen fibrils are disordered and abnormally thin. Wide fibril spacing is pronounced in the day 8, 10, and 12 knockout corneas. The day 12 lumican-null posterior stroma consists of collagen fibrils that are in very close proximity to each other (circles); by day 14 laterally fused collagen fibrils (arrows) are the result (scale bar = 200 nm).

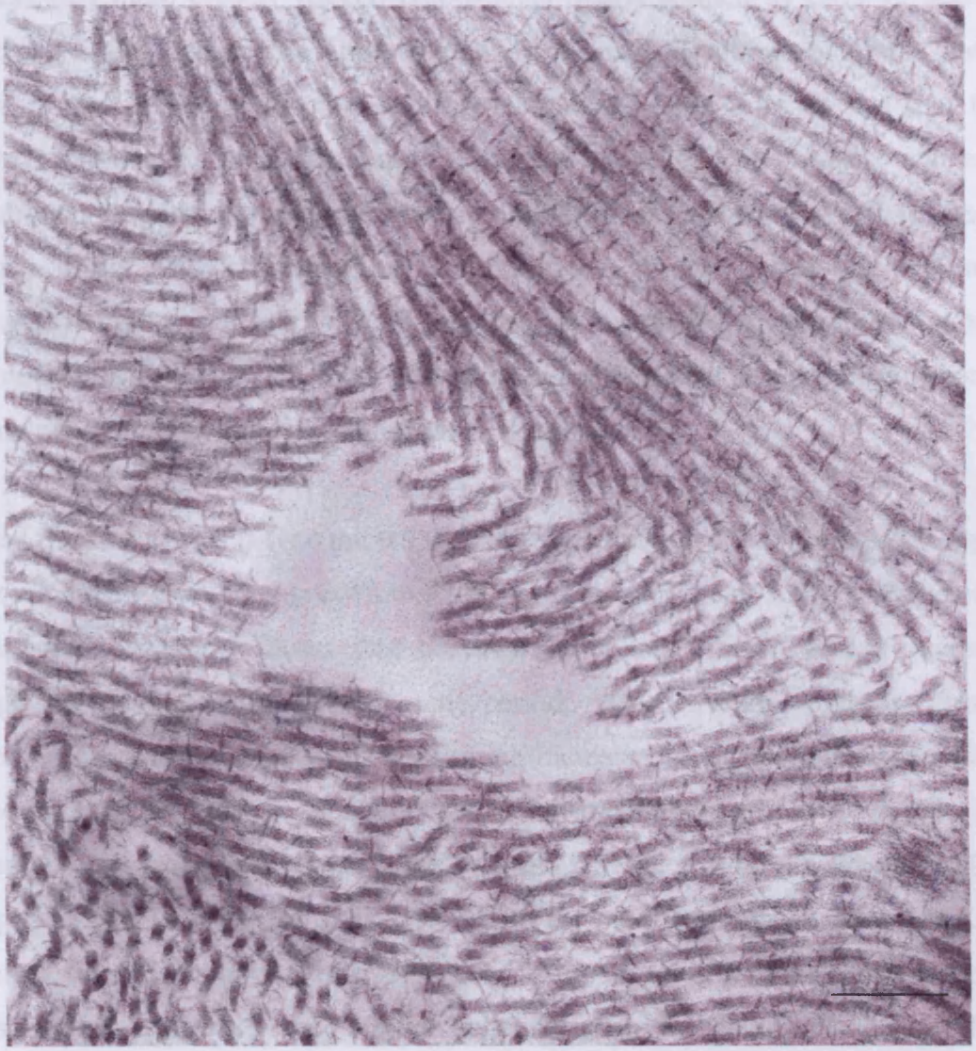

Figure 3.9. Transmission electron micrograph illustrating the presence of a 'lake' within the posterior corneal stroma of the 12-day-old neonatal wild-type mouse. Collagen fibrils surrounding the lake are reasonably well-ordered (scale bar = 300 nm).

3.4 Discussion

In vivo examinations of neonatal corneal development in the mouse have disclosed that the stroma undergoes a critical period of swelling and thinning around the time of eye opening between days 8 and 14. In order to investigate the ultrastructure of the wild-type and lumican-null corneal stroma, and to track any matrix alterations that take place, a series of XRD experiments on groups of 10 or 12 mouse corneas were performed. These results, along with the TEM findings, reveal that neonatal development of wild-type and lumican-null murine corneas is structurally distinctive. During normal development, there is a slight decrease in average fibril spacing between days 10 and 12 at the eye-opening period, and a gradual increase in the average H/W ratio values up to day 14. These findings signify the development of a

progressively more closely packed collagenous matrix formed by days 12 and 14. The compaction of collagen fibrils seen with neonatal development of the mouse cornea is also a feature of embryonic development of the chick cornea (but to a greater extent than in the neonatal mouse), where transparency develops concurrently with stromal thinning (Coulombre and Coulombre, 1958; Connon *et al*, 2004). As the collagen fibrils of normal neonates here are, on average, more widely spaced compared to collagen fibrils of more mature (i.e. 2- to 6-month-old) mouse corneas (Quantock *et al*, 2001), this implies that collagen fibrils of the developing cornea become progressively more closely packed with time.

Stromal thickness in wild-type mice transiently peaks at day 12, to decrease by day 14 and resume slow continued growth to adult thickness (Song *et al*, 2003). The current investigation, however, shows that the average collagen fibril spacing decreases through the 8 to 14 day development period. Consequently, transient stromal thickening cannot be attributed to a matching increase and decrease in fibril spacing around the day 12 window. Rather, stromal thickness changes may be the result of the temporary presence of 'lakes', areas of the corneal stroma devoid of regularly arranged collagen fibrils (Benedek, 1971). As the production of a measurable X-ray reflection depends upon the interference of X-rays scattered by regularly arranged fibrils, regions with little or no regular collagen would not contribute sufficiently to the reflection so the presence of lakes will remain unrecognised. With this reasoning, lakes may constitute cellular components of the stroma such as keratocytes as well as pockets of water. However, as keratocyte density is reported to decrease steadily from neonatal day 7 onwards (Song *et al*, 2003) the more favourable explanation is a brief increase in stromal hydration. Indeed, examination of the posterior corneal stroma from a 12-day-old wild-type mouse revealed that there are regions devoid of collagen among areas of well-organised fibrils (Figure 3.9). It is reasonable to surmise that the onset of eye opening at day 12 might necessitate a prior increase in stromal hydration to counteract atmospheric dehydration. With the knowledge that sulphation of lumican KS chains is detected from neonatal day 10 onwards (Ying *et al*, 1997), this modification may be key to ensuring that the stroma maintains a well-hydrated state. Moreover, sulphation of KS chains might be necessary to prepare the stroma for the initiation of endothelial pump activity. The endothelium is largely responsible for controlling corneal hydration (Hodson, 1971), and in the rat the

endothelial layer begins to develop adult organisation of apical junctional proteins necessary in establishing pump function around neonatal day 13 to day 20 (Joyce *et al*, 1998). It therefore appears that thinning of the stroma after eyelid opening in mice is most likely related to the establishment of endothelial pump activity.

Unlike normal mouse cornea, the lumican-null stroma presents no evidence of thickening at neonatal day 12 (Song *et al*, 2003). The XRD data reveal that the mutant corneal stroma is disorganised with wider-than-normal fibril spacing at days 8, 10, and 12 (Figure 3.4) and substantially lower H/W ratio values at all time points. The findings of a previous biophysical investigation indicate that the effects of lumican absence persist into adulthood as the corneas of 2-month-old and 6-month-old lumican-deficient mice from the same colony had collagen fibrils that tended to be, on average, 2 nm more widely spaced than those of normal littermates (Quantock *et al*, 2001) and considerably more disorganised. So far, the results of the current study suggest that prior to mutant eye opening the cornea consists of a loosely packed stromal matrix. After eye opening, this difference diminishes so that by neonatal day 14 the marginally elevated fibril spacing in the lumican-null corneas is no longer statistically significant. Nevertheless, the ramifications of this drop in fibril spacing will be explored in a moment.

In wild-type mice, the average collagen fibril diameter increases from 31 nm to 32.5 nm (Figure 3.5), similar values to those found for collagen of 4-month-old mouse corneas (Meek *et al*, 2003b). Lumican has been shown in *in vitro* studies to actively inhibit collagen fibril growth, and that this activity resides in the core protein rather than the KS side chains (Birk and Lande, 1981; Rada *et al*, 1993; Moldovan *et al*, 2001). However, this mechanism of fibrillogenesis regulation is not indicated in the lumican-deficient corneas studied here because the collagen fibrils are, throughout the period studied, smaller than normal (29.1 nm to 30.8 nm), with the difference significant or close to significant. These are average values from XRD, and previous electron microscopic studies have found a minor population of unusually large fused collagen fibrils mostly in the adult posterior stroma (Chakravarti *et al*, 2000) that may not contribute appreciably to an XRD pattern. Alternatively, increasing age and continued fibrillogenesis in the absence of lumican may eventually lead to the formation of thicker, irregularly shaped fibrils (Chakravarti *et al*, 2000). Evidence

suggests that this may be the case as 2-month-old lumican-deficient corneas consist of collagen fibrils that have, on average, normal diameters (Quantock *et al*, 2001). Indeed, the XRD data presented here show that collagen within the mutant cornea does increase in size, albeit slowly. Furthermore, the electron microscopy study conducted has, for the first time, presented evidence that with the advent of stromal thinning between days 12 and 14 (Song *et al*, 2003), collagen fibrils come into closer proximity to each other and begin to fuse in the absence of lumican by day 14 (Figure 3.8). This finding is in agreement with the statement made by Chakravarti *et al* (1998) that deregulation of fibrillogenesis has a bearing on fibrillar distance as well as fibril morphology, in that progressive lateral fusion of fibrils displaces fibrils to render the distance between them wider. This certainly appears to be the case from the examination of the posterior stroma of the neonatal day 14 lumican knockout cornea (Figure 3.8), as the area surrounding the larger, fused fibrils is collagen-poor. Similar 'fibril-poor areas' of the posterior stroma have been observed in more mature lumican-null mice (Chakravarti *et al*, 2000). Therefore, as an increase in the distance between neighbouring posterior stromal fibrils results in the loss of destructive interference and a random scattering of light, this may explain the development of corneal opacity in the lumican-deficient cornea over time (Chakravarti *et al*, 1998).

It is generally agreed that the structural characteristics of lumican are required for the development and maintenance of a well-organised corneal stroma. The core protein binds to the collagen fibril to regulate fibril growth, whilst the KS side chains prevent contact of neighbouring fibrils and keep the tissue in a hydrated state via the negatively charged sulphate residues. However, previous research has suggested that lumican is required only for postnatal maturation of the cornea. At neonatal day 7, prior to eye opening in the mouse, stromal thickness (Figure 3.3) and light scattering are not appreciably different in the mutant cornea from normal (Song *et al*, 2003). Additionally, the lumican-deficient corneal stroma appears unremarkable under routine histological examination, although lumican expression is detected in normal tissue between E13.5 and E16.5 stages of development (Chakravarti *et al*, 1998). Increasing amounts of lumican core protein are detected between neonatal days 1 and 10, a period when the eyes are still closed, but sulphated lumican KSPG only begins to accumulate after neonatal day 10 (Ying *et al*, 1997). This post-translational modification of the lumican core protein is concurrent with mouse eye opening and,

as the data gathered here indicates, is an essential component of stromal development. The lumican-deficient cornea has abnormally wider fibril spacing and significantly thinner collagen fibrils even before eye opening, suggesting that lumican is required at this early stage of development. Indeed, the lumican-deficient corneal stroma is abnormally thin both neonatally (Song *et al*, 2003) and in adulthood (Chakravarti *et al*, 2000). The transient stromal thickening witnessed in the normal cornea is not achieved in the mutant cornea, suggesting that this process is lumican dependent.

To conclude, the lumican-deficient cornea is clear at birth, but the evidence gathered indicates that ultrastructural changes are present in the newborn mutant, and that the adult mutant cornea displays remnant structural defects of earlier, postnatal developmental events.

Chapter 4. The effect of lumican mutations on cornea

4.1 Introduction

Corneal stromal architecture appears to be modulated by both collagen-collagen and proteoglycan-collagen interactions. To date, the use of transgenic technology has provided evidence that lumican is a significant element of the corneal stroma during neonatal development (Song *et al*, 2003) and adulthood (Chakravarti *et al*, 1998; 2000; Quantock *et al*, 2001) via ablation of murine lumican (*Lum*) gene expression. Recently, the role of lumican N-terminal region in collagen fibrillogenesis, and the consequences of lumican over-expression on corneal stromal morphology, have been explored.

4.1.1 The effect of lumican over-expression in the mouse cornea

The development of lumican knockout mice has shown that expression of the *Lum* gene is imperative for the development of a healthy cornea. Carlson *et al* (2005) primarily set out to determine the effect of excess lumican in cornea, and achieved tissue-specific expression of lumican in the corneas of wild-type mice via pronuclei injection of a lumican mini-gene (pSecLum) encoding lumican-c-myc-tag fusion protein (under the control of the 3.2 kb keratocan promoter). Mice were between 8- and 12-weeks-old at the time of investigation (Dr Eric Carlson, personal communication). Three transgenic mouse lines were positive for mini-gene expression, *Kera-Lum5*, *-25*, and *–38* (also termed lumWT), with lumican 3-4 fold higher in transgenic lines than non-transgenic (NTG) controls as shown by Western blot analysis. Whereas lumican absence renders the corneal stroma thinner than normal (Chakravarti *et al*, 2000), examination of corneas over-expressing lumican by *in vivo* confocal microscopy revealed no differences in epithelial and stromal thickness when compared with NTG controls (Carlson *et al*, 2005). Although the level of light scattering appeared higher in transgenic mice compared to NTG controls, this was not regarded as significant. Nevertheless, the authors reported that the corneas of mouse lines showing higher levels of transgene expression (lumWT38) show higher levels of haze than those of mouse lines with lower levels of transgene expression (lumWT5). Further investigation via TEM revealed that corneal collagen architecture of lumWT5 and lumWT38 was almost identical to that of NTG control, with similar fibril diameters, fibril spacing and packing. However, occasionally, there

was evidence of regions where collagen fibrils were less well-ordered in the transgenic lines (Figure 4.1).

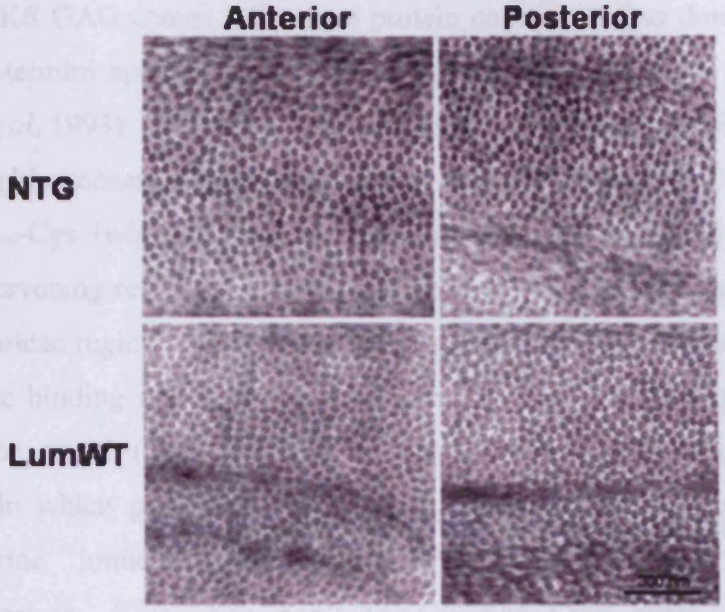

Figure 4.1. Transmission electron micrographs that show similar fibrillar architecture in the corneal stroma of NTG and lumWT mouse corneas. The collagen fibril diameters in corneas of NTG control and lumWT corneas are virtually identical. In addition, fibril packing and spacing of lumWT are unremarkable. Identical results were observed in both the anterior and posterior regions of the stroma. Bar = 300 nm (from Carlson *et al*, 2005).

During this investigation, Carlson *et al* deduced that keratocan expression is regulated by lumican at the transcriptional level. Using Western blot analysis they found that keratocan expression was upregulated to 5-6 times higher than normal when lumican is excessively expressed. Furthermore, when the lumican-null mouse cornea was intrastromally transfected with the pSecLum plasmid cDNA, not only was lumican expression now detected but also there was a 2-fold increase in keratocan expression. The authors concluded that whereas disrupted corneal morphology in the absence of lumican (Chakravarti *et al*, 1998; 2000; Quantock *et al*, 2001) indicates that precise corneal morphogenesis requires a minimal concentration of lumican KSPG, an overabundance of lumican appears to have no adverse effects on stromal collagen fibril architecture.

4.1.2 The role of lumican N-terminal region in collagen binding

The hybrid structure of lumican bestows this molecule the ability to regulate collagen fibrillogenesis via the protein core, and to modulate fibril spacing and hydration via the sulphated KS GAG chains. The core protein consists of four domains of which the N- and C-termini appear involved in collagen binding as shown by an *in vitro* study (Rada *et al*, 1993). The domain proximal to the N-terminus of lumican contains a cluster of highly conserved Cys residues with consensus sequence Cys-Xaa_{2-3}-Cys-Xaa-Cys-Xaa_{6-9}-Cys (where Xaa is any amino acid and the subscripts denote the number of intervening residues). The disulphide loop between Cys^{41} and Cys^{53} of the N-terminal lumican region may be essential for proper folding of this domain, thereby modulating the binding of lumican to collagen (Carlson *et al*, 2003). To test this theory, Carlson *et al* (2003) created a Cys-Ser substitution using site-specific mutagenesis, in which plasmid DNA encoding wild-type (termed LumWT by the authors) murine lumican (Cys^{37}-Xaa_3-**Cys^{41}**-Xaa-Cys-Xaa_9-Cys) and mutant (LumC/S) lumican (Cys^{37}-Xaa_3-**Ser^{41}**-Xaa-Cys-Xaa_9-Cys) were prepared and transfected into MK/T-1 keratocytes, an immortalised cell line derived from cultured corneal stromal cells (Gendron *et al*, 2000). When cultured, both cell lines grew a three-dimensional, multi-layered stroma *ex vivo*. However, the Cys-Ser point mutation impaired the ability of lumican to bind collagen fibrils as immunofluorescent staining revealed poor co-localisation of lumican with collagen type I in the mutant ECM. The authors obtained micrographs of lumWT and lumC/S ECMs, which they claimed to reveal disorganised collagen fibrils of varying, but mostly larger-than-normal, diameters in the mutant cell cultures (Figure 4.2).

These results suggest that the cysteine-rich domain of lumican is important in collagen fibrillogenesis and stromal matrix assembly.

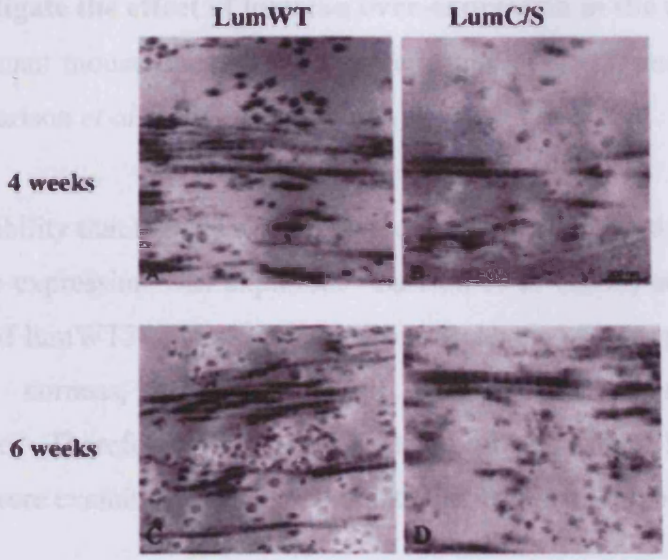

Figure 4.2. TEM of collagen fibril matrix formed by lumWT (wild-type - left panels) and lumC/S (mutant - right panels) stable transformants after 4 weeks (upper panels) and 6 weeks (lower panels). LumWT samples appear to consist of more uniform-diameter orthogonal fibrils than the lumC/S mutant, presumably perturbing collagen fibrillogenesis (Carlson *et al*, 2003) (scale bar as shown in B = 300 nm).

4.1.3 Experimental aims

Based on the findings of the aforementioned studies by Carlson *et al* (2003; 2005), the following aims were addressed:

To examine age-related structural changes in NTG control tissue

- Corneas were obtained from lumican over-expressing (lumWT) and lumican Cys/Ser mutated (lumC/S) mice of various ages, ranging from 1.5-months-old to 12-months-old. However, it was only possible to collect NTG corneas from 1.5-month-old and 2.5-month-old mice. So to determine whether data collected from older mutants could be statistically compared with that of younger controls, it was necessary to establish if collagen fibril spacing and diameter changes naturally occur with increasing age. Therefore, data collected from NTG control corneas from 1.5-month-old and 2.5-month-old mice were compared statistically.

To investigate the effect of lumican over-expression in the mouse cornea

- Three mutant mouse lines were compared; lumWT5, -25, and -38 (termed *Kera-lum* by Carlson *et al*, 2005) using XRD.

- The possibility that there is a link between corneal clarity and the level of lumican transgene expression was explored. Carlson *et al* (2005) stated that the hazier corneas of lumWT38 animals showed higher levels of transgene expression than lumWT5 corneas, although overall stromal architecture seemed largely unaffected. Therefore, prior to XRD data collection, both NTG and transgenic corneas were examined by eye to estimate the degree of corneal clarity.

- Carlson *et al* (2005) performed a TEM investigation of NTG and lumWT corneas using routine fixation with osmium tetroxide, and observed no major differences in fibril arrangement or diameter, although small isolated areas of disordered fibrils were evident. These observations led the investigators to postulate that excess lumican might not be influential due to the limited number of binding sites on each collagen fibril. So why are mutant corneas presenting slightly elevated levels of haze? It is possible that excess sulphated lumican may disturb stromal hydration by causing it to swell. Therefore, the primary aim of the TEM investigation here was to establish if the mutant corneal stroma contains 'lakes', areas devoid of collagen fibrils. In light of the knowledge that lumican over-expression results in upregulation of keratocan expression, tissue samples were prepared using cupromeronic blue staining to see if there were any obvious changes in proteoglycans. However, no quantitative measurements were made.

To investigate the role of lumican N-terminal region in collagen binding

- Carlson *et al* (2003) examined ECM deposition and fibril structure by three lumC/S cell lines (i.e. lumC/S2, -12 and -39). The primary aim of this study was to explore the implications of lumican C/S mutation *ex vivo* via the XRD investigation of corneas from lumC/S3 and lumC/S8 transgenic mice.

- The MK/T-1 cells selected for lumWT and lumC/S transfection are known to express lumican, mimecan, decorin, and collagen α1 chains, but not keratocan (Gendron *et al*, 2000), signifying that the cells may not reflect the true corneal keratocyte phenotype. Also, in view of recent evidence that the lumican-null cornea is severely affected due to significant down-regulation of keratocan (Carlson *et al*, 2005), and the possibility that MK/T-1 cells might not be capable of performing glycosylation of recombinant lumican (Carlson *et al*, 2003), it was necessary to assess the impact of this lumican mutation in corneal tissue.

- Carlson *et al* (2003) found that there was a lack of lumican-collagen binding within the multi-layered stroma produced by lumC/S cell lines, and that the collagen fibrils appeared to be of larger-than-normal diameter. Indeed, the inability of mutant lumican to bind collagen in cornea may have similar repercussions on corneal fibril morphology to a lumican-null mutation, whereby lateral fibril fusion takes place (Chakravarti *et al*, 2000). Therefore, XRD analysis was performed to gain an indication of the average collagen fibril spacing and diameter, while TEM using cupromeronic blue staining was conducted to assess collagen fibril architecture, to look for evidence of laterally fused collagen fibrils, and to look for any obvious changes in collagen-proteoglycan associations.

- In an attempt to find out if a lumC/S mutation leads to the development of corneal opacity, both NTG control and mutant corneas were examined by eye to estimate the degree of corneal clarity before XRD data collection.

4.2 Materials and Methods

4.2.1 Tissue samples

All corneas examined were kindly supplied by Professor Winston Kao, University of Cincinnati. Dr Eric Carlson generated the lumWT and lumC/S mouse lines by cloning the lumWT and lumC/S constructs created as published (Carlson *et al*, 2003) into the ClaI and SalI sites of the *Kera-lum* mini-gene (Carlson *et al*, 2005), followed by pronuclei injection into fertilized mouse eggs. Tissue specific expression of the

transgenes was achieved using the pKera promoter as oppose to pCMV (Carlson *et al*, 2004).

NTG control tissue

Corneas from 1.5-month-old (n = 7) and 2.5-month-old (n = 9) NTG mice acted as control tissue within statistical comparisons.

Lumican over-expressing corneal tissue

Corneas were from mice of three different transgenic mouse lines, namely lumWT5, lumWT25, and lumWT38. LumWT5 corneas from 1.5-month-old (n = 9) and 7-month-old (n = 9) mice were examined, as well as lumWT25 corneas from 12-month-old mice (n = 11). LumWT38 corneas from 2.5-month-old (n = 12), 4.5-month-old (n = 12) and 9.5-month-old (n = 2) mice were also examined, but data from corneas of the latter mutant age group were not included in statistical analysis due to the low sample number, but are tabulated for the reader's interest.

Lumican N-terminal C/S mutated corneal tissue

Two transgenic mouse lines were of interest, designated lumC/S3 and lumC/S8. The lumC/S3 corneas were excised from 9.5-month-old (n = 6) and 12-month-old (n = 4) mice. The lumC/S 8 corneas were collected from 1.5-month-old (n = 10), 4-month-old (n = 12) and 9-month-old (n = 3) mice.

Mice were sacrificed via CO_2 asphyxiation followed by cervical dislocation. The excision of corneal tissue (with sclera attached) using scissors and forceps was performed by the author with the help of an assistant in Professor Kao's laboratory. Each cornea was removed with sclera attached to ensure that proper alignment of the X-ray beam with the central portion of the cornea would be achieved. The next stage involved the immersion of each cornea in isopentane (cooled in liquid nitrogen) using forceps, wrapping them in clingfilm and storing them in labelled eppendorf tubes on dry ice. However, the first cornea immersed in isopentane was extremely difficult to detach from the forceps until thawed. Therefore, this cornea was discarded and the remainder were wrapped in clingfilm prior to freezing. All samples were stored on dry ice and shipped to Cardiff University. On arrival, the samples were placed in a -80°C freezer until XRD and TEM were undertaken.

4.2.2 Low-angle XRD

Prior to XRD data collection on Station 2.1, observations of corneal clarity were recorded to ascertain if there is a relationship between corneal clarity, genotype, and age of the animal at the time of tissue collection. The scores allocated were simply estimated on the basis of my own observations, as it was not possible to obtain a second opinion at the time. Therefore, the values for each group were not subjected to statistical analysis. Nevertheless, the following grading system denotes the appearance of each tissue sample prior to XRD:

Grade allocated	C/C
0	Clear
1	Slightly hazy
2	Hazy
3	Slightly milky
4	Milky
5	Slightly cloudy
6	Cloudy
7	Very cloudy

Table 4.1. Degree of corneal clarity (C/C) as judged with the naked eye.

4.2.2.1 Collection of XRD data

XRD patterns were collected as detailed in Section 2.2.2. Specifically, shutters were opened for a 2 minute exposure of each cornea, and a detector response from an 8 hour exposure to Fe^{55} was subtracted from each XRD pattern.

Data analysis was undertaken following the procedure outlined in Section 2.3, and background subtraction was undertaken as outlined in Step 2(A). Additionally, Step 5 details the calculation of interfibrillar peak H/W ratio, whereby the peak height is divided by the peak width at half-height. However, during data collection the attenuation had to be changed a number of times due to ion chamber readings exceeding 20,000 counts, which may affect the X-ray intensity (and therefore the observed peak height) from pattern-to-pattern. It was possible to determine that peak width at half-height does not change with varying X-ray intensity of a given pattern, so it was possible to use this measurement to indicate the degree of fibrillar order within each cornea i.e. the smaller the peak width value, the more ordered the collagen fibrils.

4.2.3 Transmission electron microscopy

Corneas were selected on the basis that the average fibril spacing and diameter values from XRD closely matched the values of the group they represent. NTG control tissue from a 2.5-month-old mouse (specimen 8, Table 4.2) was examined within lumican over-expression and lumican N-terminal Cys/Ser mutation studies. In the lumican over-expression study, tissue from a 1.5-month-old lumWT5 mouse (specimen 3, Table 4.3), a 2.5-month-old lumWT38 mouse (specimen 7 of Table 4.4), and a 12-month-old lumWT25 mouse (specimen 1, Table 4.5) were examined. In the lumican N-terminal C/S mutation study, tissue from a 9.5-month-old lumC/S3 mouse (specimen 4, Table 4.6) and a 9-month-old lumC/S8 mouse (specimen 1, Table 4.7) were investigated. Tissue staining and embedding, block trimming and sectioning, and staining of grid sections (2.4.3A) are outlined in Section 2.4. Sections were collected on 300 mesh hexagonal copper grids on Formvar support film.

4.3 Results of NTG control study

For details of statistical analysis, refer to Appendix 3. All *P*-values quoted were obtained by Independent samples t-test, unless otherwise stated.

Age (months)	n	C/C	IFS (nm)	CFD (nm)	P/W (nm)	t (nm)
1.5	1	0	61.6	35.7	30.5	314
	2	0	67.4	36.4	33.4	344
	3	0	58.0	33.9	30.4	276
	4	0	57.2	31.5	27.2	287
	5	0	51.6	32.8	25.7	269
	6	0	63.5	40.6	37.0	295
	7	0	66.5	42.2	36.7	321
2.5	1	0	53.4	36.7	26.7	242
	2	0	54.4	36.4	27.0	295
	3	0	56.4	37.4	26.5	299
	4	0	48.0	34.1	24.5	264
	5	0	48.0	33.9	23.3	269
	6	0	48.0	32.4	22.3	275
	7	0	63.0	40.0	37.0	295
	8	0	54.0	34.5	27.1	285
	9	0	62.0	34.8	33.0	300

Table 4.2. Degree of corneal clarity (C/C) of each NTG control specimen (n), and collagen fibril Bragg spacing (IFS), collagen fibril diameter (CFD), peak width at half-height (P/W), and coherence distance (t) values.

Corneal tissue was collected from mutant animals ranging between 1.5-months-old and 12-months-old, but unfortunately NTG tissue from animals older than 2.5 months was not available. Thus, at this stage of the investigation it was necessary to determine if the data obtained from NTG control tissue could be statistically compared with that of older transgenic tissue. Collagen fibril spacing and fibril diameter data obtained from NTG corneas of 1.5-month-old and 2.5-month-old mice were compared to establish whether these structural parameters naturally change with time. Attention was paid to the range of individual measurements within each data set, as this gives an indication of natural variability.

4.3.1 Effect of age on NTG corneal collagen morphology

All NTG control corneas appeared perfectly clear and so were allocated grade 0 (Table 4.2). Statistical comparison of NTG groups at 1.5 months (n = 7) with that of 2.5 months (n = 9) revealed that fibril spacing is wider in younger animals (60.8 ± 5.6 nm vs. 54.1 ± 5.7 nm respectively) ($P = 0.034$). However, the average collagen fibril diameter does not appear to change with time (36.2 ± 4.0 nm vs. 35.6 ± 2.3 nm) ($P = 0.718$). In order to gain an appreciation of collagen fibril order within the stroma, the interfibrillar peak width at half-height was calculated, with narrower peak widths indicative of an interfibrillar reflection created by a well-ordered collagen fibril array. The average values obtained for 1.5 month and 2.5 month groups are 31.6 ± 4.4 nm and 27.5 ± 4.7 nm respectively ($P = 0.099$). The average coherence distance values for 1.5 and 2.5 months are similar, at 301 ± 27 nm and 280 ± 20 nm respectively.

So far, the results show that the average fibril diameter has been found to remain essentially the same between 1.5 months and 2.5 months. However, the discovery that fibril spacing appears to decrease over this time period prompts further investigation to find out if wild-type data from other chapters could be used to compare with mutant data here. In order to do so, scatter graphs of individual fibril spacing and fibril diameter measurements were plotted using the NTG control data from this investigation, as well as data from wild-type corneas from 4-month-old (Chapter 5) and 10-month-old (Chapter 6) mice.

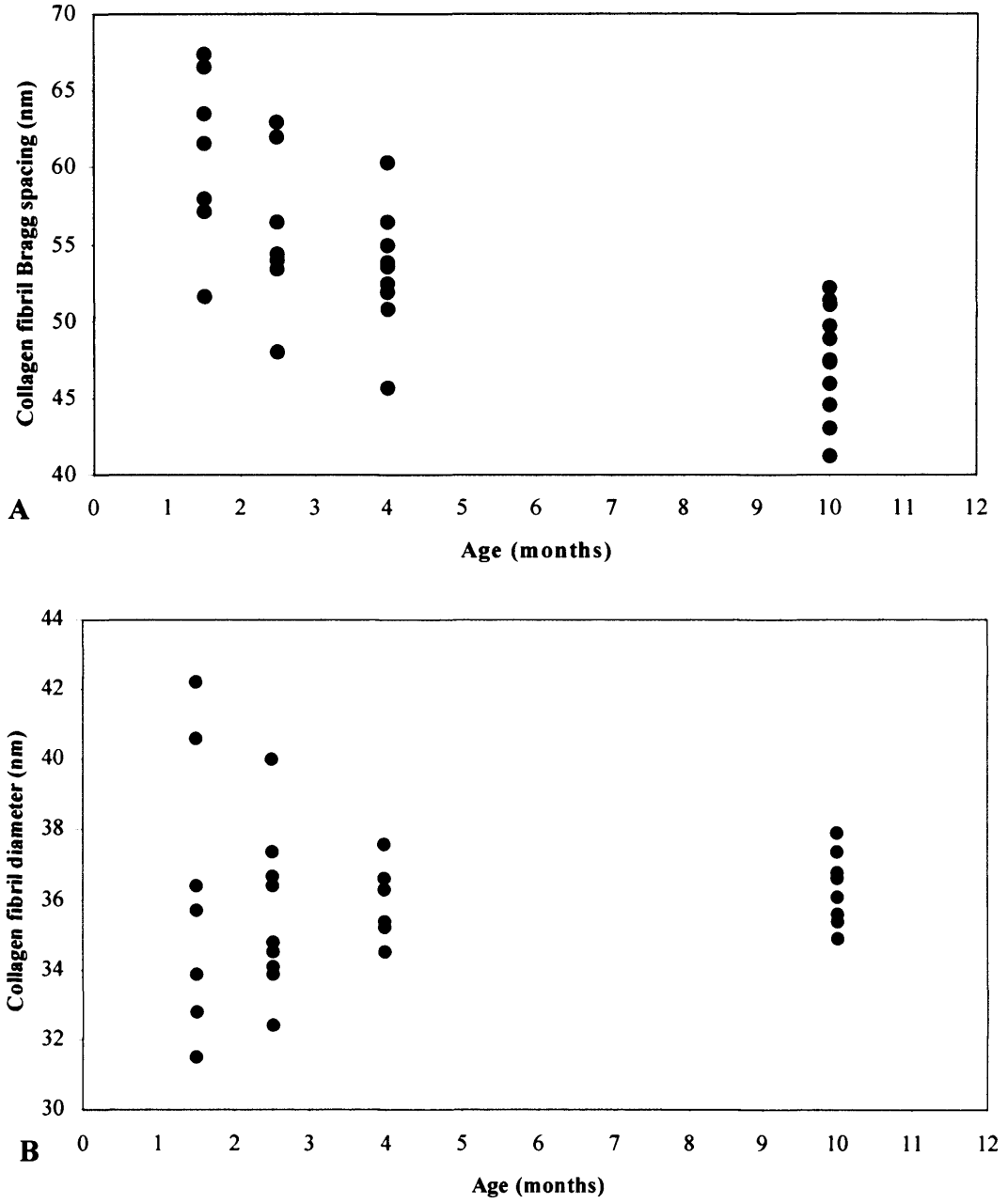

Figure 4.3. Scatter plot of individual collagen fibril Bragg spacing (A) and collagen fibril diameter (B) measurements from NTG control corneas (1.5 and 2.5 months), wild-type corneas at 4 months (Chapter 5), and wild-type corneas at 10 months (Chapter 6).

The data suggests there is a negative correlation between collagen fibril spacing and age (Figure 4.3A). Pearsons product-moment correlation coefficient reflects the extent of a linear relationship between data sets. In this case, the coefficient of determination is 0.42 or 42%, signifying that 42% of variability in fibril spacing is attributed to the variability in age. It must be stressed that this coefficient does not relay causation in any way, in that increasing age causes a decrease in fibril spacing,

purely that there is some link between the two. However, it appears that, irrespective of within-group variability, fibril diameter seems to be unrelated to age of the animal (Figure 4.3B). A coefficient of 0.01 or 1%, it was calculated, so only 1% proportion of variability in fibril diameter is attributed to the variability in age. Therefore, when studying corneal collagen fibril diameter, age is unlikely to be an important factor.

4.3.2 Discussion

The aim of this stage of the investigation was to develop an appreciation of natural variability within normal corneas through the examination of data collected from NTG control tissue. However, firm conclusions cannot be drawn from comparisons with data of previous biophysical investigations due to differences in genetic background, tissue storage, and data handling i.e. background subtraction.

Natural variations in collagen fibril spacing and collagen fibril diameter

Examination of NTG control corneas from 1.5-month-old and 2.5-month-old animals disclosed that there is natural variability in collagen spacing measurements. At 1.5 months of age, the average fibril spacing value of 60.8 ± 5.6 nm comprises individual measurements ranging from 51.6 to 67.4 nm (n = 7). Similarly, at 2.5 months fibril spacing shows variability between individuals ranging from 48 to 63 nm (n = 9) to produce an average value of 54.1 ± 5.7 nm. These natural differences have previously been found by other biophysical investigations. For instance, an XRD study conducted by Meek and Leonard (1993) revealed that the cornea of the mouse (*Mus musculus*) consists of collagen fibrils with an average fibril Bragg spacing of 64.6 ± 6.5 nm (n = 3). Also, Quantock *et al* (2001) used XRD to determine that 2-month-old wild-type mouse corneas (n = 2) have average fibril Bragg spacing measurements of 49.2 and 56 nm. Indeed, Gyi *et al* (1988) reported that natural variation is rather pronounced in rodent corneas.

An interesting finding of this study was the variation in fibril diameter measurements. At 1.5 months, an average value of 36.2 ± 4 nm consisted of five individual values ranging from 31.5 to 36.4 nm and two values at around 41 nm. Similarly, an average fibril diameter measurement of 35.6 ± 2.3 nm at 2.5 months came from eight individual diameter values ranging from 32.4 to 37.4 nm and one value at 40 nm.

These values are interesting, as collective fibril diameters have previously been shown to be relatively consistent. For instance, Quantock *et al* (2001) found individual diameter measurements from 2-month-old mouse corneas to be approximately 35 nm, while Meek and Leonard quoted a fairly consistent fibril diameter value of 39.7 ± 1.8 nm for mouse (1993). Nevertheless, these values were obtained from 2 and 3 corneas respectively, which may not truly reflect natural variation. Each group within this study consisted of a larger sample number, and when descriptive statistics were calculated the average values obtained were similar to that reported by Quantock *et al* (2001). Also, Figure 4.3B illustrates that there does tend to be more variability in collagen fibril diameter measurements within younger age groups. Therefore, with this reasoning and the normal appearance of all NTG control corneas prior to data collection, I am satisfied that these measurements should be included in statistical analysis.

Changes in collagen fibril spacing and fibril diameter with increasing age

The average collagen fibril diameter at 1.5 and 2.5 months are similar, but collagen fibril spacing is wider in the cornea of younger subjects. Similarly, Quantock *et al* (2001) showed that fibril diameter values obtained from 6-month-old wild-type mouse corneas are virtually identical to those at 2 months, but that fibril Bragg spacing appears to drop slightly over this time period. Although the methods of tissue storage and background subtraction differ to those adopted in this investigation, the current findings seem to suggest that fibril spacing naturally decreases over time. Indeed, a TEM study of gluteraldehyde fixed human corneas from 16-, 46-, and 80-year-old subjects revealed that fibril diameters are essentially unchanged with increasing age, but that aged corneal stroma displays decreased interfibrillar distances and multiple collagen-free spaces corresponding to an area of 1 or 2 collagen fibrils (Kanai and Kaufman, 1973). So, in order to extend this age study and explore the concept that the changes found continue to take place with increasing age of the mouse, the individual measurements from wild-type corneas of other Chapters were used. Indeed, the distance between the collagen fibrils of the ageing cornea appears to decrease, whereas fibril diameter does not change. So what is the significance of these findings? It is important to compare collagen fibril spacing data of transgenic mouse corneas with that of age-matched NTG control corneas only. Although the

results of this study indicate that fibril diameter data of NTG controls corneas could be compared with that of older transgenic tissue, using age-matched comparisons will ensure that fair comparisons are made, as the full implications of transgene integration are not known. For instance, Carlson *et al* (2005) showed that transgene expression could have a bearing on the expression of other genes by demonstrating that upregulation of lumican expression at the transcription level results in the upregulation of keratocan.

To conclude, the transgenic studies of lumican over-expression and lumican N-terminal C/S mutation to follow will involve the use of age-matched NTG control data. However, for those mutants without an age-matched control, the collagen fibril diameter data will be statistically compared with data of close age-matched wild-type corneas (Chapters 5 and 6). The results obtained in this situation will be examined purely to gain an indication of whether ultrastructural differences may exist.

4.4 Results of lumican over-expression study

This study deals with the investigation of corneas that over-express lumican in three transgenic mouse lines, lumWT5, lumWT25, and lumWT38. The previous study of NTG control corneas revealed that collagen fibril spacing naturally decreases with time. Consequently, lumWT5 and lumWT38 corneas were investigated for similar age-related patterns of change prior to statistical comparison with age-matched NTG controls. Then, the collagen fibril diameter data of lumWT25 corneas (collected from 12-month-old mice) were compared with that obtained from 10-month-old wild-type corneas in Chapter 6.

For details of statistical analysis refer to Appendix 3. All *P*-values quoted were obtained by Independent samples t-test unless otherwise stated.

4.4.1 LumWT5 founderline

Age (months)	n	C/C	IFS (nm)	CFD (nm)	P/W (nm)	t (nm)
1.5	1	4	60.0	39.1	31.0	301
	2	6	65.0	43.2	28.0	393
	3	6	60.0	38.3	24.8	354
	4	6	56.0	37.2	29.5	272
	5	6	65.0	40.6	36.0	324
	6	6	46.0	36.7	15.0	344
	7	6	53.7	38.0	26.7	295
	8	4	52.4	37.0	24.8	289
	9	4	63.0	40.0	26.0	379
7	1	7	68.0	38.3	39.1	314
	2	1	62.0	38.8	33.3	302
	3	5	59.0	37.2	30.0	287
	4	7	64.0	41.2	22.0	494
	5	7	47.5	36.7	16.6	342
	6	1	46.0	35.7	17.6	306
	7	5	57.5	38.8	23.0	344
	8	1	47.0	35.0	17.5	317
	9	5	58.0	36.4	27.8	302

Table 4.3. Degree of corneal clarity (C/C) of each lumWT5 specimen (n), and collagen fibril Bragg spacing (IFS), collagen fibril diameter (CFD), peak width at half-height (P/W), and coherence distance (t) values.

All lumWT5 corneas displayed some degree of haze. Scores of the 1.5-month-old group range from 4 to 6, whereas those of the 7-month-old group displayed more variation, ranging from 1 to 7 (Table 4.3).

Change in lumWT5 collagen fibril morphology with increasing age

The diameter of collagen fibrils does not appear to change with increasing age, as the average values obtained from the 1.5-month-old (38.9 ± 2.1 nm) and 7-month-old (37.6 ± 1.9 nm) groups are similar (P = 0.177). However, the earlier finding of a decrease in fibril spacing over time in NTG controls is not found in lumWT5 corneas. In fact, comparison of the average fibril spacing values at 1.5 months (57.9 ± 6.4 nm) and 7 months (56.6 ± 8.0 nm) reveals that collagen fibril spacing is essentially unchanged with time. The average peak width at half-height values of the 1.5-month-old age group (26.9 ± 5.7 nm) and 7-month-old group (25.3 ± 7.9 nm) are similar (P = 0.638); as are the coherence distance values of 1.5-month-old and 7-month-old groups (328 ± 42 nm and. 372 ± 133 nm respectively). These results indicate that, overall, the ordering of collagen fibrils in the corneal stroma of lumWT5 mice is unchanged with time.

The next step was to determine whether lumWT5 corneas are ultrastructurally distinct from NTG control counterparts at 1.5 months of age.

Effect of excess lumican in lumWT5 corneas at 1.5 months

LumWT5 corneas displayed some degree of opacity as opposed to the clear NTG corneas (Table 4.3), suggestive of ultrastructural differences. However, average fibril spacing of lumWT5 tissue (57.9 ± 6.4 nm) is similar to that of NTG control (60.8 ± 5.6 nm) (P = 0.356). Also, average fibril diameter values of mutant corneas (38.9 ± 2.1 nm) are no different from normal (36.2 ± 4.0 nm) (P = 0.095). Overall, collagen fibril architecture appears to be equally well ordered in the mutant and NTG control corneas. The average values obtained from peak width at half-height measurement for NTG control (31.6 ± 4.4 nm) and lumWT5 (26.9 ± 5.7 nm) groups are similar (P = 0.093), as are the average coherence distance values of the respective groups (301 ± 27 nm vs 372 ± 133 nm).

4.4.2 LumWT38 founderline

Age (months)	n	C/C	IFS (nm)	CFD (nm)	P/W (nm)	t (nm)
2.5	1	6	63.0	35.7	35.0	295
	2	6	62.5	37.7	32.5	310
	3	0	53.0	35.7	27.2	275
	4	4	62.0	37.2	32.3	311
	5	4	50.5	32.6	24.4	271
	6	4	56.0	33.4	23.4	315
	7	4	58.0	36.7	29.4	296
	8	4	69.6	41.9	41.0	317
	9	4	55.4	36.9	28.5	285
	10	4	62.5	38.5	30.6	327
	11	1	49.4	32.8	26.0	248
	12	1	56.0	33.4	32.0	254
4.5	1	5	55.0	36.9	21.6	353
	2	5	60.0	36.9	32.3	291
	3	5	60.0	38.8	32.3	290
	4	5	59.0	36.2	30.0	298
	5	5	52.4	36.2	21.0	317
	6	5	51.0	34.8	22.7	295
	7	1	45.0	32.6	15.5	335
	8	1	57.0	36.2	32.0	280
	9	4	65.0	44.3	26.5	419
	10	4	64.0	43.6	25.8	430
	11	4	56.5	36.4	28.1	291
	12	4	80.0	46.6	22.9	360
9.5	1	1	58.4	37.4	31.0	285
	2	1	69.0	41.9	44.6	295

Table 4.4. Degree of corneal clarity (C/C) of each lumWT38 specimen (n), and collagen fibril Bragg spacing (IFS), collagen fibril diameter (CFD), peak width at half-height (P/W), and coherence distance (t) values.

The corneal clarity scoring based on visual observations for lumWT38 corneas belonging to the 2.5-month-old group ranged from 0 to 6, while lumWT38 corneas of the 4.5-month-old group displayed scores ranging from 1 to 5 (Table 4.4).

Change in lumWT38 collagen fibril morphology with increasing age

The average collagen fibril diameter values at 2.5 months (36.0 ± 2.7 nm) and 4.5 months (38.3 ± 4.3 nm) are not significantly different (Mann-Whitney test, P = 0.284). Interestingly, collagen fibril spacing in the corneas of lumWT38 mice does not decrease with increasing age, as the average values at 2.5 months (58.1 ± 5.9 nm) and 4.5 months (58.7 ± 8.7 nm) are similar (P = 0.850). The interfibrillar peak width measurements are borderline significantly different (30.2 ± 4.9 nm vs. 25.9 ± 5.3 nm)

(P = 0.051), and the coherence distance results of 292 ± 26 nm and 329 ± 51 nm are fairly similar. These findings indicate that collagen fibril architecture of lumWT38 corneas is, on average, unchanged with increasing age of the animal.

To explore the effect of lumican over-expression in the cornea of lumWT38 mice, data was statistically compared with that of age-matched NTG controls.

Effect of excess lumican in lumWT38 corneas at 2.5 months

LumWT38 corneas appeared hazy in contrast with the clear NTG corneas. However, mutant corneas are, on average, no different to normal at the ultrastructural level. Collagen fibril spacing in lumWT38 appears slightly wider (58.2 ± 5.9 nm), but is statistically similar to NTG control values (54.1 ± 5.7 nm) (P = 0.134). The average collagen fibril diameter of mutant corneas was unremarkable when compared to age-matched controls (36.0 ± 2.7 nm vs. 35.6 ± 2.3 nm respectively; P = 0.685). These findings are supported by the similar fibril peak width measurements, with the average value for mutants being marginally wider than normal (30.2 ± 4.9 nm vs. 27.5 ± 4.7 nm respectively) but not significantly so (P = 0.218). Finally, the coherence distance values are, on average, very similar between NTG control (280 ± 20 nm) and lumWT38 (292 ± 26 nm).

Effect of excess lumican in lumWT38 corneas at 4.5 months

To gain an indication of the effect of excess lumican in the lumWT38 cornea at 4.5 months of age, a statistical comparison of the average collagen fibril diameter value was made with that of 4-month-old wild-type corneas from Chapter 5. The average collagen fibril diameter of lumWT38 corneas (38.3 ± 4.3 nm) was not significantly different from that of wild-type corneas (35.9 ± 0.9 nm) (Mann-Whitney test, P = 0.199), indicating that excess lumican may not have a marked affect on collagen fibril diameter.

4.4.3 LumWT25 founderline

Age (months)	n	C/C	IFS (nm)	CFD (nm)	P/W (nm)	t (nm)
	1	5	62.0	39.4	33.5	306
	2	5	68.0	42.2	35.6	359
	3	5	52.3	36.0	26.6	272
	4	5	68.0	41.9	32.6	370
	5	5	62.0	40.9	27.0	340
12	6	6	56.0	36.7	28.5	278
	7	6	65.0	41.9	36.6	313
	8	6	82.0	48.8	43.1	370
	9	6	61.8	36.9	35.0	280
	10	6	56.0	36.2	29.7	272
	11	5	60.6	38.3	29.7	320

Table 4.5. Degree of corneal clarity (C/C) of each lumWT25 specimen (n), and collagen fibril Bragg spacing (IFS), collagen fibril diameter (CFD), peak width at half-height (P/W), and coherence distance (t) values.

The corneal clarity scorings for lumWT25 corneas are fairly consistent, being either 5 or 6 (Table 4.5). The average collagen fibril diameter of wild-type corneas from 10-month-old mice is significantly smaller than that of lumWT25 at 12 months (36.5 ± 0.9 nm vs. 39.9 ± 3.8 nm respectively) (Mann-Whitney test; $P = 0.008$). However, although the average value of the data of this wild-type group is similar to that of the NTG controls, there is very little within-group variation, which may explain why an appreciable difference has been found.

4.4.4 Transmission electron microscopy

The XRD results of this investigation have indicated that over-expression of lumican has very little effect on corneal stromal ultrastructure in that mutant collagen architecture is, on average, similar to normal. However, with the exception of one lumWT38 cornea, all other tissue samples displayed some degree of corneal haze. It is known that lakes, areas of the corneal stroma devoid of collagen fibrils, are a source of light scattering (Benedek, 1971). Such lakes would not be evident from X-ray diffraction patterns. Therefore, a transmission electron microscopy investigation was undertaken in an attempt to determine the possible cause for corneal haze in the lumWT mouse lines.

Figure 4.4 shows that the posterior corneal stroma of lumWT5, -25, and-38 have similar collagen lamellar architecture to that of NTG control and that, interestingly,

there is no evidence of lake formation in mutant corneas. Figure 4.5 shows that NTG control collagen fibrils appear well aligned, as do the collagen fibrils of lumWT5, -25, and –38 mutants. Although there appears to be very little difference in the appearences of PG filaments in each lumWT stroma compared with NTG control, quantitative assessment would have to be carried out to see if there are changes in the size or number of these filaments.

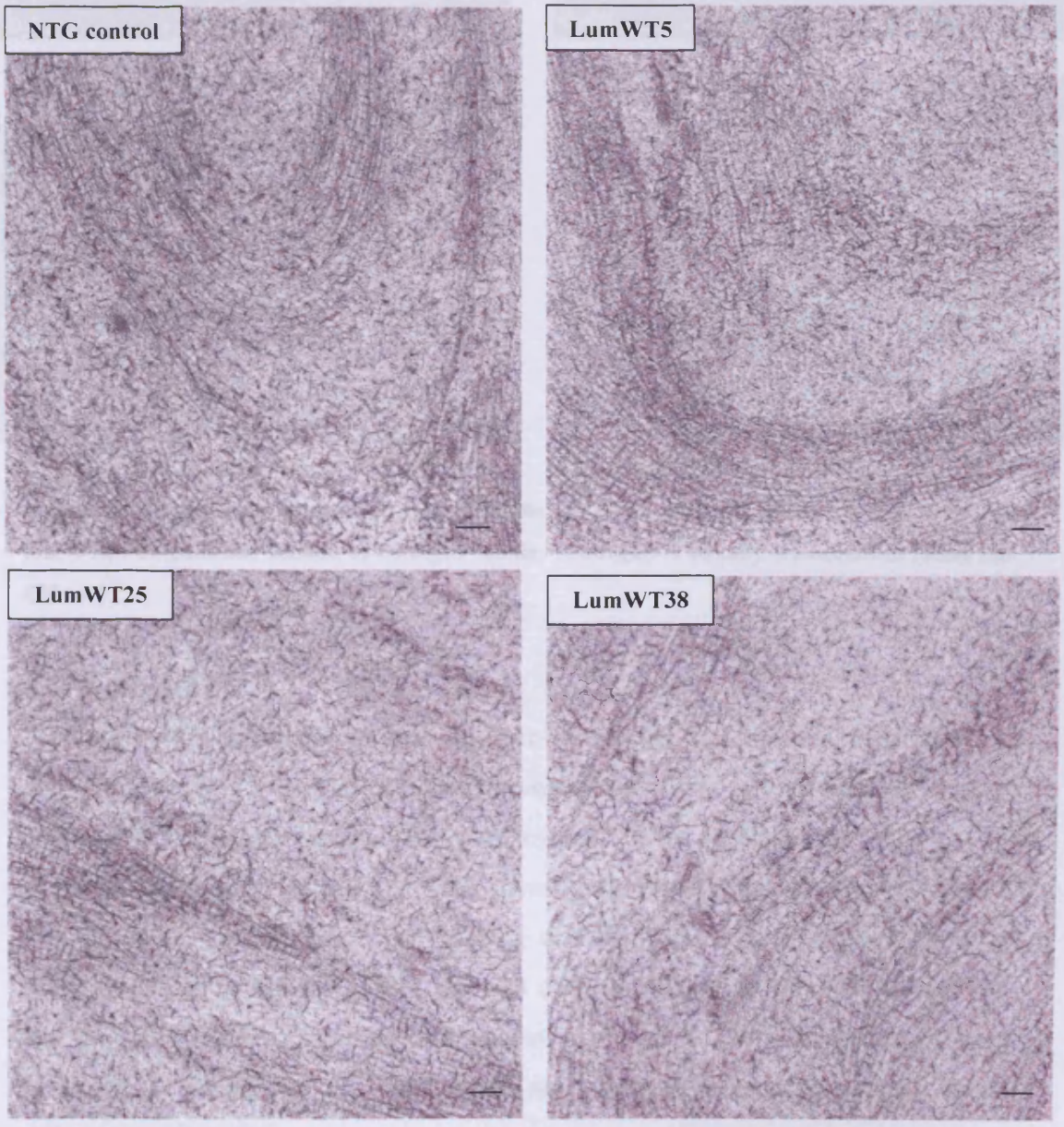

Figure 4.4. Examination of electron micrographs of NTG control, lumWT5, lumWT25, and lumWT38 stromal lamellae, indicating that there is no evidence of lakes as a result of lumican over-expression (scale bar = 300 nm).

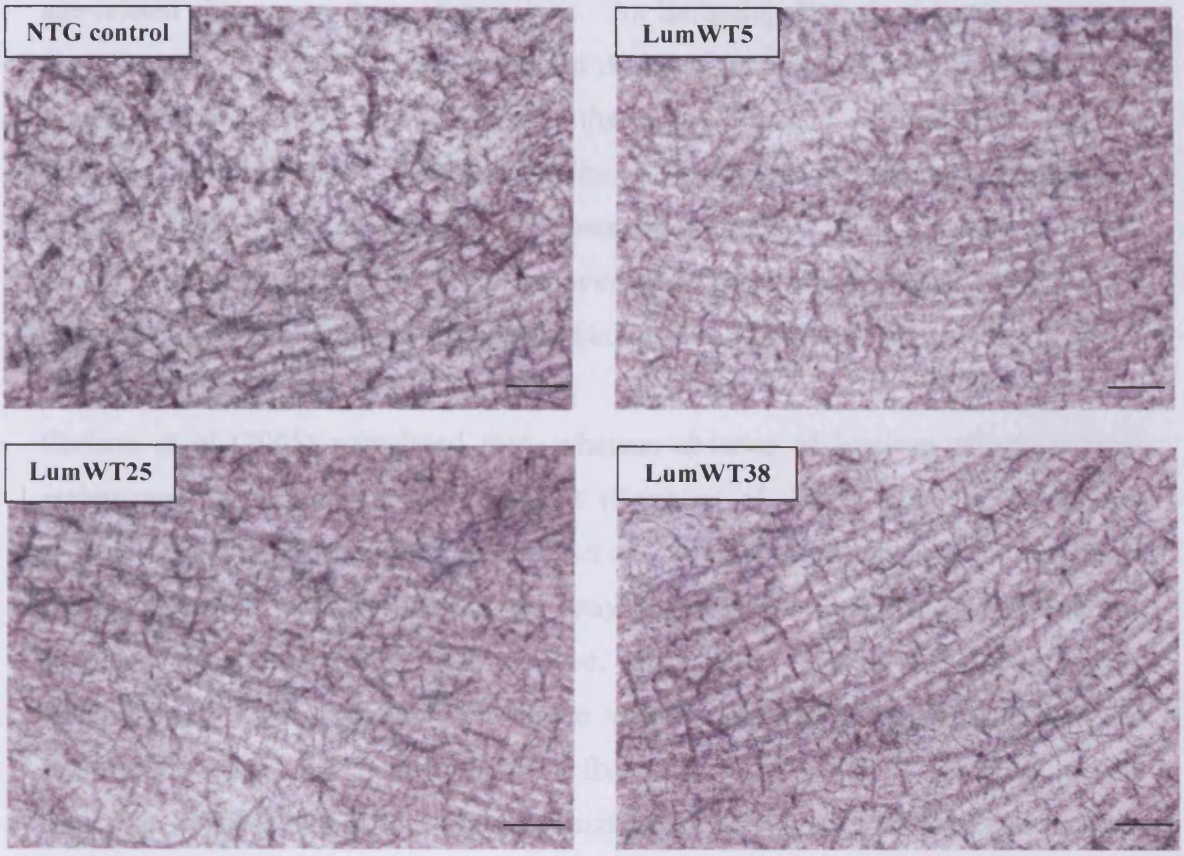

Figure 4.5. Transmission electron micrographs of NTG control, lumWT5, lumWT25, and lumWT38 longitudinal section of collagen fibrils. Collagen is equally well-ordered (scale bar = 200 nm).

4.4.5 Discussion

A recent TEM examination of lumican over-expression in the cornea of lumWT5, -25, and –38 mice by Carlson *et al* (2005) revealed that there is very little difference in collagen fibril morphology at the ultrastuctural level when compared with NTG corneas. The primary aim of this XRD investigation was to gain highly representative average values for collagen fibril spacing and fibril diameter throughout the whole tissue thickness of lumWT5, -25, and -38 corneas. Consequently, the current study has provided further evidence that excess synthesis of lumican (and presumably keratocan – Carlson *et al*, 2005) does not cause significant changes in stromal collagen architecture.

Firstly, lumWT5 and lumWT38 corneas were harvested from mice that were of different age groups, so the opportunity arose to conduct an XRD investigation of

age-related changes in these mouse lines. An intriguing feature of mutant cornea is that the spacing between fibrils does not decrease with increasing age but, in fact, remains essentially the same, suggesting that excess lumican may somehow interfere with this natural process. Nevertheless, the age-matched comparisons made between mutant and NTG controls here have shown that certainly up to 2.5 months of age there is very little difference in mutant average collagen fibril spacing. Overall, the XRD results point to relatively unchanged collagen architecture.

Carlson *et al* (2005) postulated that, whereas absence of lumican affects stromal architecture from neonatal development (Song *et al*, 2003) through to maturity (Chakravarti *et al*, 1998; 2000; Quantock *et al*, 2001), an overabundance of lumican is not detrimental to corneal morphology, maybe due to the limited number of binding sites available on collagen fibrils. Indeed, Meek and Leonard (1993) hypothesized that there is a balance of PG to collagen whereby fibrillar collagen molecules and interfibrillar GAGs are synthesised in a fixed numerical ratio. It certainly appears from the XRD data that lumican over-expression has very little effect on corneal stromal morphology. Yet, the question remains as to the origin of corneal haze. Carlson *et al* found that lumWT38 corneas display higher levels of haze than lumWT5 corneas (2005). The mutant corneas examined here appeared hazy compared to normal, but it is not possible to determine if one mouse line is collectively hazier than the other as the observations made were purely subjective. It is possible that within-group variations in haze could be linked to transgene copy number, whereby the integration of a higher copy number may intensify the effect of transgene expression. However, when genotyping the transgenic mice for the current study Dr Carlson and colleagues tested for expression of the transgene, but not copy number or insertion site. Still, the finding that all NTG control tissue appeared clear compared with transgenic corneas (bar one lumWT38) signifies that haze is somehow a product of lumican over-expression.

The corneas of lumWT mouse lines are producing excess lumican, and presumably keratocan, PGs (Carlson *et al*, 2005). However the glycosylation and sulphation of excess lumican PG is uncertain. If mutant corneas were producing surplus, maybe unbound sulphated lumican KSPG, then would this mutation have a similar effect on corneal stroma to surplus KS GAG? Mucopolysaccaridoses (MPS) are a group of

lysosomal storage diseases caused by inborn errors of metabolism, in which an inability to degrade GAGs leads to their systemic accumulation (Klintworth, 1994; in Meek and Quantock, 2001). For instance, type A MPS VI is due to deficiency of the enzyme N-acetylgalactosamine-6-sulphate-sulphatase allowing build-up of KS (Leslie *et al*, 2005), of which corneal clouding is a common feature. An XRD and TEM study suggested that corneal clouding might be a result of collagen-free areas of stroma (Rawe *et al*, 1997). Indeed, a possible cause for corneal haze here may be the development of lakes (Benedek, 1971), the reason being that excess sulphated lumican may increase the hydrophilic nature of the tissue and cause it to swell. However, there is no evidence of lake formation in the transgenic corneal stroma under TEM, signifying that excess lumican PG (and keratocan) is not equally glycosylated and sulphated.

Collagen fibril diameters and packing can influence light scattering but from this study there appear to be no significant changes between the NTG and lumWT mouse lines, so it seems unlikely that changes in collagen or its arrangement are responsible for the observed haze. The overproduction of KSPGs in the lumWT mouse lines would also be expected to influence the RI of the interfibrillar matrix, which would in turn influence light scattering (Meek *et al*, 2003a). An interesting feature of mouse cornea here is the presence of large, electron dense PGs, which enzyme digestion of wild-type cornea using keratanase and chondroitinase ABC has shown to be CS/DS PGs (Dr Phillip Lewis, personal communication). If there were more of these structures in mutant cornea, then these may contribute to light scattering either directly or by changing the RI of the interfibrillar matrix. However, there do not appear to be obvious differences in the PGs between the NTG controls and the transgenic corneal stromas, so again, this does not seem to be a likely cause of haze in this system. One cannot rule out the possibility that there is a feedback mechanism whereby the excess PG is degraded. However, this remains speculation until quantitative analysis of the PG composition of transgenic corneal stroma is carried out.

Alternatively, could light scattering be of cellular origin (Jester *et al*, 1999)? The impact of transgene integration on the expression of other genes is not known, and it is possible that the integration of the transgene into the genome may activate

keratocytes. Quiescent keratocytes appear as long, flat cells interdigitating between lamellae that scatter negligible light due to the production of enzyme-crystallins (Jester *et al*, 1999). However, upon activation the keratocytes assume a different morphology, becoming round and, among other changes, secreting lower levels of crystallins. Unfortunately, as the corneas were initially frozen it was not possible to assess keratocyte morphology using TEM, but clearly much more work is needed to identify the cause of light scattering in these corneas.

4.5 Results of lumican N-terminal C/S substitution study

This study explored the effect of a lumican N-terminal region point mutation on corneal stromal architecture in lumC/S3 and lumC/S8 mouse lines. The corneas of these mouse lines were investigated for age-related patterns of change prior to statistical comparison with age-matched NTG controls. In cases where an NTG control was not available, the collagen fibril data of wild-type corneas from other chapters were used purely to gain an indication of whether the mutant cornea is ultrastructurally different. For details of statistical analysis refer to Appendix 3. All *P*-values quoted were obtained by Independent samples t-test unless otherwise stated.

4.5.1 LumC/S3 founderline

Age (months)	n	C/C	IFS (nm)	CFD (nm)	P/W (nm)	t (nm)
9.5	1	1	55.0	35.9	28.3	271
	2	1	61.0	38.0	25.3	342
	3	3	77.0	42.9	43.5	348
	4	3	63.6	38.0	33.7	313
	5	3	54.0	36.7	28.0	278
	6	3	69.6	41.5	38.9	333
12	1	6	56.0	36.2	33.0	255
	2	5	57.0	37.7	29.2	285
	3	2	65.0	44.3	34.0	399
	4	2	52.0	36.2	24.5	290

Table 4.6. Degree of corneal clarity (C/C) of each lumC/S3 specimen (n), and collagen fibril Bragg spacing (IFS), collagen fibril diameter (CFD), peak width at half-height (P/W), and coherence distance (t) values.

Change in lumC/S3 collagen fibril morphology with increasing age

All corneas displayed some degree of haze, although scores are higher in the 12-month-old age group (Table 4.6). There is no difference in the average interfibrillar Bragg spacing measurements of corneas from 9.5-month-old (63.4 ± 8.8 nm) and 12-month-old (57.5 ± 5.4 nm) mice (P = 0.273). Additionally, the collagen fibril diameter measurements are similar in the corneas of younger and older mice (38.8 ± 2.8 nm vs. 38.6 ± 3.9 nm respectively; Mann-Whitney test; P = 0.668). The interfibrillar peak width at half-height measurements at 9.5 months (33.0 ± 7.1 nm) and 12 months (30.2 ± 4.3 nm) also reveal that there is no difference in fibrillar ordering between these ages (P = 0.508). Finally, with similar average coherence distance values from 9-month-old (314 ± 33 nm) and 12-month-old (307 ± 63 nm)

corneas, these findings point to very little change in stromal morphology with ageing. The next step was to explore the effect of the lumican mutation on lumC/S3 corneal stroma. However, due to the lack of an appropriate age-matched NTG control with which to compare either lumC/S3 age group, it was necessary to investigate the fibril diameter data of lumC/S3 9 month group using the data from close age-matched wild-type corneas (from 10-month-old mice) of chapter 6.

Effect of lumican N-terminal C/S mutation in lumC/S3 corneas at 9.5 months

All mutant corneas displayed some degree of haze, with scores ranging between 1 and 3. It was found that the average collagen fibril diameter of lumC/S3 corneas (38.8 ± 2.8 nm) is appreciably larger than wild-type (36.5 ± 0.9 nm). This result suggests that lumican might be unable to bind collagen and regulate fibrillogenesis.

4.5.2 LumC/S8 founderline

Age (months)	n	C/C	IFS (nm)	CFD (nm)	P/W (nm)	t (nm)
1.5	1	0	60.0	39.4	34.3	279
	2	0	61.7	37.7	29.9	325
	3	0	59.0	38.8	29.0	306
	4	0	72.0	43.6	40.6	341
	5	0	54.0	37.2	25.0	304
	6	0	60.0	39.4	28.3	331
	7	0	58.0	39.7	26.7	319
	8	0	65.0	41.9	34.3	322
	9	0	58.4	39.7	28.0	320
	10	0	57.0	37.2	25.6	321
4	1	0	58.0	39.1	26.8	314
	2	0	59.0	38.0	30.5	297
	3	0	61.0	40.0	26.3	348
	4	0	58.0	38.3	32.3	278
	5	0	61.4	41.2	30.3	325
	6	0	62.0	41.9	36.5	288
	7	0	64.4	40.0	36.0	306
	8	0	58.4	40.3	26.0	330
	9	0	68.0	44.7	30.0	387
	10	0	65.0	42.9	28.6	387
	11	0	51.0	38.8	22.4	304
	12	0	67.0	43.2	39.5	317
9	1	0	66.6	42.9	37.3	330
	2	0	79.0	49.7	43.0	362
	3	0	61.0	38.8	30.0	321

Table 4.7. Degree of corneal clarity (C/C) of each lumC/S8 specimen (n), and collagen fibril Bragg spacing (IFS), collagen fibril diameter (CFD), peak width at half-height (P/W), and coherence distance (t) values.

Change in lumC/S8 collagen fibril morphology with increasing age

All corneas appeared clear and so were allocated grade 0 (Table 4.7). This age study has revealed that average collagen fibril spacing does not seem to change with increasing age (One-way ANOVA; $P = 0.055$), but as this P-value was marginally higher than the 0.05 significance level, Post Hoc testing was performed to ensure that there are no underlying differences. The average collagen fibril spacing at 1.5 months (60.5 ± 5.0 nm) is similar to that at 4 months (61.1 ± 4.7 nm) (Tukey's HSD; $P = 0.963$). Average collagen fibril spacing at 9 months appears much wider (67.9 ± 7.8 nm), but Post Hoc testing confirmed that the difference is not significant when compared with 1.5 months (Tukey's HSD; $P = 0.067$) and 4 months (Tukey's HSD; $P = 0.088$).

The average collagen fibril diameter of lumC/S8 mutant corneas increases with time (One-way ANOVA; $P = 0.007$). Average fibril diameters at 1.5 months (39.5 ± 2.0 nm) and 4 months (40.7 ± 2.1 nm) are similar ($P = 0.500$). Fibril diameter at 9 months and 4 month are also similar ($P = 0.064$). However, average collagen fibril diameter at 9 months (44.2 ± 4.6 nm) is significantly larger when compared with measurements from 1.5-month-old ($P = 0.012$) mutant corneas. Examination of interfibrillar peak width at half-height measurements from corneas of 1.5-month-old (30.2 ± 4.9 nm), 4-month-old (30.4 ± 5.0 nm), and 9-month-old (33.2 ± 9.0 nm) mice has revealed that the level of fibrillar ordering does not change with time (One-way ANOVA; $P = 0.448$). This concept is supported by the similar average coherence distance measurements found (317 ± 17 nm, 323 ± 35 nm, and 338 ± 22 nm respectively).

Effect of lumican N-terminal C/S mutation in lumC/S8 corneas at 1.5 months

Average collagen fibril spacing in the lumC/S8 corneas (60.5 ± 5.0 nm) is similar to measurements from NTG control corneas (60.8 ± 5.6 nm) ($P = 0.903$). In contrast, collagen fibril diameter in these mutants is significantly larger (39.5 ± 2.0 nm) than NTG control (36.2 ± 4.0 nm) at 1.5-months-old ($P = 0.039$). Examination of interfibrillar peak width at half-height has disclosed that collagen fibrils are, on average, equally well ordered in mutant corneas (30.2 ± 4.9 nm) when compared to age-matched controls (31.6 ± 4.4 nm) ($P = 0.556$).

To gain an indication of collagen fibril diameter differences in lumC/S8 corneas at 4 months and 9 months, comparisons were made with data from 4-month-old (Chapter 5) and 10-month-old (Chapter 6) wild-type mice respectively.

Effect of lumican N-terminal C/S mutation in lumC/S8 corneas at 4 months

Statistical comparison has indicated that collagen fibrils of lumC/S8 corneas are, on average, larger (40.7 ± 2.1 nm) than wild-type (35.9 ± 0.9 nm) (Mann-Whitney test; P <0.001), indicating that mutant lumican might be unable to bind collagen to regulate fibrillogenesis.

Effect of lumican N-terminal C/S mutation in lumC/S8 corneas at 9 months

Statistical comparison has indicated that collagen fibrils of lumC/S8 corneas are, on average, thicker (44.2 ± 4.6 nm) than wild-type (36.5 ± 0.9 nm) (Mann-Whitney test; P = 0.003). This signifies that mutant lumican might be unable to bind collagen to regulate fibrillogenesis.

4.5.3 The effect of founderline on lumican C/S transgene expression

To develop a deeper understanding of the lumican mutation to be studied in these lumC/S mouse lines, the average collagen fibril spacing, fibril diameter and interfibrillar peak width values of lumC/S3 9.5 months and lumC/S8 9 months were statistically compared as they are close age-matches.

The average collagen fibril spacing of lumC/S3 (63.4 ± 8.8 nm) is similar to that of lumC/S8 (67.9 ± 7.8 nm) (P = 0.429). However, it is apparent that the average fibril diameter of lumC/S3 corneas is smaller than lumC/S8 (38.8 ± 2.8 nm vs. 44.2 ± 4.6 nm respectively; P = 0.047), signifying that maybe the mutation has had a greater effect in lumC/S8 mouse line There is very little difference in the average peak width value of lumC/S3 (33 ± 7.1 nm) and lumC/S8 (33.2 ± 9.0 nm) corneas (P = 0.970). Indeed, the coherence distance results suggest that there is very little difference in the fibrillar architecture of lumC/S3 and lumC/S8 mouse lines (314 ± 33 nm and 338 ± 22 nm respectively).

4.5.4 Transmission electron microscopy

So far, the XRD results of this study have indicated that the C/S mutation in the N-terminal region of lumican may be affecting the ability of lumican core protein to bind collagen, as the collagen fibril diameter of lumC/S8 corneas from 1.5-month-old mice is, on average, larger than those of NTG control mice. Indeed, the statistical comparison of lumC/S3 fibril diameter data with that of close age-matched wild-type corneas indicated that the diameter of mutant fibrils is larger. However, an intriguing feature of these mutant mouse lines is that only the corneas collected from lumC/S3 mice were hazy. Thus, it was important to carry out a TEM investigation, firstly to explore the possibility that the hazy appearance of lumC/S3 corneas is due to ultrastructural alterations, and secondly to ascertain whether the larger-than-normal collagen fibrils are laterally fused due to lack of lumican-collagen binding.

Figure 4.6 shows that the lamellar architecture of NTG control, lumC/S3, and lumC/S8 posterior stroma is similar. There was no evidence of 'lakes' in the hazy lumC/S3 corneas.

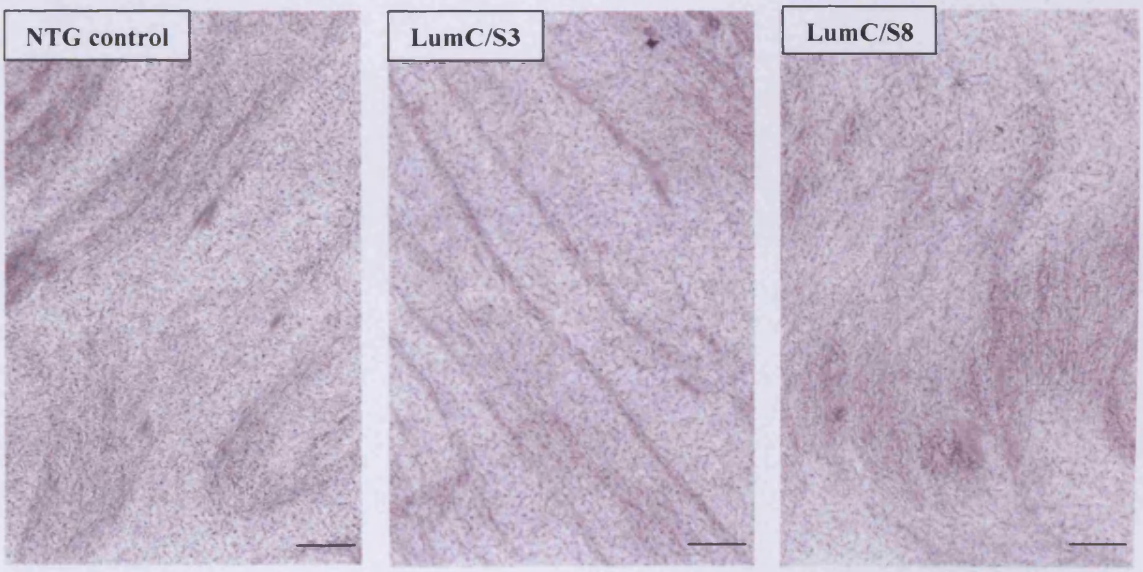

Figure 4.6. Transmission electron micrographs of NTG control, lumC/S3 and lumC/S8 corneal stromal lamellae (scale bar = 1 μm).

Yet, upon closer examination of collagen fibril architecture of NTG control and mutant corneas in Figure 4.7, mutant corneas are ultrastructurally different. First of all, in longitudinal section, NTG collagen fibrils appear to be well-spaced and seem to

maintain regular association with PGs along their length (Figure 4.7A). The collagen fibrils of lumC/S3 (Figure 4.7B) and lumC/S8 (Figure 4.7C) are also fairly well-ordered, but there appear to be a greater number of long PGs, presumably CS/DS PGs (Dr Phillip Lewis, personal communication). In transverse section, NTG control collagen fibrils are closely packed and of uniform diameter (Figure 4.7D); the collagen fibrils of lumC/S3 and lumC/S8 corneas seem to be fairly well ordered and circular in cross-section, but of more varying diameters (Figures 4.7E and F respectively). However, it is interesting that there is no evidence of laterally fused collagen fibrils in the posterior corneal stroma of either lumC/S3 or lumC/S8.

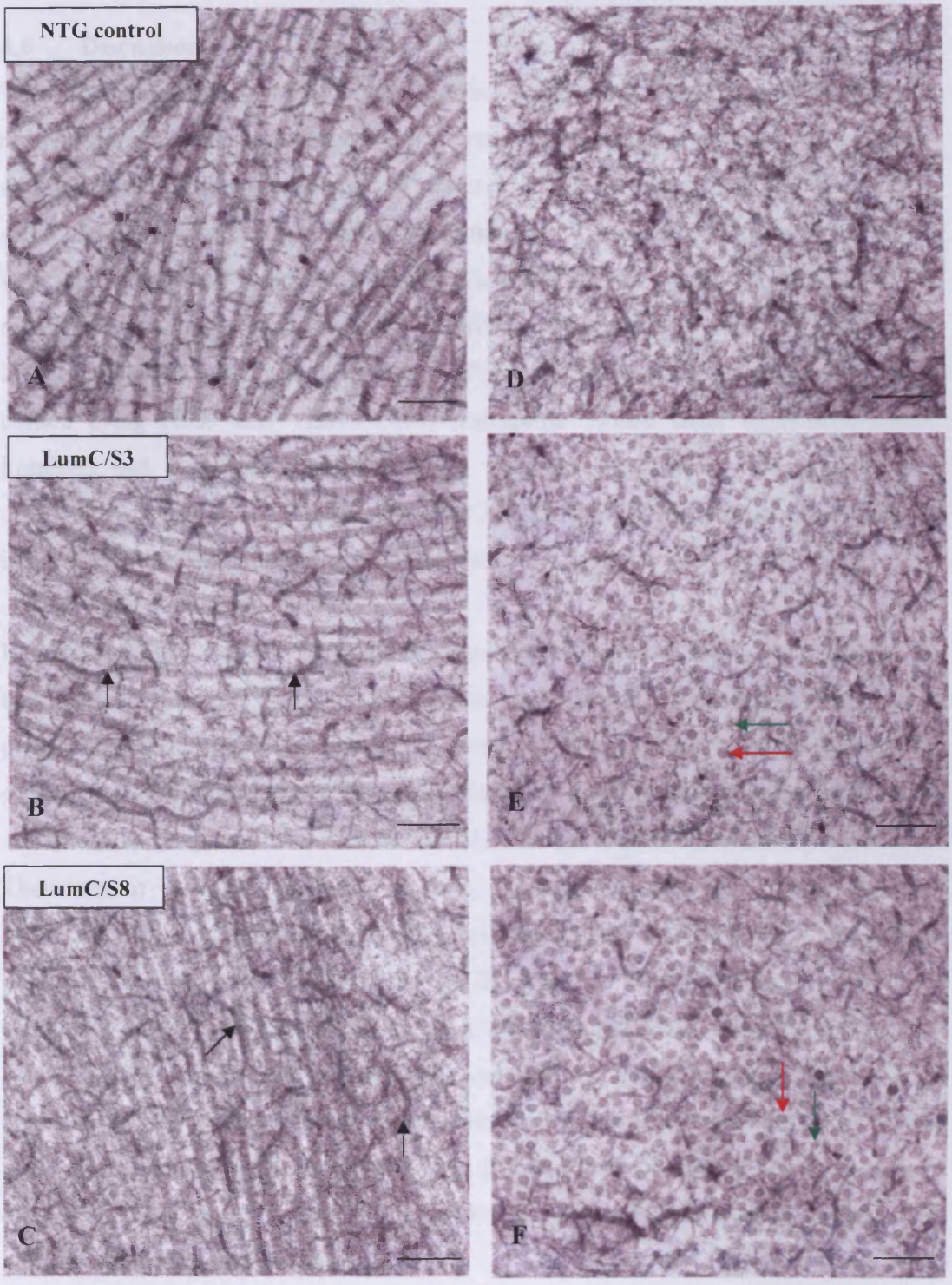

Figure 4.7. Transmission electron micrographs of NTG control, lumC/S3, and lumC/S8 longitudinal (A, B, and C respectively) and transverse (D, E, and F respectively) sections of collagen fibrils. NTG collagen fibrils maintain regular association with PGs along their length. The presence of long, dense PGs (black arrow) is evident in the stroma of lumC/S3 and lumC/S8 corneas. Collagen fibrils of mutant stromas are of various diameters; thick fibrils (red arrow) are scattered among thinner fibrils (green arrow) (scale bar = 200 nm).

4.6 Discussion

The N-terminal domain of lumican contains a region of highly conserved cysteine-rich residues that are thought to be important for proper disulphide bond formation and, therefore, binding to collagen (Rada *et al*, 1993). Carlson *et al* (2003) set out to show that cultured corneal stromal cells transfected with mutant lumican (where Cys^{41} was substituted with Ser) produce a multi-layered stroma consisting of disorganised, mostly larger-than-normal, collagen fibrils. The primary aim of the current investigation was to ascertain the impact of lumican N-terminal mutation in the mouse cornea using XRD and TEM. Two transgenic mouse lines were investigated; lumC/S3 and lumC/S8, and the corneas were collected from mice that were of different age groups. Therefore, an initial XRD investigation of age-related changes in collagen fibril morphology was conducted.

LumC/S3 corneal collagen fibril diameter remains essentially the same over time, but the distance between collagen fibrils does not decrease with increasing age as previously found in NTG controls. However, these data were collected from the corneas of 9.5-month-old and 12-month-old mice, so average collagen fibril spacing and diameter values in the cornea of animals younger than 9.5 months are not known. Therefore, it was not possible to draw firm conclusions from these findings. However, fibril spacing and diameter values obtained from the corneas of 1.5-month-old, 4-month-old, and 9-month-old lumC/S8 animals reveal intriguing age-related changes. Firstly, collagen fibril spacing does not decrease with increasing age, indicating that this natural process may be affected in the mutant cornea. More significantly, the collagen fibrils increase in diameter with advancing age, or at least there is a growing population of larger diameter fibrils among those of normal diameter. This discovery signifies that the effects of the lumican N-terminal C/S point mutation are progressive.

Carlson *et al* (2003) observed abnormal collagen fibril architecture in lumC/S mutant culture; in particular, that collagen fibrils were of larger-than-normal diameter. This XRD investigation has disclosed that the mutation may be disrupting the lumican-collagen interactions necessary for the development of uniformly sized collagen fibrils, as the collagen fibrils of lumC/S8 corneas are, on average, larger than those of NTG controls (the results obtained from close age-matched comparisons with other

wild-type corneas gave similar findings). Still, the values obtained for collagen fibril spacing and interfibrillar peak width at half-height point to a mutant corneal stroma that is unchanged in overall fibrillar organisation. Thus, at this stage of deliberation, the TEM findings will be considered as they may hold the key to these results. First of all, if C/S mutant lumican is unable to bind collagen fibrils, does the mutant cornea consist of laterally fused fibrils similar to those found in the lumican-null mouse cornea (Chakravarti *et al*, 2000)? Lateral fibril fusion may cause the displacement of fibrils and subsequently render the distance between neighbouring collagen fibrils wider. Yet the current TEM study has shown that while many of the collagen fibrils appear to be larger-than-normal, they are nonetheless circular in cross-section. So, why are fibrils not fusing in the lumC/S cornea? The recent discovery that lumican-null corneas also suffer significant down-regulation of keratocan (Carlson *et al*, 2005) suggests that the absence of both KSPGs is necessary for fibril fusion to occur. This hypothesis is substantiated by the fact that collagen fibrils of the keratocan-null mouse cornea (in which lumican mRNA expression is normal – Liu *et al*, 2003) are thicker, but circular in cross-section (Meek *et al*, 2003b). Thus, it is reasoned here that while a lack of lumican-collagen binding may be akin to absence of lumican, there is no reason to suppose that the mutation induced affects the expression of keratocan. Additionally, it is possible that mutant lumican is not glycosylated and sulphated, so having no affect upon corneal stromal hydration and therefore interfibrillar spacing.

An additional point of interest is the discovery that the lumican mutation may be more pronounced in lumC/S8 corneas from an ultrastructural point of view. Essentially, the difference between these mouse lines is potentially the insertion site of the transgene, but tests were performed to confirm transgene expression, not insertion site or copy number (Dr Eric Carlson, personal communication). The XRD data indicate that lumC/S8 corneas consist of larger fibrils than lumC/S3, although it appears from inspection of electron micrographs that the lumC/S8 corneal stroma may simply contain more of these large fibrils. In order gain an accurate assessment of stromal fibril composition, quantitative assessment would have to be undertaken.

To summarise, the cysteine-rich domain of lumican is important in collagen fibrillogenesis, as the substitution of Cys^{41} with Ser in the N-terminal region of the lumican core protein interferes with disulphide bond formation, impeding the ability

of lumican to interact with collagen. The substitution leads to the formation of a population of larger-than-normal collagen fibrils, but these are not the result of fibril fusion. With respect to haze formation, the substitution has different effects in different strains, which cannot at present be explained. However, it is evident that the spacing and organisation of the collagen fibrils are unaffected, though it appears that normal compaction of collagen that occurs with age does not occur when Cys^{41} is substituted with Ser in corneal lumican.

Chapter 5. Effect of mimecan deficiency on mouse corneal stroma

5.1 Introduction

The corneal KSPGs lumican, keratocan, and mimecan are thought to modulate collagen fibrillar architecture, and research has shown that the phenotypes presented by mice deficient in each KSPG vary. Absence of lumican produces the most extreme phenotype of all, as these unusually thin corneas develop bilateral opacity, particularly within deeper stromal layers where a disrupted stromal matrix is evident (Chakravarti *et al*, 1998; 2000; Quantock *et al*, 2001; Song *et al*, 2003). The keratocan-deficient cornea does not display opacity, but presents a thinner corneal stroma (Liu *et al*, 2003) consisting of some thicker, although circular collagen fibrils, and wider fibril spacing (Meek *et al*, 2003b). A recent investigation of mimecan-deficient corneas showed that, again, there are no obvious changes in clarity or tissue thickness, even though TEM micrographs appeared to show evidence of some alterations in collagen fibril size and arrangement at the ultrastructural level (Tasheva *et al*, 2002) (Figure 5.1).

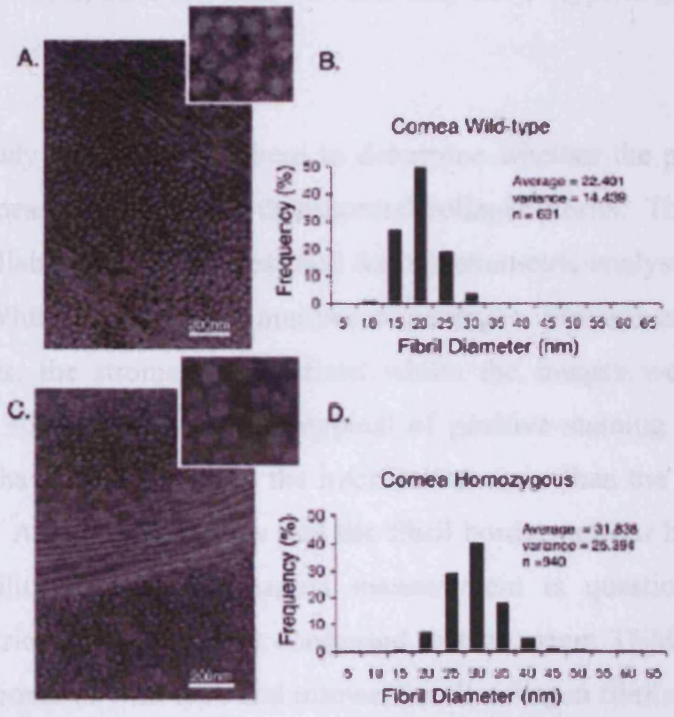

Figure 5.1. TEM micrographs containing cross-sections of collagen fibrils from corneal stroma of wild-type (A) and mutant (C) mice. Morphometric analysis of corneal collagen fibrils in wild-type (B) and in mutant (D) mice. Fibril diameter was measured morphometrically as described in the methods and presented in a histogram. The average fibril diameter, the variance and the total number (n) of fibrils measured are indicated (from Tasheva *et al*, 2002).

These research efforts have so far indicated that absence of each KSPG affects corneal stromal morphology. However, the varying degree of severity in each case points to a unique structural modulatory role for these corneal KSPGs.

5.1.1 Experimental aims

The purpose of this investigation was to gain further insight into the role of mimecan, and to what extent this molecule regulates collagen fibrillar architecture in the mouse corneal stroma. The following aims were addressed:

- Using XRD, representative average values for collagen fibril spacing and diameter were obtained for the entire thickness of normal and mutant corneal tissue, while the degree of ordering of the fibrils was investigated via the calculation of H/W ratio and coherence distance values. Tasheva *et al* (2002) investigated corneal ultrastructure of normal and mimecan-deficient mice using TEM, and stated that the diameter and spatial distribution of mutant collagen fibrils was somewhat altered. However, the small area assessed may not be typical of the entire corneal stroma.

- A TEM study was conducted here to determine whether the posterior stroma of mutant corneas contains larger-than-normal collagen fibrils. There is the question as to the reliability of the images used for morphometric analysis by Tasheva *et al* (2002). While a reasonable number of collagen fibrils were measured from micrographs, the stromal region from which the images were taken was not specified. Also, the images are atypical of positive staining whereby the stain appears to have bound more to the interfibrillar areas than the fibrils themselves. Figures 5.1 A and C inset show that the fibril borders appear hazy as a result, so the possibility of accurate manual measurement is questionable. Although morphometric analysis was not conducted in the current TEM investigation, the posterior stroma of wild-type and mimecan-null collagen fibrils were examined to determine whether mutant corneas contain larger-than-normal collagen fibrils.

5.2 Materials and methods

5.2.1 Tissue samples

Corneal tissue was kindly provided by Dr Elena Tasheva of the Division of Biology and College of Veterinary Medicine, Kansas State University, USA. Mice with a null homozygous mutation for mimecan were generated as reported previously (Tasheva *et al*, 2002). Professor Gary Conrad and colleagues removed and stored the corneas as follows. Following sacrifice of 4-month-old mice, a total of 10 wild-type and 10 mimecan-deficient corneas were excised at the limbus, and each cornea was individually wrapped in clingfilm to limit dehydration, frozen to -80°C and shipped on dry ice to Cardiff University. On arrival, the corneas remained wrapped in clingfilm and were immediately stored at -80°C until examination by XRD and TEM.

5.2.2 Low-angle XRD

5.2.2.1 Collection of XRD data

XRD patterns were collected by Professor Keith Meek and Dr Andrew Quantock as detailed in Section 2.2.2. Specifically, the beam size was 1.5 mm x 1.0 mm, and shutters were opened for a 3 minute exposure of each cornea. The detector was situated directly behind the cornea at a distance of approximately 9 m. A 14 hour exposure to Fe^{55} was subtracted from each X-ray pattern in order to account for any non-linearities in the detector.

Data analysis was performed as outlined in Section 2.3 to obtain average values for collagen fibril spacing (Step 4), fibril diameter (Step 3), H/W ratio (Step 5), and coherence distance (Step 6). Step 2(B), the alternative removal of background scatter, was undertaken.

5.2.3 Transmission electron microscopy

Tissue samples were selected on the basis of the fibril spacing and fibril diameter values falling close to the mean values of each group collected from XRD analysis. Wild-type tissue sample 6 and mimecan-null tissue sample 1 (Table 5.1) were examined. The details of tissue staining and embedding, block trimming and sectioning, and section observation are outlined in Section 2.4. However, previous staining of sections with saturated aqueous UA (Section 2.4.3A) proved to give little contrast of collagen fibrils in cross-section. Therefore, Section 2.4.3B, the procedure

outlining the use of ethanolic UA, was followed as it more readily penetrates the section.

5.3 Results

For details of statistical analysis refer to Appendix 4. All *P*-values quoted were obtained from Independent samples t-test.

5.3.1 XRD data analysis

The low-angle XRD patterns obtained from 9 wild-type and 10 mimecan-null corneas each consisted of well-defined interfibrillar reflections, of which two representative patterns are shown in Figure 5.2. Vertical transects across these XRD patterns generated similar X-ray intensity profiles for normal and mutant corneas.

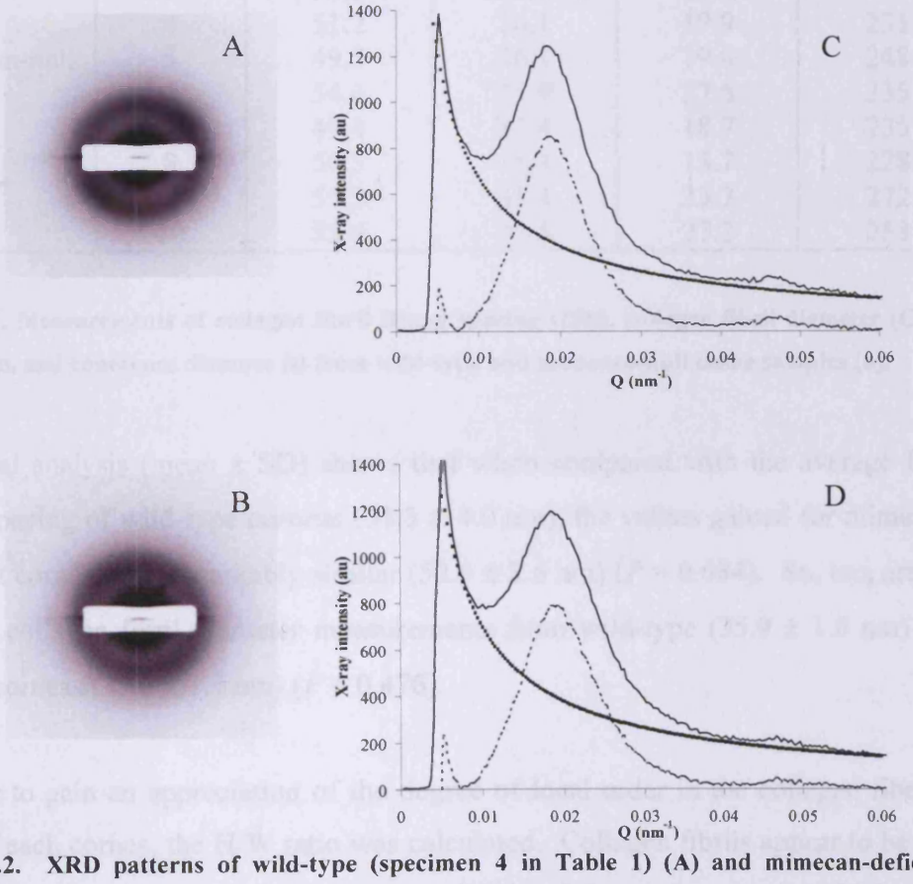

Figure 5.2. XRD patterns of wild-type (specimen 4 in Table 1) (A) and mimecan-deficient (specimen 12 in Table 1) (B) mouse corneas with similarly well-defined 1st order equatorial reflections, indicative of well-ordered corneal stromal collagen fibrils. C and D are the respective X-ray intensity profiles (solid lines), from which the fitting and subtraction of a power-law background function (squares) produces the resultant XRD pattern measured (dotted lines).

Examination of the data in Table 5.1 reveals that there is very little difference in collagen fibril morphology between wild-type and mimecan-null corneas.

Genotype	n	IFS (nm)	CFD (nm)	H/W ratio	t (nm)
Wild-type	1	52.4	36.3	35.4	272
	2	51.9	34.5	26.8	256
	3	50.8	35.2	31.2	256
	4	53.6	35.2	30.8	272
	5	54.9	36.6	26.9	276
	6	53.8	36.3	32.8	254
	7	56.5	36.3	24.7	267
	8	60.3	37.6	25.8	256
	9	45.7	35.4	19.5	237
Mimecan-null	1	51.9	34.3	33.2	241
	2	53.7	37.1	24.9	256
	3	53.5	35.4	26.1	241
	4	51.2	36.1	19.9	231
	5	49.5	36.1	19.0	248
	6	54.4	34.9	27.6	235
	7	49.4	35.4	18.7	235
	8	50.3	35.4	13.7	228
	9	57.2	37.4	23.7	272
	10	55.4	33.8	27.2	253

Table 5.1. Measurements of collagen fibril Bragg spacing (IFS), collagen fibril diameter (CFD), H/W ratio, and coherence distance (t) from wild-type and mimecan-null tissue samples (n).

Statistical analysis (mean ± SD) shows that when compared with the average fibril Bragg spacing of wild-type corneas (53.3 ± 4.0 nm), the values gained for mimecan-deficient corneas are remarkably similar (52.6 ± 2.6 nm) ($P = 0.684$). So, too, are the average collagen fibril diameter measurements from wild-type (35.9 ± 1.0 nm) and mutant corneas (35.6 ± 1.1 nm) ($P = 0.476$).

In order to gain an appreciation of the degree of local order in the collagen fibrillar array of each cornea, the H/W ratio was calculated. Collagen fibrils appear to be less well ordered in mimecan-deficient corneas (23.4 ± 5.6 nm) than normal (28.2 ± 4.8 nm) although not significantly so ($P = 0.063$). Additionally, calculation of the coherence distance revealed that mutant collagen fibrils are, on average, less well-ordered than those of wild-type (244 ± 13 nm vs. 261 ± 12 nm respectively).

5.3.2 Transmission electron microscopy

A previous electron microscopic investigation of mimecan-deficient corneas (Tasheva *et al*, 2002) presented evidence of disordered, laterally fused fibrils similar to those found in the lumican-deficient cornea (Chakravarti *et al*, 1998). So far, XRD data of this study has shown that collagen fibril morphology of the mutant corneal stroma is, on average, no different to normal. Therefore, to develop a fuller appreciation of collagen fibril architecture of mutant corneas, TEM was performed. Figure 5.3 shows images taken from the posterior stroma of wild-type and mimecan-null corneas which show that the collagen fibril morphology of mutant posterior stroma appears to be similar to that of wild-type in transverse section. Indeed, these micrographs are typical examples of the observations made throughout the sections examined.

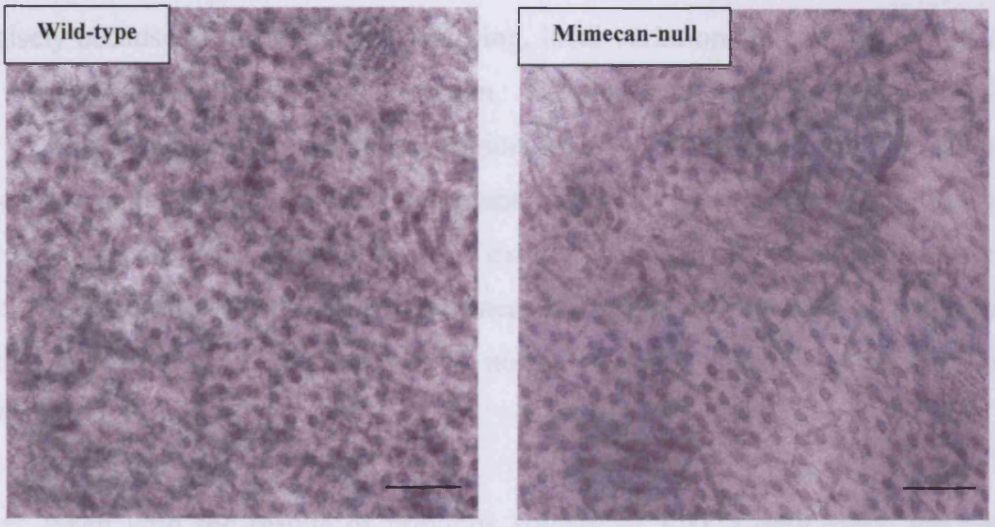

Figure 5.3. Transmission electron micrographs showing a similar degree of ordering of collagen fibrils in wild-type and mimecan-null corneas (scale bar = 200 nm).

5.4 Discussion

A TEM investigation of mimecan-null mice indicated that collagen fibrils of the mutant cornea appear thicker and more loosely packed when compared to wild-type counterparts, although corneal clarity, thickness and overall architecture are unremarkable (Tasheva *et al*, 2002). The evidence gained from the current XRD study indicates that, when taken as an average throughout the whole corneal thickness, mutant corneal collagen fibril spacing is essentially unchanged. Although the average H/W value of mutants within this study is slightly lower, this was found to be insignificant, and as the short-range ordering of collagen fibrils in mutants was

reduced to only about half the thickness of a single collagen fibril, any effects are not considered to be particularly extensive.

The average collagen fibril diameter in corneas lacking mimecan is essentially unchanged. Previous work has indicated that mimecan has the ability to regulate type I collagen fibrillogenesis *in vitro* (Ge *et al*, 2004), and examination of TEM micrographs from gluteraldehyde-fixed mutant corneas revealed what were claimed to be larger-than-normal collagen fibrils (Tasheva *et al*, 2002). The current investigation, which involved passing an X-ray beam through the entire corneal thickness, has given rise to representative average values in which all collagen fibrils encountered by the beam contribute to the X-ray pattern. This is a large number of fibrils in a tissue volume measuring 1.5 mm x 1.0 mm x corneal thickness, but precisely because of this extensive sampling, local variations in corneal ultrastructure are not detected, so TEM was undertaken. Electron micrographs taken of wild-type and mimecan-null posterior stromal regions show that collagen fibril architecture appears essentially unchanged in the mutant. Nevertheless, the findings of this study are not necessarily inconsistent with the existence of pockets of larger-than-normal, more loosely packed fibrils in mutant corneas as reported in the study by Tasheva and colleagues (2002), but overall point to normal corneal stromal architecture in the mutant.

When taken with the results of previous studies of KSPG deficiency, the current findings contribute to an appreciation of the importance of each. Lumican-deficient mouse corneas present an array of morphological abnormalities, ranging from thin, opaque corneal stroma (Chakravarti *et al*, 1998; Song *et al*, 2003), to an estimated 25% reduction in corneal KS content, including disorganised corneal stroma, and the presence of abnormally large diameter collagen fibrils in deeper tissue regions as shown by TEM (Chakravarti *et al*, 2000). Likewise, the keratocan-deficient corneal stroma is thinner-than-normal, although clear, consisting of a matrix that is less well-ordered, with more widely spaced collagen fibrils that are, on average, thicker than fibrils of normal corneas (Meek *et al*, 2003b). Corneal stromal structure at the fibrillar level is only minimally affected by the absence of mimecan. Certainly, any matrix changes measurable by XRD are negligible compared to those caused by

deletions in lumican (Quantock *et al*, 2001) and, to a lesser extent, keratocan (Meek *et al*, 2003b).

The importance of KS within the cornea of animals other than mouse has been supported on numerous occasions (Anseth, 1961b; Hassell *et al*, 1983; Cornuet *et al*, 1994). However, the extent to which KS chains are sulphated in the mouse has been speculated upon, although it is currently accepted that KS is present in mouse cornea (Funderburgh *et al*, 1995) but lacks the over-sulphated disaccharide motifs (Scott and Bosworth, 1990; Young *et al*, 2005). That said, lumican and CS/DS-carrying decorin have both been shown to regulate collagen type I fibrillogenesis *in vitro* (Rada *et al*, 1993), but corneal ultrastructure is not affected when decorin is ablated in the mouse (Danielson *et al*, 1997), therefore strengthening the concept that KSPGs play an equally important role in mouse cornea.

In the adult chick cornea, mRNA expression levels for lumican are 5-fold higher than keratocan and 38-fold higher than mimecan/osteoglycin (Dunlevy *et al*, 2000). Similar expression levels have also been reported in the embryonic quail cornea (Corpuz *et al*, 2000). In view of the results obtained from the XRD and TEM investigations conducted here, it is evident that mimecan may play only a minor role in the governance of collagen fibril architecture Maybe the loss of mimecan expression presents only subtle ultrastructural changes as this KSPG is present in corneal stroma at low levels. If this is the case, then the minimal structural defects of cornea presented in the absence of mimecan may be signifying that the role of corneal mimecan is indeed a minor one, at least in the mouse. Alternatively, compensatory mechanisms by other KSPGs may be at play (Tasheva *et al*, 2004). Nevertheless, KSPGs are considered to be instrumental in the formation and maintenance of a structurally normal murine corneal stroma.

In conclusion, there appears to be a hierarchy within the corneal KSPG population in terms of their relative influence as structural regulatory molecules: lumican, keratocan, and mimecan in decreasing order of importance.

Chapter 6. Corneal stromal architecture and *Chst5* gene absence

6.1 Introduction

In cornea, SLRPs consist of a core protein bonded to up to five GAG side chains, either the prevalent KS or CS/DS. The three PGs that bear KS side chains in cornea are lumican (Blochberger *et al*, 1992), keratocan (Corpuz *et al*, 1996; Liu *et al*, 1998), and mimecan (Funderburgh *et al*, 1997). The other main PG in cornea is decorin (Li *et al*, 1992), whose single GAG side chain consists of CS/DS. Corneal KSPGs are thought to shape the fibrillar architecture of stroma (Borcherding *et al*, 1975); while the core protein binds to collagen fibrils to regulate fibrillogenesis (Rada *et al*, 1993), the negatively charged KS GAG chains appear to ensure proper tissue hydration and regulate fibril spacing (Castoro *et al*, 1988).

Several lines of evidence suggest that GAGs/PGs play a pivotal role in the maintenance of corneal matrix structure. For instance, the avian cornea *in ovo* synthesises an unsulphated form of KS (lactosaminoglycan) at a time when the developing cornea is structurally disorganised and transmits little light, but switches to produce sulphated KS as the cornea becomes transparent and develops a more organised fibrillar architecture (Cornuet *et al*, 1994; Dunlevy *et al*, 2000; Connon *et al*, 2004). Also, opaque, disorganised corneal scar tissue of rabbit presents an altered pattern of KS sulphation (Hassell *et al*, 1983; Funderburgh *et al*, 1988; Cintron *et al*, 1990).

Mouse cornea contains relatively low levels of high sulphated KS epitope (Scott and Bosworth, 1990; Young *et al*, 2005). Even so, studies have shown that the corneas of mice deficient for lumican (Chakravarti *et al*, 1998; 2000; Quantock *et al*, 2001; Song *et al*, 2003) and keratocan (Liu *et al*, 2003; Meek *et al*, 2003b) display abnormal collagen fibril architecture, although the collagen fibril architecture of the mimecan-deficient cornea is relatively unchanged (Tasheva *et al*, 2002). These research efforts, while indicating that KSPGs are successful in the governance of corneal ultrastructure, have focused on KSPG structure/function in corneal stroma as controlled by the whole molecule. However, is it the absence of the KSPGs themselves (i.e. the core protein plus sulphated GAG side chains) that results in the structural alterations, or is the lack of sulphated KS the key?

In 2000, Akama and associates reported that the enzyme C-GlcNAc 6-*O* sulphotransferase, encoded by the human *CHST6* gene, is required for the production of sulphated KS, and that its inactivation is responsible for macular corneal dystrophy (MCD) type I. Patients suffering with this autosomal recessive hereditary disease clinically present thin cornea (Donnenfeld *et al*, 1986) and altered patterns of KS sulphation (Hassell *et al*, 1980; Klintworth *et al*, 1997; Hasegawa *et al*, 2000; Plaas *et al*, 2001b). Thus, to uncouple the role of KS GAG from the whole KSPG and ascertain the importance of KS GAG sulphation in corneal stroma, Professor Kohji Nishida and colleagues in Osaka University Medical School generated mice with a null mutation for *Chst5* (the murine ortholog of *CHST6*).

Immunoblot analysis using the monoclonal antibody 5-D-4 was performed on these animals by Dr Tomoya Akama (Burnham Institute for Medical Research) to determine that high sulphated epitopes were present in wild-type and heterozygous corneal extracts, but not in extracts from *Chst5* homozygous-null mutants. Dr Akama used a monoclonal antibody to lumican to ensure the presence of KSPG core protein in the corneas of *Chst5*-null mice. Clinical examination undertaken in Professor Nishidas' lab disclosed that the homozygous null cornea is as equally clear as counterpart genotypes, while histological examination showed normal tissue stratification, but indicated that the corneal stroma of the *Chst5*-null mutant is thinner than normal (Figure 6.1).

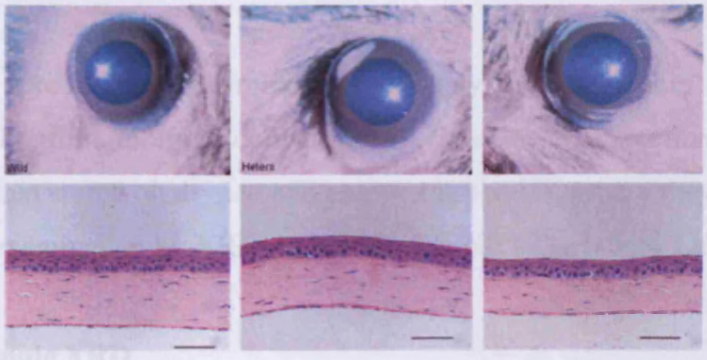

Figure 6.1. Clinical photographs of the corneas of wild-type (upper left), heterozygous-null (upper middle), and *Chst5* homozygous-null (upper right) mice showing no evidence of corneal opacification. Tissue sections indicate a thinner cornea in the homozygous *Chst5* mutant (lower right) than wild-type and heterozygous-null (lower left and middle respectively), but otherwise apparently normal stratification of the tissue (courtesy of Dr Yasutaka Hayashida).

6.1.1 Experimental aims

- In order to ascertain the necessity for sulphated KS in mouse cornea, the corneas of three genotypes were investigated; wild-type, heterozygous-null, and *Chst5* homozygous-null. An XRD investigation was carried out here, from which highly representative average values for collagen fibril spacing and fibril diameter were obtained throughout the whole tissue thickness.

- The corneas of each genotype were harvested from mice of two different age groups. Therefore, the first step in this investigation was to establish if the average collagen fibril spacing and collagen fibril diameter values of each genotype display age-related changes, and therefore if the data of these age groups could be pooled prior to statistical comparison.

6.2 Materials and Methods

6.2.1 Tissue samples

Wild-type (n = 12), heterozygous-null (n = 11), and *Chst5* homozygous-null (n = 18) corneas were kindly provided by Professor Nishida of the Department of Ophthalmology at Osaka University Medical School, Osaka. Wild-type corneas were collected from 298-day-old (n = 6) and 302-day-old (n = 6) mice. Heterozygous corneal tissue was collected from 298-day-old (n = 3) and 302-day-old (n = 8) mice. *Chst5*-null corneal tissue was collected from 151-day-old (n = 10) and 210-day-old (n = 8) mice.

Corneas were excised at the limbus immediately after sacrifice, and individually wrapped in clingfilm to limit dehydration. Specimens were immersed in liquid nitrogen and then stored on dry ice and shipped to the UK where they were stored at -80°C prior to examination by XRD on Station 2.1, SRS Daresbury Laboratory.

6.2.2 Low-angle XRD

6.2.2.1 Collection of XRD data

X-ray patterns were collected by Professor Keith Meek and Dr Andrew Quantock as detailed in Section 2.2.2. Specifically, the beam size as 1.5 mm x 1 mm, and shutters were opened for a 3 minute exposure of each cornea. The detector was situated

directly behind the cornea at a distance of approximately 9 m. A 14 hour exposure to Fe^{55} was subtracted from each X-ray pattern in order to account for any non-linearities in the detector.

Data analysis was undertaken following the procedure outlined in Section 2.3 to obtain average values for collagen fibril spacing (Step 4), fibril diameter (Step 3), H/W ratio (Step 5), and coherence distance (Step 6). Step 2(B), the alternative removal of background scatter, was followed.

6.3 Results

For details of statistical analysis refer to Appendix 5. All *P*-values quoted were obtained from Independent samples t-test, unless otherwise stated.

6.3.1 The effect of age on collagen fibril morphology

Prior to investigating the impact of a *Chst5* homozygous-null mutation on corneal stromal ultrastructure via statistical comparison with wild-type and heterozygous-null data, it was necessary to establish if there were significant changes in collagen fibril architecture between mice of different ages. When considering wild-type and heterozygous data sets, corneas were harvested from mice that were separated in age by only 4 days (298-days-old and 302-days-old). However, it was more crucial to determine whether utrastructural changes take place in the corneas of *Chst5* homozygous-null mice as there is an age gap of 51 days between the two groups (151-days-old and 210-days-old).

Effect of age on collagen fibril morphology in the wild-type cornea

Table 6.1 shows the individual measurements obtained from each age group for collagen fibril spacing, fibril diameter, H/W ratio and coherence distance. The average collagen fibril spacing values from the corneas of 298-day-old (47.7 ± 3.8 nm) and 302-day-old (47.9 ± 3.6 nm) mice are similar ($P = 0.879$). Average collagen fibril diameter of corneas from mice at 298- and 302-days-old are also unchanged (36.1 ± 1.1 nm and 36.8 ± 0.5 nm respectively; $P = 0.159$).

Age (days)	n	IFS (nm)	CFD (nm)	H/W ratio (au)	t (nm)
298	1	47.3	37.9	11.5	228
	2	45.9	35.4	29.2	255
	3	48.9	36.6	25.5	226
	4	51.1	36.1	28.7	264
	5	51.4	35.6	36.0	264
	6	41.3	34.9	10.1	222
302	1	51.0	37.4	5.2	262
	2	44.5	36.6	15.3	248
	3	47.4	37.4	20.8	264
	4	43.1	36.1	10.4	238
	5	49.7	36.6	15.1	248
	6	52.2	36.8	33.3	272

Table 6.1. The collagen fibril Bragg spacing (IFS), collagen fibril diameter (CFD), H/W ratio, and coherence distance (t) values of each wild-type tissue sample (n).

The average H/W ratio values obtained from the respective age groups are similar (23.5 ± 10.4 vs. 16.7 ± 9.7; $P = 0.268$). Finally, the coherence distance data indicates that the short-range ordering of collagen fibrils does not change over this time period. Therefore, the data of these age groups could be pooled prior to further statistical analysis, provided that data to follow from heterozygous-null and *Chst5* homozygous-null age groups do not indicate ultrastructural differences with age.

Effect of age on collagen fibril morphology in the heterozygous-null cornea

Table 6.2 shows the individual measurements obtained from each age group for collagen fibril spacing, fibril diameter, H/W ratio and coherence distance.

Age (days)	n	IFS (nm)	CFD (nm)	H/W ratio (au)	t (nm)
298	1	50.3	36.1	16.9	241
	2	47.4	36.1	11.0	231
	3	51.8	36.1	22.4	264
302	1	47.9	34.9	18.2	231
	2	45.7	34.9	12.5	219
	3	45.0	34.9	12.6	217
	4	47.9	35.6	13.6	241
	5	51.2	35.4	17.4	241
	6	47.2	36.8	9.3	235
	7	46.9	36.1	16.3	235
	8	49.9	36.1	20.1	241

Table 6.2. The collagen fibril Bragg spacing (IFS), collagen fibril diameter (CFD), H/W ratio, and coherence distance (t) values of each heterozygous tissue sample (n).

Collagen fibril spacing values obtained from corneas of mice at 298 days of age range between 47.4 and 51.8 nm, while values from corneas of 302-day-old mice range from 45 to 51.2 nm. Statistical analysis shows that the data for each group are essentially the same (Mann-Whitney test; $P = 0.152$). Interestingly, the three average collagen fibril diameter values obtained from 298-day-old mice are remarkably consistent, at 36.1 nm. Corneas from 302-day-old mice consist of collagen fibrils with diameter values ranging between 34.9 and 36.8 nm. When statistically compared, the data from each age group are not significantly different (Mann-Whitney test; $P = 0.194$). The H/W ratio values of each age group were explored. At 298 days, values range between 11 and 22.4, while those from 302-day-old mice range between 9.3 and 20.1. These measurements were found to be similar (Mann-Whitney test; $P = 0.683$). The coherence distance values for both age groups are also similar. Thus, it was established that pooling the data of these age groups is feasible prior to further statistical comparison of each genotype.

Effect of age on collagen fibril morphology in the *Chst5* homozygous-null cornea

Table 6.3 shows the individual measurements obtained from each age group for collagen fibril spacing, fibril diameter, H/W ratio and coherence distance.

Age (days)	n	IFS (nm)	CFD (nm)	H/W ratio (au)	t (nm)
151	1	40.2	35.4	4.8	184
	2	43.8	34.9	7.2	204
	3	42.4	36.6	4.8	184
	4	40.3	34.9	4.7	180
	5	44.7	34.9	6.0	201
	6	42.4	35.2	4.3	168
	7	47.7	34.3	10.1	191
	8	50.1	34.3	15.0	202
	9	47.8	34.5	12.9	192
	10	38.9	34.5	4.1	166
210	1	41.4	34.9	6.7	178
	2	41.8	34.9	6.7	188
	3	39.1	34.5	3.0	148
	4	39.3	33.8	7.3	184
	5	39.6	34.9	3.1	143
	6	38.6	34.9	2.9	219
	7	45.5	33.8	8.1	201
	8	42.5	33.8	5.9	186

Table 6.3. The collagen fibril Bragg spacing (IFS), collagen fibril diameter (CFD), H/W ratio, and coherence distance (t) values of each *Chst5* homozygous-null tissue sample (n).

Average collagen fibril spacing of corneas from mice at 151- and 210-days-old are similar (43.8 ± 3.7 nm and 40.9 ± 2.3 nm respectively; $P = 0.077$). Collagen fibril diameter measurements taken from corneas of 151-day-old mice range from 34.3 nm to 35.4 nm, while measurements from corneas of 210-day-old mice range from 33.8 nm to 34.9 nm. Statistical analysis has shown that there are no significant differences in collagen fibril diameter between these age groups (Mann-Whitney test; $P = 0.168$). The H/W ratio values obtained from corneas of 151-day-old mice range between 4.1 and 15, while those of 210-day-old mice range from 3 to 8.1. The values for each age group are not appreciably different (Mann-Whitney test; $P = 0.423$). The coherence distance each age group are not appreciably different. Therefore, the results of each age group can be pooled for further statistical analysis.

6.3.2 Collagen fibril Bragg spacing

Significant differences in fibril spacing exist between two or more of the pooled groups tested (One-way ANOVA; $P<0.001$) (Figure 6.2). Further Post Hoc testing via Tukey's HSD disclosed that the mean spacing values of wild-type (47.8 ± 3.5 nm) and heterozygous-null (48.3 ± 2.2 nm) mouse corneal collagen are no different ($P = 0.932$). However, average fibril spacing of *Chst5* homozygous-null corneas (42.6 ± 3.4 nm) is significantly lower than that of the other genotypes ($P<0.001$), signifying that disruption of the *Chst5* gene leads to the development of a corneal stroma in which the collagen fibrils are unusually close together.

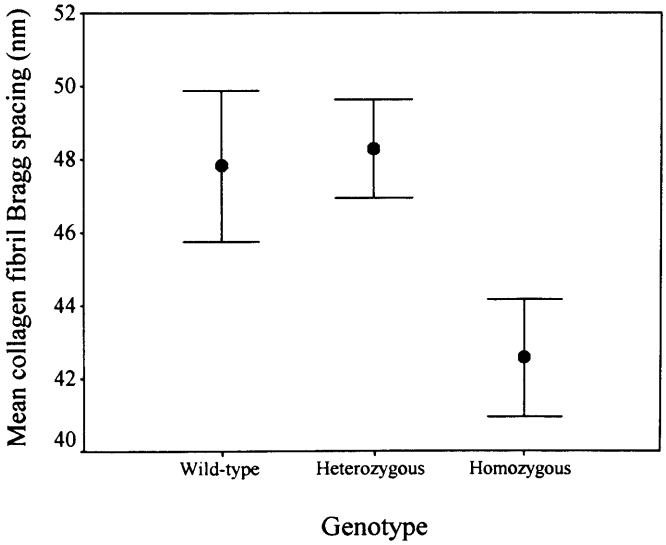

Figure 6.2. Collagen fibril Bragg spacing (nm ± SE) for wild-type, heterozygous-null, and *Chst5* homozygous-null corneas. Fibril spacing of homozygous-null collagen is appreciably smaller.

6.3.3 Collagen fibril diameter

Investigation of the collagen fibril diameter data of each genotype has shown that differences exist between the groups (Kruskal-Wallis H test; $P<0.001$) (Figure 6.3). Further Post Hoc testing via the Mann-Whitney test revealed that collagen fibril diameter values of wild-type (median value 36.6 nm) and heterozygous-null (median value 36.1 nm) corneas are borderline similar ($P = 0.045$). Nevertheless, the collagen fibril diameter data of *Chst5* homozygous-null corneas (median value 34.9 nm) points to collagen fibrils of smaller diameter than the other genotypes ($P<0.001$).

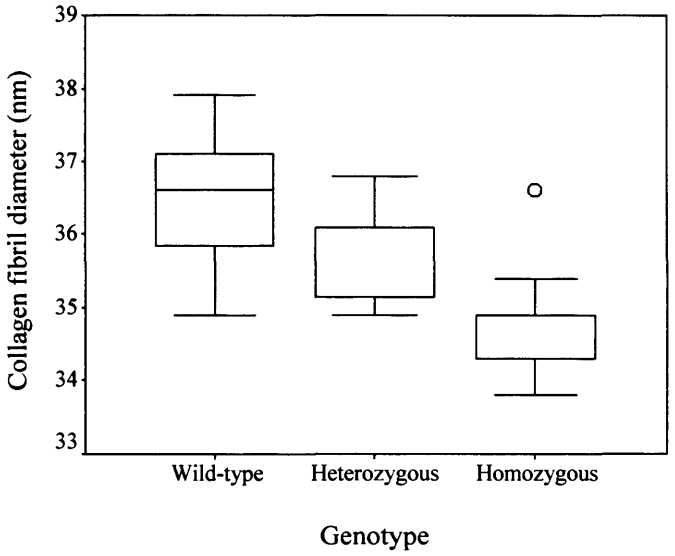

Figure 6.3. Box-and-whiskers plot of collagen fibril diameter (nm) for wild-type, heterozygous-null, and *Chst5* homozygous-null mouse corneal stroma. Wild-type and heterozygous collagen fibrils are of essentially similar diameters, but those of the homozygous-null cornea are smaller than expected (O = outlier value).

6.3.4 H/W ratio and coherence distance of corneal collagen interfibrillar peaks

Statistical analysis has revealed that differences in H/W ratio data exist between the groups (Kruskal-Wallis H test; $P<0.001$). Comparison of wild-type (median value 18.1), and heterozygous-null (median value 16.3) data reveals no significant difference (Mann-Whitney U test; $P = 0.424$). However, the *Chst5* homozygous-null H/W ratio value (median value 6.0) is significantly lower than those of wild-type and heterozygotes (Mann-Whitney; $P<0.001$) (Figure 6.4), signifying that mutant collagen fibrils are less well-ordered. Finally, the coherence distance measurements support the concept that the *Chst5* homozygous-null corneal stroma consists of less well-ordered collagen fibrils (Figure 6.5).

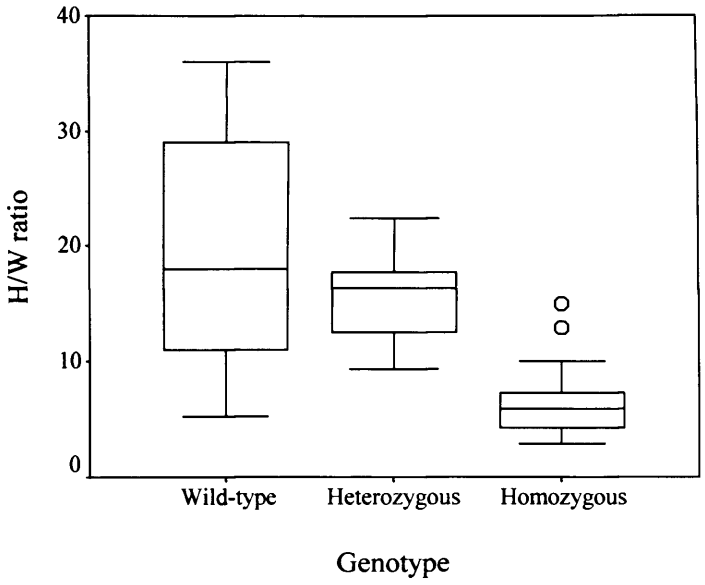

Figure 6.4. Box-and-whiskers plot of H/W ratio for wild-type, heterozygous-null, and *Chst5* homozygous-null mouse corneal stroma. Wild-type and heterozygous-null corneas are on the whole equally well-ordered, but fibrils of *Chst5* homozygous-null corneas are less organised (O = outlier value).

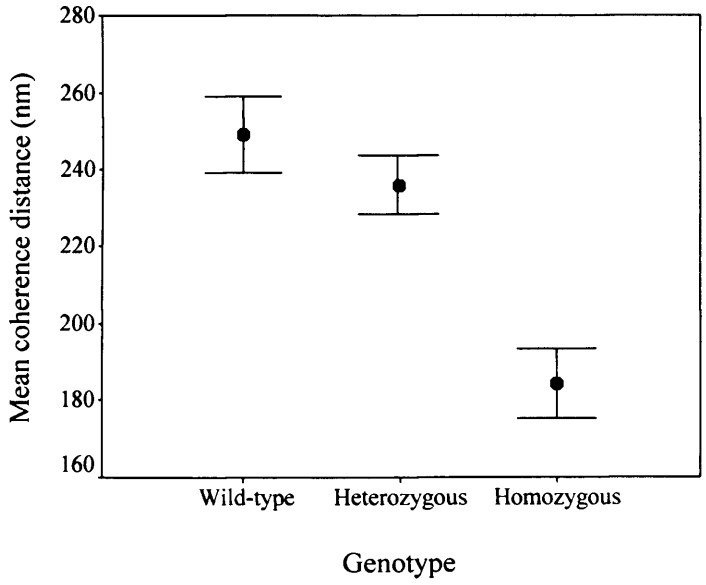

Figure 6.5. Coherence distance (mean ± SE) for wild-type, heterozygous-null, and *Chst5* homozygous-null corneal stromal collagen fibrils. The coherence distance of homozygous-null collagen fibrillar array is smaller.

6.4 Discussion

To date, the generation of gene-targeted KSPG-deficient mice has provided insight into the respective and combined functions of these molecules in the control of collagen fibril architecture (Chakravarti, 2001; Kao and Liu, 2002). The aim of this XRD investigation was to elucidate the importance of the sulphated KS side chains by obtaining highly representative structural data from the corneas of *Chst5* homozygous-null mice that lack the expression of the enzyme C-GlcNAc 6-*O* sulphotransferase.

In human, two sulphotransferase genes, *CHST5* and *CHST6*, are identified as orthologous genes of *Chst5* in mouse; however, only the sulphotransferase encoded on *CHST6* has similar substrate specificity with the enzyme encoded on *Chst5* (Hemmerich and Rosen, 2000; Akama *et al*, 2001). *Chst5* is expressed in intestine as well as corneas in mouse (Lee *et al*, 1999; Akama *et al*, 2001), whereas *CHST6* is expressed in the cornea and cartilaginous tissues such as trachea (Akama *et al*, 2000). In recent years, mutations on *CHST6* have subsequently been found on genomes of MCD patients around the world (Liu *et al*, 2000; El-Ashry *et al*, 2002; Iida-Hasegawa *et al*, 2003; Ha *et al*, 2003a; 2003b; Warren *et al*, 2003; Sultana *et al*, 2003; Abbruzzese *et al*, 2004; Aldave *et al*, 2004; El-Ashry *et al*, 2005). Mutations on *Chst5* or *CHST6*, either by causing a loss of sulphotransferase activity or by diminishing the expression of the enzyme, will result in the under-sulphation of KS.

First of all the XRD data indicates that there is a small difference in the diameter of collagen fibrils in the *Chst5* homozygous-null cornea, with fibrils approximately 2 nm thinner in diameter when compared with normal counterparts. Notwithstanding, the main point here is that the presence of lumican core protein is regulating collagen fibrillogenesis to prevent the formation of larger fibrils in the *Chst5* homozygous-null mutant, a phenomenon witnessed in the cornea of mice deficient for the lumican KSPG (Chakravarti *et al*, 2000). Indeed, Rada *et al* (1993) discovered that the *in vitro* fibrillogenesis of corneal collagen was regulated by intact lumican KSPGs, but that collagen was equally regulated by lumican core protein alone. Dr Phillip Lewis conducted an electron microscopic study via routine fixation of wild-type, heterozygous-null, and *Chst5* homozygous-null corneas that disclosed none of the large, fused collagen fibrils that are an occasional, but consistent, feature of the

lumican-deficient mouse cornea (Chakravarti *et al*, 2000). Taken together, these discoveries show that lateral fusion of collagen fibrils in the corneal stroma is prevented by lumican whether or not the core protein is modified with sulphated KS side chains.

XRD analysis has also shown that the thin *Chst5*-null cornea (Figure 6.1) consists of collagen fibrils that are, on average, closer together than those of wild-type and heterozygous corneas; a phenotype also found in the cornea of humans with MCD (Quantock *et al*, 1990). It is contended here that absence of C-GlcNAc 6-*O* sulphotransferase enzyme activity leads of lower SO_4^- charge repulsion to affect stromal hydration and allow fibrils to come closer together. Also, the KS biosynthesis model proposed by Akama *et al* (2002) detailed that sulphation of GlcNAc residues by C-GlcNAc6ST is coupled to elongation of the poly-N-acetyllactosamine chain. But what is the significance of this? Plaas *et al* (2001b) made a number of interesting observations via the examination of GAG chain fine structure in the MCD type I cornea. KS chain length is typically around 14 disaccharide units in the normal cornea, but is reduced to 3-4 disaccharides in MCD, with an absence of sulphation. It is therefore feasible that KS chain length is stunted when *Chst5* gene expression is abolished in the mouse. Therefore, if disruption of *Chst5* prevents sulphation of GlcNAc by C-GlcNa 6-*O* sulphotransferase, then elongation of the poly-N-acetyllactosamine chain might be halted, rendering the KS chain short and allowing fibrils to come closer together. Akamas' model also relays the possibility that sulphation at the C-6 position of Gal residues may depend on the sulphation of GlcNAc (2002). Indeed, several lines of evidence suggest that this is the case (Fukata *et al*, 1997; Torii *et al*, 2000). Therefore, it is clear to see that absence of sulphotransferase activity will result in the production of no or extremely low sulphated KS.

It is also known that CS/DS chain length is affected in MCD corneas, whereby length is reduced from approximately 40 disaccharide units to just 15 (Plaas *et al*, 2001b). The balance of GAG concentration is altered in the disease state, whereby there is a 24% reduction in KS, and a 60-70% increase in CS/DS (Plaas *et al*, 2001b). This finding suggests that some compensatory mechanisms might come into play when KS synthesis is altered.

It is clear from this investigation of a *Chst5* gene mutation that absence of one gene copy is not enough to affect the cornea, as the *Chst5* heterozygous-null mouse shows no changes in stromal thickness (Figure 6.1), fibril spacing, diameter, or level of fibrillar order. This in turn signifies that the mutation imposed on *Chst5* homozygous-null mice is an autosomal recessive disorder, like MCD type I, and may therefore provide a useful model with which to study this human corneal dystrophy. However, there are potential discrepancies to consider. The human MCD type I cornea suffers progressive opacification, due to the accumulation of large deposits in the keratocytes, endothelium, and between collagen lamellae (Klintworth, 1994). These deposits were later shown to consist of unsulphated KS (Lewis *et al*, 2000). Although the *Chst5*-null cornea presents an altered structural phenotype in which the collagen fibril architecture is similarly altered, there is no apparent loss of transparency (Figure 6.1). First of all, it is possible that corneal opacification may develop with advancing age as, after all, MCD in humans has an onset at around puberty, with surgical intervention not ordinarily required until the third to fifth decade of life. Additionally, a corneal stroma made up of thin, closely packed collagen fibrils may not necessarily lead to corneal cloudiness as the mouse has a cornea that is much thinner than that of human. It is likely that, although the ultrastructure of the mutant cornea is affected, the thin cornea may still allow sufficient light to pass undeterred. Thus, such a mutation may not be as catastrophic in the mouse as in other animals.

It is widely accepted that the sulphation of corneal KSPG is a necessary step in the acquisition of transparency. A biochemical species study conducted by Scott and Bosworth (1990) indicated that, compared to higher vertebrates, mouse cornea contains negligible levels of KS. However, Funderburgh *et al* later provided definitive evidence that mouse, like human, chick, and bovine, contains sulphated KS (1995).

To conclude, the discovery of structural matrix changes in *Chst5* homozygous-null corneas identifies KS GAG sulphation as a key requirement for the control of tissue morphogenesis in the corneal extracellular matrix.

Chapter 7. Concluding remarks

A strong and transparent cornea consists of a well-organised corneal stoma in which the collagen fibrils are regularly arranged and uniformly thin. Although the factors that govern this intricate architecture are not fully understood, research has so far been successful in showing that correct stromal hydration and a specific ratio of matrix constituents are the key (Kao and Liu, 2002). For instance, collagen types I and V co-assemble to produce thin heterotypic fibrils in a broad range of connective tissues, including corneal stroma (Birk *et al*, 1988). An *in vitro* study has shown that the more type V incorporated into a heterotypic fibril, the more restricted the diameter (Birk *et al*, 1990). Therefore, the fact that the corneal stroma contains a relatively high proportion of type V collagen compared to other connective tissues signifies the demand for strict regulation of collagen fibril diameters by the cornea.

This thesis has attempted to address the nature of KSPG-collagen interactions from a structural point of view. KSPGs are bi-functional macromolecules in corneal stroma, with the core protein interacting with collagen fibrils to control lateral fibril growth, and the negatively charged GAG chains extending out into the extracellular matrix to regulate fibril spacing and tissue hydration (Kao and Liu, 2002). Biochemical studies have provided information on the spatial and temporal expression of KSPGs (Funderburgh *et al*, 1997; Dunlevy *et al*, 2000), and therefore the necessity for each at specific developmental stages. However, it is through the development of transgenic and gene-targeted mice that we have developed a deeper appreciation for the role that each KSPG fulfils in the maintenance of corneal stromal architecture.

Therefore, using low-angle X-ray diffraction (XRD) and transmission electron microscopy (TEM), the overall aim of this thesis was to investigate the functional significance of KSPGs in the corneal stroma of both normal and genetically engineered mice by obtaining average values for collagen fibril spacing and collagen fibril diameter. Specifically, this thesis set out to determine the consequences of a lumican-null mutation during neonatal corneal stromal development (Chapter 3), and then to build on existing knowledge of lumican function via the investigation of corneas that express N-terminal Cys/Ser substituted lumican, and also excess lumican (Chapter 4). In Chapter 5, the consequences of a null-homozygous mutation for

mimecan were explored, followed by an attempt to uncouple the role of a KS sulphation step from that of the PG protein core via the examination of corneas from mice lacking *Chst5* gene expression (Chapter 6). These investigations have provided further evidence to support the concept that KSPGs are actively involved in the regulation of corneal stromal matrix architecture and, ultimately, transparency.

7.1 The role of the KSPG core protein in corneal collagen fibrillogenesis

The interaction of PGs with collagen fibrils at specific binding sites along the fibril axis is thought to be of importance for regulating collagen morphology (Scott and Haigh, 1985; Meek *et al*, 1986), with *in vitro* studies revealing that lumican, fibromodulin, and decorin bind fibrillar collagen via the leucine-rich repeat region to inhibit lateral fibril growth (Rada *et al*, 1993; Svensson *et al*, 1995; 2000; Kresse *et al*, 1997). Furthermore, gene-targeted mice with null mutations for either lumican (Chakravarti *et al*, 1998) or decorin (Danielson *et al*, 1997) exhibit abnormal collagen fibril architecture in skin, but only mice deficient for the former proteoglycan present a corneal phenotype.

Ultrastructural abnormalities have been detected in the neonatal lumican-null cornea (Chapter 3), whereby stromal collagen fibrils are more widely spaced, thinner-than-normal, and less well-ordered compared to wild-type counterparts as shown by XRD (Figures 3.4, 3.5, and 3.6 respectively). However, by far the most important discovery of this investigation was that fibril fusion first appears in the 14-day-old lumican-null cornea at a time when fibril spacing returns to normal (Figure 3.8), although it has very recently been indicated that these abnormal fibrils develop slightly earlier, at neonatal day 10 (Chakravarti *et al*, 2006 – in press). These findings strengthening the notion that the core protein of lumican is needed to regulate fibrillogenesis, and that the progressive development of abnormal collagen fibrils during tissue maturation leads to the structural aberrations found in the opaque cornea of mature lumican-null mice.

It is generally agreed that the role of the leucine-rich repeat region is to interact with collagen fibrils and inhibit lateral growth. However, research has shown that this interaction is dependent upon the presence of disulphide bridges at N- and C-terminal regions of the core protein, as the reduction and alkylation of bovine corneal lumican

(Rada *et al*, 1993) and skin decorin (Scott *et al*, 1986) results in a loss of collagen fibrillogenesis. In Chapter 4, the role of the N-terminal region of lumican core protein in the regulation of collagen fibrillogenesis was examined, via the XRD analysis of collagen fibril architecture in the corneas of mice that express an N-terminal Cys/Ser lumican mutant construct. It was previously reported that poor lumican-collagen interaction and a population of thicker-than-normal collagen fibrils are the consequence of this mutation (Carlson *et al*, 2003). XRD data analysis has confirmed that collagen fibrils of lumC/S3 and lumC/S8 corneas are, on average, markedly thicker (Tables 4.6 and 4.7 respectively), although circular in cross-section as shown by electron microscopy (Figures 4.7 E and F respectively). Hence, as the expression of endogenous lumican, and indeed keratocan, in the mutant cornea might be to some extent preventing lateral fibril fusion, it is suggested that future work should focus on studying expression of this construct in the lumican-null cornea to more accurately determine the consequences of this mutation. Nevertheless, the effects of this mutation seem to be progressive, as the average fibril diameter is markedly increased in the eldest lumC/S8 age group (Table 4.7), although it must be born in mind that the sample number of this group is low (n = 3). These discoveries lend support to the hypothesis that proper disulphide bond formation in the N-terminal region of lumican is a necessary process. That is not to say that the N-terminal region itself binds collagen fibrils to limit growth, but maybe that failure to undergo disulphide loop formation affects the overall quaternary structure of lumican core protein.

Chapter 4 also explored stromal ultrastructure when lumican is over-expressed to find that excess lumican has very little bearing on collagen fibril architecture, in line with the findings of Carlson *et al* (2005). Indeed, it is likely that fibril spacing, diameter, and level of fibrillar ordering are unremarkable in the corneal stroma of lumWT5, -25, and -38 mouse lines (Tables 4.3, 4.5, and 4.4 respectively), because there are only a limited number of binding sites along the collagen fibril with which lumican can interact.

So it has been found that the regulation of collagen fibril diameter depends upon the correct expression of lumican core protein. But it is clear from the investigation of mice deficient for either lumican, keratocan, or mimecan, that the corneal phenotypes presented by each mutant differ in severity, pointing to a unique role for these core

proteins. In light of recent evidence that the expression of keratocan depends upon that of lumican (Carlson *et al*, 2005), it is likely that a lumican-null mutation is most severe as the cornea suffers a down regulation of keratocan expression as well as absence of lumican. It is also clear in this situation that the expression of mimecan alone is not enough to control fibril architecture (Chapter 5). In fact, corneas lacking mimecan present only very mild changes at the ultrastructural level. The mimecan-null cornea was previously reported to consist of thicker-than-normal, more loosely packed collagen fibrils (Tasheva *et al*, 2002). Although the biophysical investigation conducted here was in agreement with this report insofar that fibrils are slightly less well ordered, fibril diameter was found to be essentially unchanged (Table 5.1); the electron microscopy investigation later confirmed, at least on a regional scale, that collagen fibrils are uniform in diameter and circular in cross-section (Figure 5.3). Therefore, the only conclusion to arise from the collective research into these mutant corneas is that thicker fibrils may well exist, but in isolated regions not detected in this instance.

The study of corneas from gene-targeted mice has provided important clues as to the necessity for the entire KSPG. However, in Chapter 6, an attempt was made to uncouple the role of the sulphated KS chains from that of the core protein via the investigation of corneas from mice lacking the expression of GlcNAc 6-*O* sulphotransferase. The examination of XRD data revealed that the collagen fibrils are, on average, 2 nm thinner-than-normal (Table 6.3) when compared to corresponding wild-type and heterozygous-null measurements (Tables 6.1 and 6.2 respectively). Notwithstanding, together with electron microscopic evidence that the fibrils are circular in cross-section (Dr Phillip Lewis, personal communication), it is clear that the core protein fulfils its role in the regulation of lateral fibril growth.

It is evident from the investigations conducted here that corneal stromal fibrillar architecture can be disrupted when lumican is knocked out (Chapter 3) or mutated (Chapter 4), and that its role in corneal stroma is a more influential one when compared to mimecan (Chapter 5). It is also apparent that when sulphation of lumican KS chains is disrupted, the interaction of lumican core protein with collagen fibrils is unaltered (Chapter 6). Nevertheless, the sulphated KS chains are equally important in the maintenance of corneal transparency, as they provide both the

physical means by which fibril spacing is maintained and the means by which stromal hydration can be controlled.

7.2 The necessity for sulphated KS chains in the corneal stroma

Corneal transparency is related to the degree of tissue hydration (Maurice, 1970) which is, in turn, dependent upon the quantity, distribution, and nature of GAGs (Bettelheim and Goetz, 1976). The corneal stroma is a very sophisticated connective tissue layer in terms of its heterogeneous structure, and particularly the in distribution of the two major GAGs, CS/DS and KS. Bettelheim and Plessy (1975) have provided evidence that the long CS/DS chains are able to interact with other side chains through Ca^{2+} bridges and hydrogen bonding, thereby creating a tight network, with the result that they have a limited water uptake but a higher degree of water retention. Conversely, the shorter KS side chains create an open network with a therefore larger swelling capacity but a lesser capacity for water retention. It therefore seems that the posterior stroma more readily swells largely due to the concentration of KSPGs in this deeper tissue region. This natural tendency of the tissue to swell is balanced by the endothelial layer, responsible for pumping water out to maintain a constant level of correct hydration. This thesis has presented evidence to support the notion that the KS chains and their modification with sulphate residues are an integral part of the corneal KSPG macromolecule and necessary for proper development of the corneal stroma.

The XRD data analysis in Chapter 3 has revealed that transient stromal thickening (Song *et al*, 2003) is not due to fibril spacing changes (Figure 3.4), but is more likely the result of the fleeting appearance of lakes within the posterior stroma at day 12 (Figure 3.9) when the stroma swells maximally. The most feasible cause for this is the modification of the polylactosamine backbone of lumican with sulphate just before eye opening (Ying *et al*, 1997) to prevent the cornea from drying out on exposure to the atmosphere but, more so, to prepare the stroma for the initiation of endothelial pump activity (Joyce *et al*, 1998). The lack of stromal thickening in the lumican-null cornea substantiates this theory; the ability of the mutant stroma to imbibe water in the days preceding eye opening is disrupted (Song *et al*, 2003), so that when the eyes open stromal hydration falls abnormally low and the tissue fails to recover normal thickness (Song *et al*, 2003).

Corneas over-expressing lumican have normal collagen fibril morphology, but present slightly elevated levels of haze (Carlson *et al*, 2005). It was postulated here that excess lumican, if glycosylated and sulphated, might lead to the formation of lakes (Chapter 4), but it became clear from electron microscopic examination that lakes were not present (Figure 4.4). Similarly, the posterior stroma of mice expressing N-terminal C/S mutated lumican did not contain lakes (Figure 4.6). Therefore, it seems that while expression of these constructs ensure the synthesis of core protein, glycosylation and sulphation might not be equally up-regulated to cause a further influx of stromal water.

The most definitive evidence for the necessity of sulphated KS chains has come from the study of *Chst5*-null mouse corneas (Chapter 6). The nature of this mutation is such that impaired sulphation of the polylactosamine backbone renders the stroma less hydrated and therefore thinner (Figure 6.1 – courtesy of Dr Yasutaka Hayashida). The effects of this mutation might be further exacerbated by the possibility that KS chain length is stunted (Plaas *et al*, 2001b), therefore allowing neighbouring fibrils to come unnaturally close together (Figure 6.2).

Mimecan is also modified with KS chains in cornea (Funderburgh *et al*, 1997). However, mimecan deficiency has no detectable effect on either corneal thickness or transparency (Tasheva *et al*, 2002), and with no obvious change in fibril architecture (Table 5.1), the effect of such a mutation on tissue hydration is minimal. This is understandable when considering that mimecan core protein is reported to carry no more than one KS chain in the mouse, as opposed to the three potential N-linked glycosylation sites identified on mouse lumican (Funderburgh *et al*, 1995) and keratocan (Dunlevy *et al*, 1998).

7.3 Understanding the effects of KSPG mutations on corneal transparency

Corneal transparency is, to a great extent, defined by corneal ultrastructure. When considering only scattering from the collagen fibrils, the fraction of light transmitted through a cornea ($F\lambda$) falls off exponentially with the product of the total scattering cross-section (σ), the collagen fibril number density (ρ), and tissue thickness (t) (Farrell, 1994), with the scattering cross-section depending upon parameters such as

fibril diameter, and the refractive indices of the fibrils and ground substance. Therefore, in order to determine the contribution of collagen scattering to decreased light transmittance in some mutant corneas, it is necessary to consider changes in all these parameters. The investigations undertaken here did not involve measurements such as corneal thickness and hydration, and as a change in one parameter is often accompanied by a change in one or more of the others (Meek *et al*, 2003a), attempts will be made here on a strictly theoretical basis to briefly consider the possible underlying causes for decreased light transmission of some mutant corneas by utilising information from the current literature and the XRD and TEM data obtained.

The neonatal lumican-null cornea is relatively clear (Song *et al*, 2003), and although the mutant cornea is thin and remains so into adulthood (Chakravarti *et al*, 1998), progressive lateral fibril fusion might displace the fibrils and eventually disrupt their mode of packing in the posterior stroma to such an extent that light scattering increases. Corneas over-expressing lumican are of normal thickness (Carlson *et al*, 2005), but present haze to varying degrees. XRD data analysis indicates that collagen fibril morphology is essentially unchanged, although Carlson *et al* did observed a few isolated regions of the posterior stroma in which fibrils were less well ordered (2005). Therefore, while it is possible that fibril packing may contribute to decreased light transmission, the possibility of cellular or extracellular origin should not be ruled out. It is difficult to deliberate the underlying causes for haze in the corneas that express N-terminal C/S mutated lumican, particularly as there is no available data regarding corneal tissue thickness. However, if we were to assume that corneal thickness remains unchanged, as does the average fibril spacing, then changes in the mode of fibril packing, cellular, or extracellular properties might bring about an increase in light scattering. Normal corneal thickness has been reported in mimecan-null mice (Tasheva *et al*, 2002) and as the XRD investigation conducted here has disclosed no significant alterations in matrix architecture in mimecan-null corneas, it may be of little surprise that these mutant corneas show no detectable loss of corneal clarity. Finally, *Chst5*-null corneas suffer from a substantial decrease in collagen fibril spacing, and disordered collagen fibrillar array, yet there is no detectable loss of transparency. These ultrastructural abnormalities might, in some respects, be compensated for by the thin corneal stroma.

7.4 Further research

The main premise of this thesis was to understand the necessity for KSPGs in the corneal stroma, and their role in the governance of fibril architecture. For future research it is recommended that quantitative analysis of collagen and PGs be undertaken in order to more clearly define the link between these mutations and disruption to stromal ultrastructure.

Additionally, as the results in Chapter 3 suggested that a thin mutant stroma consisting of widely spaced fibrils might contain less collagen material, future work could utilise a hydroxyproline assay to quantitatively determine the collagen content of corneal stroma, and thus ascertain whether collagen synthesis is affected in the mutant.

The work conducted in Chapter 4 indicated that N-terminal lumican mutation hampers the ability of this macromolecule to bind collagen. These findings are encouraging, but the author was somewhat limited in interpretation due to the lack of suitable age-matched NTG control samples, and also low sample numbers with which to conduct statistical analysis. Therefore, it is suggested that measures are taken in future to ensure that suitable control samples are available so that more conclusive evidence can be drawn from these studies. Additionally, it is recommended that the expression of this construct be studied in the lumican-null cornea to examine the full extent of this mutation.

As the lumican over-expression work in Chapter 4 employed the use of cupromeronic blue staining and TEM to observe stromal architecture in these corneas, it may be beneficial to conduct chondroitinase ABC digestion on tissue samples beforehand to more clearly observe both the distribution and association of KSPGs with collagen in the posterior stromal regions.

It was postulated in Chapter 4 that lumican transgene expression might activate keratocytes, but it was unfortunately not possible to ascertain whether keratocyte morphology differed in transgenic corneas, as freezing would destroy the cells and may lead them to adopt a different morphology. However, future work could involve

staining corneas for α-smooth muscle actin (α-SMA), one of the few phenotypic markers for the corneal fibroblast (Stramer *et al*, 2004).

Finally, in Chapter 6 it was found that the collagen fibril diameter of *Chst5*-null corneas was, on average, 2 nm smaller than those measurements taken from the corneas of wild-type counterparts. While it is plausible that such a difference is due to a less hydrated stroma, it was unfortunately not possible to take hydration measurements from these small corneas as they would rapidly lose water on exposure to the air and might, therefore, lead to inaccurate final values. However, intermolecular spacing within fibrils is sensitive to changes in hydration, and so it is suggested here that wide-angle XRD may be performed on these mutant corneas to establish whether a decrease in the intermolecular spacing has resulted in the smaller fibril diameter measurements obtained.

By exploring the change in stromal fibril architecture of mutant corneas, this thesis has provided evidence that implicate corneal KSPGs, particularly lumican, in the governance of collagen fibril arrangement. The continued research into PG deficient mice will help to more clearly establish the mechanisms by which corneal stromal ultrastructure is regulated and maintained, thereby enabling the basis for transparency to be more fully understood.

Appendix 1 – General Statistics

The following sections will provide a brief overview of the fundamental concepts of the statistical analysis performed, and the graphical presentation of data in Chapters 3 to 6.

A1.1 Descriptive statistics

Descriptive statistics provide a summary of a data set, which can be presented graphically and numerically. The following are the most commonly used numerical measures for quantitative data. Two values used to describe the average and typical value of a set of data are the mean and the median respectively. The mean (or average) of a variable is the most commonly used measure of the central tendancy (or 'middleness') of a data set, defined as the sum of all the observations divided by the number of observations. The mean is often denoted as M_x. The median value is the 'half-way' value when the data are ranked in order. In instances where there is an even number of observations, the median is defined as the average of the two central values. The median of a data set is particularly useful when a population does not follow a normal distribution (Section A1.3). The third measure of central tendency is the mode, defined as the data value that occurs with the greatest frequency. However, the mode is rarely of any practical use for continuous data.

It is necessary to assess the 'spread' or variability of data within a given sample population. The range, or the difference between the largest value and smallest value, is the simplest measure of variability of data. However, the nature by which the range is determined deems that only the two extreme values within a group are taken into account. Two more useful variability measures which incorporate all of the data are the variance (σ^2) and the standard deviation (σ). The variance is a weighted average of the squared deviations from the mean, indicating how much a set of scores vary from their mean value. The standard deviation (SD) is the positive square root of the variance, a measure of the average (standard) difference (deviation) of a score from the mean in a set of scores. Since the SD is measured in the same units as the variable and the variance is measured in squared units, the SD is often the preferred measure.

Appendix 1

The standard error of the mean (SEM) or standard error is basically the standard deviation of many sample means, defined as $\sigma/\sqrt{n}$, where σ is the standard deviation in the population and n is the size of the sample.

The confidence interval (also known as confidence limits) represents the range within which (to a given level of probability) the 'true' mean of the population would be expected to fall. Confidence intervals of 95% are typically expressed, representing a range of values from mean -1.96SE to mean +1.96SE, and will not include the true population mean value 5% of the time. Confidence intervals are based on the normal distribution (Section A1.3) and equal variance assumptions.

A1.2 Null-hypothesis and *P*-value (or alpha level)

Prior to undertaking any statistical investigation to demonstrate whether a relationship exists between two or more variables, a statement called the null-hypothesis is often constructed, which states that there is no difference between the two (or more) mean values of the populations under comparison. In order to accept or reject this hypothesis, a *P*-value (or alpha level) is calculated. *P*-values represent the probability that a particular outcome would have arisen by chance. Standard scientific practice deems $P \leq 0.05$ as statistically significant and $P \leq 0.001$ as statistically highly significant e.g. $P = 0.001$ means that there is a 0.1% probability that the difference between the two mean values considered arose by pure chance with a true null-hypothesis. Nevertheless, it is important to interpret the *P*-value appropriately, as a low *P*-value does not necessarily mean that the null-hypothesis is not true, but simply that the probability that the null-hypothesis is true is low. Equally, a *P*-value of >0.05 means that *either* there is no difference between the populations *or* that there were too few subjects to demonstrate that such a difference exists.

Finally, the *P*-value quoted throughout each chapter is two-sided (non-directional) as it is assumed that any difference between the two values compared can occur in both directions.

A1.3 Normal distribution of a variable

In order to determine what type of statistical test to implement, it is necessary to assess whether a variable is normally distributed. A variable that follows a normal distribution is symmetric about the mean value and is bell-shaped. This pattern of distribution is mirrored by many biological phenomena. There are two methods implemented for determining the distribution of a sample.

A1.3.1 Test of normality using histograms

It is possible to visually examine the shape of the variable frequency distribution by constructing a histogram and fitting a normal 'bell-shaped' function to the histogram for comparison. However, if the sample population is small then the degree of normality is difficult to assess. Thus, it is often more appropriate to assess normality using histograms when n is large.

A1.3.2 Test of normality using test statistics

The Kolmogorov-Smirnov test and Shapiro-Wilk's W test are available in SPSS 11 statistics package and can be implemented to yield a measure of the degree of data normality. However, in situations where n of a population is less than 50, the Shapiro-Wilks' W test is more appropriate for testing both small and large populations. From this test, the W statistic value is quoted, with values ≤ 0.05 signifying a data set that does not follow a normal Gaussian distribution.

A1.4 Data screening

A1.4.1 Which data screening and why

The aim of data screening is to determine whether the criteria for statistical analysis are fulfilled. The criteria for parametric testing are:

- That data for two (Independent samples t-test) or more (oneway ANOVA) groups we wish to compare follow approximately a normal distribution. If in a certain group of mouse corneas collected, the distribution of each individual measurement is similar to normal, it is reasonable to assume that within the mouse population the distribution of each variable is normal.

- That data variance in each group under comparison should be similar.

It is also beneficial if n of a population is high as central limit theorem determines that the higher the n value, the more the distribution tends to approach normality. If these criteria are not met, then non-parametric statistical methods (Kruskal-Wallis H test and Mann-Whitney U test) should be implemented. The non-parametric (or distribution-free) methods do not require any specific population distribution or any equality of variance for the data, so they are suitable for the data that do not follow the normal distribution. They use ranks rather than raw values for the statistics.

The following statistical tests were implemented within each chapter once their suitability had been established.

A1.4.2 Parametric tests

A1.4.2.1 The t-test

The t-test is one of the most popular statistical tests used to determine whether the means of two groups of scores differ to a statistically significant degree. There are two types of t-test; the independent samples t-test (for the comparison of two sets of data from two different subjects e.g. fibril spacing data from two different mice) and the non-independent samples t-test (for the evaluation of two groups of data collected from the same subject e.g. wet weight and dry weight of a cornea). The independent samples t-test was applied to much of the data analysis.

A1.4.2.2 One-way ANOVA (analysis of variance)

The one-way ANOVA is used to test for statistical significance of the differences among the means of three or more groups of data (not the 'variance' as the name may suggest). If the results of one-way ANOVA give a $P \leq 0.05$ (suggesting that there are statistical difference between some of the groups tested) further Post Hoc testing can be applied (e.g. Tukeys HSD) to determine exactly where these differences lie.

As part of Independent samples t-test and one-way ANOVA, the Levene's test is computed, which explores the homogeneity of group variances under comparison. A

Levene's statistical significance of ≤0.05 indicates that group variances are not equal, and so parametric testing is not appropriate.

A1.4.3 Non-parametric tests

A1.4.3.1 Mann-Whitney U test

The Mann-Whitney U test (or rank sum test) is one of the most commonly used non-parametric tests. It is a very powerful test (except for data that follow a normal distribution) especially if the sample number is low. Therefore, it was ideal for some of the data studied.

1.4.3.2 Kruskal-Wallis H test

The Kruskal-Wallis H test is the non-parametric equivalent of one-way ANOVA. It tests whether several independent samples are from the same population. This test was also implemented.

A1.5 Graphical presentation of data

Data sets that display a normal Gaussian distribution are presented in terms of mean value ± standard error (SE); in a normal distribution, one can be sure that the mean value depicts the central point of the data set, and that the values either side of this point are distributed fairly evenly.

Alternatively, some data sets do not follow a normal distribution, so the mean value of a data set incorrectly represents the central value. The more appropriate presentation is a Box-and-Whiskers plot. This plot consists of a box, presenting the interquartile range (the location of 50% of the data set values). The box itself is intersected by a line representing the median value; this line depicts the midpoint, whereby 50% of the values are above and 50% are below. The whiskers are lines that extend from the box to the highest and lowest values, excluding 'outliers' and 'extremes'. Essentially, SPSS 11 classifies a value lying more than 1.5 interquartile lengths beyond the box as an outlier, while a value found to be more than 3 interquartile ranges beyond the box is an extreme. SPSS 11 shows the presence of an outlier or an extreme value as a single point on the box-and-whiskers plot.

Appendix 2

A2.2 Collagen fibril diameter.

Collagen fibril diameter during normal corneal stromal development.

Age	n	Mean diameter±SD	Median	Range	W-statistic	Levene's statistic	Oneway Anova *P*-value
8	10	31.0 ± 1.3	31.1	4.7	0.243		
10	10	31.3 ± 0.8	31.4	2.7	0.748		
12	12	32.5 ± 1.2	32.3	4.1	0.068	0.759	0.002
14	12	32.3 ± 1.3	32.4	4.3	0.663		

Comparison	Tukey's HSD *P*-value
8 – 10	0.900
8 – 12	0.016
8 – 14	0.048
10 – 12	0.091
12 - 14	0.968

Collagen fibril diameter in the lumican-deficient mouse cornea.

Age	n	Mean diameter ±SD	Median	Range	W-statistic
8	12	29.1 ± 1.0	28.8	3.0	0.012
10	12	30.4 ± 1.3	30.5	5.0	0.645
12	12	30.2 ± 0.8	30.4	2.8	0.209
14	12	30.8 ± 1.4	31.2	4.8	0.186

Comparison	Levene's test	Statistical test	*P*-value
$8^{+/+} - 8^{-/-}$	N/A	Mann-Whitney	0.005
$10^{+/+} - 10^{-/-}$	0.294	Independent samples t-test	0.056
$12^{+/+} - 12^{-/-}$	0.470	Independent samples t-test	<0.001
$14^{+/+} - 14^{-/-}$	0.698	Independent samples t-test	0.015

Appendix 2

A2.3 H/W ratio of corneal collagen interfibrillar peaks.

H/W ratio during normal corneal stromal development.

Age	n	Mean H/W ratio ±SD	Median	Range	W-statistic	Levene's statistic	Oneway Anova *P*-value
8	10	4.6 ± 1.8	5.1	6.3	0.732		
10	10	6.2 ± 1.0	6.4	3.4	0.674		
12	12	7.0 ± 1.8	6.4	5.5	0.060	0.470	<0.001
14	12	7.3 ± 1.6	7.4	4.9	0.481		

Comparison	Tukey's HSD *P*-value
8 – 10	0.118
8 – 12	0.007
8 – 14	0.001
10 – 12	0.722
12 - 14	0.932

H/W ratio of lumican-deficient corneal collagen.

Age	n	Mean H/W ratio ±SD	Median	Range	W-statistic
8	12	3.1 ± 0.9	2.9	2.9	0.568
10	12	4.4 ± 1.5	4.0	5.4	0.031
12	12	3.3 ± 1.1	3.0	4.2	0.004
14	12	3.9 ± 0.9	4.1	2.9	0.250

Comparison	Levene's test	Statistical test	*P*-value
$8^{+/+} - 8^{-/-}$	0.060	Independent samples t-test	0.016
$10^{+/+} - 10^{-/-}$	N/A	Mann-Whitney	0.003
$12^{+/+} - 12^{-/-}$	N/A	Mann-Whitney	<0.001
$14^{+/+} - 14^{-/-}$	0.047	Mann-Whitney	<0.001

A2.4 Coherence distance descriptive statistics.

Mean coherence distance (nm ± SD)		
Neonatal day	$Lum^{+/+}$	$Lum^{-/-}$
8	248 ± 27	234 ± 17
10	253 ± 8	224 ± 15
12	250 ± 19	212 ± 15
14	236 ± 14	214 ± 12

Appendix 3. The effect of lumican mutations on cornea.

A3.1 NTG control results.

A3.1.1 Effect of age on NTG corneal collagen morphology.

Collagen fibril Bragg spacing

Age (months)	n	Mean IFS ± SD	Median	Range	W statistic	Levene's statistic	T-test *P*-value
1.5	7	60.8 ± 5.6	61.6	15.8	0.762		
2.5	9	54.1 ± 5.7	54.0	15.0	0.170	0.903	0.034

Collagen fibril diameter

Age (months)	n	Mean diameter ± SD	Median	Range	W statistic	Levene's statistic	T-test *P*-value
1.5	7	36.2 ± 4.0	35.7	10.7	0.560		
2.5	9	35.6 ± 2.3	34.8	7.6	0.732	0.169	0.718

Interfibrillar peak width at half-height

Age (months)	n	Mean peak width ± SD	Median	Range	W statistic	Levene's statistic	T-test *P*-value
1.5	7	31.6 ± 4.4	30.5	11.3	0.538		
2.5	9	27.5 ± 4.7	26.7	14.7	0.115	0.878	0.099

Coherence distance

Age (months)	n	Mean coherence distance ± SD
1.5	7	301 ± 27
2.5	9	280 ± 20

A3.2. Lumican over-expression results.

A3.2.1 LumWT5 founderline

Change in lumWT5 collagen fibril morphology with increasing age.

Collagen fibril Bragg spacing

Age (months)	n	Mean IFS ± SD	Median	Range	W statistic	Levene's statistic	T-test *P*-value
1.5	9	57.9 ± 6.4	60.0	19.0	0.490		
7	9	56.6 ± 8.0	58.0	22.0	0.283	0.477	0.699

Collagen fibril diameter

Age (months)	n	Mean diameter ± SD	Median	Range	W statistic	Levene's statistic	T-test *P*-value
1.5	9	38.9 ± 2.1	38.3	6.5	0.312		
7	9	37.6 ± 1.9	37.2	6.2	0.788	0.846	0.177

Appendix 3

Interfibrillar peak width at half-height

Age (months)	n	Mean peak width ± SD	Median	Range	W statistic	Levene's statistic	T-test *P*-value
1.5	9	26.9 ± 5.7	26.7	21.0	0.457		
7	9	25.3 ± 7.9	23.0	22.5	0.402	0.133	0.638

Coherence distance

Age (months)	n	Mean coherence distance ± SD
1.5	9	328 ± 42
7	9	372 ± 133

Effect of excess lumican in lumWT5 corneas at 1.5 months

Collagen fibril Bragg spacing

Genotype	n	Mean IFS ± SD	Median	Range	W statistic	Levene's statistic	T-test *P*-value
NTG control	7	60.8 ± 5.6	61.6	15.8	0.762		
Lum WT5	9	57.9 ± 6.4	60.0	19.0	0.490	0.640	0.356

Collagen fibril diameter

Genotype	n	Mean diameter ± SD	Median	Range	W statistic	Levene's statistic	T-test *P*-value
NTG control	7	36.2 ± 4.0	35.7	10.7	0.560		
Lum WT5	9	38.9 ± 2.1	38.3	6.5	0.312	0.113	0.095

Interfibrillar peak width at half-height

Genotype	n	Mean peak width ± SD	Median	Range	W statistic	Levene's statistic	T-test *P*-value
NTG control	7	31.6 ± 4.4	30.5	11.3	0.538		
Lum WT5	9	26.9 ± 5.7	26.7	21.0	0.457	0.892	0.093

Coherence distance

Genotype	n	Mean coherence distance ± SD
NTG control	7	301 ± 27
Lum WT5	9	372 ± 133

A3.2.2 LumWT38 founderline.

Change in lumWT38 collagen fibril morphology with increasing age.

Collagen fibril Bragg spacing

Age (months)	n	Mean IFS ± SD	Median	Range	W statistic	Levene's statistic	T-test *P*-value
2.5	12	58.1 ± 5.9	57.0	20.2	0.701		
4.5	12	58.7 ± 8.7	58.0	35.0	0.304	0.577	0.850

Collagen fibril diameter

Age (months)	n	Mean diameter ± SD	Median	Range	W statistic	Mann-Whitney test *P*-value
2.5	12	36.0 ± 2.7	36.2	9.3	0.377	
4.5	12	38.3 ± 4.3	36.7	14.0	0.045	0.284

Interfibrillar peak width at half-height

Age (months)	n	Mean peak width ± SD	Median	Range	W statistic	Levene's statistic	T-test *P*-value
2.5	12	30.2 ± 4.9	30.0	17.6	0.732		
4.5	12	25.9 ± 5.3	26.2	16.8	0.439	0.618	0.051

Coherence distance

Age (months)	n	Mean coherence distance ± SD
2.5	12	292 ± 26
4.5	12	329 ± 51

Effect of excess lumican in lumWT38 corneas at 2.5 months.

Collagen fibril Bragg spacing

Genotype	n	Mean IFS ± SD	Median	Range	W statistic	Levene's statistic	T-test *P*-value
NTG control	9	54.1 ± 5.7	54.0	15.0	0.170		
Lum WT38	12	58.2 ± 5.9	57.0	20.2	0.701	0.722	0.134

Collagen fibril diameter

Genotype	n	Mean diameter ± SD	Median	Range	W statistic	Levene's statistic	T-test *P*-value
NTG control	9	35.6 ± 2.3	34.8	7.6	0.732		
Lum WT38	12	36.0 ± 2.7	36.2	9.3	0.377	0.660	0.685

Interfibrillar peak width at half-height

Genotype	n	Mean peak width ± SD	Median	Range	W statistic	Levene's statistic	T-test *P*-value
NTG control	9	27.5 ± 4.7	26.7	14.7	0.115		
Lum WT38	12	30.2 ± 4.9	30.0	17.6	0.732	0.784	0.218

Coherence distance

Genotype	n	Mean coherence distance ± SD
NTG control	9	280 ± 20
LumWT38	12	292 ± 26

Effect of excess lumican in lumWT38 corneas at 4.5 months.

Collagen fibril diameter

Genotype	n	Mean diameter ± SD	Median	Range	W statistic	Mann-Whitney *P*-value
Mimecan$^{+/+}$	9	35.9 ± 0.9	36.3	3.1	0.660	
Lum WT38	12	38.3 ± 4.3	36.7	14.0	0.045	0.199

A3.2.3 LumWT25 founderline

Collagen fibril diameter

Genotype	n	Mean diameter ± SD	Median	Range	W statistic	Levene's statistic	Mann-Whitney *P*-value
Chst5$^{-/-}$	12	36.5 ± 0.9	36.6	3.0	0.936		
Lum WT25	11	39.9 ± 3.8	39.4	12.8	0.085	0.003	0.008

A3.3 Lumican N-terminal C/S substitution results.

A3.3.1 LumC/S3 founderline.

Change in lumC/S3 collagen fibril morphology with increasing age.

Collagen fibril Bragg spacing

Age (months)	n	Mean IFS ± SD	Median	Range	W statistic	Levene's statistic	T-test *P*-value
9.5	6	63.4 ± 8.8	62.3	23.0	0.672		
12	4	57.5 ± 5.4	56.5	13.0	0.598	0.324	

Collagen fibril diameter

Age (months)	n	Mean diameter ± SD	Median	Range	W statistic	Mann-Whitney test *P*-value
9.5	6	38.8 ± 2.8	38.0	7.0	0.348	
12	4	38.6 ± 3.9	37.0	8.1	0.043	0.668

Interfibrillar peak width at half-height

Age (months)	n	Mean peak width ± SD	Median	Range	W statistic	Levene's statistic	T-test *P*-value
9.5	6	33.0 ± 7.1	31.0	18.2	0.515		
12	4	30.2 ± 4.3	31.1	9.5	0.534	0.224	0.508

Coherence distance

Age (months)	n	Mean coherence distance ± SD
9.5	6	314 ± 33
12	4	307 ± 63

Effect of N-terminal C/S mutation in lumC/S3 corneas at 9.5 months.

Collagen fibril diameter

Genotype	n	Mean diameter ± SD	Median	Range	W statistic	Levene's statistic	Mann-Whitney *P*-value
Chst5$^{+/+}$	12	36.5 ± 0.9	36.6	3.0	0.936		
Lum C/S3	6	38.8 ± 2.8	38.0	7.0	0.348	0.002	0.031

A3.3.2 Lum C/S8 founderline.

Change in lumC/S8 collagen fibril morphology with increasing age.

Collagen fibril Bragg spacing

Age (months)	n	Mean IFS ± SD	Median	Range	W statistic	Levene's statistic	Oneway ANOVA *P*-value
1.5	10	60.5 ± 5.0	59.5	18.0	0.138		
4	12	61.1 ± 4.7	61.2	17.0	0.656	0.530	0.055
9	3	67.9 ± 7.8	65.8	18.0	0.350		

Post Hoc testing (Tukey's HSD)

Age comparison	*P*-value
1.5 - 4	0.963
1.5 – 9	0.067
4 - 9	0.088

Collagen fibril diameter

Age (months)	n	Mean diameter ± SD	Median	Range	W statistic	Levene's statistic	Oneway ANOVA *P*-value
1.5	10	39.5 ± 2.0	39.4	6.4	0.201		
4	12	40.7 ± 2.1	40.2	6.7	0.602	0.091	0.007
9	3	44.2 ± 4.6	44.2	10.9	0.999		

Post Hoc testing (Tukey's HSD)

Age comparison	*P*-value
1.5 - 4	0.500
1.5 – 9	0.012
4 - 9	0.064

Interfibrillar peak width at half-height

Age (months)	n	Mean peak width ± SD	Median	Range	W statistic	Levene's statistic	Oneway ANOVA *P*-value
1.5	10	30.2 ± 4.9	28.7	15.6	0.148		
4	12	30.4 ± 5.0	30.2	17.1	0.851	0.177	0.448
9	3	33.2 ± 9.0	33.7	20.7	0.934		

Post Hoc testing (Tukey's HSD)

Age comparison	*P*-value
1.5 - 4	0.993
1.5 – 9	0.648
4 - 9	0.684

Coherence distance

Age (months)	n	Mean coherence distance ± SD
1.5	10	317 ± 17
4	12	323 ± 35
9	3	338 ± 22

Effect of lumican N-terminal C/S mutation in lumC/S8 corneas at 1.5 months.

Collagen fibril Bragg spacing

Genotype	n	Mean IFS ± SD	Median	Range	W statistic	Levene's statistic	T-test *P*-value
NTG control	7	60.8 ± 5.6	61.6	15.8	0.762		
Lum C/S8	10	60.5 ± 5.0	59.5	18.0	0.138	0.515	0.903

Collagen fibril diameter

Genotype	n	Mean diameter ± SD	Median	Range	W statistic	Levene's statistic	T-test *P*-value
NTG control	7	36.2 ± 4.0	35.7	10.7	0.560		
Lum C/S8	10	39.5 ± 2.0	39.4	6.4	0.201	0.074	0.039

Interfibrillar peak width at half-height

Genotype	n	Mean peak width ± SD	Median	Range	W statistic	Levene's statistic	T-test *P*-value
NTG control	7	31.6 ± 4.4	30.5	11.3	0.538		
Lum C/S8	10	30.2 ± 4.9	28.7	15.6	0.148	0.885	0.556

Appendix 3

Coherence distance

Genotype	n	Mean coherence distance ± SD
NTG control	7	301 ± 27
Lum C/S8	10	317 ± 17

Effect of lumican N-terminal C/S mutation in lumC/S8 corneas at 4 months.

Collagen fibril diameter

Genotype	n	Mean diameter ± SD	Median	Range	W statistic	Levene's statistic	Mann-Whitney *P*-value
Mimecan$^{+/+}$	9	35.9 ± 0.9	36.3	3.1	0.660		
Lum C/S8	12	40.7 ± 2.1	40.2	6.7	0.602	0.022	<0.001

Effect of lumican N-terminal C/S mutation in lumC/S8 corneas at 9 months.

Collagen fibril diameter

Genotype	n	Mean diameter ± SD	Median	Range	W statistic	Levene's statistic	Mann-Whitney *P*-value
Chst5$^{+/+}$	12	36.5 ± 0.9	36.6	3.0	0.936		
Lum C/S8	3	44.2 ± 4.6	44.2	10.9	0.999	0.002	0.003

The effect of founderline on lumican C/S transgene expression.

Collagen fibril Bragg spacing

Genotype	n	Mean IFS ± SD	Median	Range	W statistic	Levene's statistic	T-test *P*-value
Lum C/S3	6	63.4 ± 8.8	62.3	23.0	0.672		
Lum C/S8	3	67.9 ± 7.8	65.8	18.0	0.350	0.714	0.429

Collagen fibril diameter

Genotype	n	Mean diameter ± SD	Median	Range	W statistic	Levene's statistic	T-test *P*-value
Lum C/S3	6	38.8 ± 2.8	38.0	7.0	0.348		
Lum C/S8	3	44.2 ± 4.6	44.2	10.9	0.999	0.367	0.047

Interfibrillar peak width at half-height

Genotype	n	Mean peak width ± SD	Median	Range	W statistic	Levene's statistic	T-test *P*-value
Lum C/S3	6	33.0 ± 7.1	31.0	18.2	0.518		
Lum C/S8	3	33.2 ± 9.0	33.7	20.7	0.934	0.598	0.970

Appendix 3

Coherence distance

Genotype	n	Mean coherence distance ± SD
Lum C/S3	6	314 ± 33
Lum C/S8	3	338 ± 22

Appendix 4 – The effect of mimecan deficiency on mouse corneal stroma.

A4.1 Collagen fibril Bragg spacing.

Genotype	n	Mean IFS ± SD	Median	Range	W statistic	Levene's statistic	T-test *P*-value
Mimecan$^{+/+}$	9	53.3 ± 4.0	53.6	14.6	0.876		
Mimecan$^{-/-}$	10	52.7 ± 2.6	52.7	7.8	0.675	0.548	0.668

A4.2 Collagen fibril diameter.

Genotype	n	Mean fibril diameter± SD	Median	Range	W statistic	Levene's statistic	T-test *P*-value
Mimecan$^{+/+}$	9	35.9 ± 0.9	36.3	3.1	0.660		
Mimecan$^{-/-}$	10	35.6 ± 1.1	35.4	3.6	0.804	0.700	0.484

A4.3 H/W ratio of corneal collagen interfibrillar peaks.

Genotype	n	Mean H/W ratio ± SD	Median	Range	W statistic	Levene's statistic	T-test *P*-value
Mimecan$^{+/+}$	9	28.2 ± 4.8	26.9	15.9	0.896		
Mimecan$^{-/-}$	10	23.4 ± 5.6	24.3	19.5	0.930	0.652	0.063

A4.4 Coherence distance descriptive statistics.

Genotype	n	Mean ± SD	Median	Range	W statistic
Mimecan$^{+/+}$	9	261 ± 12	256	39	0.293
Mimecan$^{-/-}$	10	244 ± 13	241	44	0.442

Appendix 5 – Corneal stromal architecture and *Chst5* gene absence.

A5.1 The effect of age on collagen fibril morphology.

A5.1.1 Wild-type

Collagen fibril Bragg spacing (IFS).

Age	n	Mean IFS ± SD	Median	Range	W-statistic	Levene's statistic	T-test *P*-value
298	6	47.7 ± 3.8	48.1	10.1	0.523		
302	6	47.9 ± 3.6	48.6	9.1	0.646	0.882	0.879

Pooling of these groups is feasible provided that age is shown to have no affect on fibril spacing in the following age groups.

Collagen fibril diameter (CFD).

Age	n	Mean CFD ± SD	Median	Range	W-statistic	Levene's statistic	T-test *P*-value
298	6	36.1 ± 1.1	35.9	3.0	0.670		
302	6	36.8 ± 0.5	36.7	1.3	0.387	0.191	0.159

The data of both age groups could be pooled prior to further statistical analysis.

H/W ratio

Age	n	Mean H/W ratio ± SD	Median	Range	W-statistic	Levene's statistic	T-test *P*-value
298	6	23.5 ± 10.4	27.1	25.9	0.283		
302	6	16.7 ± 9.7	15.2	28.1	0.668	0.631	0.268

These groups can be pooled prior to further statistical analysis.

A5.1.2 Heterozygous-null.

Collagen fibril Bragg spacing

Age	n	Mean IFS ± SD	Median	Range	W-statistic	Mann-Whitney *P*-value*
298	3	49.8 ± 2.2	50.3	4.4	0.653	
302	8	47.7 ± 2.0	47.6	6.2	0.763	0.152

The data for the heterozygous-null age groups can be pooled for further statistical analysis.

Collagen fibril diameter

Age	n	Mean CFD ± SD	Median	Range	W-statistic	Mann-Whitney *P*-value*
298	3	36.1 ± 0.0	NA^{Ψ}	NA^{Ψ}	NA^{Ψ}	
302	8	35.6 ± 0.7	35.5	1.9	0.227	0.194

The data of both age groups could be pooled before further statistical analysis.

H/W ratio

Age	n	Mean H/W ratio ± SD	Median	Range	W-statistic	Mann-Whitney *P*-value*
298	3	16.8 ± 5.7	16.9	11.4	0.961	
302	8	15.0 ± 3.6	15.0	10.8	0.862	0.683

These groups can be pooled prior to further statistical analysis.

A5.1.3 *Chst5* homozygous-null.

Collagen fibril Bragg spacing

Age	n	Mean IFS ± SD	Median	Range	W-statistic	Levene's statistic	T-test *P*-value
151	10	43.8 ± 3.7	43.1	11.2	0.588		
210	8	40.9 ± 2.3	40.5	6.9	0.252	0.165	0.077

The data of these homozygous-null age groups can be pooled.

Collagen fibril diameter

Age	n	Mean CFD ± SD	Median	Range	W-statistic	Mann-Whitney *P*-value
151	10	34.9 ± 0.7	34.9	2.3	0.036	
210	8	34.4 ± 0.5	34.7	1.1	0.004	0.168

The data from each group could now be pooled for further analysis.

H/W ratio

Age	n	Mean H/W ratio ± SD	Median	Range	W-statistic	Mann-Whitney *P*-value
151	10	7.4 ± 3.9	5.4	10.9	0.018	
210	8	5.5 ± 2.1	6.3	5.2	0.084	0.423

These groups can be pooled prior to further statistical analysis.

Appendix 5

A5.2 Statistical analysis of pooled data

A5.2.1 Collagen fibril Bragg spacing.

Genotype	n	Mean IFS ± SD	Median	Range	W statistic	Levene's statistic	Oneway Anova *P*-value
Wild-type	12	47.8 ± 3.5	48.2	10.9	0.463		
Heterozygous	11	48.3 ± 2.2	47.9	6.8	0.599	0.304	<0.001
Homozygous	18	42.6 ± 3.4	42.1	11.5	0.089		

Comparison	Tukey's HSD *P*-value
Wild-type - heterozygous	0.932
Wild-type - homozygous	<0.001
Heterozygous - homozygous	<0.001

A5.2.2 Collagen fibril diameter.

Genotype	n	Mean CFD ± SD	Median	Range	W statistic	Kruskal-Wallis H *P*-value
Wild-type	12	36.5 ± 0.9	36.6	3.0	0.936	
Heterozygous	11	35.7 ± 0.6	36.1	1.9	0.073	<0.001
Homozygous	18	34.7 ± 0.7	34.9	2.8	0.024	

Comparison	Mann-Whitney *P*-value
Wild-type - heterozygous	0.045
Wild-type - homozygous	<0.001
Heterozygous - homozygous	<0.001

A5.2.3 H/W ratio of corneal collagen interfibrillar peaks.

Genotype	n	Mean H/W ratio ± SD	Median	Range	W statistic	Kruskal-Wallis *P*-value
Wild-type	12	20.1 ± 10.2	18.1	30.9	0.459	
Heterozygous	11	15.5 ± 4.0	16.3	13.1	0.922	<0.001
Homozygous	18	6.5 ± 3.3	6.0	12.1	0.019	

Comparison	Mann-Whitney *P*-value
Wild-type – heterozygous	0.424
Wild-type – homozygous	<0.001
Heterozygous - homozygous	<0.001

Appendix 5

A5.2.4 Coherence distance descriptive statistics.

Genotype	n	Mean t ± SD	Median	Range	W-statistic
Wild-type	12	249 ± 17	251	51	0.202
Heterozygous	11	236 ± 13	235	47	0.197
Homozygous	18	184 ± 19	185	76	0.430

Neonatal Development of the Corneal Stroma in Wild-Type and Lumican-Null Mice

Nicola Beecher,[1] *Shukti Chakravarti,*[2] *Sarah Joyce,*[2] *Keith M. Meek,*[1] *and Andrew J. Quantock*[1]

Purpose. Between days 8 and 14 of neonatal development, the corneal stroma of the mouse undergoes critical changes in tissue thickness, cell density, and light scattering. The authors investigate the stromal matrix structure in wild-type and lumican-deficient corneas in this developmental phase.

Methods. Wild-type (n = 44) and lumican-deficient (n = 42) mouse corneas at neonatal days 8, 10, 12, and 14 were investigated by synchrotron x-ray diffraction to establish the average collagen fibril spacing, average collagen fibril diameter, and level of fibrillar organization in the stromal matrix.

Results. Collagen interfibrillar spacing in the normal mouse cornea became more closely packed between days 8 and 14, though not significantly so. In lumican-null mice, interfibrillar spacing was significantly elevated at days 8, 10, and 12, but not day 14, compared with that in wild-type mice. At all stages investigated, collagen fibrils were, on average, marginally thinner than normal in lumican-null mutants, and the spatial distribution of the fibrils was less well organized.

Conclusions. Transient thickening of the corneal stroma of the normal mouse at eye opening is probably not caused by widespread, homogeneous rearrangement of collagen fibrils but more likely by a temporary increase in cell or stromal "lake" volume. Lumican, structurally influential in adult mouse corneas, is also a key molecule in the neonatal development of the stromal matrix. (*Invest Ophthalmol Vis Sci.* 2006;47:146–150) DOI:10.1167/iovs.05-0907

In the corneal stroma, collagen fibrils are uniformly thin, regularly spaced, and aligned with high spatial order. This arrangement is necessary for light transmittance,[1] with proteoglycans in the extracellular stromal matrix implicated in the control of the collagen fibrillar architecture. The role of proteoglycans in the governance of corneal structure has long been a matter of interest. For example, after the discovery by Anseth[2] that the wound area and the surrounding tissue of rabbit corneas have high levels of chondroitin sulfate and dermatan sulfate and low levels of keratan sulfate, Hassell and colleagues[3] reported that opaque corneal scar tissue in rabbits contains negligible amounts of keratan sulfate and displays large interfibrillar spaces. A subsequent increase in keratan sulfate is accompanied by a return to normal fibril spacing. A significant reduction in keratan sulfate levels in the cornea is also often seen in patients with the most common form of macular corneal dystrophy,[4,5] a disease that renders the cornea significantly thinner than normal with more closely packed collagen fibrils.[6] In development, too, keratan sulfate has long been linked with stromal ultrastructure,[7] and the appearance of the sulfated proteoglycan form of lumican after embryonic day 12 in the chick cornea has given rise to the idea that it might be associated with changes in corneal structure, though other regulatory mechanisms are likely involved.[8,9]

Three types of small corneal proteoglycan have been identified that contain the keratan sulfate side chains lumican,[10] keratocan,[11] and mimecan.[12] Advances in the field of molecular genetics have allowed the generation of mice with targeted proteoglycan deficiencies, allowing investigations into the functional roles of specific corneal proteoglycans. This work has shown that, in maturity, neither keratocan-deficient nor mimecan-deficient corneas exhibit obvious corneal opacities.[13,14] The adult lumican-deficient mouse, on the other hand, displays a severe phenotype, with homozygous mutants exhibiting pronounced corneal opacification, especially in deeper stromal layers.[15] What is not known in any detail, however, is whether ultrastructural matrix aberrations caused by the lack of lumican are late-evolving phenomena or early events in neonatal development that persist into adulthood.

The mouse cornea is well formed at birth but undergoes significant growth afterward, characterized by changes in tissue thickness, cell density, and light scattering.[16] The highly organized stromal matrix, centrally important for light transmittance, clearly must adjust structurally during this developmental phase, but little is known about the manner in which it does so. The mouse as an animal model for corneal research is increasingly gaining importance because of the availability of gene-targeted mutants, and systematic examination of the collagen architecture in the mouse cornea by transmission electron microscopy has begun to address the important question of postnatal development with a view to understanding the acquisition of corneal transparency. This will provide a good assessment of collagen fibril ultrastructure in ultrathin tissue sections. We can also carry out x-ray scattering experiments on intact, isolated corneas to ascertain the spatial dimensions of fibrillar collagen in the corneal stroma. In recent years we have used this approach to study the mature corneas of normal mice and of mice with null mutations in lumican, keratocan, or mimecan.[17–19] Synchrotron x-ray fiber diffraction is a technique by which an intense beam of monochromatic x-rays, focused in the current series of experiments to 1 mm × 0.5 mm at the specimen, is passed through the whole thickness of a cornea. As with the passage of light through the cornea, each collagen fibril in the path of the x-ray beam acts as an independent scatterer of x-rays. Fiber diffraction patterns of com-

From the [1]Structural Biophysics Group, Cardiff School of Optometry and Vision Sciences, Cardiff University, Cardiff, United Kingdom; and the [2]Departments of Medicine, Cell Biology and Ophthalmology, Johns Hopkins University, Baltimore, Maryland.

Supported by the Biotechnology and Biological Sciences Research Council Project Grant 72/B18021 (AJQ), the National Institutes of Health Grant EY11654 (SC), the Medical Research Council Programme Grant G0001033 (KMM, AJQ), and the Council for the Central Laboratory of the Research Councils for beam time at the Synchotron Radiation Source (SRS), Daresbury Laboratory, Cheshire, UK (KMM, AJQ).

Submitted for publication July 14, 2005; revised August 19, 2005; accepted November 15, 2005.

Disclosure: **N. Beecher**, None; **S. Chakravarti**, None; **S. Joyce**, None; **K.M. Meek**, None; **A.J. Quantock**, None

The publication costs of this article were defrayed in part by page charge payment. This article must therefore be marked "*advertisement*" in accordance with 18 U.S.C. §1734 solely to indicate this fact.

Corresponding author: Andrew J. Quantock, Structural Biophysics Group, Cardiff School of Optometry and Vision Sciences, Cardiff University, Redwood Building, King Edward VII Avenue, Cathays Park, Cardiff CF10 3NB, UK; quantockaj@cf.ac.uk.

Investigative Ophthalmology & Visual Science, January 2006, Vol. 47, No. 1

bined x-ray scatter are recorded from individual corneas and analyzed to provide highly representative average values for the spatial dimensions of collagen fibrils in the corneal stroma.[20] Our studies on 2- to 6-month-old corneas disclosed structural matrix changes in lumican-null and keratocan-null mutants but not, to any great extent, mimecan-null mutants.[17-19]

Recently, it was discovered that during neonatal development the mouse corneal stroma sustains a transient alteration in its physical thickness between days 8 and 14.[16] This does not happen in the corneas of lumican-null neonates. Here, we use synchrotron x-ray fiber diffraction to investigate matrix architecture during neonatal development in wild-type and lumican-deficient corneas throughout the day 8 to 14 developmental phase. Our study provides new insights into how the collagen fibril diameter, interfibrillar spacing, and structural order adjust in the normal mouse cornea as it grows, thickens, and condenses before and after eyelid opening. Furthermore, in seeking to elucidate whether the structural defects reported in the adult lumican-null mouse cornea are caused by poor regulation of the dynamic fibrillar architecture during neonatal maturation, we provide clear evidence for a developmental role for lumican in establishing and maintaining the corneal matrix architecture.

Materials and Methods

Specimens

Normal mouse (CD-1) corneas at neonatal development day 8 (n = 10), day 10 (n = 10), day 12 (n = 12), and day 14 (n = 12), along with lumican-null corneas at day 8 (n = 12), day 10 (n = 12), day 12 (n = 12), and day 14 (n = 12) were carefully dissected at the limbus. Because of the small size of each cornea, we thought it was more appropriate to use chemical fixation as a method of preservation rather than freezing as has been done previously, so each cornea was immediately immersed in 4% paraformaldehyde and shipped to Cardiff University in the United Kingdom. The mice were from a colony with a null homozygous mutation for lumican.[15] On arrival, the corneas remained in the fixative solution at 4°C for a week until low-angle x-ray diffraction analysis was undertaken. All procedures were carried out in accordance with the ARVO Statement for the Use of Animals in Ophthalmic and Vision Research.

Data Collection

The corneas, secured in sealed specimen holders between two sheets of mylar, were analyzed at the Synchotron Radiation Source (SRS; Daresbury Laboratory, Cheshire, UK). Each specimen was placed in the path of a focused (1 × 0.5 mm), monochromatic (λ = 0.154 nm) x-ray beam on SRS Station 2.1, and the shutters were opened to expose the cornea for 2 minutes. Low-angle x-ray scattering patterns for all specimens were recorded on a multiwire, gas-proportional area detector situated directly behind the cornea at a distance of 8.25 m. An evacuated tube with polyester film windows separated the specimen from the detector to reduce air scatter. The window nearest the detector contained a lead beam stop that purposely blocked the direct x-ray beam that passed through the cornea undeviated.

Data Processing

X-ray patterns (512 × 512 pixels) were analyzed with software, graphics, and statistics packages (Unix-based software; Statistica; Statsoft, Tulsa, OK). They were initially normalized using ion chamber counts to account for beam intensity decay. A detector response from a 9-hour exposure to a radioactive source (Fe^{55}) was then subtracted from each x-ray pattern to correct for any nonlinearities in the detector. Next, a vertical scan, 26 pixels wide, of x-ray intensity (I) versus reciprocal space coordinate (R) was taken across the center of the pattern to obtain the intensity profile of the first-order equatorial x-ray reflection corrected for the fact that the scan across the circular x-ray pattern was linear. Patterns were then analyzed to obtain values for the average collagen interfibrillar spacing and average collagen fibril diameter, as described elsewhere.[17] Various methods of subtracting background x-ray scatter were tried, and after all of them the overall pattern of structural change that we report remained essentially the same.

In addition to providing a measure of collagen fibril separation, the interfibrillar reflection provides an indication of the degree of local order in the arrangement of the collagen fibrils in the cornea, based on the angular width of the interfibrillar reflection. In accordance with Stokes[21] and Regini et al.,[22] we represent this as the coherence distance with higher values reflective of more local order in the fibrillar array.

Results

X-ray intensity profiles from wild-type and lumican-null corneas in the neonatal day 8 to day 14 time frame contain intensity maxima representing the collagen interfibrillar x-ray reflection (Fig. 1). Before eye opening (days 8 and 10), these maxima are generally better defined in the intensity profiles from wild-type corneas than from lumican-null corneas. This indicates that the fibrillar matrix is relatively well ordered in the normal mouse cornea throughout the developmental period studied—that is, before and after eye opening. Analysis of all x-ray patterns from the 92 corneas examined was undertaken to ascertain average collagen fibril spacing, average collagen fibril diameter, and extent of local order in the fibrillar array.

Collagen Fibril Spacing

The average center-to-center collagen interfibrillar Bragg spacing in the mouse corneal stroma did not change appreciably between postnatal days 8 and 10; it remained approximately 65 nm (P = 0.953; Table 1). After eye opening, at days 12 and 14, collagen fibril spacing was marginally lower than it was before eye opening, measuring 61 to 63 nm (Table 1), though this difference was not statistically significant (days 8-12, P = 0.414; days 8-14, P = 0.063). At days 8, 10, and 12, lumican-deficient corneas had significantly higher fibril spacings than their wild-type counterparts (Table 1). Later, however, at day 14, when the average collagen fibril spacing in the lumican-null corneas decreased, no difference in collagen fibril spacing was detected between wild-type and mutant corneas (Table 1).

Collagen Fibril Diameter

In the normal mouse cornea, average collagen fibril diameters during the stated developmental period were in the 31-nm to 32.5-nm range (Table 1). The average collagen fibril diameter in the same period in the lumican-null corneas was in the 29.1-nm to 30.8-nm range, lower than that in wild-types mice, with the difference significant or close to significance at all time points investigated (Table 1).

Coherence Distance

As an average value for all corneas examined at days 10, 12, and 14, the coherence distance of the collagen fibrillar array in the corneas of lumican-null mice was low with respect to the corresponding value in the corneas of wild-type counterparts (Table 1). This points to a stromal matrix in the mouse cornea at days 10 to 14 that was less well ordered when lumican was absent, with short-range order extending approximately 30 to 50 nm less. In the current analyses, we were unable to reliably obtain measurements of the coherence distance from day 8 lumican-null corneas because many of the interfibrillar reflections were too diffuse. This was indicative of lower levels of structural short-range order at this time point in the mutant corneas compared to later times in these corneas.

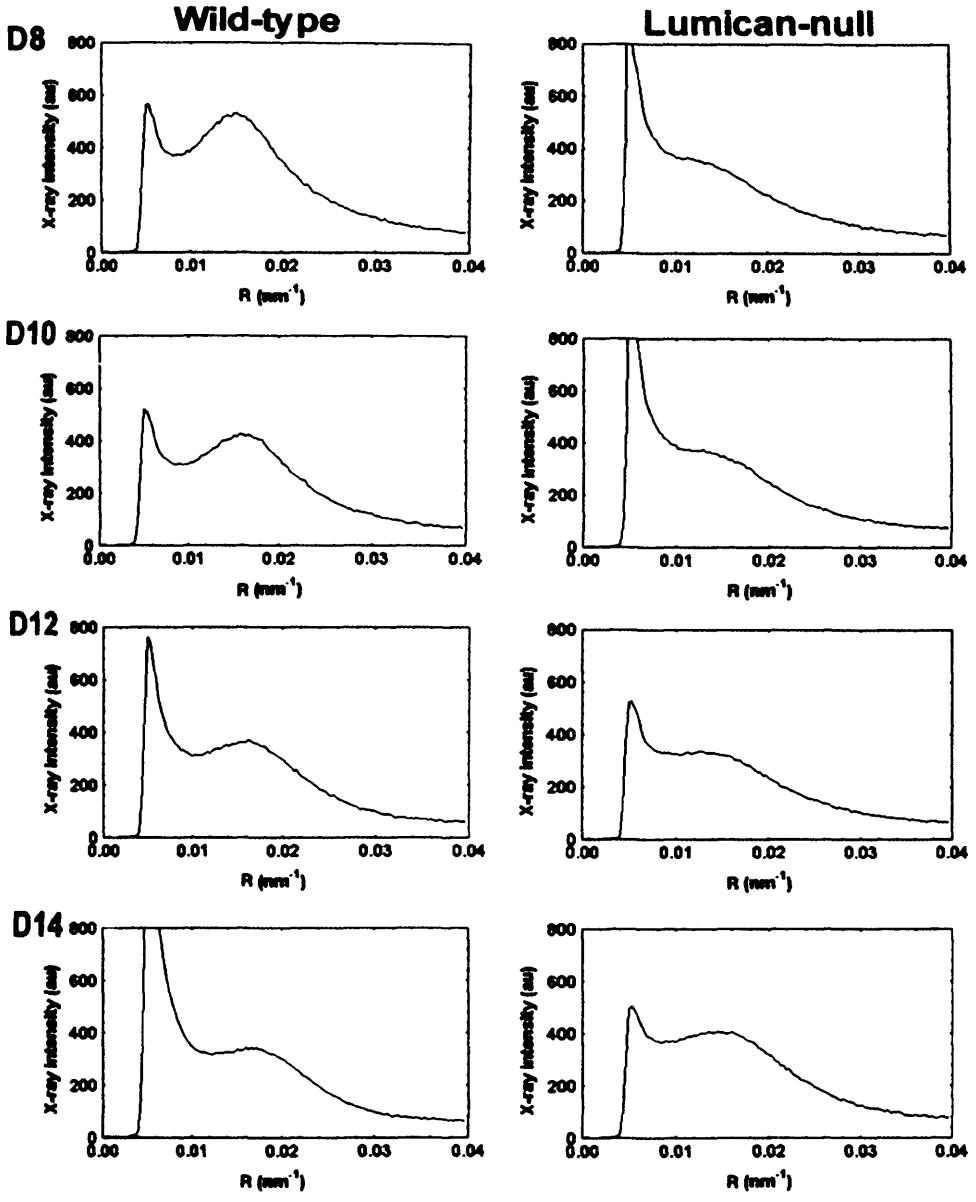

FIGURE 1. X-ray intensity scans across low-angle synchrotron x-ray diffraction patterns from the corneas of day 8 (D8) to 14 wild-type and lumican-null mice. The peak in the region of 0.013 to 0.018 nm^{-1} represents the collagen interfibrillar x-ray reflection that arises from the regularly arranged collagen fibrils that constitute the stromal extracellular matrix.

DISCUSSION

In vivo examinations of neonatal corneal development in the mouse have disclosed that the stroma undergoes a critical period of swelling and thinning around the time of eye opening in the day 8 to 14 interval.[16] We performed a series of synchrotron x-ray diffraction experiments on groups of 10 or 12 normal mouse corneas obtained every two days during this developmental period to investigate the internal fine structure of the stroma and to chart any matrix alterations. Data revealed that in normal mice, the average collagen fibril spacing remained relatively unchanged between days 8 and 10 (Table 1). It then decreased around the time of eye opening (days 10–12), so that a progressively more closely packed collagenous matrix was formed by day 14. Despite differences in tissue preservation and data acquisition/analysis, collagen fibrils in the neonatal mouse cornea throughout the day 8–14 time frame were more widely spaced, on average, than collagen fibrils in the corneas of more mature (i.e., 2- to 6-month-old) mice.[17,19]

Confocal microscopy has found that, in vivo, stromal thickness in normal mice transiently peaks at day 12, only to decrease by day 14 before resuming slow continued growth to adult thickness.[16] The present data have not indicated an increase in average collagen interfibrillar spacing at day 12, leading us to conclude that stromal thickening at this time cannot be ascribed to homogeneous moving apart of collagen fibrils. (A preliminary report at the ARVO 2003 annual meeting presented initial evidence for elevated collagen fibril spacing at day 12 in the normal mouse stroma, but this is not substantiated by the current, more extensive data.) An alternative explanation for the transient day 12 stromal thickening might be the temporary presence of regions of the corneal stroma that are devoid of regularly arranged collagen fibrils, the so-called collagen-free lakes that have been evoked by Benedek[23] among others. As alluded to earlier, x-rays scattered by a corneal matrix of collagen fibrils with some spatial regularity will interfere to form a recordable interfibrillar x-ray reflection. Through analysis, this yields a value for the average center-to-

TABLE 1. Average Structural Parameters for $Lum^{+/+}$ and $Lum^{-/-}$ Mouse Corneas

	Fibril Spacing, nm		Fibril Diameter, nm		Coherence Distance, nm	
Day	$Lum^{+/+}$	$Lum^{-/-}$	$Lum^{+/+}$	$Lum^{-/-}$	$Lum^{+/+}$	$Lum^{-/-}$
8	65.4 ± 3.6	75.6 ± 3.8 $P < 0.001$	31.0 ± 1.3	29.1 ± 1.0 $P = 0.005$*	247 ± 23	N/O
10	64.6 ± 3.4	69.2 ± 3.4 $P = 0.005$	31.3 ± 0.8	30.4 ± 1.3 $P = 0.056$	239 ± 14	197 ± 15 $P < 0.001$
12	63.0 ± 3.6	68.4 ± 3.2 $P < 0.001$	32.5 ± 1.2	30.2 ± 0.8 $P < 0.001$	227 ± 16	181 ± 10 $P < 0.001$
14	61.4 ± 3.7	63.8 ± 3.1 $P = 0.104$	32.3 ± 1.3	30.8 ± 1.4 $P = 0.015$	227 ± 14	199 ± 14 $P < 0.001$

All values are mean ± SD.

Comparison of neonatal murine $Lum^{+/+}$ and $Lum^{-/-}$ corneal collagen interfibrillar Bragg spacing, collagen fibril diameter, and level of fibrillar organization defined as the coherence distance, with higher numbers indicative of more local order in the stromal matrix. Collagen interfibrillar spacing is significantly higher in the lumican null corneal stroma at days 8, 10, and 12, whereas fibril diameter is marginally reduced in the lumican null corneas almost throughout.

N/O indicates data not obtainable because of marked lack of local order in fibrillar array.

* Nonparametric testing because of nonnormal data distribution.

center collagen interfibrillar spacing. Regions of the cornea with little or no regularly arranged collagen, on the other hand, do not contribute sufficiently to the interfibrillar reflection; thus, the presence of lakes would remain unrecognized in the current analysis. It should be borne in mind that the lakes as envisaged here may constitute cellular components of the stroma. Therefore, the transient day 12 increase in stromal thickness can be reconciled with the current findings if it were caused by a passing increase in the overall keratocyte cell volume. Consequently, our interpretation of the data favors a mechanism of temporary stromal thickening in which expansion and contraction of stromal lakes, cellular or not, occur at approximately day 12 rather than a process involving a widespread, homogeneous adjustment of the collagen fibrillar array.

Unlike normal mouse cornea, the corneas of lumican-null mutants do not become thicker at neonatal day 12.[16] The x-ray data indicated that at days 8, 10, and 12, lumican-null corneas exhibited a significant increase in average collagen fibril spacing compared with their age-matched, wild-type counterparts (Table 1). This was particularly noticeable at day 8. By day 14, the average fibril spacing in the corneas of mutant mice was marginally higher than the corresponding wild-type value, but not significantly so. A previous investigation[17] shows that the corneas of mature (2- to 6-month-old) lumican-deficient mice from the same colony have collagen fibrils that tend to be more widely spaced than collagen fibrils in the corneas of age-matched wild-type littermates by an average of 2 nm. Taken with the current findings, a picture emerges of a neonatal mouse cornea before eye opening that has a loosely packed stromal matrix in the absence of lumican. After eye opening, this difference recedes so that by day 14 the marginally elevated interfibrillar spacing in lumican-null corneas is not statistically significant (Table 1). As the tissue gains maturity, the evidence is that the fibrillar array becomes more compact in wild-type and lumican-null corneas alike, with x-ray diffraction data suggesting that a small average elevation in fibril spacing in the lumican-null cornea of approximately 2 nm persists. In some respects the finding of a marginally more loosely packed fibrillar stroma in the absence of a molecule, lumican, which ordinarily contains hydrophilic keratan sulfate side chains, is counterintuitive, but we point out that keratan sulfate tends to be less highly sulfated in the mouse cornea than in that of other species.[24] Additionally, perhaps the hydrophilic nature of its stroma in the lumican-null situation is maintained by other matrix components.

In the normal mouse cornea, the average collagen fibril diameter during the day 8 to 14 neonatal period lies in the 31-nm to 32.5-nm range (Table 1), the same as for 4-month-old mouse corneas that were examined by synchrotron x-ray diffraction after chemical fixation.[18] (Aldehyde fixation causes shrinkage of corneal tissue,[25] with the average collagen fibril diameters in hydrated, unfixed normal adult mouse corneas closer to 35 nm.[17,19]) At all time points investigated here, the average collagen fibril diameter in lumican-null corneas was lower (29.1–30.8 nm) than the average collagen fibril diameter in normal corneas, with the difference significant or close to significant (Table 1). We emphasize that this is a representative average value from x-ray diffraction. Previous electron microscopic studies have found unusually large, fused collagen fibrils in the lumican-null cornea.[26] These fused fibrils are mostly in the posterior stroma, but because they are present only at low levels, they will not contribute appreciably to the x-ray diffraction pattern. Previous experiments have shown that lumican, extracted from bovine cornea by salt or guanidine treatment, is active in inhibiting the in vitro fibrillogenesis of purified collagen monomers, also obtained from ox cornea.[27] In those experiments, fibrils that were formed in the absence of lumican achieved significantly higher final diameters. Ostensibly, this is at odds with the data presented here because the average fibril diameter in our lumican-deficient mice is, throughout the developmental period studied, lower than normal. The discrepancy between the findings of the in vitro experiments with bovine corneal extracts[27] and the transgenic mouse work presented here is difficult to pinpoint, but perhaps it is attributed to a host of reasons. Maybe other stromal proteoglycans or matrix components compensate for the lack of lumican in our mouse model. After all, decorin proteoglycan and decorin core protein also have the ability to regulate collagen fibril diameter.[27] We should also consider that collagen type V has been identified as a regulator of fibril diameter in the hybrid type I/V fibrils that are found in cornea.[28] Thus, it is possible that a differential influence of collagen type V might have contributed to the disparate results in the two systems (the in vitro bovine work used an estimated mixture of 91% collagen type I and 9% collagen type V[27]). We can also speculate that some type of fibril fusion might have taken place in the in vitro bovine fibrillogenesis experiments.[27]

Coherence distance measurements for the wild-type corneas between days 8 and 14 are not markedly different (Table 1), indicating that the level of local order in the normal mouse

stroma does not change appreciably between days 8, 10, 12, and 14. Put another way, we can conclude that the corneal stroma of the normal mouse is already structurally well organized before eye opening, and that its becoming organized is not a consequence of the stromal condensation that occurs after eye opening. The corneal stroma of the lumican-null mouse, on the other hand, is, at all times studied, less well-organized than the corneal stroma of the normal mouse. At day 8, in particular, the stromal matrix of the lumican-null mouse was so disorganized that it did not enable us to make reliable measurements of the coherence distance across all corneas in that group. Stromal disorganization in lumican-deficient mice persists into adulthood.[17] It is also a feature of mature keratocan-deficient corneas,[18] though not, to any great extent, mature mimecan-deficient corneas.[19]

The current findings point to a key role for lumican in the establishment of a properly organized stromal matrix in the neonatal developmental phase, presumably through its interaction with collagen and other matrix components, and suggest that the structural defects seen in adult lumican-null corneas are not structural problems that arise de novo with age, but stem from early postnatal events.

Acknowledgments

The authors thank Gunter Grossmann for help at the Synchotron Radiation Source (Daresbury Laboratory, Cheshire, UK) and Rob Young for useful discussions.

References

1. Maurice DM. The structure and transparency of the cornea. *J Physiol.* 1957;136:263-286.
2. Anseth A. Glycosaminoglycans in corneal regeneration. *Exp Eye Res.* 1961;1:122-127.
3. Hassell JR, Cintron C, Kublin C, Newsome DA. Proteoglycan changes during restoration of transparency in corneal scars. *Arch Biochem Biophys.* 1983;222:362-369.
4. Nakazawa K, Hassell JR, Hascall VC, Lohmander LS, Newsome DA, Krachmer J. Defective processing of keratan sulfate in macular corneal dystrophy. *J Biol Chem.* 1984;259:22:13751-13757.
5. Yang CJ, SundarRaj N, Thonar J-Ma, Klintworth GK. Immunohistochemical evidence of heterogeneity in macular corneal dystrophy. *Am J Ophthalmol.* 1988;106:65-71.
6. Quantock AJ, Meek KM, Ridgway AEA, Bron AJ, Thonar EJ-MA. Macular corneal dystrophy: reduction in both corneal thickness and collagen interfibrillar spacing. *Curr Eye Res.* 1990;9:4:393-398.
7. Anseth A. Glycosaminoglycans in the developing corneal stroma. *Exp Eye Res.* 1961;1:116-121.
8. Cornuet PK, Blochberger TC, Hassell JR. Molecular polymorphism of lumican during corneal development. *Invest Ophthalmol Vis Sci.* 1994;35:870-877.
9. Connon CJ, Meek KM, Kinoshita S, Quantock AJ. Spatial and temporal alterations in the collagen fibrillar array during the onset of transparency in the avian cornea. *Exp Eye Res.* 2004;78:909-915.
10. Blochberger TC, Vergnes JP, Hempel J, Hassell JR. cDNA to chick lumican (corneal keratan sulfate proteoglycan) reveals homology to the small interstitial proteoglycan gene family and expression in muscle and intestine. *J Biol Chem.* 1992;267:1:347-352.
11. Corpuz LM, Funderburgh JL, Funderburgh ML, Bottomley GS, Prakash S, Conrad GW. Molecular cloning and tissue distribution of keratocan: bovine corneal keratan sulfate proteoglycan 37A. *J Biol Chem.* 1996;271:16:9759-9763.
12. Funderburgh JL, Corpuz LM, Roth MR, Funderburgh ML, Tasheva ES, Conrad GW. Mimecan, the 25-kDa corneal keratan sulfate proteoglycan, is a product of the gene producing osteoglycin. *J Biol Chem.* 1997;272:44:28089-28095.
13. Liu CY, Birk DE, Hassell JR, Kane B, Kao WWY. Keratocan-deficient mice display alterations in corneal structure. *J Biol Chem.* 2003;278:21672-21677.
14. Tasheva ES, Koester A, Paulson AQ, et al. Mimecan/osteoglycin-deficient mice have collagen fibril abnormalities. *Mol Vis.* 2002;8:407-415.
15. Chakravarti S, Magnuson T, Lass JH, Jepsen KJ, LaMantia C, Carroll H. Lumican regulates collagen fibril assembly: skin fragility and corneal opacity in the absence of lumican. *J Cell Biol.* 1998;141:1277-1286.
16. Song J, Lee Y-G, Houston J, et al. Neonatal corneal stromal development in the normal and lumican-deficient mouse. *Invest Ophthalmol Vis Sci.* 2003;44:548-557.
17. Quantock AJ, Meek KM, Chakravarti S. An x-ray diffraction investigation of corneal structure in lumican-deficient mice. *Invest Ophthalmol Vis Sci.* 2001;42:1750-1756.
18. Meek KM, Quantock AJ, Boote C, Liu CY, Kao WWY. An x-ray investigation of corneal structure in keratocan-deficient mice. *Matrix Biol.* 2003;22:467-475.
19. Beecher N, Carlson C, Allen BR, et al. An x-ray diffraction study of corneal structure in mimecan-deficient mice. *Invest Ophthalmol Vis Sci.* 2005;46:4046-4049.
20. Meek KM, Quantock AJ. The use of x-ray scattering techniques to determine corneal ultrastructure. *Prog Ret Eye Res.* 2001;20:95-137.
21. Stokes AR. The theory of x-ray fibre diagrams. *Prog Biophys.* 1955;5:5-167.
22. Regini JW, Elliott GF, Hodson SA. The ordering of corneal collagen fibrils with increasing ionic strength. *J Mol Biol.* 2004;336:179-186.
23. Benedek GB. Theory of transparency of the eye. *Applied Optics.* 1971;10:3:459-473.
24. Young RD, Tudor D, Hayes AJ, et al. Atypical composition and ultrastructure of proteoglycans in the mouse corneal stroma. *Invest Ophthalmol Vis Sci.* 2005;1973-1978.
25. Fullwood NJ, Meek KM. A synchrotron x-ray study of the changes occurring in the corneal stroma during processing for electron microscopy. *J Microsc.* 1992;169:53-60.
26. Chakravarti S, Petroll WM, Hassell JR, et al. Corneal opacity in lumican-null mice: defects in collagen fibril structure and packing in the posterior stroma. *Invest Ophthalmol Vis Sci.* 2000;41:11:3365-3373.
27. Rada JA, Cornuet PK, Hassell JR. Regulation of corneal collagen fibrillogenesis in vitro by corneal proteoglycan (lumican and decorin) core proteins. *Exp Eye Res.* 1993;56:635-648.
28. Birk DE, Fitch JM, Babiarz JP, Doane KJ, Linsenmayer TF. Collagen fibrillogenesis in vitro—interaction of type-I and type-V collagen regulates fibril diameter. *J Cell Sci.* 1990;95:649-657.

An X-Ray Diffraction Study of Corneal Structure in Mimecan-Deficient Mice

Nicola Beecher,[1,2] *Connie Carlson,*[3] *Bryan R. Allen,*[3] *Rogers Kipchumba,*[3] *Gary W. Conrad,*[3] *Keith M. Meek,*[1,2] *and Andrew J. Quantock*[1,2]

Purpose. Keratan sulfate proteoglycans (KSPGs) in the corneal stroma are believed to influence collagen fibrillar arrangement. This study was performed to investigate the fibrillar architecture of the corneal stroma in mice homozygous for a null mutation in the corneal KSPG, mimecan.

Methods. Wild-type (n = 9) and mimecan-deficient (n = 10) mouse corneas were investigated by low-angle synchrotron x-ray diffraction to establish the average collagen fibrillar spacing, average collagen fibril diameter, and level of fibrillar organization in the stromal array.

Results. The mean collagen fibril diameter in the corneas of mimecan-null mice, as an average throughout the whole thickness of the tissue, was not appreciably different from normal (35.6 ± 1.1 nm vs. 35.9 ± 1.0 nm). Average center-to-center collagen fibrillar spacing in the mutant corneas measured 52.6 ± 2.6 nm, similar to the 53.3 ± 4.0 nm found in wild-type mice. The degree of local order in the collagen fibrillar array, as indicated by the height-width (H:W) ratio of the background-subtracted interfibrillar x-ray reflection, was also not significantly changed in mimecan-null corneas (23.4 ± 5.6), when compared with the corneas of wild-types (28.2 ± 4.8).

Conclusions. On average, throughout the whole depth of the corneal stroma, collagen fibrils in mimecan-null mice, unlike collagen fibrils in lumican-null mice and keratocan-null mice, are of a normal diameter and are normally spaced and arranged. This indicates that, compared with lumican and keratocan, mimecan has a lesser role in the control of stromal architecture in mouse cornea. (*Invest Ophthalmol Vis Sci.* 2005;46: 4046-4049) DOI:10.1167/iovs.05-0325

Corneal clarity relies on the maintenance of a stromal matrix consisting of uniformly small-diameter collagen fibrils, equally spaced and fairly well ordered, to satisfy the requirements for light transmittance.[1,2] Small leucine-rich proteoglycans (PGs) within the matrix are believed to be necessary elements for the development and maintenance of a well-ordered corneal stroma. Within the cornea, PGs carry either keratan sulfate (KS) or chondroitin sulfate/dermatan sulfate (CS/DS) side-chains, the former population comprising the KSPGs lumican,[3] keratocan,[4] and mimecan.[5] Sulfation of corneal GAGs lends them an overall negative charge and high water-binding capacity,[6] and evidence from several animal models suggests that KS plays a pivotal role in the regulation of corneal stromal structure. For example, the accumulation of KS after developmental day 12 in chick cornea coincides with the onset of corneal transparency from day 14 onward.[7,8] Also, the wound area and surrounding tissue of rabbit corneas contains high levels of CS and DS and low levels of KS.[9] These scars, which display large interfibrillar spaces, later regain normal fibrillar spacing along with an increase in KS levels.[10]

The generation of mice deficient in one or more PGs has allowed researchers to investigate the role of these molecules in corneal ultrastructure, and several studies have been undertaken in an attempt to determine the function of all three KSPGs. These research efforts have indicated that lumican-null murine corneas display a severe phenotype. They are significantly thinner than normal and develop bilateral corneal opacification and a disrupted stromal matrix.[11-15] The corneas of keratocan-deficient mice, in contrast, are virtually indistinguishable from the wild-type in corneal clarity. Nevertheless, they have a thinner corneal stroma,[16] with x-ray scattering studies disclosing collagen fibrils that have a larger-than-normal average diameter and increased interfibrillar spacing.[17] A recent investigation of mimecan-deficient mice disclosed that mutant corneas also appear clinically normal, with no obvious changes in clarity, even though alterations in collagen fibril size are indicated by electron microscopy.[18] The purpose of this investigation was to use x-ray fiber diffraction methodologies to determine to what extent mimecan regulates the overall collagen fibrillar architecture in the mouse cornea.

Materials and Methods

Mimecan-null mice and wild-type counterparts were housed at the Division of Biology, Kansas State University, and handled at all times in accordance with the ARVO Statement for the Use of Animals in Ophthalmic and Vision Research.

The production of the mutants has been reported previously.[18] Ten four-month-old animals were killed by cervical dislocation and the corneas excised at the limbus. Each cornea was individually wrapped in plastic film to limit dehydration, frozen immediately in liquid nitrogen, stored at −80°C, and shipped on dry ice to the United Kingdom. Freezing is an accepted way of storing corneas for investigation of extracellular matrix structure by synchrotron x-ray scattering,[19] and tissues remained wrapped at −80°C before examination of 9 wild-type and 10 mimecan-null corneas. Experiments were performed at the Synchrotron Radiation Source ([SRS], Daresbury Laboratory, Cheshire, UK).

For data collection, corneas were secured in a sealed specimen holder between two sheets of Mylar, where they were allowed to thaw. Each specimen was then placed in turn in the path of a focused (1.5 × 1.0 mm), monochromatic (λ = 0.154 nm) x-ray beam on SRS

From the [1]Structural Biophysics Group, School of Optometry and Vision Sciences, and the [2]Cardiff Institute of Tissue Engineering and Repair, Cardiff University, Cardiff, Wales, United Kingdom; and the [3]Division of Biology, Kansas State University, Manhattan, Kansas.

Supported by Medical Research Council Programme Grant G0001033 (KMM, AJQ), National Eye Institute Grant EY13395 (GWC, EST), and Biotechnology and Biological Sciences Research Council (BBSRC) Project Grant 72/B18021 (AJQ). Mice used in this study were produced by Eli Lilly, Inc., and made available to the authors.

Submitted for publication March 14, 2005; revised April 22, 2005; accepted September 13, 2005.

Disclosure: **N. Beecher**, None; **C. Carlson**, None; **B.R. Allen**, None; **R. Kipchumba**, None; **G.W. Conrad**, Eli Lilly (F); **K.M. Meek**, None; **A.J. Quantock**, None

The publication costs of this article were defrayed in part by page charge payment. This article must therefore be marked "*advertisement*" in accordance with 18 U.S.C. §1734 solely to indicate this fact.

Corresponding author: Andrew J. Quantock, Structural Biophysics Group, School of Optometry and Vision Sciences, Cardiff University, Redwood Building, King Edward VII Ave., Cathays Park, Cardiff CF10 3NB, UK; quantockaj@cf.ac.uk.

Investigative Ophthalmology & Visual Science, November 2005, Vol. 46, No. 11

Station 2.1. The shutters were opened for a 3-minute exposure of each cornea. X-ray fiber diffraction patterns were recorded on a multiwire, gas proportional area detector situated directly behind the cornea at a distance of approximately 9 m. An evacuated tube with polyester film windows separated the specimen from the detector to reduce air scatter. The window nearest the detector contained a small lead beam-stop that purposely blocked the direct x-ray beam, which passed through the cornea undeviated, and thus allowed x-ray diffraction patterns to be recorded. The analytical procedures used to calculate the average collagen interfibrillar spacing, average collagen fibril diameter, and level of the local order in the fibrillar array (i.e., the H:W ratio) have been described previously.[14,20,21] All data were calculated after calibration of the system according to the meridional reflections arising from the 67 nm axial D-periodic collagen repeat in hydrated rat tail tendon.

Results

Low-angle x-ray fiber diffraction patterns obtained from wild-type and mimecan-null mouse corneas, in both cases, consisted of well-defined interfibrillar reflections formed by the interference of x-rays scattered by collagen fibrils with some degree of lateral order (Fig. 1). Vertical transects across these diffraction patterns generated x-ray scattering–intensity plots for wild-type and mimecan-null corneas with similar profiles (Fig. 2). The major scattering elements in the cornea are the stromal collagen fibrils, but a degree of background scatter is produced by nonfibrillar elements in the tissue. After subtracting a power-law background from the experimental data and measuring the position of the background-subtracted interfibrillar reflection (Fig. 2), we obtained data for the mean center-to-center collagen interfibrillar Bragg spacing in each of 9 wild-type and 10 mimecan-null corneas (Table 1). Statistical analysis (±SD) shows that this value in wild-type (53.3 ± 4.0 nm) and mimecan-null (52.6 ± 2.6 nm) corneas is not significantly different (independent samples *t*-test; $P = 0.684$). The collagen interfibrillar Bragg value is quoted for consistency with other structural x-ray studies. Bragg spacing differs from the actual center-to-center collagen interfibrillar spacing in the cornea because the mode of fibrillar packing is not taken into account. If, for example, pseudohexagonal packing of collagen fibrils is assumed, the interfibrillar Bragg spacing must be increased by a 1.12 multiplication factor.[22]

The angular width of a collagen interfibrillar x-ray reflection is an indicator of the degree of local order in the fibrillar array, with narrower reflections formed by more well-ordered spatial arrangements. Narrower reflections give rise to sharper peaks in the x-ray intensity profile of the interfibrillar reflection, and in this study we used the H-W ratio (i.e., height of the background-subtracted peak divided by peak width at half height) to represent a reflection's sharpness.[20,21] Accordingly, a higher H:W ratio is indicative of a matrix arrangement with more local order. The data (Table 1) show that the extent of local order in the collagen fibrillar array was less in mimecan-null corneas (H:W ratio = 23.4 ± 5.6 vs. 28.2 ± 4.8 in wild-types), but not significantly so (independent samples *t*-test; $P = 0.063$).

Analyses of the first subsidiary equatorial reflections in the x-ray intensity profiles (Fig. 2) disclosed that the average collagen fibril diameter in mimecan-null corneas (35.6 ± 1.1 nm) was not appreciably different from normal (35.9 ± 1.0 nm; independent samples *t*-test; $P = 0.476$; Table 1). Thus, for all parameters measured, the fibrillar architecture of the mimecan-deficient mouse cornea, taken as an average throughout the whole corneal thickness, did not differ appreciably from that of wild-type corneas.

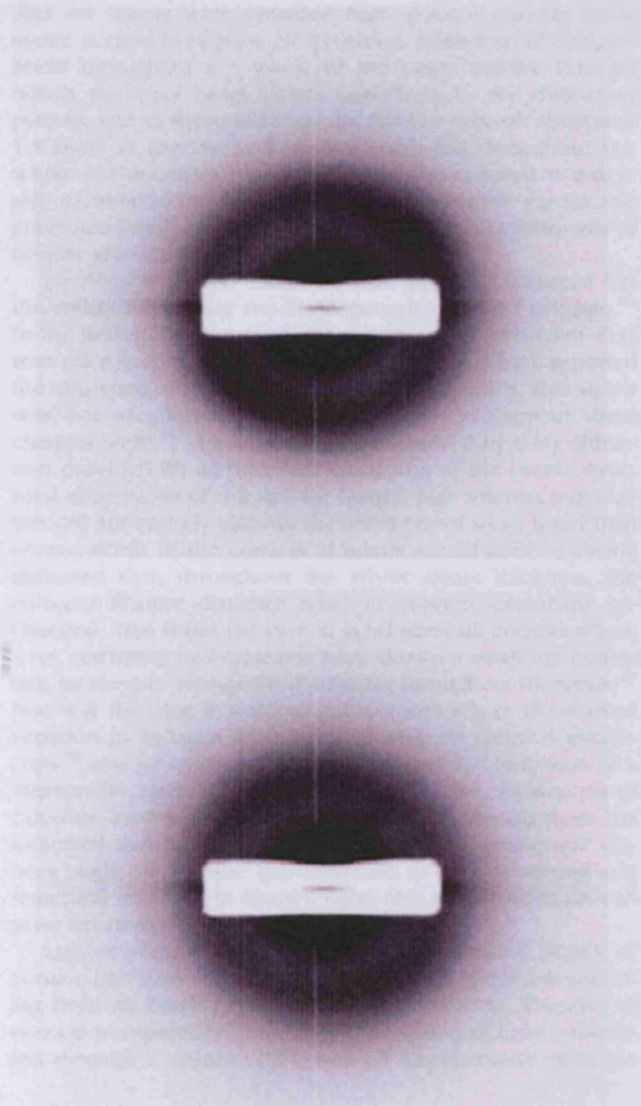

Figure 1. *Top*: a low-angle x-ray diffraction pattern from wild-type mouse cornea (Table 1, specimen 4) containing a dark, circular interfibrillar x-ray reflection produced by x-rays scattered by regularly arranged stromal collagen fibrils. *Bottom*: corresponding diffraction pattern from a mimecan-null cornea (Table 1, specimen 12). The two were not appreciably different.

Discussion

An appreciation of the respective structural roles of the three stromal matrix KSPGs in the cornea is of fundamental importance for a fuller understanding of corneal ultrastructure and transparency. X-ray fiber diffraction studies of the corneas of lumican-null mice and keratocan-null mice have disclosed clear matrix changes, though to different extents.[14,17] In the current investigation, we used similar methodologies to probe the fine structure of the cornea in mice lacking the other main corneal KSPG, mimecan. The results showed that (1) the average collagen interfibrillar spacing in mimecan null corneas was not significantly different from that in wild-type corneas, (2) the level of local order in the fibrillar array was similar in the two tissues, and (3) the mean collagen fibrillar diameter in the corneas of mimecan-null mice was essentially unchanged. The

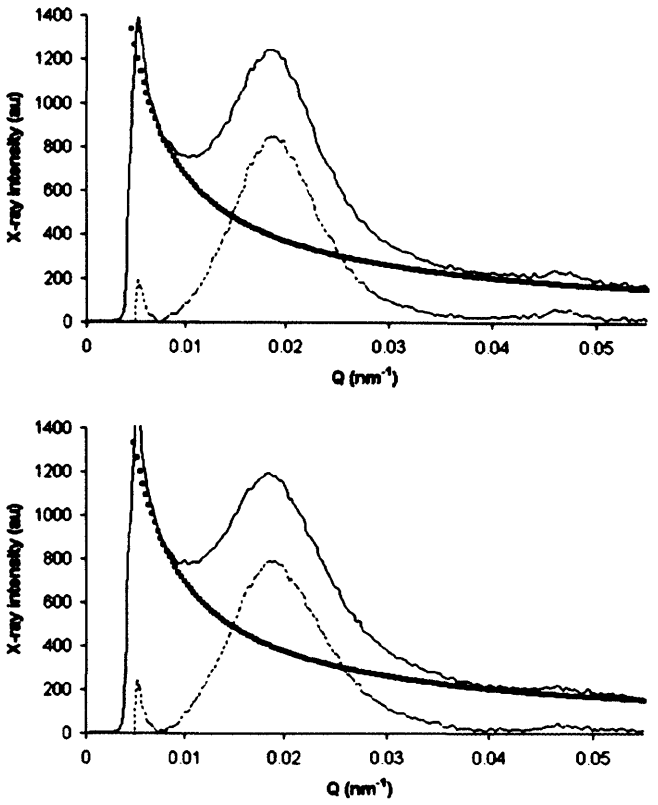

FIGURE 2. X-ray scattering-intensity plots from the wild-type (*top*) and mimecan-null (*bottom*) corneas shown in Figure 1. *Solid line*: x-ray-intensity scan radiating outward from the center of the pattern. A power-law background function (•) is fitted to each experimental data set. *Dashed lines*: x-ray intensity after background removal, with the interfibrillar peak visible at approximately $Q = 0.02$ nm^{-1} and the first subsidiary equatorial reflection used to calculate fibril diameter seen at approximately $Q = 0.047$ nm^{-1}.

data we report were obtained from unfixed corneas maintained at close to physiologic hydration. Moreover, all collagen fibrils throughout the whole of the tissue volume through which the x-ray beam passes contribute to the diffraction pattern, and in these experiments this is a volume measuring 1.5 mm^2 at the cornea's surface extended throughout the whole of the cornea's thickness. Thus, we sampled an extensive number of the collagen fibrils in the mouse cornea and generated highly representative, quantitative measurements of fibrillar architecture.

Previous work has indicated that, in vitro, mimecan has the ability to regulate the fibrillogenesis of type I collagen.[23] In the mimecan-null cornea, manual measurements from electron micrographs of glutaraldehyde-fixed tissue have reported the existence of larger than normal collagen fibrils, although it was not ascertained quantitatively how widespread these changes were.[18] The large sampling achieved by x-ray diffraction provided for an excellent evaluation of the overall structural dimensions of the stromal matrix, and whereas our analysis did not entirely rule out the existence of some larger than normal fibrils in the corneas of mimecan-null mice, it clearly indicated that, throughout the whole tissue thickness, the collagen fibrillar diameter was, on average, essentially unchanged. This is not the case in keratocan-null corneas where x-ray scattering investigations have shown a small but consistent increase in average fibril diameter throughout the tissue.[17] Nor is it the case in lumican-null corneas where the marked variation in collagen fibril diameter seen on electron microscopy[12] was so extensive that it precluded the formation of a measurable x-ray reflection that would have allowed us to calculate average collagen fibril diameter.[14] Recent work has indicated that the severity of phenotype in lumican-null corneas might be because this molecule, as well as serving as a structural regulator in its own right, also modulates keratocan gene expression.[24]

Light-scattering from the extracellular stromal matrix of cornea, like x-ray scattering, is based on the combined scattering from all fibrils in the path of the radiation. Theories of corneal transparency[2] state that the fraction of light transmitted through a cornea, $F(\lambda)$, falls off exponentially with the

TABLE 1. Individual and Average Measurements in the Stroma of Wild-Type and Mimecan-Deficient Mouse Corneas

Genotype	Specimen	Collagen Interfibrillar Spacing (nm)	Collagen Fibril Diameter (nm)	Height/Width Ratio
Mimecan$^{+/+}$	1	52.4	36.3	35.4
	2	51.9	34.5	26.8
	3	50.8	35.2	31.2
	4	53.6	35.2	30.8
	5	54.9	36.6	26.9
	6	53.8	36.3	32.8
	7	56.5	36.3	24.7
	8	60.3	37.6	25.8
	9	45.7	35.4	19.5
	Mean	53.3 ± 4.0	35.9 ± 1.0	28.2 ± 4.8
Mimecan$^{-/-}$	10	51.9	34.3	33.2
	11	53.7	37.1	24.9
	12	53.5	35.4	26.1
	13	51.2	36.1	19.9
	14	49.5	36.1	19.0
	15	54.4	34.9	27.6
	16	49.4	35.4	18.7
	17	50.3	35.4	13.7
	18	57.2	37.4	23.7
	19	55.4	33.8	27.2
	Mean	52.6 ± 2.6	35.6 ± 1.1	23.4 ± 5.6

product of the total scattering cross-section (σ), the collagen fibril number density (ρ), and the thickness of the tissue (t):

$$F(\lambda) = e^{-\sigma\rho t}$$

Detailed calculations of corneal transparency are not trivial, particularly because σ is itself a complex function of the wavelength of light, the diameters of the collagen fibrils, their mode of packing, and the ratio of the refractive index of the hydrated fibrils to the refractive index of the extrafibrillar matrix.[2] Nevertheless, when considering the transparency of lumican-deficient corneas, one could reasonably argue that the increased average interfibrillar spacing seen by x-ray diffraction[14] is indicative of a lower ρ. The lumican-null cornea is considerably thinner than normal, and so t is also reduced.[12] Both of these changes point to an increase in $F(\lambda)$, the corollary being that the alterations in matrix structure must increase the value of σ sufficiently to bring about the three-fold increase in backscattered light from the corneal stroma that is seen in the lumican-null mouse.[12] Keratocan-null corneas are also thinner than normal, with a wider average interfibrillar spacing (and therefore lower t and ρ), but no detectable reduction in corneal clarity.[16,17] This can be explained if we accept that stromal matrix alterations in this mutant are less extensive than in the lumican-null animal, leading to less pronounced changes in σ. Normal corneal thickness (t) has been reported in mimecan-null mice.[18] Because the current investigation discloses no significant alterations in matrix architecture in mimecan-null corneas we can reasonably surmise that any changes in σ and ρ are small. Thus, it is not surprising that these corneas show no detectable loss of corneal clarity.[18]

Mouse cornea, unlike the corneas of most other species that have been investigated, contains KS that is predominantly undersulfated.[25,26] Nevertheless, these PGs are considered to be instrumental in the formation and maintenance of a structurally normal corneal stroma.[11,12,16,18] Based on the findings of this and previous[14,17] x-ray scattering experiments on all three KSPG-null mouse corneas, there appears to be a hierarchy within the KSPG population in terms of their relative influence as structural regulatory molecules: lumican, keratocan, and mimecan in decreasing order of importance.

Acknowledgments

The authors thank Gunter Grossmann for help with data collection at the SRS, and Craig Boote for help with data handling.

References

1. Maurice DM. The structure and transparency of the cornea. *J Physiol.* 1957;136:263-286.
2. Farrell RA. Corneal transparency. In: Albert DM, Jacobiec SA, eds. *Principles and Practice of Ophthalmology.* Philadelphia: Saunders; 1994.
3. Blochberger TC, Vergnes JP, Hempel J, Hassell JR. cDNA to chick lumican (corneal keratan sulfate proteoglycan) reveals homology to the small interstitial proteoglycan gene family and expression in muscle and intestine. *J Biol Chem.* 1992;267:347-352.
4. Corpuz LM, Funderburgh JL, Funderburgh ML, Bottomley GS, Prakash S, Conrad GW. Molecular cloning and tissue distribution of keratocan: bovine corneal keratan sulfate proteoglycan 37A. *J Biol Chem.* 1996;271:9759-9763.
5. Funderburgh JL, Corpuz LM, Roth MR, Funderburgh ML, Tasheva ES, Conrad GW. Mimecan, the 25-kDa corneal keratan sulfate proteoglycan, is a product of the gene producing osteoglycin. *J Biol Chem.* 1997;272:28089-28095.
6. Castoro JA, Bettelheim AA, Bettelheim FA. Water gradients across bovine cornea. *Invest Ophthalmol Vis Sci.* 1988;29:963-968.
7. Hart GW. Biosynthesis of glycosaminoglycans during corneal development. *J Biol Chem.* 1976;251:6513-6521.
8. Cornuet PK, Blochberger TC, Hassell JR. Molecular polymorphism of lumican during corneal development. *Invest Ophthalmol Vis Sci.* 1994;35:870-877.
9. Anseth A. Glycosaminoglycans in corneal regeneration. *Exp Eye Res.* 1961;1:122-127.
10. Hassell JR, Cintron C, Kublin C, Newsome DA. Proteoglycan changes during restoration of transparency in corneal scars. *Arch Biochem Biophys.* 1983;222:362-369.
11. Chakravarti S, Magnuson T, Lass JH, Jepsen KJ, LaMantia C, Carroll H. Lumican regulates collagen fibril assembly: skin fragility and corneal opacity in the absence of lumican. *J Cell Biol.* 1998;141:1277-1286.
12. Chakravarti S, Petroll WM, Hassell JR, et al. Corneal opacity in lumican-null mice: defects in collagen fibril structure and packing in the posterior stroma. *Invest Ophthalmol Vis Sci.* 2000;41:3365-3373.
13. Saika S, Shiraishi A, Saika S, et al. Role of lumican in the corneal epithelium during wound healing. *J Biol Chem.* 2000;275:2607-2612.
14. Quantock AJ, Meek KM, Chakravarti S. An x-ray diffraction investigation of corneal structure in lumican-deficient mice. *Invest Ophthalmol Vis Sci.* 2001;42:1750-1756.
15. Song J, Lee Y-G, Houston J, et al. Neonatal corneal stromal development in the normal and lumican-deficient mouse. *Invest Ophthalmol Vis Sci.* 2003;44:548-557.
16. Liu C-Y, Birk DE, Hassell JR, Kane B, Kao WW-Y. Keratocan-deficient mice display alterations in corneal structure. *J Biol Chem.* 2003;278:21672-21677.
17. Meek KM, Quantock AJ, Boote C, Liu CY, Kao WW-Y. An x-ray diffraction investigation of corneal structure in keratocan-deficient mice. *Matrix Biol.* 2003;22:467-475.
18. Tasheva ES, Koester A, Paulson AQ, et al. Mimecan/osteoglycin-deficient mice have collagen fibril abnormalities. *Mol Vis.* 2002;8:407-415.
19. Fullwood NJ, Meek KM. An ultrastructural, time-resolved study of freezing in the corneal stroma. *J Mol Biol.* 1994;236:749-758.
20. Meek KM, Quantock AJ. The use of x-ray scattering techniques to determine corneal ultrastructure. *Prog Retin Eye Res.* 2001;20:95-137.
21. Rawe IM, Meek KM, Leonard DW, Takahashi T, Cintron C. Structure of corneal scar tissue: an x-ray diffraction study. *Biophys J.* 1994;67:1743-1748.
22. Worthington CR, Inoye H. X-ray diffraction study of the cornea. *Int J Biol Macromol.* 1985;7:2-8.
23. Ge G, Seo NS, Liang X, Hopkins DR, Hook M, Greenspan DS. Bone morphogenetic protein-1/tolloid-related metalloproteinases process osteoglycin and enhance its ability to regulate collagen fibrillogenesis. *J Biol Chem.* 2004;279:41626-41633.
24. Carlson EC, Liu CY, Chikama TI, et al. Keratocan, a cornea-specific keratan sulfate proteoglycan, is regulated by lumican. *J Biol Chem.* 2005;280:25541-25547.
25. Scott JE, Bosworth TR. A comparative biochemical and ultrastructural study of proteoglycan-collagen interactions in corneal stroma. *Biochem J.* 1990;270:491-497.
26. Young RD, Tudor D, Hayes AJ, et al. Atypical composition and ultrastructure of proteoglycans in the mouse corneal stroma. *Invest Ophthalmol Vis Sci.* 2005;46:1973-1978.

Matrix morphogenesis in cornea is mediated by the modification of keratan sulfate by GlcNAc 6-*O*-sulfotransferase

Yasutaka Hayashida*, Tomoya O. Akama†, Nicola Beecher‡, Philip Lewis‡, Robert D. Young‡, Keith M. Meek‡, Briedgeen Kerr§, Clare E. Hughes§, Bruce Caterson§, Akira Tanigami¶, Jun Nakayama‖, Michiko N. Fukada†, Yasuo Tano*, Kohji Nishida**††, and Andrew J. Quantock‡

*Department of Ophthalmology, Osaka University Medical School, 2-2 Yamadaoka, Suita, Osaka 565-0871, Japan; †Glycobiology Program, Burnham Institute for Medical Research, 10901 North Torrey Pines Road, La Jolla, CA 92037; ‡Structural Biophysics Group, School of Optometry and Vision Sciences, Cardiff University, Redwood Building, Cathays Park, Cardiff CF10 3NB, United Kingdom; §Connective Tissue Biology Laboratory, School of Biosciences, Cardiff University, Museum Avenue, Cathays Park, Cardiff CF10 3US, United Kingdom; ¶Otsuka GEN Research Institute, Otsuka Pharmaceutical Co. Ltd., Tokushima 771-0192, Japan; ‖Department of Pathology, Shinshu University School of Medicine, Matsumoto 390-8621, Japan; and **Department of Ophthalmology, Tohoku University Medical School, 1-1 Seiryo-cho, Aobaku, Sendai, Miyagi 980-8574, Japan

Edited by Stuart A. Kornfeld, Washington University School of Medicine, St. Louis, MO, and approved July 12, 2006 (received for review June 29, 2006)

Matrix assembly and homeostasis in collagen-rich tissues are mediated by interactions with proteoglycans (PGs) substituted with sulfated glycosaminoglycans (GAGs). The major GAG in cornea is keratan sulfate (KS), which is N-linked to one of three PG core proteins. To ascertain the importance of the carbohydrate chain sulfation step in KS functionality, we generated a strain of mice with a targeted gene deletion in *Chst5*, which encodes an *N*-acetylglucosamine-6-*O*-sulfotransferase that is integral to the sulfation of KS chains. Corneas of homozygous mutants were significantly thinner than those of WT or heterozygous mice. They lacked high-sulfated KS, but contained the core protein of the major corneal KSPG, lumican. Histochemically stained KSPGs coassociated with fibrillar collagen in WT corneas, but were not identified in the *Chst5*-null tissue. Conversely, abnormally large chondroitin sulfate/dermatan sulfate PG complexes were abundant throughout the *Chst5*-deficient cornea, indicating an alteration of controlled PG production in the mutant cornea. The corneal stroma of the *Chst5*-null mouse exhibited widespread structural alterations in collagen fibrillar architecture, including decreased interfibrillar spacing and a more spatially disorganized collagen array. The enzymatic sulfation of KS GAG chains is thus identified as a key requirement for PG biosynthesis and collagen matrix organization.

collagen | glycosaminoglycans | proteoglycans

Glycosaminoglycans (GAGs) substituted on proteoglycans (PGs) are influential in defining collagen fibrillar architecture in a wide range of connective tissue matrices. Keratan sulfate (KS) is an important constituent of several collagen-rich tissues and is the major GAG in cornea where it is N-linked to asparagine residues in one of three PG core proteins: lumican (1), keratocan (2), and mimecan/osteoglycin (3). Human corneal GlcNAc 6-*O*-sulfotransferase (also known as human GlcNAc6ST-5 and GST4β) is the responsible enzyme for the synthesis of high-sulfated KS via the transfer of sulfate onto the GlcNAc 6-*O* position of the KS backbone (4).

Fairly compelling evidence exists for a regulatory role for KSPGs in the maintenance of corneal matrix structure in a number of species. The avian cornea *in ovo*, for example, synthesizes an unsulfated form of KS midway through development when it is structurally disorganized and transmits relatively little light, but switches to produce a sulfated KS GAG as it becomes transparent and attains a more well ordered collagen fibrillar ultrastructure (5, 6). KS sulfation patterns are also altered in opaque, structurally disorganized corneal scar tissue in rabbits (7, 8) and in cloudy human corneas with the inherited disease, macular corneal dystrophy (9), which is caused by mutations in *CHST6*, a gene encoding human corneal GlcNAc 6-*O*-sulfotransferase (10).

Hybrid type I/V collagen fibrils are the cornea's main nonspecular light-scattering elements and are formed into wide, interweaving belts or lamellae that lie approximately in the tissue plane (11). Within each lamella the fibrils are regularly spaced and have remarkably uniform diameters. It is this configuration that sets the cornea apart from other collagenous (and opaque) connective tissues and is responsible for its transmission of visible light (12). KSPGs are believed to shape the architecture of the cornea via interactions with fibrillar collagen.

Investigations of the corneas of mice with null mutations in lumican (13–17) or keratocan (18, 19) have disclosed specific abnormalities in tissue architecture. Deletions of mimecan, on the other hand, have minimal influence on corneal matrix assembly (20, 21). These observations stimulated several questions that are pivotal to our understanding of the functional roles of the component molecular domains of PGs. To better understand the role of KS sulfation motifs in corneal matrix morphogenesis and uncouple the role of KS GAG from KSPG we investigated the corneas of a newly generated mouse strain with a null mutation in *Chst5*, which encodes a GlcNAc 6-*O*-sulfotransferase that is responsible for the sulfation of KS GAG chains.

Results

To elucidate the biological functions of sulfated KS GAG in mouse cornea *in vivo*, a target vector was constructed that contained a *Chst5* DNA fragment with a neomycin-resistant gene that substituted the ORF of *Chst5*. Homologous recombinant ES cells were produced (Fig. 1*A*) and used to generate *Chst5*-null mice by intercrossing *Chst5* heterozygotes (Fig. 1*B*). Homozygous mutants did not express *Chst5* mRNA (Fig. 1*C*). Genotyping at 3 weeks of age disclosed that ≈25% of pups were *Chst5*-null. The null mice were normally developed at their embryonic stage and born without any critical deficiencies. Follow-up study after 1 yr showed that *Chst5* mutations were nonlethal and the mice developed normally with no outward signs of abnormal gait or skeletal deformities. On slit-lamp examination corneas were transparent in the homozygous, heterozygous, and WT animals. *Chst5*-null corneas displayed normal tissue stratification on histological examination, but were significantly thinner than normal with a stroma that measured 51.1 ± 4.5 μm (n = 12) compared with 63.1 ± 4.6 μm (n = 12) in heterozygous mice ($P < 0.001$) and 66.3 ± 9.0 μm (n = 16) in WT

Conflict of interest statement: No conflicts declared.

This paper was submitted directly (Track II) to the PNAS office.

Abbreviations: KS, keratan sulfate; CS, chondroitin sulfate; DS, dermatan sulfate; PG, proteoglycan; GAG, glycosaminoglycan.

††To whom correspondence should be addressed. E-mail: knishida@oph.med.tohoku.ac.jp.

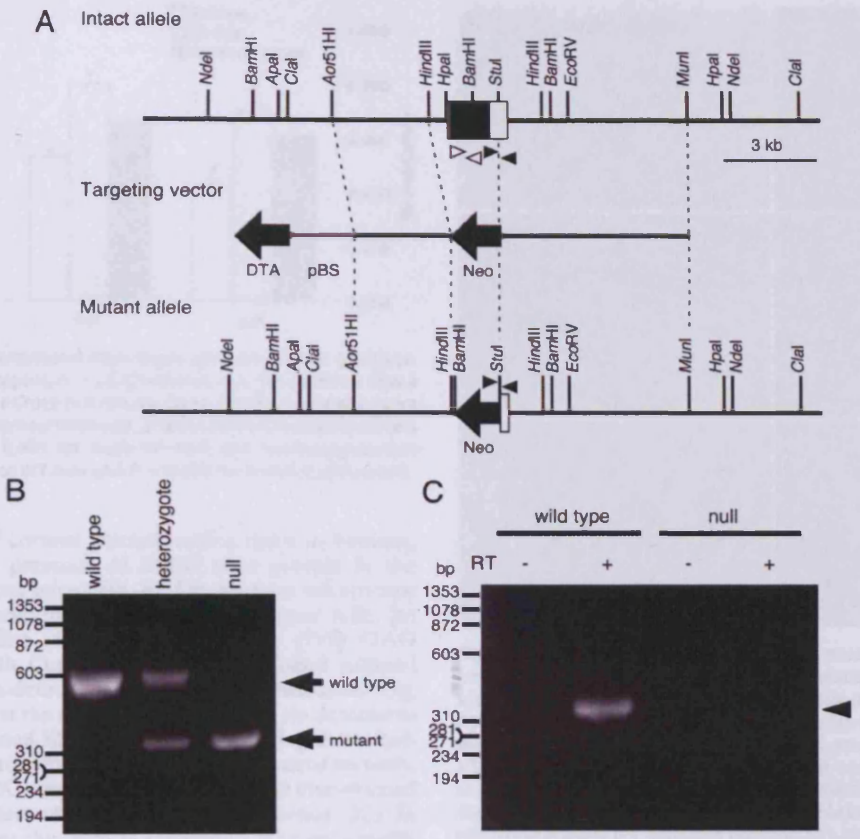

Fig. 1. Generation of *Chst5*-null mice. (*A*) Structure of the targeting vector and generated mutant allele. *Chst5* exon 2 (white box) including a single ORF (black box) was replaced with a neomycin-resistant gene (Neo, shown by a black arrow) in the targeting vector and generated mutant allele. The negative selection marker, DTA, and plasmid vector backbone, pBS, are shown by a black arrow and a gray line, respectively. (*B*) Normal and mutant alleles generated by homologous recombination with the targeting vector were detected by genomic PCR analysis using specific primers shown as black arrowheads in *A*. (*C*) RT-PCR analysis using primers indicated as white arrowheads in *A* also confirmed the presence and absence of *Chst5* mRNA (indicated by an arrowhead) in the whole eyes of WT and *Chst5*-null mice, respectively.

mice ($P < 0.001$) (Figs. 2 and 3). Epithelial thickness, as evidenced by the cornea/stroma thickness ratios, was unaffected (Fig. 3).

PG Composition. Previously, we found comparatively low levels of sulfated KS in normal mouse cornea based on immunoreactivity with 5D4 (22), a mAb that recognizes high sulfated sequences of residues (minimally penta-sulfated) on poly *N*-acetyllactosamine disaccharides of KS (23, 24). In the current study these KS epitopes were detected in extracts of WT and heterozygous corneas, but not in corneal extracts from homozygous *Chst5*-null mice (Fig. 4).

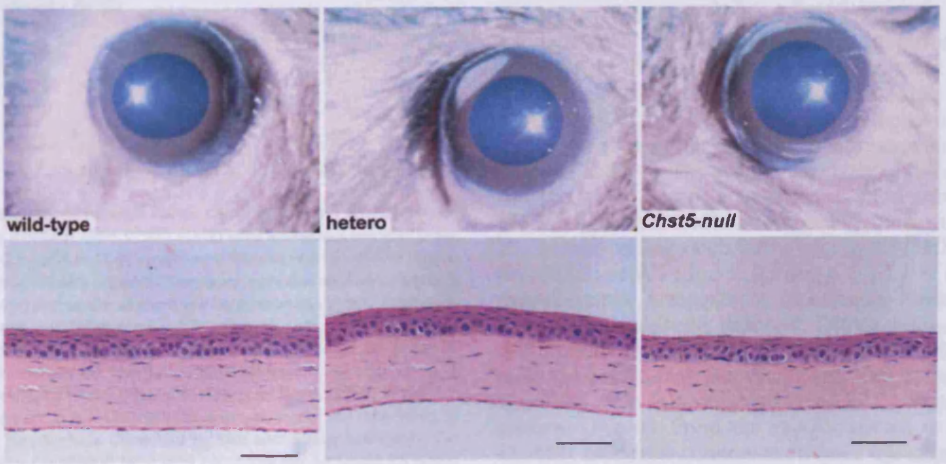

Fig. 2. Corneas of WT, heterozygous, and homozygous *Chst5*-null mice with no evidence of tissue opacification. Histologic sections show normal tissue stratification, but with an indication of a relatively thin stroma in the mutant mouse. (Scale bars: 50 μm.)

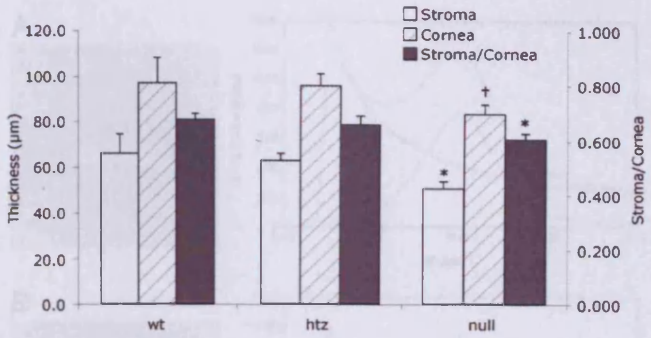

Fig. 3. Corneal thickness measured from tissue sections in each genotype group (WT, $n = 12$; heterozygous, $n = 12$; *Chst5*-null, $n = 16$) confirms that a thin stroma is a feature of the *Chst5*-null mouse. Open, hatched, and filled bars indicate stromal thickness, corneal thickness, and the stroma/cornea thickness ratio, respectively. *, $P < 0.001$ for both WT-null and heterozygous-null comparisons. †, $P < 0.003$ for WT-null and $P < 0.001$ for heterozygous-null.

Immunoblot analysis of corneal extracts with a mAb to lumican, however, identifies the presence of KSPG core protein in the corneas of *Chst5*-deficient mice (Fig. 4). On electron microscopy WT corneas that had been incubated in chondroitinase ABC [to digest chondroitin sulfate (CS)/dermatan sulfate (DS) GAG chains] and stained with Cupromeronic blue exhibited sulfated KSPGs as small electron-dense, collagen-associated filaments (Fig. 5). *Chst5*-null corneas, on the other hand, contained no detectable Cupromeronic blue-stained KSPG filaments, indicating their abolishment by the *Chst5* mutation (Fig. 5). As was discovered recently, large chondroitinase ABC-susceptible, Cupromeronic blue-stained PG filaments are a feature of the normal mouse cornea (22). In *Chst5*-null mouse corneas the large PG filaments take on a highly unusual branched "caterpillar-like" morphology (Fig. 5). They are removed from the tissue by incubation in chondroitinase ABC, but not keratanase I, indicating a significant CS/DS component.

Collagen Matrix Architecture. In all genotypes, electron microscopy revealed a typical lamellar organization of aligned collagen fibrils

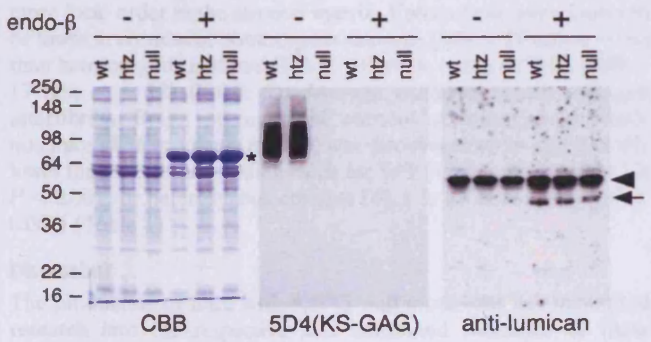

Fig. 4. Immunoblot analysis of corneal KSPG. Corneal protein extracts were stained with Coomasie brilliant blue (CBB) (*Left*) and analyzed for the presence of sulfated KS-GAG by 5D4 mAb (*Center*) and the expression of KSPG core protein by antilumican antibody (*Right*). Lanes of corneal protein extracts from *Chst5*-WT, heterozygote, and null mice are indicated as wt, htz, and null, respectively. Each extract was incubated with (+) and without (−) endo-β-galactosidase before SDS/PAGE. A major band found in lanes of endo-β-galactosidase-digested protein on the SDS/PAGE pattern (marked by *) is exogenous BSA included with endo-β-galactosidase as a stabilizer. A prominent band (arrowhead) on the immunoblot with antilumican antibody is endogenous mouse Ig heavy chain detected by the secondary antibody. On 5D4 immunostaining, the *Chst5*-null lane was negative for sulfated KS GAG. Lumican protein (arrow) was detected in endo-β-galactosidase-treated lanes in corneal extracts from all three genotypes.

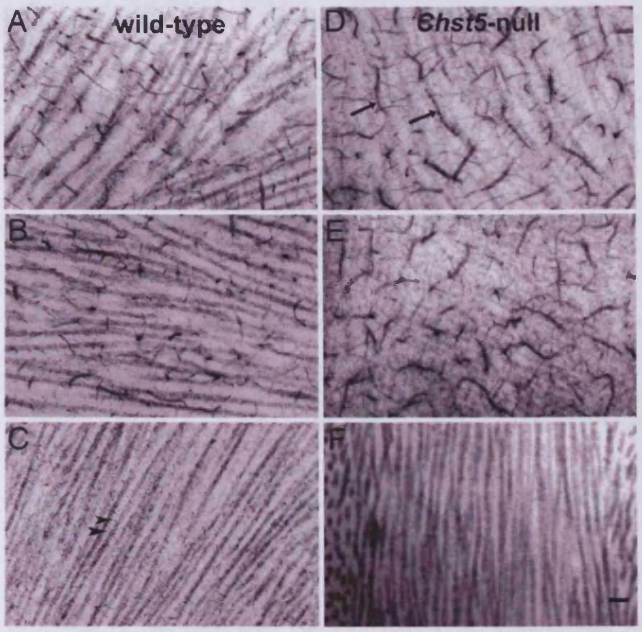

Fig. 5. Electron micrographs of the corneal stroma in WT (*Left*) and homozygous *Chst5*-null mice (*Right*), showing PGs stained with Cupromeronic blue after incubation in buffer (*A* and *D*), keratanase (*B* and *E*), and chondroitinase ABC (*C* and *F*). Small collagen-associated PG filaments remaining after chondroitinase ABC digestion in the WT cornea (*C*, arrowheads) represent sulfated KSPGs. These are not present in *Chst5*-null cornea (*F*). Abnormally large, caterpillar-like PGs (arrows), not present in the WT stroma (*A*), are evident in the *Chst5*-null cornea (*D*). These are susceptible to chondroitinase ABC (*F*), but not to keratanase (*E*), digestion pointing to a significant CS/DS component. (Scale bar: 300 nm.)

with uniform diameters and no evidence in *Chst5*-null corneas of the large, fused collagen fibrils that form in the corneas of mice with targeted gene deletions of the major corneal KSPG, lumican (data not shown) (14). To discover whether *Chst5* deletions have a bearing on the overall corneal matrix structure we undertook a series of synchrotron x-ray fiber diffraction experiments. Resultant diffraction patterns produced by corneas of homozygous *Chst5*-null mice were noticeably different from the corresponding diffraction patterns obtained from the corneas of WT or heterozygous mice (Fig. 6). X-ray data were acquired from whole, isolated corneas maintained close to physiologic hydration, and collagen fibrils throughout the whole of the cornea's thickness in the tissue volume through which the x-ray beam passes contribute to the diffraction pattern (25). Thus, sampling is extensive, generating representative measurements of collagen matrix architecture.

Analyses of the x-ray diffraction patterns indicated a marked alteration in the collagen fibrillar ultrastructure in the *Chst5*-null cornea (Table 1). The average diameter of collagen fibrils throughout the whole depth of the corneal stroma in homozygous mice (34.7 ± 0.7 nm; $n = 18$) was marginally, but significantly, lower than the corresponding value for heterozygous (35.7 ± 0.6 nm; $n = 11$; $P < 0.001$) or WT (36.5 ± 0.9 nm; $n = 12$; $P < 0.001$) corneas. The overall spatial arrangement of collagen fibrils in the *Chst5*-null cornea was manifestly different. Diffraction patterns from *Chst5*-null corneas all possessed a first-order equatorial (i.e., interfibrillar) x-ray reflection that was visibly less well defined than the corresponding reflection obtained from WT corneas or heterozygous corneas (Fig. 6). From the angular spread of these reflections a quantity called the coherence distance was calculated according to Regini and associates (26). Described by Stokes (27) as "the average distance over which exact periodicity [of the collagen fibrillar array]

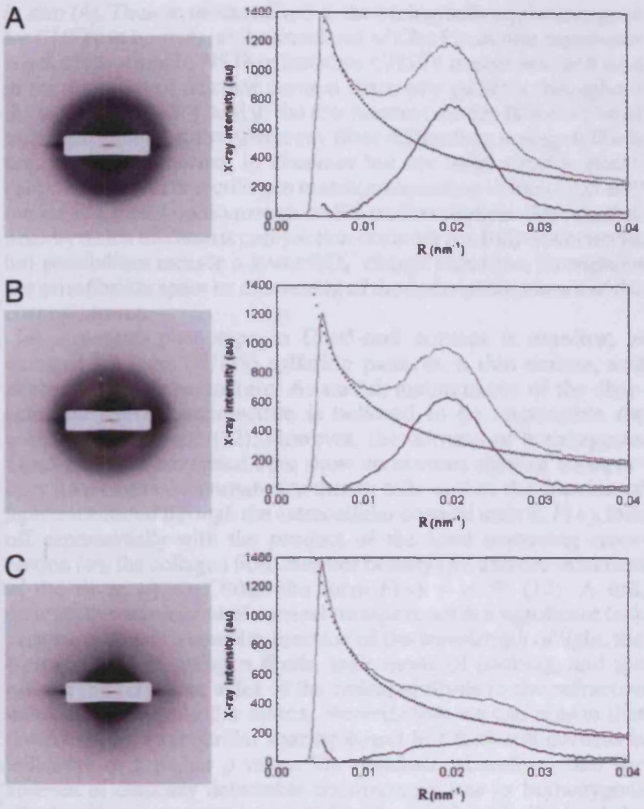

Fig. 6. Synchrotron x-ray fiber diffraction patterns from the corneas of WT (*A*), heterozygous (*B*), and homozygous (*C*) *Chst5*-null mice revealing a more diffuse collagen interfibrillar x-ray reflection in the homozygous situation. Background-subtracted peaks in the x-ray intensity profiles from the patterns confirm the diffuseness of the interfibrillar reflection and enable calculation of the mean center-to-center collagen interfibrillar Bragg spacing.

begins to fail," higher coherence distance values are indicative of more local order in the stromal matrix. Values here were found to be lower in corneas of homozygous mutants (184 ± 19 nm; $n = 18$) than heterozygous mutants (236 ± 13 nm; $n = 11$) or WTs (249 ± 17 nm; $n = 12$) (Table 1). Average center-to-center collagen interfibrillar Bragg spacing in the corneas of homozygous *Chst5*-null mice (42.6 ± 3.4 nm; $n = 18$) was discovered to be significantly lower than the corresponding value for WT (47.8 ± 3.5 nm; $n = 12$; $P < 0.001$) or heterozygous corneas (48.3 ± 2.2 nm; $n = 11$; $P < 0.001$) (Table 1).

Discussion

The production of mice with KSPG-null mutations has facilitated research into the respective and combined functions of these molecules in the control of extracellular matrix morphogenesis (28–30). Broadly stated, of the three KSPGs in cornea, lumican and keratocan are required to maintain collagen fibrils in a specific spatial conformation (13–19). The influence of mimecan, on the other hand, is minimal (21). Recent work has also shown that lumican and keratocan are related PGs, and that lumican has a regulatory influence over the expression of keratocan at the transcriptional level (31). All KSPG-deficient mice studied thus far are gene-targeted mutants that have had the synthesis of a particular KSPG core protein disturbed. To help uncouple the role of KS GAG from KSPG and ascertain the importance of the sulfation of the KS side chains in the governance of matrix ultrastructure, the corneas of a new gene-targeted mouse with *Chst5* mutations were investigated.

Table 1. Average collagen fibril spacing, diameter, and coherence distances (± SD) in WT, heterozygous, and homozygous *Chst5* corneas

Genotype	*n*	Mean collagen fibril Bragg spacing, nm	Mean collagen fibril diameter, nm	Mean coherence distance, nm
Chst5$^{+/+}$	12	47.8 ± 3.5	36.5 ± 0.9	249.3 ± 17.2
Chst5$^{+/-}$	11	48.3 ± 2.2	35.7 ± 0.6	236.0 ± 12.7
Chst5$^{-/-}$	18	42.6 ± 3.4*	34.7 ± 0.7*	184.2 ± 19.2*

*, $P < 0.001$ for both WT-null and heterozygote-null comparisons.

Chst5 encodes intestinal GlcNAc 6-*O*-sulfotransferase, a carbohydrate sulfotransferase that is expressed in the intestine and cornea in mouse (4, 32), and which acts on transferring sulfate onto the 6-*O* position of the nonreducing terminal GlcNAc on KS (4). This sulfation step is coupled with the elongation of the KS backbone (33, 34). Sulfation at the 6-*O* position on the galactose residue may depend on the sulfation of GlcNAc (35, 36), thus it can be appreciated how an absence of sulfotransferase activity results in the production of no or extremely low sulfated KS in *Chst5*-null mice. It may also be possible that elongation of the KS backbone is disturbed in the *Chst5*-null cornea because of dramatic loss of hydrophilic residues on the carbohydrate. It is not known whether the absence of GlcNAc sulfation affects the KS chain elongation step in the corneas of homozygous *Chst5*-null mice. Nevertheless, it is now established that, although the tissue continues to express the major corneal KSPG core protein, lumican, it lacks both immunodetectable epitopes of high sulfated KS GAG sequences and histochemically identifiable sulfated KSPG filaments.

The large, caterpillar-like CS/DS PG filaments discovered in the stroma of *Chst5*-deficient corneas on Cupromeronic blue staining appear specific to this tissue. Previous investigations of human corneas have reported an oversulfation of CS/DS PGs in macular corneal dystrophy and suggested that the lack of KS sulfation might lead to an oversulfation of CS/DS (37, 38). It is also possible that the inability to sulfate KS GAG in the *Chst5*-null mouse cornea might result in a compensatory oversulfation of CS/DS and the resultant appearance of chondroitinase ABC-susceptible, caterpillar-like staining complexes.

In vitro work by Rada and associates (39) has demonstrated that the fibrillogenesis of corneal collagen is regulated by intact lumican PGs, but that it is equally regulated by lumican core protein alone. The current analysis of isolated whole corneas shows marginally thinner fibrils, on average, in the *Chst5*-null situation, indicating that the sulfation of KS side chains is not a major requirement for the inhibition of collagen fibril growth in the cornea *in situ*. Electron microscopy of *Chst5*-deficient corneas, moreover, found none of the isolated, fused collagen fibrils that are a consistent feature of the lumican-deficient mouse cornea (14). Thus, we conclude that lumican is required to prevent the fusion of collagen fibrils in the corneal stroma, but that this function can be met whether or not the PG is modified with sulfated KS side chains.

The foremost structural change seen in corneas of homozygous *Chst5*-null mice is the abnormally close collagen fibrillar packing (Table 1). *Chst5* is a murine ortholog of *CHST6*, the carbohydrate sulfotransferase gene that in humans is causative for macular corneal dystrophy (10). Interestingly, the human genome has an additional sulfotransferase gene, *CHST5*, as an ortholog for *Chst5* in mouse (4, 10, 32). Because of their high homology, *CHST5* and *CHST6* seem to be created by gene duplication during evolution (10). The coding sequences of the three human and mouse genes are highly homologous, and all of the gene products have sulfotransferase activity over nonreducing terminal GlcNAc (4, 40). Nevertheless, only the enzymes encoded on *CHST6* and *Chst5* have similar substrate specificity and the ability to produce sulfated KS

in vitro (4). Thus, in mouse, *Chst5* is the biologically equivalent gene for *CHST6* in humans, and a knockout of *Chst5* in mouse represents a lack of functional *CHST6* in humans. *CHST6* mutations are found in the genomes of macular corneal dystrophy patients throughout the world (10, 41–50), and in the few human corneas that have been examined postoperatively by x-ray fiber diffraction, collagen fibrils are, on average, normal in diameter but are more closely spaced (51). We contend that collagen matrix compaction in the *Chst5*-null mouse is a direct consequence of KS undersulfation. The mechanism by which this matrix compaction occurs is not fully understood, but possibilities include a lower SO_4^- charge repulsion throughout the extrafibrillar space or a lessening of the hydrophilic nature of the corneal stroma.

A structural phenotype in *Chst5*-null corneas is manifest in changed KS (and CS/DS) sulfation patterns, a thin stroma, and altered matrix ultrastructure. As stated, maintenance of the characteristic stromal architecture is believed to be responsible for corneal transparency (12). However, the corneas of homozygous *Chst5*-null mice examined here show no obvious signs of transparency loss. Corneal transparency theory tells us that the fraction of light transmitted through the extracellular corneal matrix, $F(\lambda)$, falls off exponentially with the product of the total scattering cross-section (σ), the collagen fibril number density (ρ), and the thickness of the tissue (t), and takes the form $F(\lambda) = e^{-\sigma\rho t}$ (12). A full, quantitative assessment of corneal transparency is a significant task because σ is itself a complex function of the wavelength of light, the diameters of the collagen fibrils, their mode of packing, and the ratio of the refractive index of the hydrated fibrils to the refractive index of the extrafibrillar matrix. Nevertheless, we can reason that the decreased interfibrillar spacing found in *Chst5*-null corneas is indicative of a higher ρ value. We conclude, therefore, that the absence of clinically detectable transparency loss in homozygous *Chst5*-null corneas must be caused by the combined effects of the thin stroma in these animals (i.e., reduced t), possibly augmented by changes in stromal architecture that lead to a lower σ value.

In summary, mutations on *Chst5* result in the undersulfation of KS GAG in murine cornea, the loss of collagen-associated KSPG filaments, and the altered sulfation of CS/DS. Collagen matrix changes also occur in homozygous *Chst5*-null corneas, identifying the sulfation step in KS GAG biosynthesis as a fundamental requirement for tissue morphogenesis.

Materials and Methods

Generation of *Chst5*-Null Mice. To construct the targeting vector, a mouse genomic P1 clone (VJ129 strain) containing *Chst5* was isolated by PCR-based screening. From this screening a 12-kbp DNA fragment, which contained *Chst5* exon 2, was obtained by Aor51H1 and MunI digestion and subcloned into pBluescript II SK vector. The entire ORF of *Chst5* encoded on exon 2 was then replaced with MC1-neo, and diphtheria toxin A subunit sequence was added at the 5′ region of *Chst5*. The constructed targeting vector DNA was linearized with SalI and used to transfect a 129-derived mouse ES cell line. Homologous recombinant ES cells were used to produce chimeric and heterozygote mutant mice. Obtained heterozygotes were subsequently backcrossed to C57BL/6 mice for five to eight generations, after which the mice were intercrossed to obtain null mutants. Genotyping of WT and mutant alleles was performed by PCR analysis using three primers, Ch5WTF1 (5′-GCTGCTGGGTTACCGGTCTGTGCATT-3′), a specific forward primer for intact allele, Ch5KOF2 (5′-GACCGCGCCGCCCCGAC-3′), a specific forward primer for mutant allele, and Ch5R1 (5′-CAGCCCACAGCCGCGCCTTT-3′), a reverse primer for both alleles. Amplification reactions were carried out in a AB2720 Thermal Cycler (Applied Biosystems, Foster City, CA) by 5-min denaturation at 96°C before cycling, 35 cycles of denaturation at 96°C for 30 s, annealing at 66°C for 30 s, extension at 72°C for 30 s, and further extension at 72°C for 5 min.

To confirm expression of *Chst5* transcripts, RT-PCR was performed as follows. Twelve whole eyes were obtained, and total RNA was extracted by using TRIzol reagent (Invitrogen, Carlsbad, CA) according to the manufacturer's instruction. Five micrograms of total RNA was reverse-transcribed by SuperScript II (Invitrogen) and oligo(dT)$_{12-18}$ primer, and an aliquot of the resulted cDNA mixture was examined by PCR analysis using mIGn6RTF primer (5′-GCAGAAGCGCAGCGGGCAG-3′) and mIGn6RTR primer (5′-GTCACGCACGGCCATGTGGAG-3′). The reaction conditions were as described above, except for the use of 45 cycles.

Light and Electron Microscopy. Excised eyes of 20 mice (6 WT, 6 heterozygous, and 8 mutant) were fixed in 4% paraformaldehyde and embedded in paraffin. Sections were taken through the central corneas of all 40 eyes, and after staining with hematoxylin and eosin, measurements were made of corneal thickness, stromal thickness, and the corneal/stromal thickness ratio. For electron microscopy excised corneas were fixed in 2.5% glutaraldehyde in 25 mM sodium acetate buffer with Cupromeronic blue (Europa Bioproducts, Cambridge, U.K.) included in the fixative at 0.01% (wt/vol) to stain sulfated PGs in a critical electrolyte concentration mode competing with $MgCl_2$ at 0.1 M (22). Before this process some corneas were incubated in either keratanase I (MP Biomedicals, Costa Mesa, CA; 1 unit/ml in Tris-acetate buffer at pH 8.0) to degrade KS, or chondroitinase ABC (Sigma, St. Louis, MO; 2.5 units/ml in Tris-acetate buffer at pH 7.4), to degrade 0-, 4- and 6-sulfated CS and DS in line with published protocols (22, 38). Ultrathin (silver/gold) sections were stained with 1% aqueous phosphotungstic acid and 0.5% aqueous uranyl acetate (40°C for 40 min in both cases) before examination in a Philips (Eindhoven, The Netherlands) EM208 transmission electron microscope at ×32,000 magnification.

Immunoblot Analysis of Corneal Protein Extracts. Twenty mouse corneas were collected into a 1.5-ml microcentrifuge tube and homogenized in 1 ml of guanidine·HCl buffer (4 M guanidine·HCl/50 mM Tris·HCl, pH 8.0/10 mM EDTA, pH 8.0/1 mM PMSF) containing 2 μl of Protease Inhibitor Mixture (Sigma-Aldrich, St. Louis, MO), using a metal blade homogenizer. The homogenate was shaken at 4°C overnight, and the supernatant was separated by centrifugation and collected. The remaining precipitate was again extracted with 1 ml of guanidine·HCl buffer by shaking at 4°C overnight, and the supernatants were combined. They were then dialyzed against urea buffer (6 M urea/50 mM Tris·HCl, pH 6.8) at 4°C for 24 h, and the resultant solution was recovered in a microcentrifuge tube. After measurement of protein concentration, the solution was adjusted to 1 μg protein/μl concentration by urea buffer and stored at −20°C until its use as corneal protein extract for the following experiments.

Twenty micrograms of corneal protein extract was incubated for 12 h at 37°C with or without 1 unit of endo-β-galactosidase (Associates of Cape Cod, East Falmouth, MA) in 300 μl of 50 mM sodium acetate, pH 6.5, containing 2 μl of Protease Inhibitor Mixture. This reaction was stopped by acetone precipitation, after which the resultant protein precipitate was dissolved into 20 μl of SDS/PAGE sample buffer and subjected to SDS/PAGE. After electrophoresis, separated proteins were either visualized by CBB-R250 staining or transferred onto a PVDF membrane for immunoblotting. For detection of sulfated KS GAG, the filter was blocked with 10% skim milk in PBST5.3 (PBS-0.05% Tween 20, pH 5.3, adjusted with HCl) at room temperature for 1.5 h, and then reacted with diluted 5D4 antibody (Associates of Cape Cod) in 10% skim milk-PBST5.3 for 1 h. The filter was then washed three times with PBST5.3 and reacted with diluted HRP-labeled anti-mouse Ig antibody (Pierce Biotech, Rockford, IL) in 0.3% skim milk-PBST5.3 for 1 h. After washing three times with PBST5.3, the filter was reacted with SuperSignal West Pico chemiluminescent substrate (Pierce Biotech) for 5 min followed by exposure to an x-ray film. For detection of lumican KSPG core protein, the blotted filter

was blocked with 5% BSA in PBST (PBS-0.05% Tween 20) for 1.5 h at room temperature and reacted with diluted mouse monoclonal antilumican antibody in 5% BSA-PBST for 1 h. The filter was then washed three times with PBST followed by incubation with HRP-labeled anti-mouse Ig antibody in 0.3% BSA-PBST for 1 h. After washing three times with PBST, detected signals were visualized as described above.

Synchrotron X-Ray Fiber Diffraction. Corneas from 21 mice (9 homozygous mutants, 6 heterozygous mutants, and 6 WTs) were excised at the limbus immediately after death and individually wrapped in Clingfilm to limit dehydration. Specimens were then frozen in dry ice and stored at −80°C before examination by x-ray diffraction at the Synchrotron Radiation Source (SRS), Daresbury Laboratory, Cheshire, U.K (25). Freezing is an accepted way of storing corneas for investigations of matrix structure by synchrotron x-ray scattering (52). For data collection corneas were, in turn, individually secured in a sealed specimen holder between two sheets of Mylar and positioned in the path of the x-ray beam on SRS Station 2.1, such that when the shutters were opened (3-min exposures were used) monochromatic radiation of wavelength 0.154 nm focused to 1.5 × 1.0 mm at the specimen passed through the full thickness of the cornea. Camera length was 9 meters, and fiber diffraction patterns were recorded on a multiwire, gas proportional area detector. Initial data handling using purpose-written, Unix-based software and graphics/statistics packages (Statistica; Statsoft, Tulsa, OK) consisted of normalization with ion chamber counts to correct for beam intensity decay, followed by the subtraction of a detector response from a 14-h exposure to a Fe^{55} radioactive source to correct for any nonlinearities in the detector. X-ray intensity profiles across each diffraction pattern were generated by taking a vertical scan, 26 pixels wide, of x-ray intensity (I) versus radial position (r). The symmetrical diffraction pattern was then summed about its center to improve the signal-to-noise ratio. As a result the x-ray intensity scans shown in Fig. 6 represent the first-order equatorial x-reflection as a single peak plotted against R, the reciprocal space coordinate. The average center-to-center collagen interfibrillar Bragg spacing and average collagen fibril diameter were calculated, respectively, from the positions of the first-order equatorial x-ray reflection and the position of the first subsidiary maximum as described by Meek and Quantock (25). The angular width of the first-order equatorial (i.e., interfibrillar) reflection was used to obtain an appreciation of the degree of local order in the fibrillar array by calculating the coherence distance as described by Regini and associates (26).

We thank Dr. Gunter Grossmann and staff at the Synchrotron Radiation Source for help with data collection and the Central Laboratory of the Research Councils for beamtime at the Synchrotron Radiation Source (K.M.M. and A.J.Q.). This work was supported by Biotechnology and Biological Sciences Research Council Project Grant 72/B18021 (to A.J.Q. and B.C.), National Institutes of Health Grants CA071932 (to M.N.F.) and EY014620 (to T.O.A.), Medical Research Council Program Grant G0001033 (to K.M.M., B.C., and A.J.Q.), and the Arthritis Research Campaign U.K.

1. Blochberger, T. C., Vergnes, J.-P., Hempel, J. & Hassell, J. R. (1992) *J. Biol. Chem.* **267,** 347–352.
2. Corpuz, L. M., Funderburgh, J. L., Funderburgh, M. L., Bottomley, G. S., Prakash, S. & Conrad, G. W. (1996) *J. Biol. Chem.* **271,** 9759–9763.
3. Funderburgh, J. L., Corpuz, L. M., Roth, M. R., Funderburgh, M. L., Tasheva, E. S. & Conrad, G. W. (1997) *J. Biol. Chem.* **272,** 28089–28095.
4. Akama, T. O., Nakayama, J., Nishida, K., Hiraoka, N., Suzuki, M., McAuliffe, J., Hindsgaul, O., Fukuda, M. & Fukuda, M. N. (2001) *J. Biol. Chem.* **276,** 16271–16278.
5. Cornuet, P. K., Blochberger, T. C. & Hassell, J. R. (1994) *Invest. Ophthalmol. Visual Sci.* **35,** 870–877.
6. Connon, C. J., Meek, K. M., Kinoshita, S. & Quantock, A. J. (2004) *Exp. Eye Res.* **78,** 909–915.
7. Funderburgh, J. L., Cintron, C., Covington, H. I. & Conrad, G. W. (1988) *Invest. Ophthalmol. Visual Sci.* **29,** 1116–1124.
8. Cintron, C., Gregory, J. D., Dalme, S. P. & Kublin, C. L. (1990) *Invest. Ophthalmol. Visual Sci.* **31,** 1975–1981.
9. Hassell, J. R, Newsome, D. A., Krachmer, J. H. & Rodrigues, M. M. (1980) *Proc. Natl. Acad. Sci. USA* **77,** 3705–3709.
10. Akama, T. O., Nishida, K., Nakayama, J., Watanabe, H., Ozaki, K., Nakamura, T., Dota, A., Kawasaki, S., Inoue, Y., Maeda, N., *et al.* (2000) *Nat. Genet.* **26,** 237–241.
11. Komai, Y. & Ushiki, T. (1991) *Invest. Ophthalmol. Visual Sci.* **32,** 2244–2258.
12. Farrell, R. A. (1994) in *Principles and Practice of Ophthalmology*, eds. Albert, D. M. & Jacobiec, S. A. (Saunders, Philadelphia), pp. 64–81.
13. Chakravarti, S., Magnuson, T., Lass, J. H., Jepsen, K. J., LaMantia, C. & Carroll, H. (1998) *J. Cell Biol.* **141,** 1277–1286.
14. Chakravarti, S., Petroll, W. M., Hassell, J. R., Jester, J. V., Lass, J. H., Paul, J. & Birk, D. E. (2000) *Invest. Ophthalmol. Visual Sci.* **41,** 3365–3373.
15. Quantock, A. J, Meek, K. M. & Chakravarti, S. (2001) *Invest. Ophthalmol. Visual Sci.* **42,** 1750–1756.
16. Song, J., Lee, Y.-G., Houston, J., Petroll, W. A. Chakravarti, S., Cavanagh, H. D. & Jester, J. V. (2003) *Invest. Ophthalmol. Visual Sci.* **44,** 548–557.
17. Beecher, N., Chakravarti, S., Joyce, S., Meek, K. M. & Quantock. A. J. (2006) *Invest. Ophthalmol. Visual Sci.* **47,** 146–150.
18. Liu, C. Y., Birk, D. E., Hassell, J. R., Kane, B. & Kao, W. W. Y. (2003) *J. Biol. Chem.* **278,** 21672–21677.
19. Meek, K. M., Quantock, A. J., Boote, C., Liu, C. Y. & Kao. W. W. Y. (2003) *Matrix Biol.* **22,** 467–475.
20. Tasheva, E. S., Koester, A., Paulson, A. Q., Garrett, A. S., Boyle, D. L., Davidson, H. J., Song, M., Fox, N. & Conrad, G. W. (2002) *Mol. Vis.* **8,** 407–415.
21. Beecher, N., Carlson, C., Allen, B. R., Kipchumba, R., Conrad, G. W., Meek, K. M. & Quantock, A. J. (2005) *Invest. Ophthalmol. Visual Sci.* **46,** 4046–4049.
22. Young, R. D., Tudor, D., Hayes, A. J., Kerr, B., Hayashida, Y., Nishida, K., Meek, K. M., Caterson, B. & Quantock, A. J. (2005) *Invest. Ophthalmol. Visual Sci.* **46,** 1973–1978.
23. Caterson, B., Christner, J. E. & Baker, J. R. (1983) *J. Biol. Chem.* **258,** 8848–8854.
24. Mehmet, H., Scudder, P., Tang, P. W., Hounsell, E. F., Caterson, B. & Feizi, T. (1986) *Eur. J. Biochem.* **157,** 385–391.
25. Meek, K. M. & Quantock, A. J. (2001) *Prog. Ret. Eye Res.* **20,** 95–137.
26. Regini, J. W., Elliott, G. F. & Hodson, S. A. (2004) *J. Mol. Biol.* **336,** 179–186.
27. Stokes, A. R. (1955) *Prog. Biophys.* **5,** 5–167.
28. Chakravarti, S. (2001) *Exp. Eye Res.* **73,** 411–419.
29. Chakravarti, S. (2002) *Glycoconjugate J.* **19,** 287–293.
30. Kao, W. W. Y. & Liu, C. Y. (2002) *Glycoconjugate J.* **19,** 275–285.
31. Carlson, E. C., Liu, C. Y., Chikama, T. I., Hayashi, Y., Kao, C. W. C., Birk, D. E., Funderburgh, J. L, Jester, J. V. & Kao, W. W. Y. (2005) *J. Biol. Chem.* **280,** 25541–25547.
32. Lee, J. K., Bhakta, S., Rosen, S. D. & Hemmerich, S. (1999) *Biochem. Biophys. Res. Commun.* **263,** 543–549.
33. Funderburgh, J. L. (2000) *Glycobiology* **10,** 951–958.
34. Akama, T. O., Misra, A. K., Hindsgaul, O. & Fukuda, M. N. (2002) *J. Biol. Chem.* **277,** 42505–42513.
35. Fukuta, M., Inazawa, J., Torii, T., Tsuzuki, K., Shimada, E. & Habuchi, O. (1997) *J. Biol. Chem.* **272,** 32321–32328.
36. Torii, T., Fukuta, M. & Habuchi, O. (2000) *Glycobiology* **10,** 203–211.
37. Plaas, A. H., West, L. A., Thonar, E. J.-M. A., Karcioglu, Z. A., Smith, C. J., Klintworth, G. K. & Hascall, V. C. (2001) *J. Biol. Chem.* **276,** 39788–39796.
38. Meek, K. M., Quantock, A. J., Elliott, G. F., Ridgway, A. E. A., Tullo, A. B., Bron, A. J. & Thonar, E. J.-M. A. (1989) *Exp. Eye. Res.* **49,** 941–958.
39. Rada, J., Cornuet, P. K. & Hassell, J. R. (1993) *Exp. Eye. Res.* **56,** 635–648.
40. Hemmerich, S. & Rosen, S. D. (2000) *Glycobiology* **10,** 849–856.
41. Lui, N.-P., Sew-Knight, S., Rayner, M., Jonasson, F., Akama, T. O., Fukuda, M. N., Bao, W., Gilbert, J. R., Vance, J. M. & Klintworth, G. K. (2000) *Mol. Vis.* **6,** 261–264.
42. El-Ashry, M. F., Abd El-Aziz, M. M., Wilkins, S., Cheetham, M. E., Wilkie, S. E., Hardcastle, A. J., Halford, S., Bayoumi, A. Y., Ficker, L. A., Tuft, S., *et al.* (2002) *Invest. Ophthalmol. Visual Sci.* **43,** 377–382.
43. Iida-Hasegawa, N., Furuhata, A., Hayatsu, H., Murakami, A., Fujiki, K., Nakayasu, K. & Kanai, A. (2003) *Invest. Ophthalmol. Visual Sci.* **44,** 3272–3277.
44. Sultana, A., Sridhar, M. S., Jagannathan, A., Balasubramanian, D., Kannabiran, C. & Klintworth, G. K. (2003) *Mol. Vis.* **9,** 730–734.
45. Warren, J. F., Aldave, A. J., Srinivasan, M., Thonar, E. J., Kumar, A. B., Cevallos, V., Whitcher, J. P. & Margolis, T. P. (2003) *Arch. Ophthalmol.* **121,** 1608–1612.
46. Ha, N. T., Chau, H. M., Cung, L. X., Thanh, T. K., Fujiki, K., Murakami, A., Hiratsuka, Y. & Kanai, A. (2003) *Invest. Ophthalmol. Visual Sci.* **44,** 3310–3316.
47. Ha, N. T., Chau, H. M., Cung, L. X., Kim, T. T., Fujiki, K., Murakami, A., Hiratsuka, Y., Hasegawa, N. & Kanai, A. (2003) *Cornea* **22,** 508–511.
48. Aldave, A. J., Yellore, V. S., Thonar, E. J., Udar, N., Warren, J. F., Yoon, M. K., Cohen, E. J., Rapuano, C. J., Laibson, P. R., Margolis, T. P. & Small, K. (2004) *Am. J. Ophthalmol.* **137,** 465–473.
49. Abbruzzese, C., Kuhn, U., Molina, F., Rama, P. & De Luca, M. (2004) *Clin. Genet.* **65,** 120–125.
50. El-Ashry, M. F., Abd El-Aziz, M. M., Shalaby, O., Wilkins, S., Poopalasundaram, S., Cheetham, M., Tuft, S. J., Hardcastle, A. J., Bhattacharya, S. S. & Ebenezer, N. D. (2005) *Am. J. Ophthalmol.* **139,** 192–193.
51. Quantock, A. J., Meek, K. M., Ridgway, A. E. A., Bron, A. J. & Thonar, E. J.-M. A. (1990) *Curr. Eye Res.* **9,** 393–398.
52. Fullwood, N. J. & Meek, K. M. (1994) *J. Mol. Biol.* **236,** 749–758.

Bibliography

Abbruzzese, C., Kuhn, U., Molina, F. *et al.* 2004. Novel mutations in the *CHST6* gene causing macular corneal dystrophy. *Clinical Genetics* 65, 120-125.

Akama, T.O., Nishida, K., Nakayama, J. *et al.* 2000. Macular corneal dystrophy type I and type II are caused by distinct mutations in a new sulphotransferase gene. *Nature Genetics* 26 (2), 237-241.

Akama, T.O., Nakayama, J., Nishida, K. *et al.* 2001. Human corneal GlcNAc 6-O-sulfotransferase and mouse intestinal GlcNac 6-O-sulfotransferase both produce keratan sulfate. *Journal of Biological Chemistry* 276 (19), 16271-16278.

Akama, T.O., Misra, A.K., Hindsgaul, O. *et al.* 2002. Enzymatic synthesis *in vitro* of the disulfated disaccharide unit of corneal keratan sulfate. *Journal of Biological Chemistry* 277 (45), 42505-42513.

Akimoto, Y., Yamakawa, N., Furukawa, K. *et al.* 2002. Changes in distribution of the long form of type XII collagen during chicken corneal development. *Journal of Histochemistry and Cytochemistry* 50 (6), 851-862.

Aldave, A.J., Yellore, V.S., Thonar, E.J. *et al.* 2004. Novel mutations in the carbohydrate sulfotransferase gene (*CHST6*) in American patients with macular corneal dystrophy. *American Journal of Ophthalmology* 137, 465-473.

Anseth, A. 1961a. Glycosaminoglycans in corneal regeneration. *Experimental Eye Research* 1, 122-127.

Anseth, A. 1961b. Glycosaminoglycans in the developing corneal stroma. *Experimental Eye Research* 1, 116-121.

Bibliography

Anseth, A. 1969. Studies on corneal polysaccharides. V. Changes in corneal glycosaminoglycans in transient stromal edema. *Experimental Eye Research* 8 (3), 297-301.

Armstrong, D.J., Hiscott, P., Batterbury, M. *et al.* 2002. Corneal stromal cells (keratocytes) express thrombospondins 2 and 3 in wound repair phenotype. *International Journal of Biochemistry and Cell Biology* 34 (6), 588-593.

Axelsson, I. and Heinegard, D. 1978. Characterization of the keratan sulphate proteoglycans from bovine corneal stroma. *Biochemical Journal* 169 (3), 517-530.

Bella, J., Eaton, M., Brodsky, B. *et al.* 1994. Crystal and molecular structure of a collagen-like peptide at 1.9 A resolution. *Science* 226 (5182), 75-81.

Benedek, G.B. 1971. Theory of transparency of the eye. *Applied Optics* 10 (3), 459-473.

Bettelheim, F. A. and Goetz, D. 1976. Distribution of hexosamines in bovine cornea. *Investigative Ophthalmology* 15 (4), 301-304.

Bettelheim, F.A. and Plessy, B. 1975. The hydration of proteoglycans of bovine cornea. *Biochimica et Biophysica Acta*, 381; 203-214.

Birk, D. E., Fitch, J. M., Babiarz, J. P. *et al.* 1990. Collagen fibrillogenesis *in vitro*: interaction of types I and V collagen regulates fibril diameter. *Journal of Cell Science* 95 (4), 649-657.

Birk, D. E., Fitch, J. M., Babiarz, J.P. *et al.* 1988. Collagen type I and type V are present in the same fibril in the avian corneal stroma. *Journal of Cell Biology* 106 (3), 999-1008.

Birk, D.E. and Lande, M.A. 1981. Corneal and scleral collagen fiber formation *in vitro*. *Biochimica et Biophysica Acta* 670 (3), 362-369.

Bibliography

Blochberger, T.C., Vergnes, J.P., Hempel, J. *et al.* 1992. cDNA to chick lumican (corneal keratan sulfate proteoglycan) reveals homology to the small interstitial proteoglycan gene family and expression in muscle and intestine. *Journal of Biological Chemistry* 267 (1), 347-352.

Bonaldo, P., Mucignat, M.T., Colombatti, A. 1990. Efficient expression of chicken alpha 1 (VI) collagen chain in transiently transfected mammalian cells. *Matrix* 10 (3), 139-147.

Boote, C., Dennis, S., Huang, Y. *et al.* 2005. Lamellar orientation in human cornea in relation to mechanical properties. *Journal of Structural Biology* 149 (1), 1-6.

Boot-Handford, R. P., Tuckwell, D. S., Plumb, D. A. *et al.* 2003. A novel and highly conserved collagen (pro(alpha)1(XXVII)) with a unique expression pattern and unusual molecular characteristics establishes a new clade within the vertebrate fibrillar collagen family. *Journal of Biological Chemistry* 278 (33), 31067-31077.

Borcherding, M.S., Blacik, L.J., Sittig, R.A. *et al.* 1975. Proteoglycans and collagen fibre organization in human corneoscleral tissue. *Experimental Eye Research* 21 (1), 59-70.

Bozzola, J.J. and Russell, L.D. ed./eds. 1992. *Electron microscopy: principles and techniques for biologists*. Boston: Jones and Bartlett Publishers.

Bron, A.J. 2001. Editorial: The architecture of the corneal stroma. *British Journal of Ophthalmology* 85, 379-383.

Bron, A.J., Tripathi, A.C., Tripathi, B.J. 1997. *The cornea and sclera.* London: Chapman and Hall Medical.

Bruns, R. R., Press, W., Engvall, E. *et al.* 1986. Type VI collagen in extracellular, 100-nm periodic filaments and fibrils: identification by immunoelectron microscopy. *Journal of Cell Biology* 103 (2), 393-404.

Bibliography

Carlson, E.C., Liu, C-Y., Chikama, T.I. *et al.* 2005. Keratocan, a cornea-specific keratan sulfate proteoglycan, is regulated by lumican. *Journal of Biological Chemistry* 280 (27), 25541-25547.

Carlson, E.C., Liu, C-Y., Yang, X. *et al.* 2004. *In vivo* gene delivery and visualization of corneal stromal cells using an adenoviral vector and keratocyte-specific promoter. *Investigative Ophthalmology and Visual Science* 45 (7), 2194-2200.

Carlson, E.C., Mamiya, K., Liu, C-Y. *et al.* 2003. Role of Cys^{41} in the N-terminal domain of lumican in *ex vivo* collagen fibrillogenesis by cultured corneal stromal cells. *Biochemical Journal* 369 (3), 461-468.

Castoro, J.A., Bettelheim, A.A., Bettelheim, F.A. 1988. Water gradients across bovine cornea. *Investigative Ophthalmology and Visual Science* 29 (6), 963-968.

Chakravarti, S. 2001. The cornea through the eyes of knockout mice. *Experimental Eye Research* 73 (4), 411-419.

Chakravarti, S. and Magnuson, T. 1995. Localization of mouse lumican (keratan sulfate proteoglycan) to distal chromosome 10. *Mammalian Genome* 6 (5), 367-368.

Chakravarti, S., Magnuson, T., Lass, J.H. *et al.* 1998. Lumican regulates collagen fibril assembly: skin fragility and corneal opacity in the absence of lumican. *Journal of Cell Biology* 141 (5), 1277-1286.

Chakravarti, S., Petroll, W.M., Hassell, J.R. *et al.* 2000. Corneal opacity in lumican-null mice: defects in collagen fibril structure and packing in the posterior stroma. *Investigative Ophthalmology and Visual Science* 41 (11), 3365-3373.

Chakravarti, S., Zhang, G., Chervoneva, I. *et al.* 2006. Collagen fibril assembly during postnatal development and dysfunctional regulation in the lumican-deficient murine cornea. *Developmental Dynamics* - in press.

Bibliography

Chapman, J.A., Tzaphlidou, M., Meek, K.M. *et al* 1990. The collagen fibril – a model system for studying the staining and fixation of a protein. *Electron Microscopy Review* 3, 143-182.

Cintron, C., Covington, H.I., Kublin, C.L. 1983. Morphogenesis of rabbit corneal stroma. *Investigative Ophthalmology and Visual Science* 24 (5), 543-546.

Cintron, C., Covington, H.I., Kublin, C.L. 1990. Morphologic analyses of proteoglycans in rabbit corneal scars. *Investigative Ophthalmology and Visual Science* 31 (9), 1789-1798.

Connon, C.J., Meek, K.M., Kinoshita, S. *et al.* 2004. Spatial and temporal alterations in the collagen fibrillar array during the onset of transparency in the avian cornea. *Experimental Eye Research* 78 (5), 909-1015.

Cornuet, P.K., Blochberger, T.C., Hassell, J.R. 1994. Molecular polymorphism of lumican during corneal development. *Investigative Ophthalmology and Visual Science* 35 (3), 870-877.

Corpuz, L.M., Funderburgh, J.L., Funderburgh, M.L. *et al.* 1996. Molecular cloning and tissue distribution of keratocan. Bovine corneal keratan sulfate proteoglycan 37A. *Journal of Biological Chemistry* 271 (16), 9759-9763.

Corpuz, L.M., Dunlevy, J.R., Hassell, J.R. *et al.* 2000. Molecular cloning and relative tissue expression of keratocan and mimecan in embryonic quail cornea. *Matrix Biology* 19 (7), 693-698.

Coulombre, A.J. and Coulombre, J.L. 1958. Corneal development. I. Corneal transparency. *Journal of Cell Physiology* 51 (1), 1-11.

Danielson, K.G., Baribault, H., Holmes, D.F. *et al.* 1997. Targeted disruption of decorin leads to abnormal collagen fibril morphology and skin fragility. *Journal of Cell Biology* 136 (3), 729-743.

Bibliography

Davis, N.R., Risen, O.M., Pringle, G.A. 1975. Stable, nonreducible cross-links of mature collagen. *Biochemistry* 14 (9), 2031-2036.

Davson, H. 1984. *The Eye, Volume IB* (3rd edition) New York, Academic Press.

Daxer, A. and Fratzl, P. 1997. Collagen fibril orientation in the human corneal stroma and its implication in keratoconus. *Investigative Ophthalmology and Visual Science* 38 (1), 121-129.

Degroote, S., Lo-Guidice, J.M., Strecker, G. *et al.* 1997. Characterization of an N-acetylglucosamine-6-O-sulfotransferase from human respiratory mucosa active on mucin carbohydrate chains. *Journal of Biological Chemistry* 272 (47), 29493-29501.

DeLuca. S., Richmond, M.E., Silbert, J.E. 1973. Biosynthesis of chondroitin sulfate. Sulfation of the polysaccharide chain. *Biochemistry* 12 (20), 3911-3915.

Dickenson, J.M., Huckerby, T.N., Nieduszynski, I.A. 1991. A non-reducing terminal fragment from tracheal cartilage keratan sulphate chains contains alpha (2-3)-linked N-acetylneuraminic acid. *Biochemical Journal* 278, 779-785.

Doetschman, T., Gregg, R.G., Maeda, N. *et al.* 1987. Targetted correction of a mutant HPRT gene in mouse embryonic stem cells. *Nature* 330 (6148), 576-578.

Donnenfeld, E.D., Cohen, E.J., Ingraham, H.J. *et al.* 1986. Corneal thinning in macular corneal dystrophy. *American Journal of Ophthalmology* 101 (1), 112-113.

Dunlevy, J.R., Beales, M.P., Berryhill, B.L. *et al.* 2000. Expression of the keratan sulfate proteoglycans lumican, keratocan and osteoglycin/mimecan during chick corneal development. *Experimental Eye Research* 70 (3), 349-362.

Bibliography

Dunlevy, J.R., Chakravarti, S., Gyalzen, P. *et al.* 1998. Cloning and chromosomal localization of mouse keratocan, a corneal keratan sulfate proteoglycan. *Mammalian Genome* 9, 316-319.

El-Ashry, M.F., Abd El-Aziz, M.M., Wilkins, S. *et al.* 2002. Identification of novel mutations in the carbohydrate sulfotransferase gene (*CHST6*) causing macular corneal dystrophy. *Investigative Ophthalmology and Visual Science* 43, 377-382.

El-Ashry, M.F., Abd El-Aziz, M.M., Shalaby, O. *et al.* 2005. Novel *CHST6* nonsense and missense mutations responsible for macular corneal dystrophy. *American Journal of Ophthalmology* 139, 192-193.

Ezura, Y., Chakravarti, S., Oldberg, A. *et al.* 2000. Differential expression of lumican and fibromodulin regulate collagen fibrillogenesis in developing mouse tendons. *Journal of Cell Biology* 151 (4), 779-788.

Farrell R.A. 1994. Corneal Transparency. In: Albert, D.M. and Jacobiec, S.A. ed./eds. *Principles and Practice of Ophthalmology*. Philadelphia: Saunders.

Farrell, R.A. and McCally, R.L. 2000. Corneal transparency. In: Albert, D.M. and Jakobeic F.A. ed/eds. *Principles and Practice of Ophthalmology*. Philadelphia: Saunders.

Fessler LI, Morris NP, Fessler JH. 1975. Procollagen: biological scission of amino and carboxyl extension peptides. *Proceedings of the National Academy of Sciences USA* 72 (12), 4905-4909.

Findlater, G. S., McDougall, R. D., Kaufman, M. H. 1993. Eyelid development, fusion and subsequent reopening in the mouse. *Journal of Anatomy* 183 (1), 121-129.

Bibliography

Fitch, J. M., Mentzer, A., Mayne, R. *et al.* 1988. Acquisition of type IX collagen by the developing avian primary corneal stroma and vitreous. *Developmental Biology* 128 (2), 396-405.

Forrester, J., Dick, A., McMenamin, P. *et al.* 1999. *The eye: basic sciences in practice*. London: WB Saunders.

Forrester, J., Dick, A., McMenamin, P. *et al.* 2002. *The eye: basic sciences in practice* 2nd ed London: WB Saunders.

Fosang, A.J. and Hardingham, T.E. 1996. Matrix proteoglycans. In: Comper, W.D. ed. *Extracellular matrix, Volume 2, Molecular Components and Interactions.* OCA (Overseas Publishers Association): Harwood Academic Publishers.

Freund, D.E., McCally, R.L., Farrell, R.A. *et al.* 1995. Ultrastructure in anterior and posterior stroma of perfused human and rabbit corneas. Relation to transparency. *Investigative Ophthalmology and Visual Science* 36 (8), 1508-1523.

Fukuta, M., Inazawa, J., Torii, T. *et al.* 1997. Molecular cloning and characterization of human keratan sulfate Gal-6-sulfotransferase. *Journal of Biological Chemistry* 272 (51), 32321-32328.

Fullwood, N.J. and Meek, K.M. 1993. A synchrotron x-ray study of the changes occurring in the corneal stroma during processing for electron microscopy. *Journal of Microscopy* 169 (1), 53-60.

Fullwood, N.J. and Meek, K.M. 1994. An ultrastructural, time-resolved study of freezing in the corneal stroma. *Journal of Molecular Biology* 236 (3), 749-758.

Funderburgh, J.L. 2000. Keratan sulfate: structure, biosynthesis, and function. *Glycobiology* 10 (10), 951-958.

Bibliography

Funderburgh, J.L., Perchellet, A.L., Swiergiel, P. *et al.* 1998. Keratocan (Kera), a corneal keratan sulfate proteoglycan, maps to the distal end of mouse chromosome 10. *Genomics* 52, 110-111.

Funderburgh, J.L., Cintron, C., Covington, H.I. *et al.* 1988. Immunoanalysis of keratan sulphate proteoglycan from corneal scars. *Investigative Ophthalmology and Visual Science* 29, 1116-1124.

Funderburgh, J. L. and Conrad, G. W. 1990. Isoforms of corneal keratan sulfate proteoglycan. *Journal of Biological Chemistry* 265 (14), 8297-8303.

Funderburgh, J.L., Corpuz, L.M., Roth, M.R. *et al.* 1997. Mimecan, the 25-kDa corneal keratan sulfate proteoglycan, is a product of the gene producing osteoglycin. *Journal of Biological Chemistry* 272 (44), 28089-28095.

Funderburgh, J. L., Funderburgh, M. L., Hevelone, N. D. *et al.* 1995. Sequence, molecular properties, and chromosomal mapping of mouse lumican. *Investigative Ophthalmology and Visual Science* 36 (11), 2296-2303.

Ge, G., Seo, N-S., Liang, X. *et al.* 2004. Bone morphogenic protein-1/tolloid-related metalloproteinase process osteoglycin and enhance its ability to regulate collagen fibrillogenesis. *Journal of Biological Chemistry* 279 (40), 41626-41633.

Gendron, R.L., Liu, C.Y., Paradis, H. *et al.* 2000. MK/T-1, an immortalized fibroblast cell line derived using cultures of mouse corneal stroma. *Molecular Vision* 7, 107-113.

Gipson, I.K. and Anderson, R.A. 1977. Response of the lysosomal system of the corneal epithelium to tyrosine-induced cell injury. *Journal of Histochemistry and Cytochemistry* 25 (12), 1351-1362.

Bibliography

Glauert, A.M. and Lewis, P.R. 1998. Biological specimen preparation for transmission electron microscopy. In: Glauert A.M. ed. *Practical methods in electron microscopy: Volume* 17. London: Portland Press.

Goldman, J.N. and Benedek, G.B. 1967. The relationship between morphology and transparency in the nonswelling corneal stroma of the shark. *Investigative Ophthalmology* 6 (6), 574-600.

Goodfellow, J.M., Elliott, G.F., Woolgar, A.E. 1978. X-ray diffraction studies of the corneal stroma. *Journal of Molecular Biology* 119 (2), 237-252.

Gordon, G.W. and Ruddle, F.H. 1981. Integration and stable germline transmission of genes injected into mouse pronuclei. *Science* 214 (4526), 1244-1246.

Gordon, M. K., Gerecke, D. R., Dublet, B. *et al.* 1989. Type XII collagen. A large multidomain molecule with partial homology to type IX collagen. *Journal of Biological Chemistry* 264 (33), 19772-19778.

Gordon, G.W., Scangos, G.A., Plotkin, D.J. *et al.* 1980. Genetic transformation of mouse embryos by microinjection of purified DNA. *Proceedings of the National Academy of Sciences USA* 77 (12), 7380-7384.

Gross, J. 1974. Collagen biology: structure, degradation, and disease. *Harvey Lecture* 68, 351-482.

Gurwood, A.S. 2000. Managing corneal abrasions. *Optometry Today* (December) 26-29.

Gyi, T.J., Meek, K.M., Elliott, G.F. 1988. Collagen interfibrillar distances in corneal stroma using synchrotron x-ray diffraction: a species study. *International Journal of Biological Macromolecules* 10, 265-269.

Bibliography

Ha, N.T., Chau, H.M., Cung, L.X. *et al.* 2003a. Identification of novel mutations of the *CHST6* gene in Vietnamese families affected with macular corneal dystrophy in two generations. *Cornea* 22, 508-511.

Ha, N.T., Chau, H.M., Cung, L.X. *et al.* 2003b. Mutation analysis of the carbohydrate sulfotransferase gene in Vietnamese with macular corneal dystrophy. *Investigative Ophthalmology and Visual Science* 44, 3310-3316.

Hardingham, T.E. and Fosang, A.J. 1992. Proteoglycans: many forms and many functions. *FASEB Journal* 6 (3), 861-870.

Hart, R.W. and Farrell, R.A. 1969. Light scattering in the cornea. *Journal of the Optical Society of America* 59, 766-774.

Hasegawa, N., Torii, T., Miyajima, H. *et al.* 2000. Decreased GlcNAc 6-O-sulphotransferase activity in the cornea with macular corneal dystrophy. *Investigative Ophthalmology and Visual Science* 41, 3670-3677.

Hassell, J.R., Cintron, C., Kublin, C. *et al.* 1983. Proteoglycan changes during restoration of transparency in corneal scars. *Archives of Biochemistry and Biophysics* 222 (2), 362-369.

Hassell, J.R., Newsome, D.A., Krachmer, J.H. *et al.* 1980. Macular corneal dystrophy: failure to synthesize a mature keratan sulfate proteoglycan. *Proceedings of the National Academy of Sciences USA* 77 (6), 3705-3709.

Haustein J. 1983. On the ultrastructure of the developing and adult mouse corneal stroma. *Anatomy and Embryology (Berlin)* 168 (2), 291-305.

Hay, E.D. 1991. *Cell biology of extracellular matrix* (2nd edition) New York: Plenum Press.

Bibliography

Hayashi, S., Osawa, T., Tohyama, K. 2002. Comparative observations on corneas, with special reference to Bowman's layer and Descemet's membrane in mammals and amphibians. *Journal of Morphology* 254 (3), 247-258.

Hedbom, E. and Heinegard, D. 1993. Binding of fibromodulin and decorin to separate sites on fibrillar collagens. *Journal of Biological Chemistry* 268 (36), 27307-27312.

Hemmerich, S. and Rosen, S.D. 2000. Carbohydrate sulfotransferase in lymphocyte homing. *Glycobiology* 10, 849-856.

Hendrix, M.J., Hay, E.D., von der Mark, K. *et al.* 1982. Immunohistochemical localisation of collagen types I and II in the developing chick cornea and tibia by electron microscopy. *Investigative Ophthalmology and Visual Science* 22 (3), 359-375.

Hocking, A.M., Shinomura, T., McQuillan, D.J. 1998. Leucine-rich repeat glycoproteins of the extracellular matrix. *Matrix Biology* 17 (1), 1-19.

Hodge, A.J. and Petruska, J.A. 1963. Recent studies with the electron microscope on ordered aggregates of the tropocollagen molecule. In: Ramachandran, G.N. ed. *Aspects of protein chemistry*. London: Academic Press.

Hodson S. 1971. Evidence for a bicarbonate-dependent sodium pump in corneal endothelium. *Experimental Eye Research* 11 (1), 20-29.

Holmes, D.F., Gilpin, C.J., Baldock, C. *et al.* 2001. Corneal collagen fibril structure in three dimensions: Structural insights into fibril assembly, mechanical properties, and tissue organization. *Proceedings of the National Academy of Sciences USA* 98 (13), 7307-7312.

Huang, Y. and Meek, K.M. 1999. Swelling studies on the cornea and sclera: the effects of pH and ionic strength. *Biophysical Journal* 77 (3), 1655-1665.

Bibliography

Iida-Hasegawa, N., Furuhata, A., Hayatsu, H. *et al.* 2003. Mutations in the *CHST6* gene in patients with macular corneal dystrophy: Immunohistochemical evidence of heterogeneity. *Investigative Ophthalmology and Visual Science* 44, 3272-3277.

Iozzo, R.V. 1999. The biology of the small leucine-rich proteoglycans. Functional network of interactive proteins. *Journal of Biological Chemistry* 274 (27), 18843-18846.

Jacobsen, I.E., Jensen, O.A., Prause, J.U. 1984. Structure and composition of Bowman's membrane. Study by frozen resin cracking. *Acta Ophthalmologica (Copenhagen)* 62 (1), 39-53.

Jenkins, E., Moss, J.B., Pace, J.M. *et al.* 2005. The new collagen gene COL27A1 contains SOX9-responsive enhancer elements. *Matrix Biology* 24 (3), 177-184.

Jester, J.V., Ghee Lee, Y., Li, J. *et al.* 2001. Measurement of corneal sublayer thickness and transparency in transgenic mice with altered corneal clarity using *in vivo* confocal microscopy. *Vision Research* 41 (10-11), 1283-1290.

Jester, J.V., Moller-Pedersen, T., Huang, J. *et al.* 1999. The cellular basis of corneal transparency: evidence for 'corneal crystallins'. *Journal of Cell Science* 112 (5), 613-22.

Joyce, N.C., Harris, D.L., Zieske, J.D. 1998. Mitotic inhibition of corneal endothelium in neonatal rats. *Investigative Ophthalmology and Visual Science* 39 (13); 2572-2583.

Kanai, A. and Kaufman, H.E. 1973. Electron microscopic studies of corneal stroma: aging changes of collagen fibers. *Annals of Ophthalmology* 5 (3), 285-287.

Bibliography

Kang, G.M. and Ko, M.K. 2005. Morphological characteristics and intercellular connections of corneal keratocytes. *Korean Journal of Ophthalmology* 19 (3), 213-218.

Kao, W.W. and Liu, C.Y. 2002. Roles of lumican and keratocan on corneal transparency. *Glycoconjugate Journal* 19 (4-5), 275-285.

Kay, G.I. 1969. Stereologic measurement of cell volume fraction of rabbit corneal stroma. *Archives of Ophthalmology* 82 (6), 792-794.

Klintworth, G.K. 1994. Disorders of glycosaminoglycans (mucopolysaccharides) and proteoglycans. In: Klintworh, G.K. and Garner, A. ed./eds. *The Pathobiology of Ocular Disease: A Dynamic Approach.* New York: Marcel Decker.

Klintworth, G.K., Oshima, E., al-Rajhi, A. *et al.* 1997. Macular corneal dystrophy in Saudi Arabia: a study of 56 cases and recognition of a new immunophenotype. *American Journal of Ophthalmology* 124 (1), 9-18.

Klyce, S.D. 1977. Enhancing fluid secretion by the corneal epithelium. *Investigative Ophthalmology and Visual Science* 16 (10), 968-973.

Klyce, S.D. and Beuerman, R.W. 1988. Structure and function of the cornea. In: Kaufmann, H.E. ed. *The cornea.* New York: Churchill Livingston.

Komai, Y. and Ushiki, T. 1991. The three-dimensional organization of collagen fibrils in the human cornea and sclera. *Investigative Ophthalmology and Visual Science* 32 (8), 2244-2258.

Kresse, H., Liszio, C., Schonherr, E. *et al.* 1997. Critical role of glutamate in a central leucine-rich repeat of decorin for interaction with type I collagen. *Journal of Biological Chemistry* 272, 1804-1810.

Bibliography

Lander, A.D. 1999. Proteoglycans. In: Kreis, T. and Vale, R. ed/eds *Guidebook to the extracellular matrix, anchor, and adhesion proteins*. A Sambrook and Tooze Publication at Oxford University Press (2nd edition), 351-356.

Lee, D. and Wilson, G. 1981. Non-uniform swelling properties of the corneal stroma. *Current Eye Research* 1 (8), 457-461.

Lee, J.K., Bhakta, S., Rosen, S.D. *et al.* 1999. Cloning and characterization of a mammalian N-acetylglucosamine-6-sulfotransferase that is highly restricted to intestinal tissue. *Biochemical and Biophysical Research Communications* 263 (2), 543-549.

Lee, R.E. and Davison, P.F. 1984. The collagens of the developing bovine cornea. *Experimental Eye Research* 39 (5), 639-652.

Leonard, D.W. and Meek, K.M. 1997. Refractive indices of the collagen fibrils and extrafibrillar material of the corneal stroma. *Biophysical Journal* 72 (3), 1382-1387.

Leslie, T., Siddiqui, M.A.R., Aitken, D.A. *et al.* 2005. Morquio syndrome: electron microscopic findings. *British Journal of Ophthalmology online* 89, 925-926.

Lewis, D., Davies, Y., Nieduszynski, I.A. *et al.* 2000. Ultrastructural localization of sulfated and unsulfated keratan sulfate in normal and macular corneal dystrophy type I. *Glycobiology* 10 (3), 305-312.

Li, W., Vergnes, J.P., Cornuet, P.K. *et al.* 1992. cDNA clone to chick corneal chondroitin/dermatan sulfate proteoglycan reveals identity to decorin. *Archives of Biochemistry and Biophysics* 296 (1), 190-197.

Linsenmayer, T. F., Bruns, R. R., Mentzer, A. *et al.* 1986. Type VI collagen: immunohistochemical identification as a filamentous component of the extracellular matrix of the developing avian corneal stroma. *Developmental Biology* 118 (2), 425-431.

Bibliography

Linsenmayer, T. F., Fitch, J. M., Birk, D. E. 1990. Heterotypic collagen fibrils and stabilizing collagens. Controlling elements in corneal morphogenesis? *Annals New York Academy of Sciences* 580, 143-160.

Linsenmayer, T. F., Fitch, J. M., Mayne, R. 1984. Extracellular matrices in the developing avian eye: type V collagen in corneal and noncorneal tissues. *Investigative Ophthalmology and Visual Science* 25 (1), 41-47.

Liu, C-Y., Birk, D.E., Hassell, J.R. *et al.* 2003. Keratocan-deficient mice display alterations in corneal structure. *Journal of Biological Chemistry* 278 (24), 21672-21677.

Liu, C-Y., Shiraishi, A., Kao, C.W.C. *et al.* 1998. The cloning of mouse keratocan cDNA and genomic DNA and the characterization of its expression during eye development. *Journal of Biological Chemistry* 273 (35), 22584-22588.

Liu, N.P., Sew-Knight, S., Rayner M. *et al.* 2000. Mutations in corneal carbohydrate sulphotransferase 6 gene (*CHST6*) cause macular corneal dystrophy in Iceland. *Molecular Vision* 6, 261-264.

Ljubimov, A.V., Alba, S.A., Burgeson, R.E. *et al.* 1998. Extracellular matrix changes in human corneas after radial keratotomy. *Experimental Eye Research* 67 (3), 265-272.

Mao, J-R. and Bristow, J. 2001. The Ehlers-Danlos syndrome: on beyond collagens. *Journal of Clinical Investigation* 107 (9), 1063-1069.

Marchini, M., Morocutti, M., Ruggeri, A. *et al.* 1986. Differences in the fibril structure of corneal and tendon collagen. An electron microscopy and X-ray diffraction investigation. *Connective Tissue Research* 15 (4), 269-281.

Marshall, G.E., Konstas, A.G., Lee, W.R. 1993. Collagens in ocular tissues. *British Journal of Ophthalmology* 77 (8), 515-524.

Bibliography

Mathews, C.K. and van Holde, K.E. 1995. In: *Biochemistry* (2nd edition). The Benjamin/Cummings Publishing Company, Inc.

Maurice, D.M. 1957. The structure and transparency of the cornea. *Journal of Physiology* 136, 263-286.

Maurice, D.M. 1969. The cornea and sclera. In: Davson, H. ed. *The eye*. New York: Academic Press. pp. 489-599.

Maurice, D.M. 1970. The transparency of the corneal stroma. Vision Research 10, 107-108.

Maurice, D.M. 1984. The cornea and sclera. In: Davson, H. ed. *The eye*. New York: Academic Press. pp. 1-158.

Maurice, D.M. and Monroe, F. 1990. Cohesive strength of corneal lamellae. *Experimental Eye Research* 50 (1), 59-63.

Maurice, D.M. and Riley, M.V. 1970. The cornea. In: Graymore, C. ed. *Biochemistry of the eye*. London: Academic Press.

Mayer, K., Linker, A., Davidson, E.A. *et al.* 1953. The mucopolysaccharides of the cornea. *Journal of Biological Chemistry* 205, 611-616.

Meek, K.M. 2002. The cornea. In: Roberts, D. (editor). *Signals and Perception: the fundamentals of human sensation* 103-114. Open University Publication.

Meek, K.M., Blamires, T., Elliott, G.F. *et al.* 1987. The organisation of collagen fibrils in the human corneal stroma: a synchrotron X-ray diffraction study. *Current Eye Research* 6 (7), 841-846.

Bibliography

Meek, K.M., Elliott, G.F., Nave, C. 1986. A synchrotron X-ray diffraction study of bovine cornea stained with cupromeronic blue. *Collagen Related Research* 6 (2), 203-218.

Meek, K.M., Elliott, G.F., Sayers, Z. *et al.* 1981. Interpretation of the meridional X-ray diffraction pattern from collagen fibrils in corneal stroma. *Journal of Molecular Biology* 149 (3), 477-488.

Meek, K.M. and Leonard, D.W. 1993. Ultrastructure of the corneal stroma: a comparative study. *Biophysical Journal* 64 (1), 273-280.

Meek, K.M., Leonard, D.W., Connon, C.J. *et al.* 2003a. Transparency, swelling and scarring in the corneal stroma. *Eye* 17 (8), 927-936.

Meek, K.M. and Quantock, A.J. 2001. The use of x-ray scattering techniques to determine corneal ultrastructure. *Progress in Retinal and Eye Research* 20 (1), 95-137.

Meek, K.M., Quantock, A.J., Boote, C. *et al.* 2003b. An X-ray scattering investigation of corneal structure in keratocan-deficient mice. *Matrix Biology* 22 (6), 467-475.

McIlwain, J.T. 1998. *An introduction to the biology of vision.* Cambridge University Press.

Melcher, A. H. and Chan, J. 1978. The relationship between section thickness and the ultrastructural visualization of collagen fibrils: importance in studies on resorption of collagen. *Archives of Oral Biology* 23 (3), 231-233.

Moldovan, L., Zarnescu, O., Oancea, A. *et al.* 2001. Corneal collagen interaction with proteoglycans and glycosaminoglycans. *Romanian Biotechnological Letters* 6 (2), 137-145.

Bibliography

Muller, L.J., Pels, E., Vrensen, G.F. 2001. The specific architecture of the anterior stroma accounts for maintenance of corneal curvature. *British Journal of Ophthalmology* 85 (4), 437-443.

Nakayasu, K. Tanaka, M., Konomi, H. *et al.* 1986. Distribution of types I, II, III, IV and V collagen in normal and keratoconus corneas. *Ophthalmic Research* 18 (1), 1-10.

Newsome, D. A., Gross, J., Hassell, J. R. 1982. Human corneal stroma contains three distinct collagens. *Investigative Ophthalmology and Visual Science* 22 (3), 376-381.

Newton, R.H. and Meek, K.M. 1998a. Circumcorneal annulus of collagen fibrils in the human limbus. *Investigative Ophthalmology and Visual Science* 39 (7), 1125-1134.

Newton, R.H. and Meek, K.M. 1998b. The integration of the corneal and limbal fibrils in the human eye. *Biophysical Journal* 75 (5), 2508-2512.

Nilsson, B., Nakazawa, K., Hassell, J.R. *et al.* 1983. Structure of oligosaccharides and the linkage region between keratan sulfate and the core protein on proteoglycans from monkey cornea. *Journal of Biological Chemistry* 258 (10), 6056-6063.

Nishiyama, T., McDonough, A.M., Bruns, R.R. *et al.* 1994. Type XII and XIV collagens mediate interactions between banded collagen fibers *in vitro* and may modulate extracellular matrix deformability. *Journal of Biological Chemistry* 269 (45), 28193-28199.

Oeben, M., Keller, R., Stuhlsatz, H.W. *et al.* 1987. Constant and variable domains of different disaccharide structure in corneal keratan sulphate chains. *Biochemical Journal* 248 (1), 85-93.

Bibliography

Oldberg, A., Antonsson, P., Lindblom, K. *et al.* 1989. A collagen-binding 59-kd protein (fibromodulin) is structurally related to the small interstitial proteoglycans PG-S1 and PG-S2 (decorin). *EMBO Journal* 8 (9), 2601-2604.

Orgel, J. P., Miller, A., Irving, T. C. *et al.* 2001. The *in situ* supermolecular structure of type I collagen. *Structure (Cambridge)* 9 (11), 1061-1069.

Otvos, L. Jr, Cappelletto, B., Varga, I. *et al.* 1996. The effects of post-translational side-chain modifications on the stimulatory activity, serum stability and conformation of synthetic peptides carrying T helper cell epitopes. *Biochimica et Biophysica Acta* 1313 (1), 11-19.

Pace, J.M., Corrado, M., Missero, C. *et al.* 2003. Identification, characterization and expression analysis of a new fibrillar collagen gene, COL27A1. *Matrix Biology* 22 (1), 3-14.

Patel, S., Marshall, J., Fitzke, III F.W. 1995. Refractive index of the human corneal epithelium and stroma. *Journal of Refractive Surgery* 11 (2), 100-105.

Plaas, A.H., West, L.A., Midura, R.J. 2001a. Keratan sulfate disaccharide composition determined by FACE analysis of keratanase II and endo-beta-galactosidase digestion products. *Glycobiology* 11 (10), 779-790.

Plaas, A.H., West, L.A., Thonar, E.J. *et al.* 2001b. Altered fine structures of corneal and skeletal keratan sulfate and chondroitin/dermatan sulfate in macular corneal dystrophy. *Journal of Biological Chemistry* 276 (43), 39788-39796.

Plaas, A. H. and Wong-Palms, S. 1993. Biosynthetic mechanisms for the addition of polylactosamine to chondrocyte fibromodulin. *Journal of Biological Chemistry* 268 (35), 26634-26644.

Polack, F. M. 1961. Morphology of the cornea. I. Study with silver stains. *American Journal of Ophthalmology* 51, 1051-1056.

Bibliography

Quantock, A. J., Dennis, S., Adachi, W. *et al.* 2003. Annulus of collagen fibrils in mouse cornea and structural matrix alterations in a murine-specific keratopathy. *Investigative Ophthalmology and Visual Science* 44 (5), 1906-1911.

Quantock, A. J., Kinoshita, S., Capel, M. S. *et al.* 1998. A synchrotron x-ray diffraction study of developing chick corneas. *Biophysical Journal* 74 (2), 995-998.

Quantock, A.J., Meek, K.M., Chakravarti, S. 2001. An x-ray diffraction investigation of corneal structure in lumican-deficient mice. *Investigative Ophthalmology and Visual Science* 42 (8), 1750-1756.

Quantock, A.J., Meek, K.M., Ridgway, A.E.A. *et al.* 1990. Macular corneal dystrophy: reduction in both corneal thickness and collagen interfibrillar spacing. *Current Eye Research* 9 (4), 393-398.

Quantock, A. J., Sano, Y., Young, R. D. *et al.* 2005. Stromal architecture and immune tolerance in additive corneal xenografts in rodents. *Acta Ophthalmologica Scandinavica* 83 (4), 462-466.

Rada, J.A., Cornuet, P.K., Hassell, J.R. 1993. Regulation of corneal collagen fibrillogenesis in vitro by corneal proteoglycan (lumican and decorin) core proteins. *Experimental Eye Research* 56 (6), 635-648.

Radner, W. and Mallinger, R. 2002. Interlacing of collagen lamellae in the midstroma of the human cornea. *Cornea* 21 (6), 598-601.

Ramachandran, G.N., Bansal. M., Bhatnagar, R.S. 1973. A hypothesis on the role of hydroxyproline in stabilizing collagen structure. *Biochimica et Biophysica Acta* 322 (1), 166-171.

Ramachandran, G.N. and Kartha, G. 1954. Structure of collagen. *Nature* 174, 269-270.

Bibliography

Ramachandran, G.N. and Kartha, G. 1955. Structure of collagen. *Nature* 176, 593-595.

Rawe, I.M., Leonard, D.W., Meek, K.M. *et al.* 1997. X-ray diffraction and transmission electron microscopy of Morquio syndrome type A cornea: a structural analysis. *Cornea* 16, 369-376.

Regini, J.W., Elliott, G.F., Hodson, S.A. 2004. The ordering of corneal collagen fibrils with increasing ionic strength. *Journal of Molecular Biology* 336 (1), 179-186.

Robert, L., Legeais, J.M., Robert, A.M. *et al.* 2001. Corneal collagens. *Pathologie Biologie (Paris)* 49 (4), 353-363.

Ruggiero, F., Burillon, C., Garrone, R. 1996. Human corneal fibrillogenesis. Collagen V structural analysis and fibrillar assembly by stromal fibroblasts in culture. *Investigative Ophthalmology and Visual Science* 37 (9), 1749-1760.

Ruter, E.R. and Kresse, H. 1984. Partial purification and characterization of 3'-phosphoadenylylsulfate: keratan sulfate sulfotransferases. *Journal of Biological Chemistry* 259 (19), 11771-11776.

Saika, S., Shiraishi, A., Liu, C-Y. *et al.* 2000. Role of lumican in the corneal epithelium during wound healing. *Journal of Biological Chemistry* 275 (4), 2607-2612.

Sawada, H., Konomi, H., Hirosawa, K. 1990. Characterization of the collagen in the hexagonal lattice of Descemet's membrane: its relation to type VIII collagen. *Journal of Cell Biology* 110 (1), 219-227.

Schmitt, F. O., Gross, J., Highberger, J. H. 1955. Tropocollagen and the properties of fibrous collagen. *Experimental Cell Research* (Supplement) 3, 326-334.

Bibliography

Schmut, O. 1977. The identification of type III collagen in calf and bovine cornea and sclera. *Experimental Eye Research* 25 (5), 505-509.

Scott, J.E. 1988. Proteoglycan-fibrillar collagen interactions. *Biochemical Journal* 252 (2), 313-323.

Scott, J.E. 1990. Proteoglycan-collagen interactions and sub-fibrillar structure in collagen fibrils: implications in the development and remodelling of connective tissues. *Biochemical Society Transcripts* 18 (3), 489-490.

Scott, J.E. 1992. Supramolecular organization of extracellular matrix glycosaminoglycans, *in vitro* and in the tissues. *FASEB Journal* 6 (9), 2639-2645.

Scott, J.E. and Bosworth, T.R. 1990. A comparative biochemical and ultrastructural study of proteoglycan-collagen interactions in corneal stroma. Functional and metabolic implications. *Biochemical Journal* 270 (2), 491-497.

Scott, J.E. and Haigh, M. 1985. 'Small'-proteoglycan:collagen interactions: keratan sulphate proteoglycan associates with rabbit corneal collagen fibrils at the 'a' and 'c' bands. *Bioscience Reports* 5 (9), 765-774.

Scott, P.G., Winterbottom, N., Dodd, C.M. *et al.* 1986. A role for disulphide bridges in the protein core in the interaction of proteodermatan sulphate and collagen. *Biochemical and Biophysical Research Communications* 138, 1348-1354.

Smith, J.W. 1968. Molecular pattern in native collagen. *Nature* 219 (150), 157-158.

Smith, J.W. 1969. The transparency of the corneal stroma. *Vision Research* 9, 393-396.

Smith, R.S., Kao, W.W.Y., John, S.W.M. 2002. Ocular development. In: John, S.W.M., Nishina, P.M., Sundberg, J.P. ed./eds. *Systematic evaluation of the mouse eye: anatomy, pathology, and biomethods*. CRC Press.

Bibliography

Smolin, G. and Thoft, R.A. 1994. *The cornea: scientific foundations and clinical practice* (3rd edition) 22-30 Boston: Little Brown Publishers.

Song, J., Lee, Y.G., Houston, J. *et al.* 2003. Neonatal corneal stromal development in the normal and lumican-deficient mouse. *Investigative Ophthalmology and Visual Science* 44 (2), 548-557.

Soriano, E.S., Campos, M.S., Michelacci, Y.M. 2000. Effect of epithelial debridement on glycosaminoglycan synthesis by human corneal explants. *Clinica Chimica Acta* 295 (1-2), 41-62.

Stokes, A.R. 1955. *The theory of x-ray fibre diagrams*. London: Pergamon Press Ltd. pp.140-167.

Stramer, B.M., Kwok, M.G., Farthing-Nayak, P.J. *et al.* 2004. Monoclonal Antibody (3G5) – defined ganglioside: cell surface marker of corneal keratocyte. *Investigative Ophthalmology and Visual Science* 45, 807-812.

Sultana, A., Sridhar, M.S., Jagannathan, A. *et al.* 2003. Novel mutations of the carbohydrate sulfotransferase-6 (*CHST6*) gene causing macular corneal dystrophy in India. *Molecular Vision* 9, 730-734.

Suzuki, M. 1939. Prosthetic group of cornea mucoid. *Journal of Biochemistry* 30, 185-191.

Svensson, L., Aszodi, A., Reinholt, F.P. *et al.* 1999. Fibromodulin-null mice have abnormal collagen fibrils, tissue organisation, and altered lumican deposition in tendon. *Journal of Biological Chemistry* 274 (14), 9636-9647.

Svensson, L., Heinegard, D., Oldberg, A. 1995. Decorin-binding sites for collagen type I are mainly located in leucine-rich repeats 4-5. *Journal of Biological Chemistry* 270, 20712-20716.

Bibliography

Svensson, L., Narlid, I., Oldberg, A. 2000. Fibromodulin and lumican bind to the same region on collagen type I fibril. *FEBS Letters* 470, 178-182.

Svensson, L., Oldberg, A., Heinegard, D. 2001. Collagen binding proteins. *Osteoarthritis Cartilage* 9 (Supplement A), S23-S28.

Tai, G.H., Huckerby, T.N., Nieduszynski, I.A. 1996. Multiple non-reducing chain termini isolated from bovine corneal keratan sulfates. *Journal of Biological Chemistry* 271, 23535-23546.

Tai, G.H., Nieduszynski, I.A., Fullwood, N.J. *et al.* 1997. Human corneal keratan sulfates. *Journal of Biological Chemistry* 272 (45), 28227-28231.

Tasheva, E.S., Corpuz, L.M., Funderburgh, J.L. *et al.* 1997. Differential splicing and alternative polyadenylation generate multiple mimecan mRNA transcripts. *Journal of Biological Chemistry* 272 (51), 32551-32556.

Tasheva, E.S., Funderburgh, M.L., McReynolds, J. *et al.* 1999. The bovine mimecan gene. Molecular cloning and characterization of two major RNA transcripts generated by alternative use of two splice acceptor sites in the third exon. *Journal of Biological Chemistry* 274 (26), 18693-18701.

Tasheva, E.S., Klocke, B., Conrad, G.W. 2004. Analysis of transcriptional regulation of the small leucine rich proteoglycans. *Molecular Vision* 10, 758-772.

Tasheva, E.S., Koester, A., Paulsen, A.Q. *et al.* 2002. Mimecan/osteoglycin-deficient mice have collagen fibril abnormalities. *Molecular Vision* 8, 407-415.

Taylor, B.A., Burmeister, M., Bryda, E.C. 1997. Mouse chromosome 10. *Mammalian Genome* 7, S176-S189.

Toda, N. and Seno, N. 1970. Sialic acid in the KS fraction of whale cartilage. *Biochimica et Biophysica Acta* 208, 227-235.

Bibliography

Thomas, K.R. and Capecchi, M.R. 1987. Site-directed mutagenesis by gene targeting in mouse embryo-derived stem cells. *Cell* 51 (3), 503-512.

Torii, T., Fukuda, M., Habuchi, O. 2000. Sulphation of sialyl N-acetyllactosamine oligosaccharides and fetuin oligosaccharides by keratan sulfate Gal-6-sulfotransferase. *Glycobiology* 10, 203-211.

Turss, R., Friend, J., Reim, M. *et al.* 1971. Glucose concentration and hydration of the corneal stroma. *Opthalamic Research* 2, 253-260.

Ujita, M., Shinomura, T., Kimata, K. 1995. Molecular cloning of the mouse osteoglycin-encoding gene. *Gene* 158, 237-240.

van der Rest, M., Dublet, B., Champliaud, M.F. 1990. Fibril-associated collagens. *Biomaterials* 11, 28-31.

Vogel, K.G., Paulsson, M., Heinegard, D. 1984. Specific inhibition of type I and type II collagen fibrillogenesis by the small proteoglycan of tendon. *Biochemical Journal* 223 (3), 589-597.

von der Mark, H., Aumailley, M., Wick, G. *et al.* 1984. Immunochemistry, genuine size and tissue localization of collagen VI. *European Journal of Biochemistry* 142 (3), 493-502.

Warren, J.F., Aldave, A.J., Srinivasan, M. *et al.* 2003. Novel mutations in the *CHST6* gene associated with macular corneal dystrophy in Southern India. *Archives of Ophthalmology* 121, 1608-1612.

Weber, I.T., Harrison, R.W., Iozzo, R.V. 1996. Model structure of decorin and implications for collagen fibrillogenesis. *Journal of Biological Chemistry* 271 (50), 31767-31770.

Bibliography

Wess, T. J., Hammersley, A. P., Wess, L. *et al.* 1998. A consensus model for molecular packing of type I collagen. *Journal of Structural Biology* 122 (1-2), 92-100.

Wessel, H., Anderson, S., Fite, D. *et al.* 1997. Type XII collagen contributes to diversities in human corneal and limbal extracellular matrices. *Investigative Ophthalmology and Visual Science* 38 (11), 2408-2422.

Wilson, S.E. and Hong, J.W. 2000. Bowman's layer structure and function: critical or dispensable to corneal function? A hypothesis. *Cornea* 19 (4), 417-420.

Woodhead-Galloway, J. 1982. Structure of the collagen fibril: an interpretation. In: Weiss, J.B. and Jayson, M.I.V. ed./eds. *Collagen in health and disease*. 28-48 Churchill Livingston Press.

Worthington, C.R. and Inouye, H. 1985. X-ray diffraction study of the cornea. *International Journal of Biological Macromolecules* 7, 2-8.

Xu, T., Bianco, P., Fisher, L.W. *et al.* 1998. Targeted disruption of the biglycan gene leads to an osteoporosis-like phenotype in mice. *Nature Genetics* 20 (1), 78-82.

Ying, S., Shiraishi, A., Kao, C.W. *et al.* 1997. Characterization and expression of the mouse lumican gene. *Journal of Biological Chemistry* 272 (48), 30306-30313.

Young, R.D., Tudor, D., Hayes, A.J. *et al.* 2005. Atypical composition and ultrastructure of proteoglycans in the mouse corneal stroma. *Investigative Ophthalmology and Visual Science* 46 (6), 1973-1978.

Yue, B. Y., Baum, J. L., Smith, B. D. 1979. Collagen synthesis by cultures of stromal cells from normal human and keratoconus corneas. *Biochemical and Biophysical Research Communications* 86 (3), 465-472.

Bibliography

Zieske, J.D. 2004. Corneal development associated with eyelid opening. *International Journal of Developmental Biology* 48 (8-9), 903-911.